COMPARATIVE NEUROTOXICITY OF METHYLMERCURY AND MERCURIC CHLORIDE *IN VIVO* AND *IN VITRO*

A Dissertation

by

KERRY ALMEDA THUETT

Submitted to the Office of Graduate Studies of
Texas A&M University
in partial fulfillment of the requirements for the degree of

DOCTOR OF PHILOSOPHY

August 2009

Major Subject: Toxicology

COMPARATIVE NEUROTOXICITY OF METHYLMERCURY AND MERCURIC CHLORIDE *IN VIVO* AND *IN VITRO*

A Dissertation

by

KERRY ALMEDA THUETT

Submitted to the Office of Graduate Studies of
Texas A&M University
in partial fulfillment of the requirements for the degree of

DOCTOR OF PHILOSOPHY

Approved by:

Co-Chairs of Committee,	Louise C. Abbott
	Evelyn Tiffany-Castiglioni
Committee Members,	Wei-Jung A. Chen
	Timothy D. Phillips
Chair of Toxicology Faculty,	Robert C. Burghardt

August 2009

Major Subject: Toxicology

ABSTRACT

Comparative Neurotoxicity of Methylmercury and Mercuric Chloride

In Vivo and *In Vitro*. (August 2009)

Kerry Almeda Thuett, B.S.; M.S., Texas Tech University

Co-Chairs of Advisory Committee: Dr. Louise C. Abbott
Dr. Evelyn Tiffany-Castiglioni

It is impossible to remove methylmercury (MeHg) from biological systems because MeHg is found throughout our environment in many fresh and salt water fish. The consumption of fish is important to human nutrition and health. The mechanism of MeHg neurotoxicity must be understood to minimize adverse exposure consequences. The dissertation objective was to: 1) compare mechanisms of MeHg neurotoxicity between animals exposed as adults and those exposed during gestation, and 2) develop an *in vitro* test model of *in vivo* MeHg exposure.

Total mercury (Hg) levels in tissue / cells were determined by combustion / trapping / atomic absorption. Cell death was determined by Fluoro-Jade histochemical staining and activated caspase 3 immunohistochemistry for *in vivo* studies, and Trypan blue exclusion, lactate dehydrogenase activity, and cytotoxicity assays for *in vitro* studies. Mitochondrial membrane potential (MMP), intracellular calcium ion concentration ($[Ca^{2+}]_i$), and production of reactive oxygen species (ROS) were determined using fluorescence microscopy or microplate reader assays. Young adult C57Bl/6 mice were exposed to a total dose of 0, 1.0, or 5.0 mg/kg body weight MeHg divided over postnatal days (P)35 to 39. Pregnant female mice were exposed to a total does of 0, 0.1, or 1.0 mg/kg body weight MeHg divided over gestational days (G)8 to 18. SY5Y cells were exposed to 0, 0.01, 0.1, or 1.0 μM MeHg or $HgCl_2$ for 24, 48, or 72 hours.

Total Hg in brains of young adult mice, mouse pups, and SY5Y cells accumulated in a dose-dependent manner. Cell death increased in SY5Y cells exposed to the highest concentrations of MeHg and $HgCl_2$ used in this study. Cell death increased in the molecular and granule cerebellar cell layers of young adult mice exposed to the highest doses of MeHg used in this study. P0 mouse pups showed no increase in cell death within the cerebellum following MeHg exposure. Cerebella of mice at P10 exhibited decreased dying cells only in the external germinal layer.

Low concentrations of MeHg affected MMP in both *in vivo* and *in vitro* studies, but did not result in decreased MMP typically associated with higher MeHg concentrations. $[Ca^{2+}]_i$ was increased throughout the *in vivo* experiments in an age- , sex- and brain region-dependent manner. Generation of ROS was decreased in both *in vivo* and *in vitro* studies with both the MeHg and $HgCl_2$ (*in vitro*) treatments.

In summary, low and moderate MeHg exposure, both *in vivo* and *in vitro*, altered mitochondrial function, Ca^{2+} homeostasis, and ROS differently than what is reported in the literature for higher MeHg exposure concentrations. SY5Y cells were sensitive to low-levels of MeHg and $HgCl_2$ and responded similarly to cells in the whole animal studies, thus making SY5Y cells realistic candidates for mechanistic MeHg studies.

Cell culture and whole animal neuronal functional studies at chronic low-level MeHg exposure are limited. These data suggest that low-levels of MeHg may affect neuronal function. Therefore, further chronic low-level MeHg neuronal functional studies are warranted.

DEDICATION

There are people in my life that I love more than life itself. They mean more to me than any degree I could earn, more than any praise or accolade I will ever receive. To these pillars upon whom my dissertation is founded, I dedicate these words:

> "God is our refuge and strength, a very present help in trouble." (Psalms 46:1)
>
> "Come to Me, all who are weary and heavy-laden, and I will give you rest." (Matthew 11:28)
>
> "Every good thing bestowed and every perfect gift is from above, coming down from the Father of lights, with whom there is no variation, or shifting shadow." (James 1:17)
>
> "In all your ways acknowledge Him, and He will make your paths straight." (Proverbs 3:6)
>
> *Drawn from The Holy Bible, New American Standard Version.*

Ronald and Nancy, you are the greatest parents ever given to any child. Trevor, Jodi, Dalton and Caelan, I love you all; we need to play more Guitar Hero! Casey Donnelly and Tim Knight, you are the best; thanks for the many fun celebrations. Deanna Mueller Keene, Catherine Mueller Glaze, and Jennafer Todd Chaddrick, you are my very best friends, and I thank you endlessly for keeping in touch when I had retreated from the world. Sarah Wills, I am a better person because of you, and I am grateful. Ian Murray, thank you for being a supportive scientist and friend; thanks also for bringing Kevin to Salsa class. Kevin Joy, where did you come from?! You entered my life at a time that was most needed; I know, without a doubt, that you were sent from God to ensure that my Ph.D was completed. Nick Garcia, Nickercizing with the Nick-elodeon was a daily respite from the tedium of research; as you abused my body, you freed my mind; because of your excellent skills and training, I am stronger and healthier today than I have ever been in my life.

ACKNOWLEDGEMENTS

I would like to thank my committee co-chairs, Dr. Louise Abbott and Dr. Evelyn Castiglioni, and my committee members, Dr. Wei-Jung Chen and Dr. Tim Phillips for their guidance and support throughout the course of this research. These individuals were consistently supportive, patient, and understanding as I made my way through the process of attaining a Ph.D. Their direction and expertise in whole animal, cell culture, statistical, and environmental toxicological research played a pivotal role in my success.

Thanks also go to Dr. Robert Burghardt and Dr. Rola Baroumi in the College of Veterinary Medicine and Biomedical Sciences Image Analysis lab for their mentoring, time, and attention. These two individuals and the equipment they provided were instrumental in my successful and proper completion of over half of my dissertation research.

Dr. Yongchang Qian, was a continual support and source of knowledge during my cell culture research. He provided mentoring as well as the space and supplies necessary for the *in vitro* portion of my project. He and Ying Zheng, together helped make my cell culture research a success.

Throughout my time at Texas A&M, several undergraduate students participated in portions of my research. Heather Thompson, Rene Ramon, Susan Hernandez, Raul Grajeda, Francisco Gomez, Ian Windsor, Tania Kanadan, and Devang Ghandi have earned my deepest gratitude for their eagerness to work, willingness to learn, and dedication to the end goal.

I would like to thank Sang-Soep Nahm, Tamy Frank-Cannon, Sairam Bellum, Bhupinder Bawa, Sarah Wills, and Pei-San Huang for their expertise, kindness, and ultimately, their friendship. These lab colleagues taught me techniques and skills and provided helping hands when needed.

TABLE OF CONTENTS

CHAPTER Page

LIST OF FIGURES

FIGURE Page

FIGURE Page

FIGURE Page

FIGURE Page

LIST OF TABLES

CHAPTER I

INTRODUCTION

HIPPOCAMPAL FORMATION

Historical perspective

The hippocampal formation is a part of each cerebral hemisphere that lies beneath the cortical surface and functions in emotion, learning, and memory. Its anatomy and function have been studied for more than 400 years. As referenced in Gurunluoglu and Gurunluoglu (2008), the term "hippocampus" (sea horse) was first used by Arantius in 1587 who thought the three dimensional form of the human hippocampus looked like a sea horse. In the 19th century, Pierre Paul Broca first observed the association of the hippocampus and other C-shaped structures with emotional states. Broca named this region *le grande lobe limbique* (*limbus*, Latin for "border") because it encircles the diencephalon and borders the cerebral cortex (Broca, 1878; Finger, 2004). At this same time, Alois Alzheimer, a German neuroanatomist, observed that characteristic pathologic changes in the hippocampal formation were associated with dementia (Graeber *et al.*, 1997). In 1937, at Cornell University, James Papez observed neurodegenerative changes in the hippocampus, mammillary bodies, thalamus, and cingulate in post-mortem examinations of the brains of individuals with psychiatric disorders. He suggested that a complex set of specific connections between structures of the limbic lobe formed a circuit for emotional experience (Papez, 1937). Wilder Penfield was the first person to obtain evidence that memory processes might be localized to specific regions of the brain. In the 1940s, he began using electrical stimulation to map the motor, sensory and language functions in the cerebral cortex of patients undergoing brain surgery to relieve focal epilepsy. He found that stimulation of the temporal lobes produced coherent recollections of earlier experiences (Penfield, 1958a; Penfield, 1958b; Penfield, 1958c).

This dissertation follows the style of *Toxicological Sciences*.

Corroborating this evidence were studies of behavior in patients whose medial temporal lobe of the cerebrum had been ablated to ameliorate symptoms of temporal lobe epilepsy. In the 1950's, Brenda Milner and William Scoville (Neylan, 2000) studied the patient "H.M.". He had bilateral temporal lobe removal, which resulted in a lesion in the hippocampus. H.M. lost the ability to consolidate short-term memory into long-term memory; however, he retained the memory of events occurring before the surgery. Current research suggests that limbic areas associated with the medial temporal lobe have a role in learning, memory, cognition, and behavioral expression. These structures include the cingulate gyrus, parahippocampal gyrus, perirhinal cortex, entorhinal cortex, amygdala, mammillary bodies, and the hippocampal formation, particularly the hippocampus.

Gross and histological structure and fiber connections

The hippocampal formation and its efferent pathways (fornix) form a concentric ring that surrounds the diencephalon and midbrain (Fig I-1). There are three components comprising the hippocampal formation: dentate gyrus, hippocampus proper, and subiculum (Fig I-2). The components are organized as strips running rostrocaudally within the temporal lobe and together forming a cylinder. They are folded upon each other into the configuration of a "jelly-roll" pastry (Fig I-1). Each of the three components contains three cell layers. The dentate gyrus contains the molecular, granule cell, and hilus layers. The molecular layer is composed of apical dendrites of granule cells, but few cell bodies. Axons of granule cells synapse on other neurons of the hippocampal formation. The hilus contains interneurons. This region is complex and is often considered the "CA4" field, as opposed to a part of the dentate gyrus (Amaral, 1978). However, it has been shown that cells originating in the hilus project only to the dentate gyrus and to no other field of the hippocampal formation (Laurberg and Sørensen, 1981). The three layers of the hippocampus proper and the subiculum are analogous to those of the dentate gyrus. However, the granule cell layer is replaced with

the pyramidal layer that contains pyramidal cells that are the major output neurons of the hippocampal formation (Kandel *et al.*, 2000; Martin, 1996).

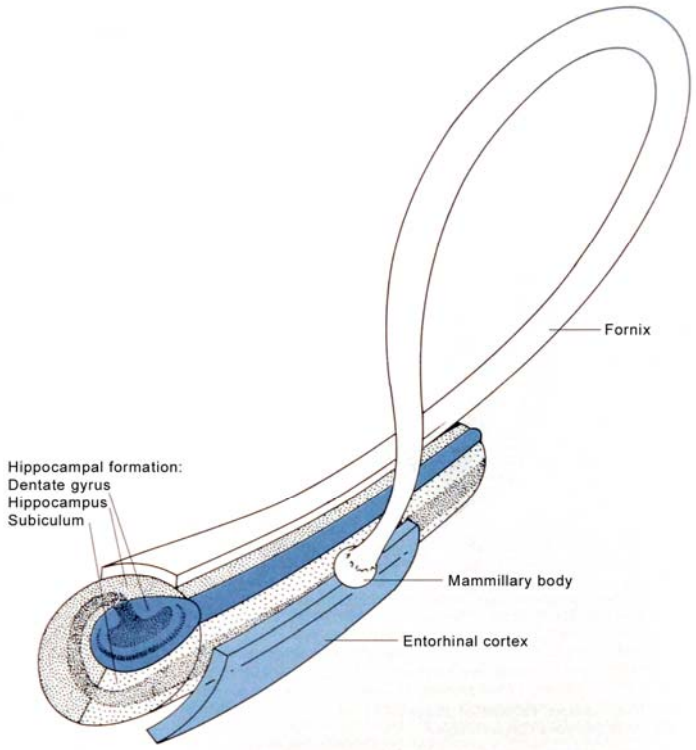

FIG. I-1. General spatial relationships of components of the hippocampal formation, its efferent pathway (fornix), and the entorhinal cortex. Modified from Martin, J. H. (1996). Neuroanatomy Text and Atlas. 2 ed., p. 452. Appleton & Lange, Stamford.

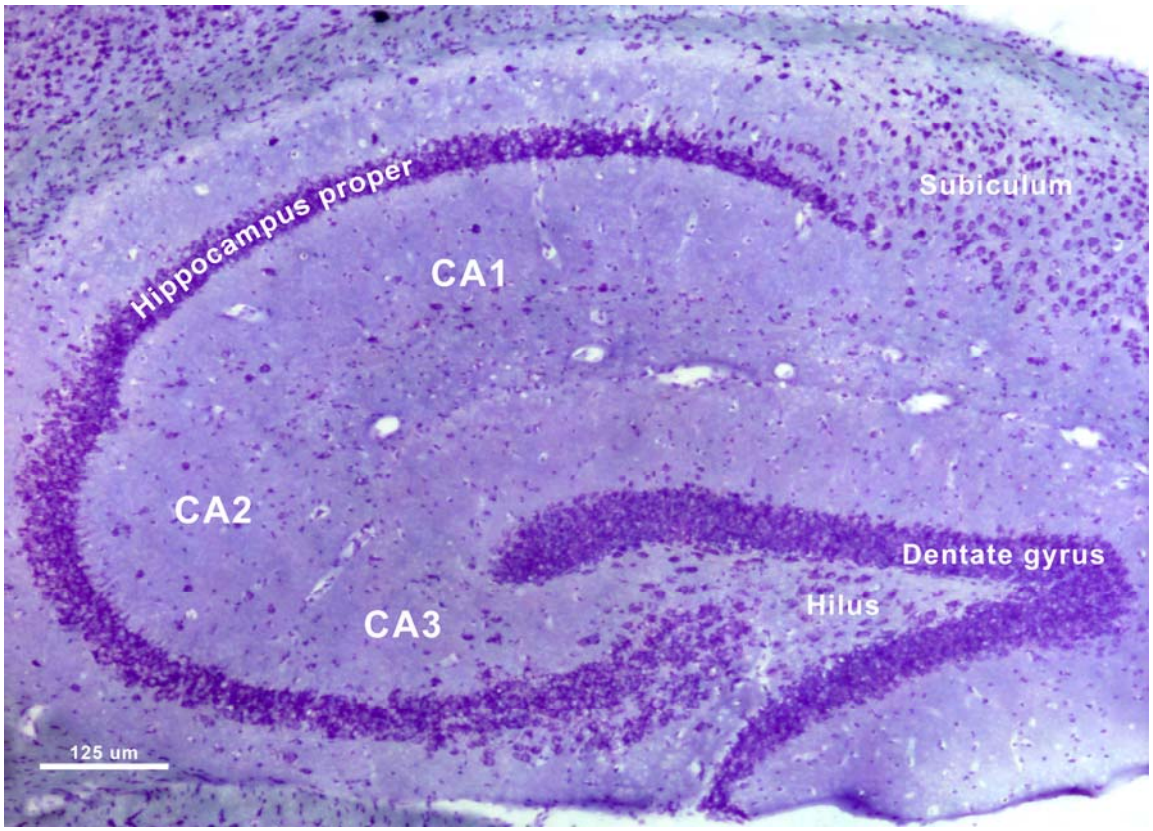

FIG. I-2. Hippocampal subfields of a forty-day-old mouse. The subiculum, dentate gyrus and three regions of the hippocampus proper (Cornu Ammonis, Ammon's horn) are labeled: CA1, CA2, and CA3. The image is a paraformaldehyde-fixed, frozen sagittal section stained with 1% thionin. Scale bar is 125 um.

The major input to the hippocampal formation is the entorhinal cortex, located on the parahippocampal gyrus adjacent to the hippocampal formation (Fig I-1 and I-3). Other portions of the limbic cortex indirectly influence the hippocampal formation through the entorhinal cortex (Fig I-3). The perforant fiber pathway from the entorhinal cortex forms excitatory connections with the granule cells of the dentate gyrus (Fig I-3) (Andersen *et al.*, 1966; Witter and Amaral, 1991). The small (7 µm), highly compact granule cells give rise to axons that form the mossy fiber pathway, which connects to the pyramidal cells in the CA3 region of the hippocampus proper (Blackstad *et al.*, 1970).

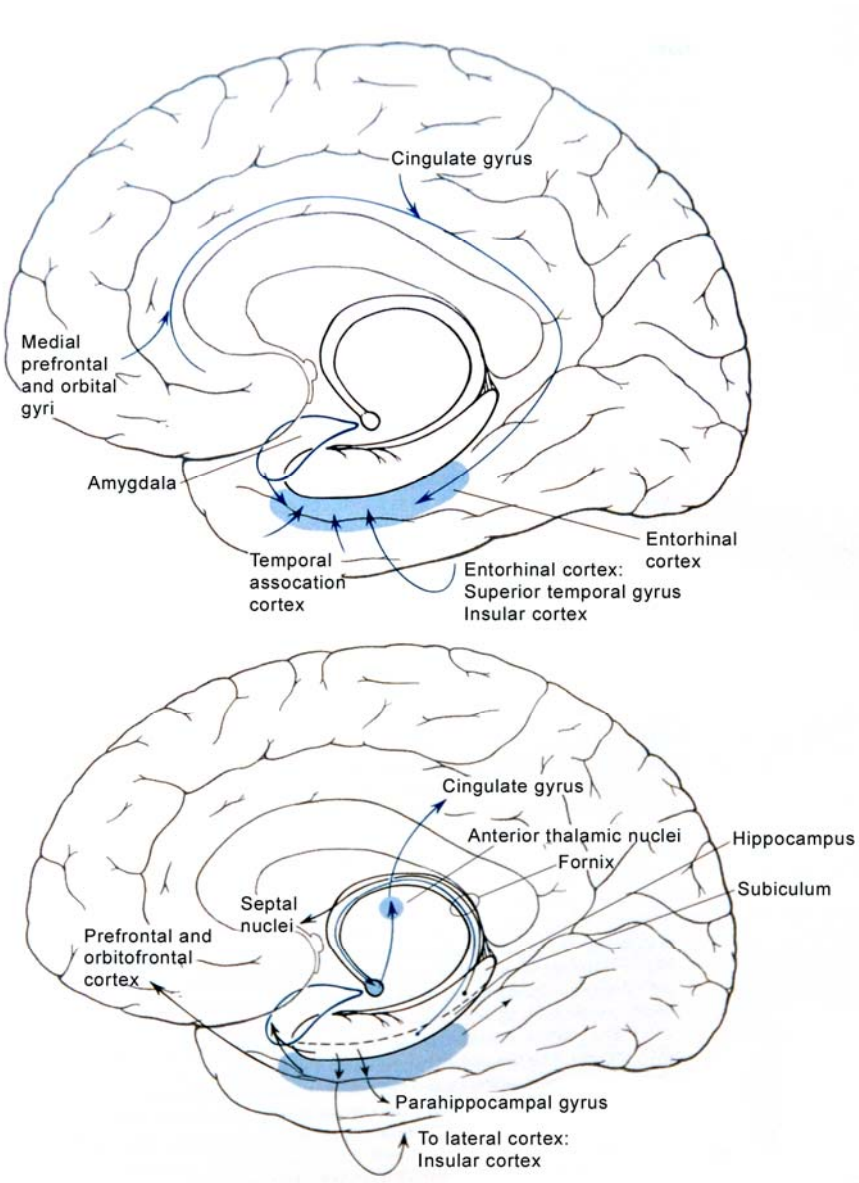

FIG. I-3. Principal afferent connections (A) and efferent projections (B) of the hippocampal formation. Inputs from the cingulate gyrus and other association areas of the cerebral cortex are transmitted to the hippocampal formation from the entorhinal cortex. Efferent projections from the subiculum and hippocampus to the rostral diencephalon and telencephalon are located in the fornix. Modified from Martin, J. H. (1996). Neuroanatomy Text and Atlas. 2 ed., p. 455. Appleton & Lange, Stamford.

The hippocampus proper (also called *Corno Ammonis* or Ammon's horn) has three distinct fields: CA3, CA2, and CA1 (Lorente de No, 1933) (Fig I-2). The subfields have different cell shapes and sizes, connectivity, electrophysiological properties and

susceptibility to insults (Taupin, 2007). Field CA3 borders the hilus of the dentate gyrus on one end and the CA2 region on the other. The CA3 region is larger and contains more cells than the CA2 region (Seress, 1988). Pyramidal cells in CA3 receive input from axons of granule cells from the dentate gyrus and are known as mossy fibers. Mossy fibers travel through the hilar region to synapse on CA3 pyramidal cells. Schaffer collateral project from CA3 pyramidal cells to the pyramidal cells in CA1. The CA2 region is the smallest and most compact of the pyramidal cell regions, which is the main distinguishing characteristic of the CA2 region. The CA1 region borders the CA2 region on the end opposite CA3. The CA1 region is larger and contains more cells than either the CA2 or the CA3 region (Seress, 1988). Efferent collaterals of the CA1 pyramidal cells collect on the surface of the hippocampal formation to form a compact fiber bundle called the fornix, which contains axons that project to the subcortical telencephalon and diencephalon (Fig. I-3).

Although each of the hippocampal fields is essentially one cell layer comprised of pyramidal cells, the plexiform layers above and below the pyramidal cell layer also have been named (Insausti and Amaral, 2004). The alveus is the outermost layer located nearest the lateral ventricle. It is composed of axons of pyramidal cells. The stratum oriens lies between the alveus and the pyramidal cell layer. It is composed mainly of basal dendrites of pyramidal cells and various interneurons. The region on the other side of the pyramidal cell layer, nearest the hippocampal fissure, contains apical dendrites of pyramidal cells and various interneurons. This plexiform layer has been divided into three layers: stratum lucidum, stratum radiatum, and stratum lacunosum-moleculare. The stratum lucidum contains mossy fibers from granule cells that travel through or synapse on proximal dendrites of pyramidal cells. The stratum lucidum only appears adjacent to CA3, because CA2 and CA1 do not receive mossy fiber inputs. The stratum radiatum of CA3 and CA2 contain associational projections from other regions of the hippocampus as well as subcortical inputs such as from the septal nuclei and the supramammillary region. The stratum radiatum and stratum lacunosum-moleculare of the CA1 region contain projections from CA3 and CA2 pyramidal cells (Schaffer collaterals) (Ishizuka

et al., 1990). The Schaffer collaterals form the last synapse in a powerful excitatory synaptic chain which includes the entorhinal cortex, dentate gyrus granule cells, and CA3 and CA1 pyramidal cells (Anderson *et al.*, 1971).

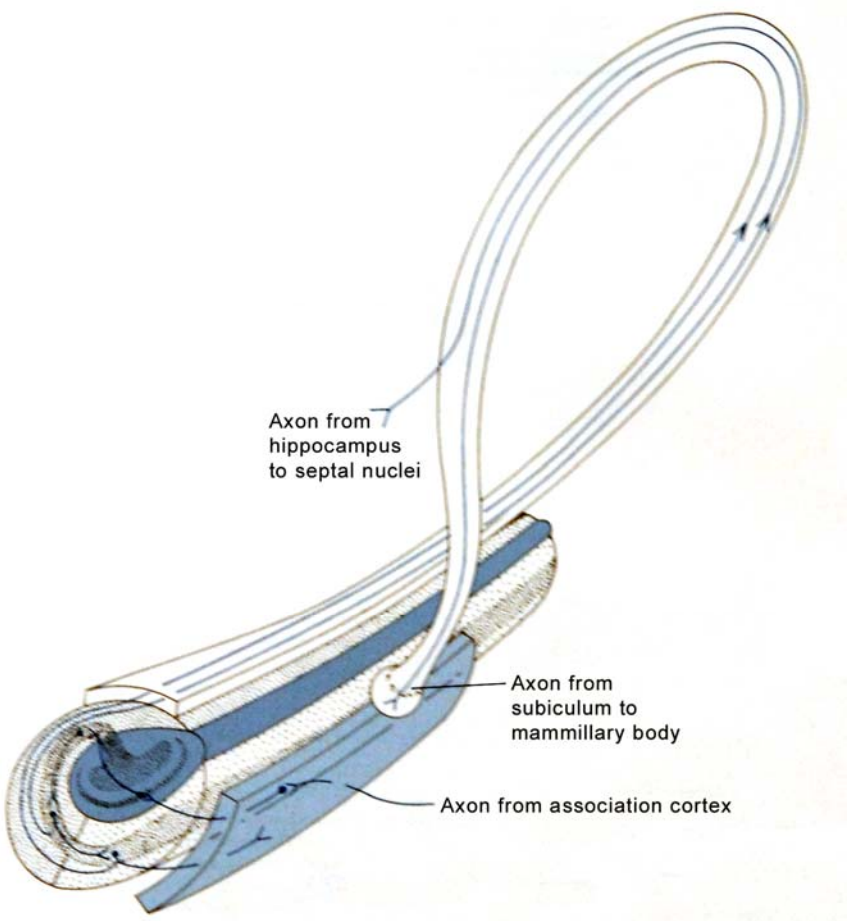

FIG. I-4. Simplified serial circuit from the entorhinal cortex to the hippocampal formation. Two outputs are shown: the fornix, which has a major projection to the septal nucleus and mammillary body, and the projection back to the entorhinal cortex. Modified from (Martin, J. H. (1996). Neuroanatomy Text and Atlas. 2 ed., p. 453. Appleton & Lange, Stamford.

Axons from the CA1 region of the hippocampus synapse primarily in the subiculum (Finch and Babb, 1981) and the lateral septal nuclei in the rostral forebrain (Alonso and Köhler, 1984; Swanson and Cowan, 1977). Axons project from the subiculum and the lateral septal nuclei to a large portion of the cerebral forebrain, thus

connecting the hippocampus indirectly to major learning, memory, and behavioral pathways (Fig I-3). Pyramidal cell axons from the subiculum synapse in the mammillary bodies, lateral septal nuclei, anterior thalamic nuclei, amygdala, entorhinal cortex, and nucleus accumbens (Kandel *et al.*, 2000; Krettek and Price, 1977; Martin, 1996; Sørensen and Shipley, 1979). Projections from the septal nuclei travel through the fornix back to the hippocampus as a regulatory mechanism. Other brain areas that have connections to and from the hippocampal formation include: the hypothalamus (Segal and Landis, 1974), nucleus accumbens (Groenewegen *et al.*, 1982), caudate nucleus and putamen (Groenewegen *et al.*, 1982), and the thalamus (Chronister *et al.*, 1975) (Fig I-3).

Adult neurogenesis

The hippocampus is of particular interest because of the presence of adult neurogenesis that takes place in this brain region. In the mammalian CNS, most neurons are born during the prenatal phase of development, with the exception of the granule cells of the dentate gyrus of the hippocampus and the granule cells of the cerebellum, which are primarily born during the first two postnatal weeks in rats (Bayer, 1980). In guinea pigs, postnatal development in the dentate gyrus is high up to P20 then begins to slow significantly after P30 (Guidi *et al.*, 2005).

Previously, it was thought that the adult brain did not generate new nerve cells, and that the adult brain was devoid of stem cells. In the early 1960's, Altman and Das (Altman, 1962; Altman and Das, 1965) published data suggesting the generation of new neuronal cells in specific areas of the adult brain, the subventricular zone and the dentate gyrus. In the 1980's, adult neurogenesis was confirmed in mammals, including primates (Gross, 2000; Taupin and Gage, 2002). Reynolds and Weiss (1992) isolated adult neural stem cells from the rodent central nervous system (CNS). Eriksson *et al.* (1998) identified the subgranular zone of the dentate gyrus as one of the two major locations where adult neurogenesis occurs. In the dentate gyrus of mammals, newly generated neuronal cells in the subgranular zone migrate to the granule cell layer, where they

differentiate into neuronal cells, extend axonal projections and establish functional connections (Cameron *et al.*, 1993; Eriksson *et al.*, 1998; Gould *et al.*, 1999; van Praag *et al.*, 2002) (Fig I-5). In rats, new granule cells extend axons to the CA3 regions in four to ten days following mitosis (Hastings and Gould, 1999). It has been shown that newly established neurons in adult humans live for at least two years (Eriksson *et al.*, 1998).

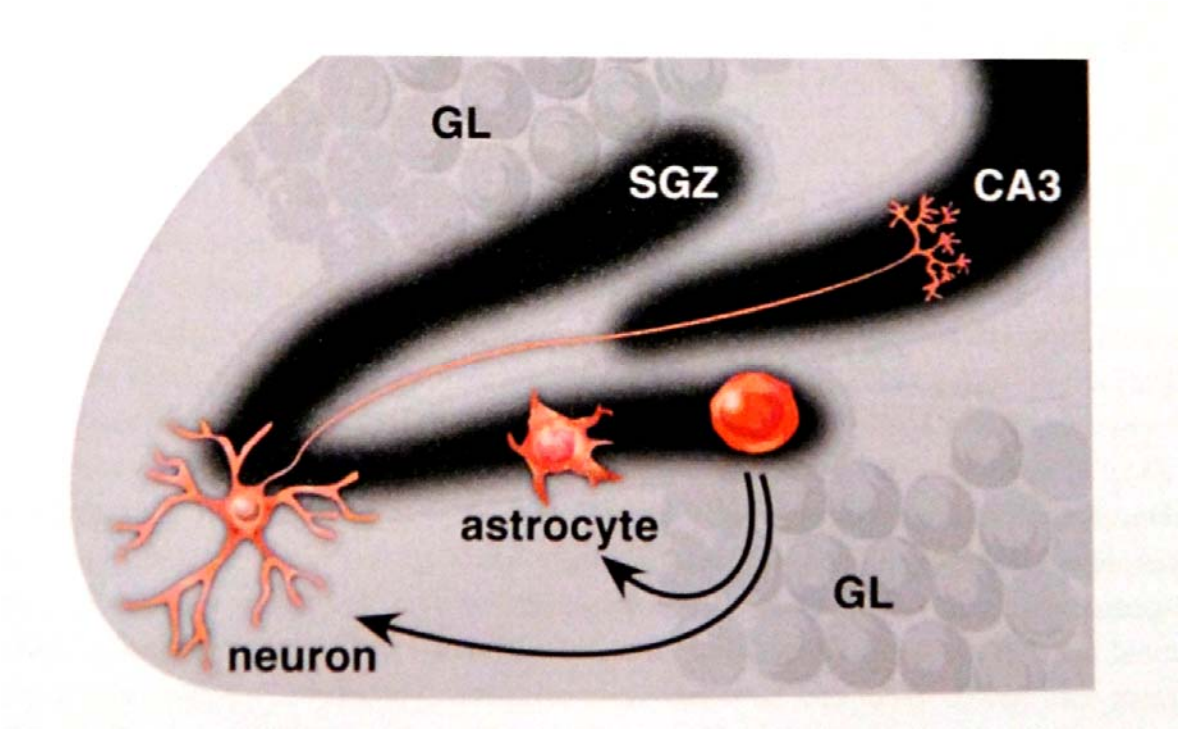

FIG. I-5. Neurogenesis in the adult dentate gyrus. New neuronal cells in the subgranular zone of the dentate gyrus migrate to the granule layer and differentiate into neuronal cells and astrocytes. The new neurons in the granule layer extend axons to the CA3 region of the hippocampus. Modified from Taupin, P. (2007). The Hippocampus - Neurotransmission and Plasticity in the Nervous System. p. 103. Nova Science Publishers, New York.

Confirmation of adult neurogenesis suggests that the development of the brain may be a lifelong process, and the CNS may be amenable to repair (Taupin, 2007), or susceptible to developmental disorders. Just as alterations in early developmental neurogenesis may result in abnormal hippocampal function, so also could alteration in

adult neurogenesis. The presence of adult neurogenesis has consequences for our understanding of CNS development, function, and therapeutic approaches.

Learning and memory

The major role of the hippocampus is the consolidation of learning and memory. As stated previously, hippocampal lesions may result in a type of amnesia in which memories of events prior to the damage are retained, but new information is not. This amnesia applies only to specific facts and events (explicit or declarative memory) and not to the learning of new skills and procedures (implicit memory). Basically, learning and memory not associated with conscious recall of specific items, such as pattern recognition, habits, conditioned autonomic reactions to stimuli, and motor skills, do not depend on the hippocampus, whereas consolidation of explicit memories of facts and events does depend on the hippocampus (Kandel *et al.*, 2000; Martin, 1996).

Donald Hebb (Hebb, 1950) postulated that use-dependent changes in synaptic strength were the elemental units of learning. The CA1 region of the hippocampus is important in long-term potentiation (LTP). LTP is a brief period of synaptic activity that causes a long-lasting increase in the strength of activated synapses (Bliss and Gardner-Medwin, 1973). Potentiation may last from two hours to many days. Treatments that block LTP decrease the formation of long-term memories (Morris, 2003). LTP is induced when repetitive synaptic activation causes sufficient depolarization of the postsynaptic neuron to relieve the constitutive block of the N-methyl-D-aspartate receptor (NMDAR)-gated ion channel by Mg^{2+} in the extracellular fluid (Malenka and Nicoll, 1999; Malinow, 2003). These channels allow calcium ions (Ca^{2+}) to enter the postsynaptic cell and activate various second messengers. Second messenger pathways may increase insertion of new glutamate receptors or increase phosphorylation of pre-existing receptors, thereby increasing the cell's ability to generate current (Malenka and Bear, 2004). In addition, second messenger pathways may lead to changes in gene expression and the encoding of proteins that underlie maintenance of the potentiation (Martin *et al.*, 2000).

Other ways to increase the synaptic connection between neurons and enhance LTP include: 1) increasing the number of sites of contact between the two, 2) increasing the size of the dendritic spine heads to accommodate more receptors, or 3) increasing the diameter of the dendritic spine neck so that depolarization of the spine more readily translates to the whole dendrite (Fifková and Anderson, 1981; Fischer *et al.*, 1998; Moser *et al.*, 1994). A unifying theme throughout the hypotheses of enhanced synaptic transmission is the idea that Ca^{2+} is involved. Proper functioning of the NMDAR-gated ion channel allows Ca^{2+} to enter the cell. The Ca^{2+}-calmodulin-dependent protein kinase, CaMK, is a second messenger involved in LTP and spine morphogenesis (Jourdain *et al.*, 2003); spines contain intracellular organelles that regulate $[Ca^{2+}]_i$ (Cooney *et al.*, 2002). Blocking voltage-gated Ca^{2+} channels reduces synaptic transmission and the appearance of new spines (Engert and Bonhoeffer, 1999). Proper Ca^{2+} function and concentration appear to be instrumental in the morphological changes of neurons that are necessary for learning and memory.

Disorders of the hippocampus

Because the hippocampus is associated with many types of learning and memory and is connected to the cerebral cortex as well as the hypothalamus, alterations in normal hippocampal function can produce a wide variety of behavioral symptoms in addition to the abnormalities in declarative learning and memory already discussed. Altered hippocampal function has been associated with impaired odor-discrimination learning (Martin *et al.*, 2007), decreased avoidance learning (Simonyi *et al.*, 2007), altered spatial memory (Barhwal *et al.*, 2007), depression (Campbell and Macqueen, 2004) , post-traumatic stress disorder (Gilbertson *et al.*, 2007), the acquisition and consolidation of memories associated with fear (Wallenstein and Vago, 2001), epilepsy (Myhrer, 2007), Alzheimer's disease (Thompson *et al.*, 2004), schizophrenia (Nestor *et al.*, 2007), and autism (Dager *et al.*, 2007).

Cell loss in the hippocampal formation is associated with epilepsy (Sommer, 1880). Two-thirds of the cases of temporal lobe epilepsy show the hippocampal

formation as the only structure with pathological modification (Meldrum and Corsellis, 1984). Cell loss is mainly in CA1, while granule cell dispersion and organization changes occur in the dentate gyrus (Houser *et al.*, 1992). Studies suggest that a hippocampal-seizure relationship may be established following episodes of infantile seizures (Meldrum and Corsellis, 1984).

A large portion of memory loss associated with Alzheimer's disease is linked to damage to the hippocampal formation. Recent studies showed that only the subiculum and the hilus of the dentate gyrus show substantial cell loss in normal aging (West, 1993; West *et al.*, 1994). This cell loss, however, is not the case in individuals with Alzheimer's disease. Afflicted patients have significant cell loss in the subiculum and dentate gyrus as well as in the entorhinal cortex (Insausti *et al.*, 1998; Price *et al.*, 2001; Simic *et al.*, 1997; West *et al.*, 1994). As the disease develops, the hippocampal formation essentially becomes functionally disconnected from its major afferent and efferent interactions (Hyman *et al.*, 1984).

Abnormalities in the development of the hippocampal system may contribute to schizophrenia. There is an altered distribution of nicotinamide-adenine dinucleotide phosphate-diaphorase-containing cells in the hippocampal formation of schizophrenic patients (Akbarian *et al.*, 1993; Ribak and Seress, 1983; Sobreviela and Mufson, 1995). In addition, Jakob and Beckmann (1994; 1986) suggested that disturbances in neuronal migration might explain disorganization observed in the entorhinal cortex of individuals with schizophrenia.

Finally, altered hippocampal function has been described in individuals with autism and related disorders (Lord *et al.*, 2000). Bauman and Kemper (1985) reported an increase in cell density in all three fields of the hippocampus, as well as in the entorhinal cortex of autistic patients. More recently, MRI scans of autistic individuals showed an increase in the total volume of the left hippocampus (Rojas *et al.*, 2006). In addition, neuropsychological tasks that determine the integrity of brain circuits linking the dorsolateral prefrontal cortex and the hippocampus indicated that individuals with autism performed poorer than those without autism (Loveland *et al.*, 2008). The

research in this area is new and incomplete; a clear connection between the hippocampus and autism has not been confirmed.

CEREBELLUM

Gross structure

The cerebellum is a major subdivision of the CNS and is responsible for coordination of motor function and balance. It controls rate, range, and force of motion by monitoring sensory input from the body, head, eyes, and ears, as well as from the cerebral motor cortex (Nolte and Sundsten, 2001). The cerebellum has been the focus of extensive neurological research due, in part, to its simple and well documented organizational structure (Angevine *et al.*, 1961; Jansen, 1954; Ziehen, 1934).

The cerebellum is located dorsal to the 4th ventricle and caudal to the cerebral hemispheres. Grossly, it is divided into three regions: the vermis, two hemispheres, and the flocculonodular lobe (Fig I-6). The vermis is responsible for spinocerebellar/ somatosensory functions. The hemispheres are involved in motor planning for coordination of motor function of the limbs; the hemispheres are also involved in motor learning. The flocculonodular lobe is responsible for balance and equilibrium (Nolte and Sundsten, 2001). The primary fissure separates the cerebellum into rostral (anterior) and caudal (posterior) portions. The posterolateral fissure defines the flocculonodular lobe. (Altman and Bayer, 1997; Marani and Voogd, 1979).

The cerebellum is highly lobulated. There are 10 defined lobules (folia) (Altman and Bayer, 1997; Voogd and Glickstein, 1998). Different nomenclature is used for the lobules when referring to humans and mice (Table I-1). In mice, the vermis lobules I and II are fused, as are lobules IV and V (Marani and Voogd, 1979) (Fig I-7).

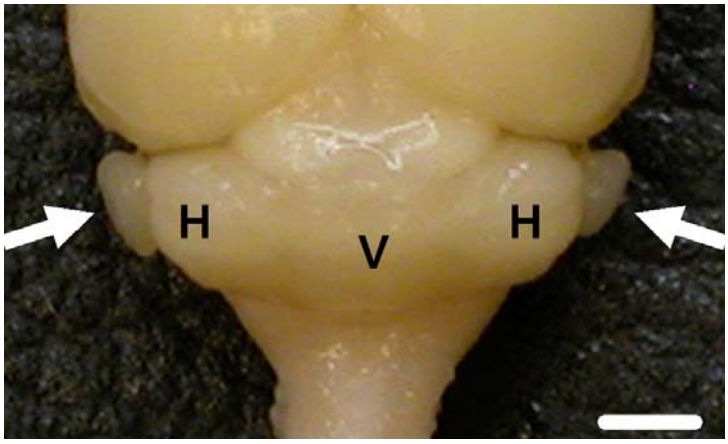

FIG. I-6. Dorsal view of the adult mouse cerebellum. V indicates vermis, H indicates hemispheres and arrows indicate flocculi. Scale bar is 2 mm.

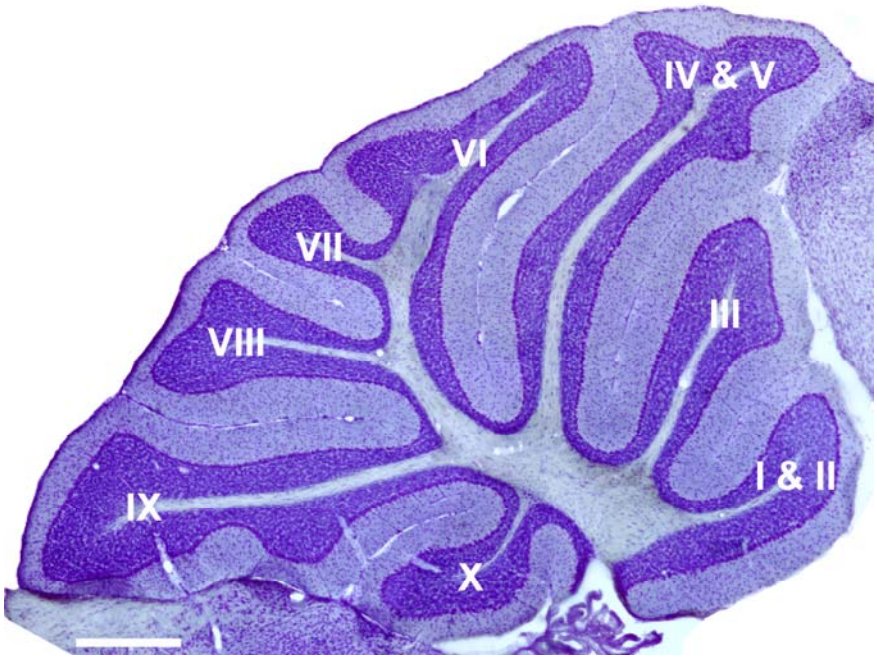

FIG. I-7. Microscopic anatomy of the adult mouse cerebellum. Sagittal view of a mouse cerebellar vermis showing lobules I through X. Section is paraformaldehyde-fixed, frozen, and stained with 1% thionin. Scale bar is 500 µm.

TABLE I-1
Nomenclature of Cerebellar Lobules

Vermis		Hemispheres	
Human	**Other mammals**	**Human**	**Other mammals**
Lingual	Lobule I	Vincingulum lingulae	Anterior lobule
Central	Lobule II & III	Ala lobulus centralis	Anterior lobule
Culmen	Lobule IV & V	Anterior quadrangulate lobule	Anterior lobule
Declive	Lobule IV	Posterior quadrangulate lobule	Lobule simplex
Folium	Lobule VIIA	Superior semilunar lobule	Ansiform lobule Crus I
Tuber	Lobule VIIB	Inferior semilunar & gracile lobule	Ansiform lobule Crus II
Pyramis	Lobule VIII	Biventral lobule	Paramedian lobule
Uvula	Lobule IX	Tonsilla	Dorsal paraflocculus
Nodulus	Lobule X	Accessory paraflocculus	Ventral paraflocculus
		Flocculus	Flocculus

(Altman and Bayer, 1997; Voogd and Glickstein, 1998)

Microscopic anatomy and circuitry

The cerebellar cortex is arranged into three layers: the molecular, Purkinje, and granule cell layers (Fig I-8). The molecular layer contains stellate and basket cells, dendrites of Purkinje cells, axons of granule cells, known as parallel fibers, and inferior olive neurons (climbing fibers). The Purkinje layer is a single cell layer containing the cell bodies of Purkinje neurons. The granule cell layer is made up of granule cell neurons, unipolar brush cell interneurons, Golgi cell interneurons, and axons of Purkinje cells (Altman and Bayer, 1997).

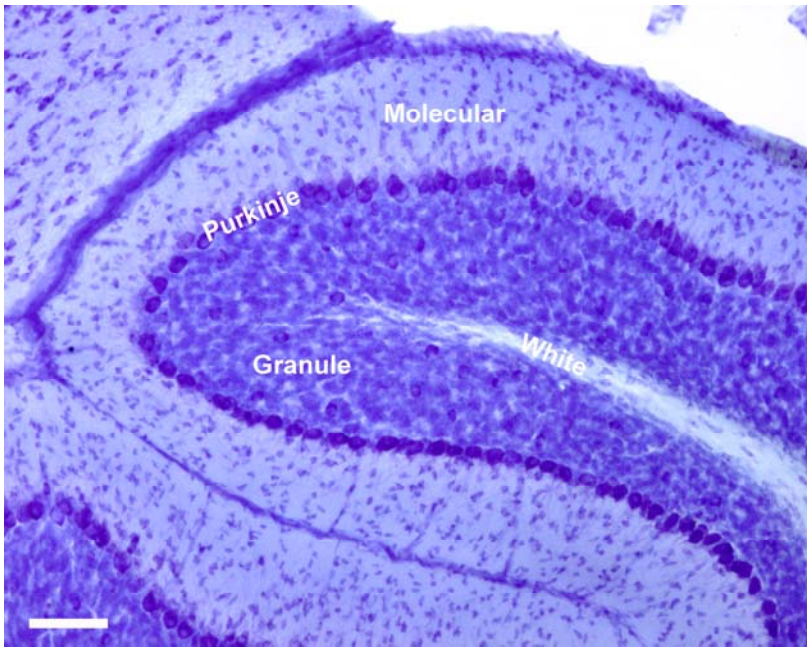

FIG. I-8. Cell layers of the adult mouse cerebellum. Sagittal view of lobule VI of a mouse cerebellar vermis showing the molecular layer, the Purkinje cell layer, the granule cell layer, and the white matter or medullary layer. The section is paraformaldehyde-fixed, frozen, and stained with 1% thionin. Scale bar is 100 µm.

Purkinje cells have a pear-shaped cell body and a fan-shaped dendritic arbor that is oriented in the sagittal plane and extends the width of the cerebellar molecular layer. Purkinje cells are one of the largest cells in the brain with a cell body approximately 50 – 80 µm in diameter (Ghez and Thach, 2000). Purkinje cells are inhibitory and are the only efferent neurons within the cerebellar cortex. They project primarily to the deep cerebellar nuclei and to the vestibular nuclei. The deep cerebellar nuclei include the fastigial, interpositus, and dentate nuclei (Marani and Voogd, 1979). The fastigial nuclei receive axons from the cerebellar vermis, while the interpositus and dentate nuclei receive axons from the paravermis and hemispheres, respectively. The fastigial and interpositus are responsible for modulation of motor activity. The dentate nuclei are involved in motor function and planning (Nolte and Sundsten, 2001). Purkinje cells in the flocculonodular lobe project to the vestibular nuclei and influence balance and equilibrium (Angaut and Brodal, 1967; De Zeeuw *et al.*, 1994). The excitation of Purkinje cells produces inhibition in the target structure (Ito, 1984c).

Granule cells are the smallest and most numerous neurons of the cerebellar cortex and are approximately 5 – 8 μm in diameter. The initial vertical portion of the granule cell axon passes through the granular and Purkinje cell layers perpendicular to the surface of the lobule. In the molecular layer, the granule cell axon bifurcates and forms two "parallel fibers" that traverse the long axis of the cerebellum. They excite Purkinje neurons that synapse with them along the length of the parallel fibers (Palkovits *et al.*, 1971). In addition to excitation of Purkinje neurons, granule cells also excite basket, stellate, and Golgi cells, which also are inhibitory neurons. The net result of granule cell excitation is the inhibition of all other neuronal cell types within the cerebellum (Altman and Bayer, 1997).

Basket cells are located in the lower one third to one half of the molecular layer. They are excited by granule cells and exert inhibitory action upon Purkinje neurons (Ito, 1984b). Stellate cells are typically located in the upper two thirds of the molecular layer. They are excited by granule cells and exert inhibitory action upon Purkinje neurons (Rakic, 1972). Golgi cells are located in the granule cell layer where they receive information from Purkinje cells (Eccles, 1967) and inhibit the activity of granule cells, resulting in a negative feedback loop. Unipolar brush cells, in contrast, receive input from mossy fibers and are excitatory to cerebellar granule cells, resulting in a positive feedback loop (Diño *et al.*, 2000).

There are two excitatory afferents associated with the cerebellum, the climbing fiber and the mossy fiber. Climbing fibers originate in the contralateral inferior olive (Courville and Faraco-Cantin, 1978; Szentagothai and Rajkovits, 1959) and enter the cerebellum through the inferior cerebellar peduncle (Campbell and Armstrong, 1983). They ascend through the medullary layer, traverse the granule cell layer, and then "climb" up and the dendritic trees of Purkinje cells. Climbing fibers carry

somatosensory, visual, and cerebral cortical information and excite Purkinje neurons (Eccles *et al.*, 1964). Mossy fibers carry sensory information from the periphery as well as information from the cerebral cortex to the granule cells. The axons of mossy fibers terminate in the glomeruli of granule cells as a large swelling called a rosette (Altman and Bayer, 1997). Fig I-9 provides an overview of the cerebellar neurons and circuitry. Table I-2 provides a summary of the postsynaptic targets and the neurotransmitters of the cerebellar neurons.

The cerebellum has three functional divisions. The spinocerebellum receives somatic sensory input from the spinal cord and controls posture and movement of the trunk and limbs. The cerebellar components of the spinocerebellum are the vermis and the intermediate hemisphere, which project to the fastigial and interposed nuclei, respectively. The cerebrocerebellum receives input from the cerebral cortex via the pontine nuclei, and controls planning of movement. The cerebellar component of the cerebrocerebellum is the lateral hemisphere that projects to the dentate nucleus. The vestibulocerebellum receives input from the vestibular labyrinth, the eye, and the ear and controls head and eye movements and maintains balance. The cerebellar component of the vestibulocerebellum is the flocculonodular lobe that projects to the vestibular nuclei (Fig I-10).

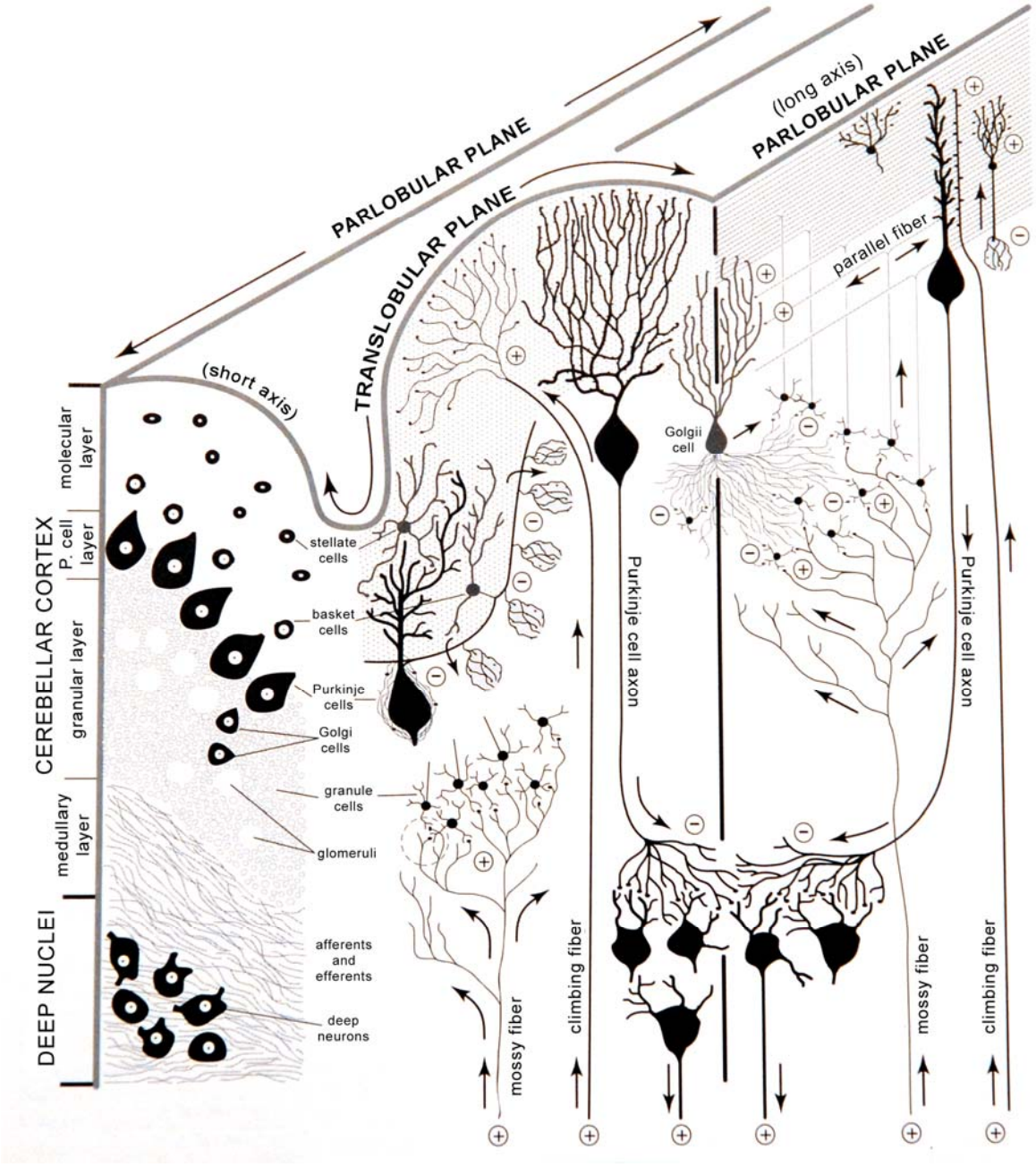

FIG. I-9. Cytological organization and functional circuitry of the cerebellum. The distribution, orientation, connections, excitatory (+) or inhibitory (-) influence, and the target of principal cerebellar neurons is depicted. P cell layer is the Purkinje cell layer. Arrows indicate stimulus direction. Modified from Altman, J. and Bayer, S. A. (1997). Development of the Cerebellar System: In Relation to its Evolution, Structure, and Functions. CRC Press, Boca Raton.

TABLE I-2

Neurons of the Cerebellum, Their Postsynaptic Targets, and the Various Neurotransmitters Involved

Presynaptic fibers	Neurotransmitter	Postsynaptic targets
Mossy fibers	Glutamate, Acetylcholine	Granule cells
	Glutamate	Unipolar brush cells
Climbing fibers	Aspartate, CRF	Purkinje cells
	CRF	Deep cerebellar nuclei
Granule cells	Glutamate	Purkinje cells
Purkinje cells	GABA	Deep cerebellar nuclei
		Golgi cells
Golgi cells	GABA, Glycine	Granule cells
Basket cells	GABA	Purkinje cells
Stellate cells	GABA, Taurine	Purkinje cells
Deep cerebellar nuclei	GABA	Inferior olivary nuclei (ION)
	Aspartate, Glutamate	Non-ION targets
Unipolar brush cells	Glutamate	Granule cells

CRF = corticotrophin releasing factor, GABA = gamma amino butyric acid
(Altman and Bayer, 1997; Diño *et al.*, 2000; Voogd and Glickstein, 1998)

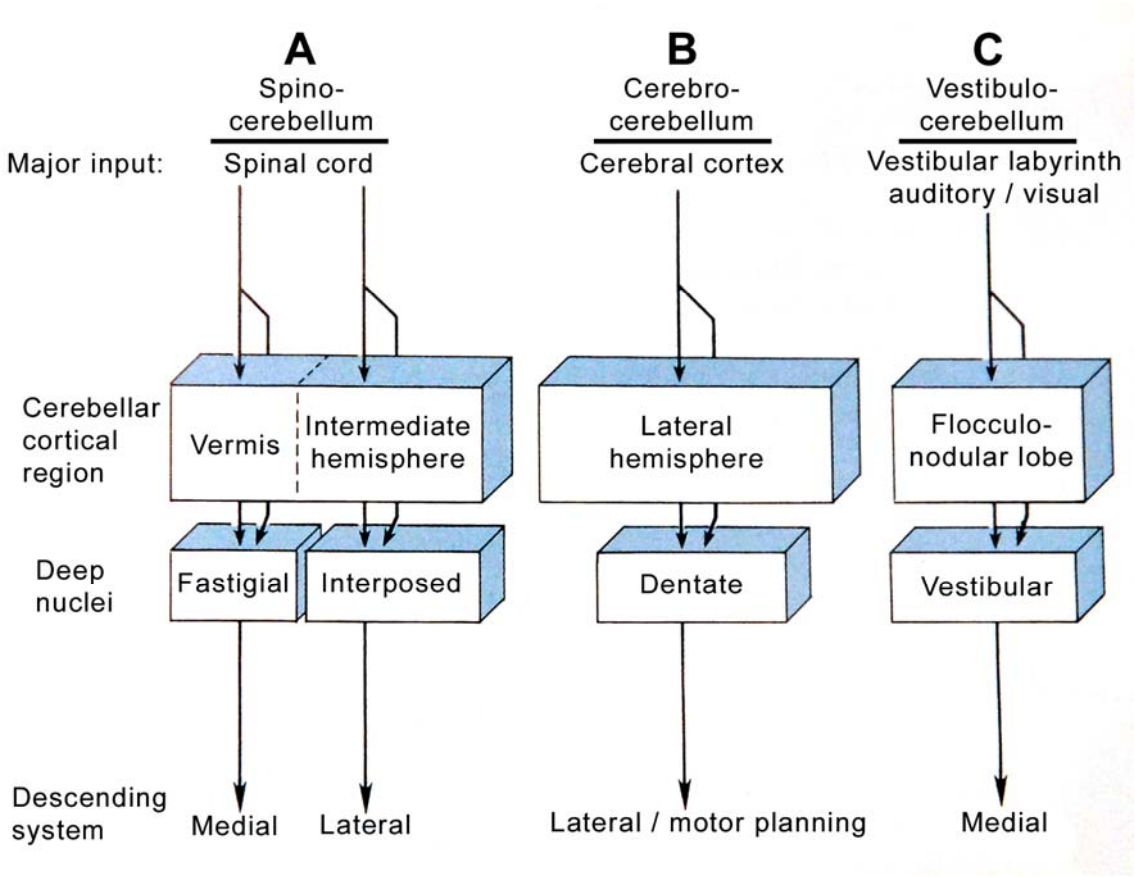

FIG. I-10. Key features of the functional divisions of the cerebellum. The functional organization of the spinocerebellum (A), the cerebrocerebellum (B), and the vestibulocerebellum (C) are represented with their major inputs and the associated cerebellar region and deep nuclei. Modified from Martin, J. H. (1996). Neuroanatomy: Text and Atlas. 2nd ed. p. 297. Appleton & Lange, Stamford.

In the cerebellum and throughout the CNS, glia cells as well as neurons are present. The ratio of glia to neurons in the CNS is approximately 1.7 in humans (Friede, 1954; Hawkins and Olszewski, 1957). Glia in the cerebellum include: 1) microglia, which are phagocytic and respond to infection and damage, 2) oligodendrocytes, which form the myelin sheath around axons, 3) astrocytes, mainly protoplasmic, which are important for structure and the maintenance of neuronal metabolic function and environment, and 4) Golgi epithelial cells, a. k. a. Bergmann (radial) glia (Kierszenbaum, 2002). Microglia and oligodendrocytes are found mainly in the medullary layer (Ito, 1984a). Astrocytes are located primarily in the granule layer. They scavenge ions and remnants of neuronal metabolism, such as K^+, glutamate (Hamberger *et al.*, 1979), and α-aminobutyric acid that may accumulate in the neuronal environment.

The most distinctive of the cerebellar glia are the Golgi epithelial cells, not to be confused with Golgi neurons. Their cell bodies lie in the upper border of the granule layer, just beneath the Purkinje cells; their long processes, known as Bergmann fibers, ascend through the molecular layer and form conical endfeet in contact with the pia (Bergmann, 1857). The ascending processes of radial glia are arranged tightly as thin walls, or palisades, in the parlobular plane, and between the palisades are broader, glia-free vertical stacks of parallel fibers from granule cells. Several radial glia palisades cut across the dendritic arbor of individual Purkinje cells that are oriented in the translobular plane (Fig I-11) (Altman and Bayer, 1997). Radial glia fibers enwrap synapses on Purkinje cell dendrites (Yamada and Watanabe, 2002).

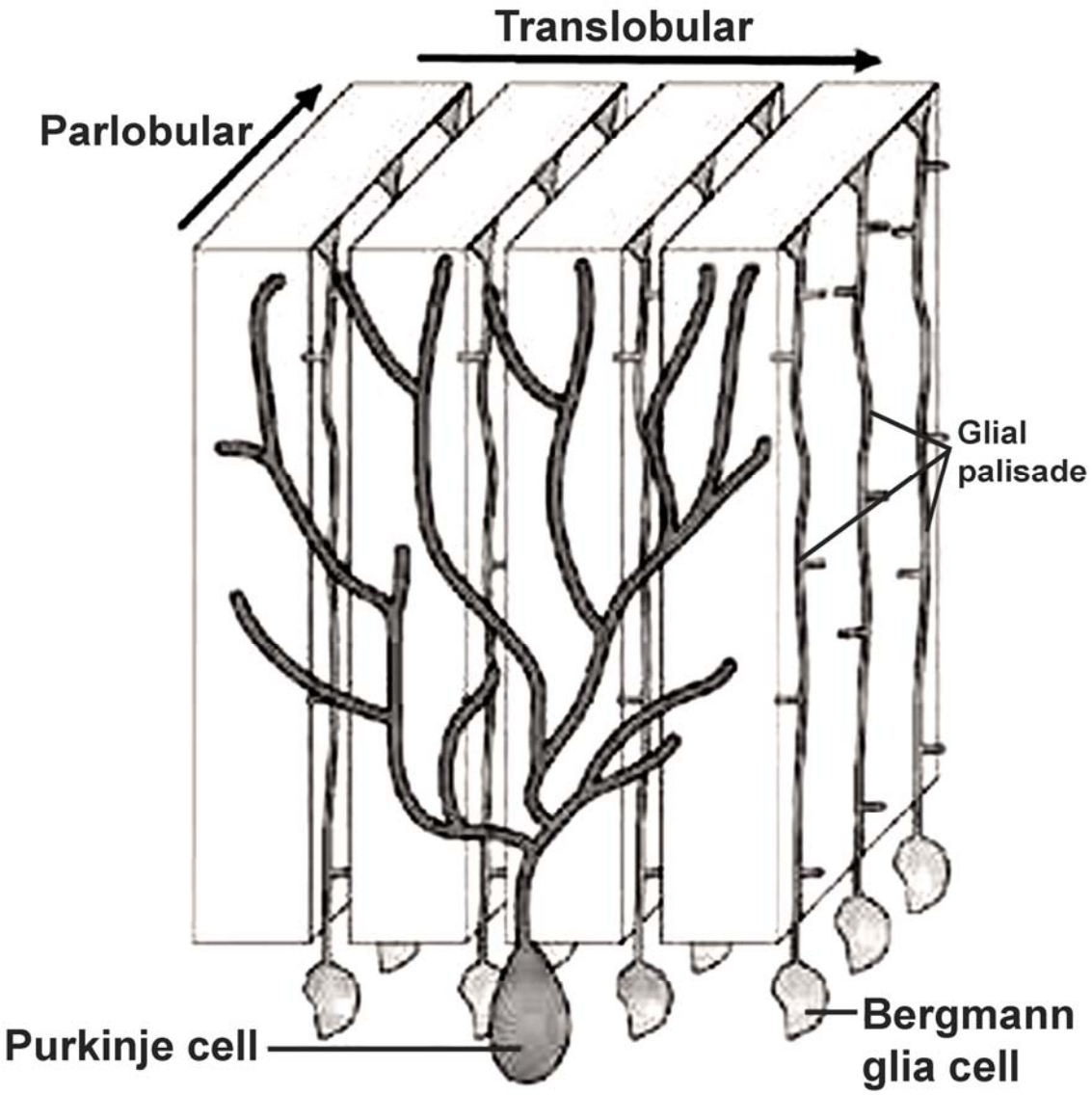

FIG. I-11. Schematic depicting the spatial relationship between Bergmann glial cells and Purkinje cells. Purkinje cell dendrites are restricted to the translobular plane of the cerebellar cortex. Radial fibers from neighboring Bergmann glial cells are aligned into palisades in the parlobular plane, and cut across and impinge upon Purkinje cell dendrites in a vertical orientation. Modified from Huang, Z. J., Di Cristo, G., and Ango, F. (2007). Development of GABA innervation in the cerebral and cerebellar cortices. *Nature Rev Neurosci* 8, 673-686, 10.1038/nrn2188.

Translobular zones in the cerebellar cortex

In addition to the gross longitudinal compartmentalization of the cerebellum defined as vermis, paravermis, and hemispheres (Chambers and Sprague, 1955a; Chambers and Sprague, 1955b), one can also observe zonal longitudinal divisions based on the distribution of climbing fibers, histochemistry, and the immunocytochemical heterogeneity of Purkinje cells. Climbing fibers from specific portions of the inferior olive climb and terminate in specific areas within the cerebellum. This results in a translobular pattern of climbing fiber projections (Buisseret-Delmas and Angaut, 1993; Buisseret-Delmas *et al.*, 1993). Longitudinally oriented light and dark stained 5'-nucleotidase bands occur in the molecular layer of the vermis. Approximately twenty translobular alternating light and dark bands on each side of the cerebellar cortex have also been observed (Marani, 1986). The significance of this banding is currently unknown. In addition to this banding, (Chan-Palay *et al.*, 1981) showed that motilin-immunoreactive Purkinje cells alternate with glutamic acid decarboxylase-immunoreactive Purkinje cells in the cerebellar cortex, and that neurons containing taurine are aligned in four active bands separated by three inactive bands. The taurine neurons included Purkinje, basket, and Golgi cells. Several other monoclonal antibody specific translobular molecules have been found (Herrup and Kuemerle, 1997). These include B1 (Ingram *et al.*, 1985), zebrin I and zebrin II (Leclerc *et al.*, 1992), tyrosine hydroxylase (Hess and Wilson, 1991) and calbindin (Wassef *et al.*, 1985). Fig I-12 shows a comparison of zebrin stripe patterns in various mammals (Sillitoe *et al.*, 2005). Although the basic structure of the cerebellum is simple and well understood, the microscopic and genetic organization and patterning within the cerebellum is far more complex. This complex organization may significantly influence the pattern of neuronal dysfunction and cell death, which occurs in disorders of the cerebellum.

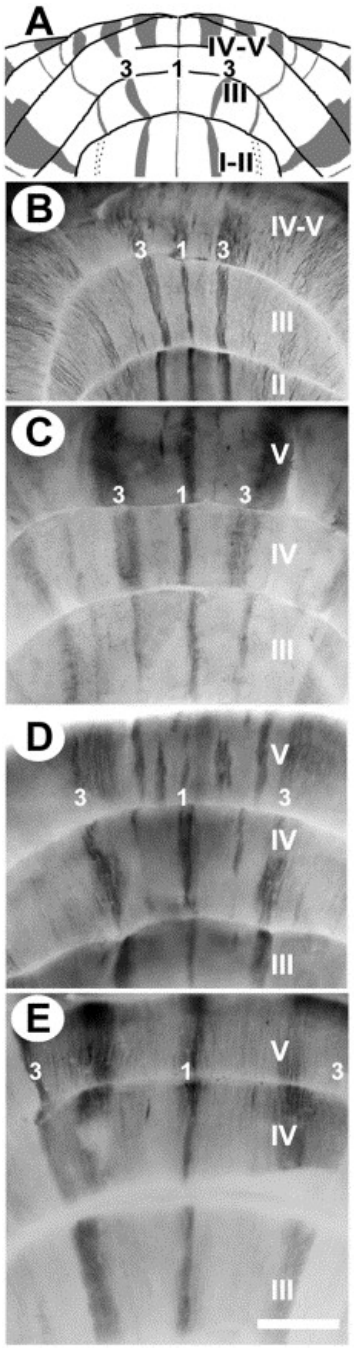

FIG. I-12. Comparison stripe patterns of the anterior lobe vermis of adult rodent cerebella. (A) Cartoon of zebrin II +/- compartmentalization in the mouse. P1+ stripe straddles the midline and strong P2 and P3+ stripes are visible on either side. A weak P4+ stripe lies at the interface of the vermis and the hemisphere. The P2+ stripe does not extend into more anterior lobules, but the P1 and P3+ stripes remain prominent. (B) Mouse anterior lobe vermis. (C) Hamster anterior lobe vermis. (D) Rat anterior lobe vermis. (E) Guinea pig anterior lobe vermis. Scale bar is 1 mm. Modified from Sillitoe, R. V., Marzban, H., Larouche, M., Zahedi, S., Affanni, J. and Hawkes, R. (2005). Conservation of the architecture of the anterior lobe vermis of the cerebellum across mammalian species. Prog Brain Res 148, 283-297.

Motor learning

Motor learning by the cerebellum is a relatively new concept. Studies indicate that the cerebellum is associated with trial-and-error practice-type motor adaptation and learning. David Marr (Marr, 1969) and James Albus (Albus, 1971) proposed that climbing fiber inputs to Purkinje neurons modify the response to mossy fibers, and that this modification could occur over a prolonged time. Their theory was that during repetitive movement, climbing fibers provide error signals that depress parallel fibers and allow "correct" movements to emerge. This has been termed, long-term depression (LTD) (Ito, 1986; Ito *et al.*, 1982). In LTD, climbing fibers weaken parallel fiber-Purkinje cell synapses (Ekerot and Kano, 1985; Ekerot and Oscarsson, 1981; Ito, 1986). Cerebellar damage often impairs this type of learning. In the vestibule-ocular reflex, a coordinated response maintains the eyes on a fixed target when the head is rotated. When humans wore prism glasses that reversed the visual field, the reflex was flawed. After wearing the glasses for several days, the reflex becomes reversed from "normal" (Ito, 1982). Vestibulocerebellar lesions block this adaptation. In addition, control of limb movements can be altered by wearing prism glasses. When people throw darts at a target with glasses that reverse the field of vision, the initial throw is off-target. After ten to thirty throws, the direction-of-throw becomes altered such that the darts then land on-target (Martin *et al.*, 1996a; Martin *et al.*, 1996b). Individuals with damaged cerebellar cortex or inferior olive are unable to adapt in this situation. Finally, studies also indicate that the cerebellum may be involved in associative learning. McCormick and Thompson (1984) and Yeo (1984) showed that cerebellar lesions disrupted the acquisition and retention of classically conditioned eyeblink reflex in rabbits.

Disorders of the cerebellum

Cerebellar disorders have three basic and distinct signs: 1) hypotonia, abnormally low muscle tone, 2) ataxia, abnormal execution of voluntary movements and lack of coordination, and 3) intention tremor (Ghez and Thach, 2000). Intention tremor is most obvious at the end of the movement when the antagonist muscle is engaged. Studies

show that newborn rats with decreased numbers of cells in the external germinal cell layer of the cerebellum have severe locomotor abilities that appear between postnatal day 22 and 29 and persist throughout life (Altman *et al.*, 1971). In addition, these animals were unable to sit and maintain balance without forelimb support (Altman *et al.*, 1971). These disabilities made it difficult for the animals to use their paws for picking up food items and grooming themselves. Finally, skills such as learning to descend from a vertical rod head-down and learning to climb a rod to an overhead platform to escape danger were not mastered by the rats with extensive loss of external germinal layer cells (Altman *et al.*, 1971).

CENTRAL NERVOUS SYSTEM DEVELOPMENT

General overview

The embryonic period of mammalian development is particularly important because it is during this course that most major malformations occur. The developing embryo is highly sensitive to insult during early development (Muller and O'Rahilly, 2004). The human prenatal period is divided into the embryonic period, which is eight weeks post-fertilization, and the fetal period, eight weeks post-fertilization to birth (Fig I-13). Specific morphological stages of brain development have been identified during the embryonic phase (Table I-3).

Vertebrate embryos have three principal (germ) cell layers: ectoderm (outer), mesoderm (middle), and endoderm (inner). A specialized region of the ectoderm, the neural plate, is the source of the neurons and glia of the nervous system and lies along the midline of the embryo. Marginal cells of the neural plate proliferate and alter their shape to form a neural groove that deepens. The edges eventually shift dorsally and medially to appose each other, and then close to form a hollow neural tube. The caudal portion of the neural tube forms the spinal cord; the rostral portion forms the brain. Three layers exist around the neural tube: the innermost ependymal layer, which is also called neuroepithelium that gives rise to immature nerve cells; the middle or mantle layer, which forms specialized glia that serve as a scaffold for migrating neurons; and

the outermost marginal layer, which primarily contains the axonal processes of developing neurons. In the mature spinal cord these three embryonic layers of the wall of the neural tube can still be identified. The ependymal layer lines the ventricular system, the mantle layer becomes the gray matter, and the marginal layer becomes the white matter (Jessell and Sanes, 2000; Martin, 1996; Sadler, 2006). In the mature brain, the ependymal layer still lines the ventricular system, but the other two layers are no longer clearly recognizable due to the complex growth and remodeling that takes place as the brain matures.

From rostral to caudal, the cranial end of the neural tube develops into five brain regions: the telencephalon that becomes the cerebral hemispheres, the diencephalon that becomes the epithalamus, thalamus and hypothalamus, the mesencephalon that becomes the midbrain, the metencephalon that becomes the pons and cerebellum, and the myelencephalon that becomes the medulla. The large cavity within the developing neural tube forms the ventricular system that is filled with cerebrospinal fluid produced by the choroid plexus. Two lateral ventricles form in the region of the telencephalon; they are connected by the interventricular foramina to the third ventricle that forms in the diencephalon. The fourth ventricle develops in the region of the metencephalon and myelencephalon; it is connected to the third ventricle by the cerebral aquaduct that is located in the region of the mesencephalon (Jessell and Sanes, 2000; Martin, 1996; Sadler, 2006).

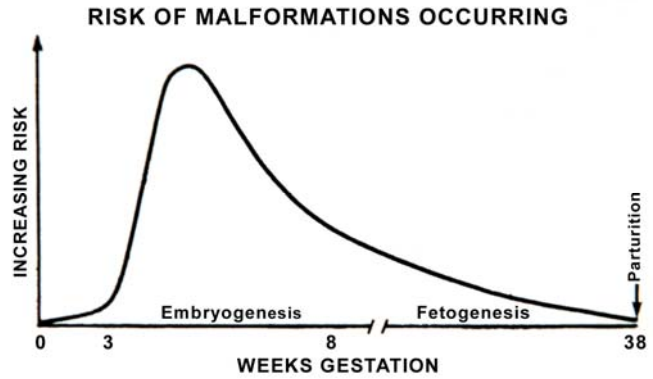

FIG. I-13. Gestational timeline of human developmental malformation potential. The risk of malformations is highest between gestational weeks 3 and 8. Gestational days 0, 3, 8 and 38 are identified. / / indicates a break in the progression of time. Modified from Sadler, T. W. (2006). Langman's Medical Embryology. 10th ed. Lippincott, Williams & Wilkins, Philadelphia.

TABLE I-3

Initial Appearance of Various Features of the Human Nervous System

Features	Stage	Weeks
Neural folds and groove	8	
Mesencephalic flexure; primary neuromeres; rhombencephalon, mesencephalon, prosencephalon	9	
Neural tube begins; telencephalon, medium and diencephalon	10	4
Rostral neuropore closes	11	
Caudal neuropore closes; secondary neurulation begins	12	4.5
Closed neural tube; cerebellar primordium; isthmus	13	
Pontine flexure; medial ventricular eminence; future cerebral hemispheres; all 16 neuromeres present	14	
Myelencephalon, metencephalon; hippocampal thickening; lateral ventricular eminence	15	5
Epiphysial evagination	15,16	
Thalamus; all cranial nerves present	16	
Internal and external cerebellar swellings; neurophypophysial evagination; synapses in primordial plexiform layer	17	6
Future corpus striatum; defined interventricular foramina; choroids fissure; dentate nucleus; inferior cerebellar peduncles	18	
Olfactory bulb; insula; choroid plexus of fourth ventricle	19	
Choroid plexus of lateral ventricles	20	7
Cortical plate; anterior and inferior horns of lateral ventricle; circulus arteriosus complete	21	
Internal and external capsules; claustrum	22	
Caudate nucleus and putamen; anterior commissure begins; external germinal layer in cerebellum	23	8

The weeks given are post-fertilizational.
Modified from Muller, F. and O'Rahilly, R. (2004). The Human Nervous System (G. Paxinos and J. K. Mai, Eds.), 2nd ed., p. 23. Elsevier Academic Press, San Diego.

Some developing areas of the embryo have inductive influence on other developing areas. These include the prechordal plate, the primitive streak, and the notochord process. The prechordal plate is in close contact with the neural groove, or future forebrain and provides signals to suppress the medial portion of the unseparated optic field, which induces two separate eye fields (retinas) to form. The primitive streak is a temporary caudal axial structure that exists during the process of gastrulation and lacks a basement membrane, allowing the emigration of surface epiblast cells to form the trilaminar embryo. The epiblast cells that migrate through the primitive streak gives rise to all three germ layers and most importantly to the paraxial mesoderm, notochord process, and endoderm. The notochord process becomes the notochord that, along with the adjacent paraxial mesoderm, induces formation of the floor plate in the neural plate by means of diffusible factors. The floor plate regulates differentiation of motor neurons and axonal growth in the developing neural tube (Muller and O'Rahilly, 2004).

Inductive influence occurs through gene expression. Sonic hedgehog (*SHH*) is expressed in the prechordal plate and is involved in signaling the development of the hypothalamus and diencephalons in the cranial region of the neural tube. *FOXG1* regulates the development of the telencephalon. *EN1*, *EN2* and *WNT1* are involved in patterning of the mesencephalon and metencephalon in humans and mice (Song *et al.*, 1996). *EN1* regulates development of the tectum and the cerebellum; *EN2* is involved in cerebellar development only. *WNT1* interacts with *EN1* and *EN2* to regulate the development of the cerebellum from as early as the neural plate stage (Fig I-14). *PAX3* is expressed in the neural groove and neural tube and later in the mesencephalon, rhombencephalon, and spinal cord once they are formed. *PAX5* is expressed in the mes-rhombencephalic boundary and the spinal cord. *PAX6* is expressed in the optic neuromeres of the neural tube and in the rhombencephalon and spinal cord (Gerard *et al.*, 1995). In addition, *HOX* genes (Fig I-15) are expressed in human rhombomeres and pharyngeal arches (Vieille-Grosjean *et al.*, 1997). The expression of many *HOX* genes determine position along the anterior-posterior axis of the hindbrain and identifies the rhombomeres and their derivatives (Sadler, 2006).

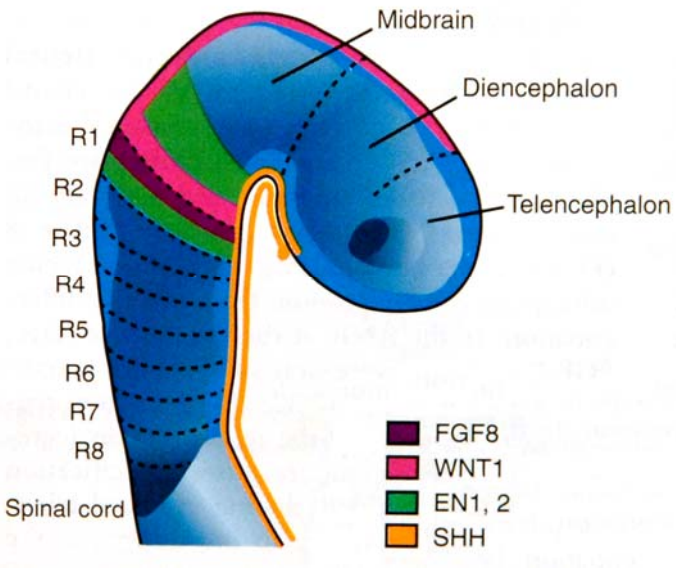

FIG. I-14. Patterns of gene expression for *WNT1*, *EN1*, *EN2*, and *SHH*, and for the signaling molecule, fibroblast growth factor 8 (FGF8). FGF8 signals the expression of these genes. The genes are involved in development of the mesencephalon and metencephalon. Modified from Sadler, T. W. (2006). Langman's Medical Embryology. 10th ed. p. 306. Lippincott, Williams & Wilkins, Philadelphia.

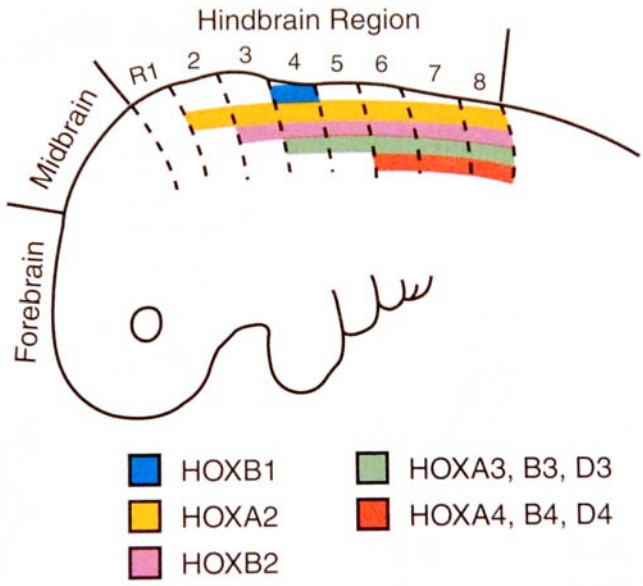

FIG. I-15. Patterns of *HOX* gene expression in the hindbrain. *HOX* genes are expressed in overlapping patterns ending at specific rhombomere boundaries. These genes confer positional value along the anterior-posterior axis of the hindbrain. They determine the identity of the rhombomeres and their derivatives. Modified from Sadler, T. W. (2006). Langman's Medical Embryology. 10th ed. Lippincott, Williams & Wilkins, Philadelphia.

The above listed genes represent only a small portion of the numerous genes that must be activated and/or inactivated at the appropriate time and sequence in the developmental process. The exact regulation and specific timing of gene expression is of utmost importance to proper embryonic development. Any event, such as a chemical insult, that interferes with this time-course could have negative consequences for the embryo or fetus.

Hippocampal development

As the cerebral cortex develops, it encircles the diencephalon, that remains basically spherical, and takes on the shape of the letter C. Structures that take on the C-shape have both a dorsal and a ventral component within the brain. These structures include the lateral ventricles, caudate nucleus, hippocampal formation, cingulated and parahippocampal gyri, and the fornix (Jessell and Sanes, 2000; Martin, 1996; Sadler, 2006).

The following summary of the development of the hippocampus is based on what is known for the human (Insausti and Amaral, 2004). Early in development, the hippocampus is located dorsal to the corpus callosum, but later is "dragged" into the temporal lobe. The hippocampal formation begins to enfold into the temporal lobe. As the hippocampal sulcus forms, the dentate gyrus and the subiculum become apposed. The pial surface of these structures fuses (Fig I-16). By nine weeks of gestation, the hippocampal area is located in the medial aspect of the developing cerebral hemisphere (Arnold and Trojanowski, 1996). The hippocampal fissure appears at ten weeks (Humphrey, 1967). The subiculum, the hippocampal fields, and the three layers of the dentate gyrus become apparent between fifteen and nineteen weeks of gestation. At twenty-five weeks, the hippocampal fissure is more pronounced and the fields have expanded. The dentate gyrus is greatly expanded, but many of the cells have immature features. At thirty-four weeks, the hippocampal formation has a basic mature appearance. The hippocampus is decreased in size slightly from earlier time points due to apoptosis and growth of neuronal processes. No significant morphological changes

occur into adulthood other than progressive myelination to completion. In contrast, the development of the entorhinal cortex, the primary hippocampal input, continues to develop until the end of the second postnatal year (Grateron *et al.*, 1996).

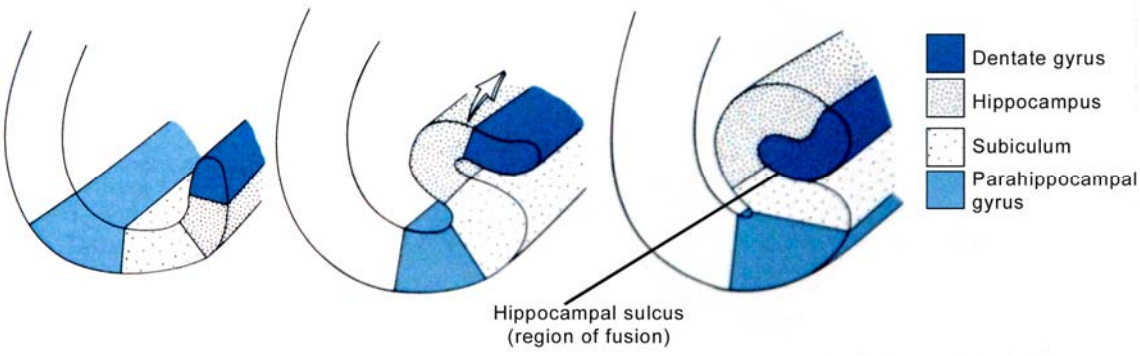

FIG. I-16. Schematic of the hippocampal formation during development. The hippocampal sulcus forms and the dentate gyrus and subiculum become apposed and fuse. The apparatus resembles a "jelly roll". The arrow indicates the direction of movement. Modified from Martin, J. H. (1996). Neuroanatomy: Text and Atlas. 2nd ed. p. 469. Appleton & Lange, Stamford.

In mice, neural progenitor cells that become pyramidal cells of the CA regions of the hippocampus are born on embryonic (E) day 10.5 (Angevine, 1965). By E14.5, most of the progenitor cells have migrated to their final positions, and most of these will become pyramidal cells between E15 and E19 (Supèr and Soriano, 1994). The CA regions continue to develop and mature until the third postnatal week (Grove and Tole, 1999; Zimmer, 1978). The afferent fibers from the septum arrive at the CA regions at E17.5, and the afferent fibers from the entorhinal cortex reach the dentate gyrus at E. 19.5 (Supèr and Soriano, 1994).

The granule cells of the dentate gyrus exhibit a different pattern of development compared to the pyramidal cells of the CA regions. In mice, the birth of the granule cells occurs mainly after birth from postnatal (P) day 20 to two weeks (Altman and Bayer, 1990). The first 15% of the granule cells are generated at the same time as the pyramidal cells, E10.5. The next 70% are generated during the first two postnatal weeks, and the last 15% appear after P16 (Bayer, 1980). The mossy fiber projections from the granule

cells to the CA3 pyramidal cells grow, mature, and make their final connections between P3 and P21 (Amaral and Dent, 1981; Gaarskjaer, 1986).

Cerebellar development

The cerebellum develops from neuroblasts located from a specific region in the alar plate of the dorsolateral metencephalon called the rhombic lip. At first, the rhombic lips are widely separated, but eventually fuse long the midline. The midline region becomes the vermis, and the two lateral regions become the hemispheres. Fissures form on the cerebellar surface and are oriented from medial to lateral. The fissures divide the cerebellum into three lobes: anterior, posterior, and flocculonodular (Altman and Bayer, 1997; Martin, 1996; Sadler, 2006).

A summary of the development of the cerebellum is shown in Fig I-17. The rhombencephalon surrounds the fourth ventricle and is the source of neurons of the hindbrain. It can be divided into the myelencephalon (primordial medulla) and the metencephalon, (primordial cerebellum and pons) (Patten and Carlson, 1974), which both contain an alar (dorsal) and basal (ventral) plate. In rats and mice the cerebellum is derived from the alar plate just after neural tube closure at E8.5 (McMahon and Bradley, 1990; Herrup and Kuemerle, 1997). Between E13 and E16 in rats, the medullary velum invaginates into the 4^{th} ventricle; there is an increase in pontine flexure, and an increase in size and backward growth of the tectal primordium, which results in the permanent location placement of the cerebellum. By E16, differentiating zones have begun to develop within the primordial cerebellum. Between E17 and E22, the external germinal cell layer (ECL) is dispersed over the surface of the cerebellum, and the Purkinje cells have migrated to a location just below the ECL (Altman and Bayer, 1997).

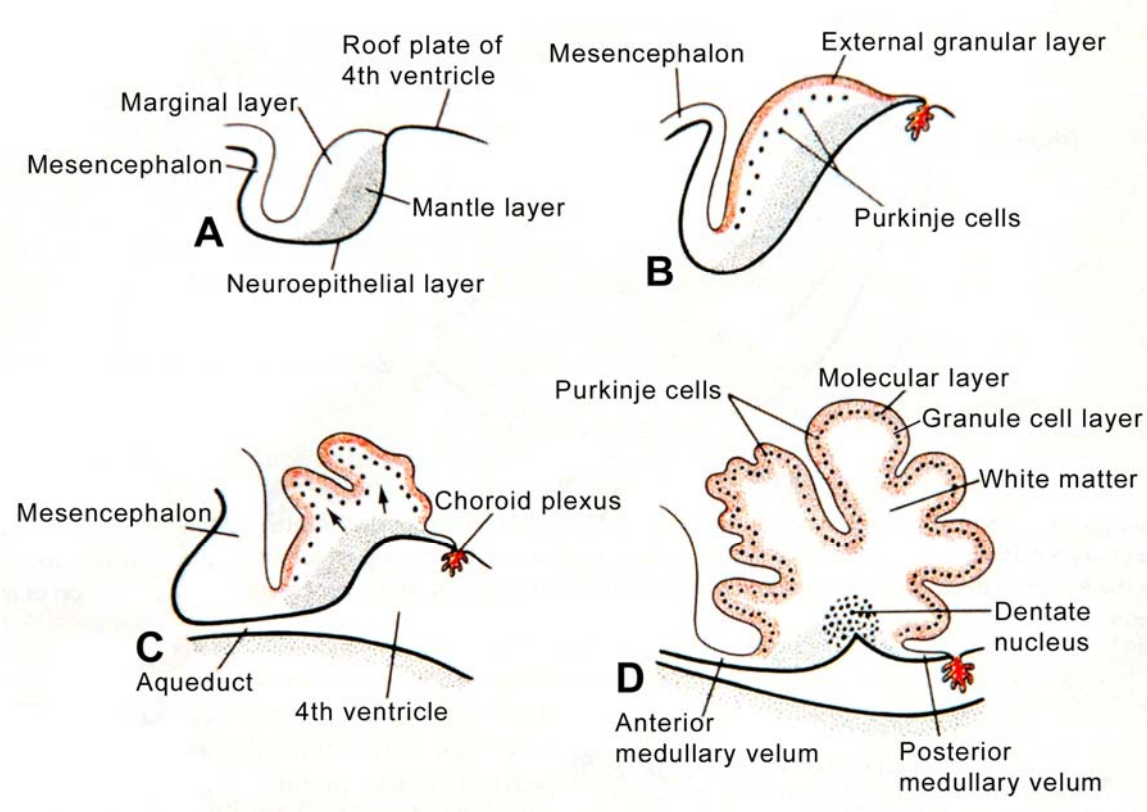

FIG. I-17. The development of the cerebellum in the rat. (A) is embryonic day (E) 13 to E15 and shows the invagination of the medullary velum into the fourth ventricle. (B) is E16 to E20 showing the formation of the external granular and Purkinje cell layer. (C) is E22 at the beginning of lobulation and granule cell migration. (D) is the mature cerebellum with full lobulation and complete migration of cerebellar neurons to their final locations. Modified from Sadler, T. W. (2006). Langman's Medical Embryology. 10th ed. p. 298. Lippincott Williams & Wilkins, Philadelphia.

The cells in the cerebellum originate from two separate germinal zones. Purkinje cell, Golgi cells, and some glial cells emerge from the ventricular cell matrix, which covers the ventricular surface of the cerebellar plates. Granule, basket, stellate, and some glial cells are derived from the external granular layer, near the outer surface of the cerebellar plates. The cells migrate from the ventricular matrix and the external granular layer in opposite directions to their final destination (Fig I-18).

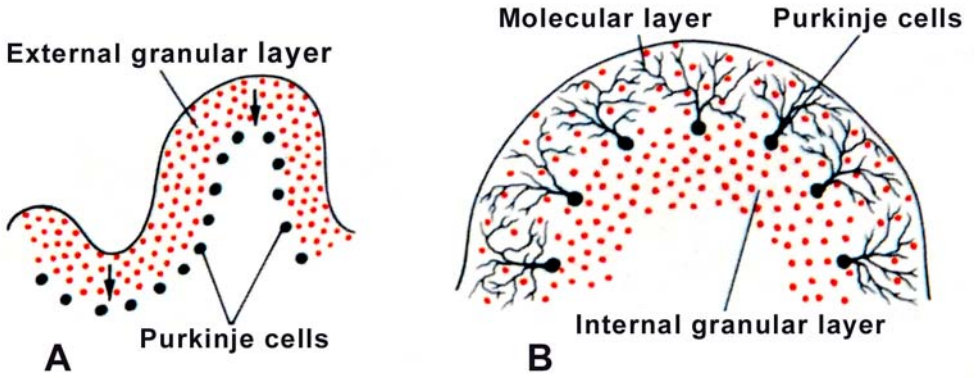

FIG. I-18. Development of the cerebellar cortex. (A) shows a developing cerebellar cortex with the external granular layer on the pial surface of the cerebellum and the immature Purkinje cells layered below. In (B), the mature cerebellum has a molecular layer, a single Purkinje cell layer, and an internal granule cell layer. Modified from Sadler, T. W. (2006). Langman's Medical Embryology. 10th ed. p. 298. Lippincott Williams & Wilkins, Philadelphia.

Radial glial cells are some of the earliest cell types to appear during embryonic development. They have been linked to direct neuronal migration and laminar patterning of the cerebral and cerebellar cortex. During the perinatal period, radial glial cells are replaced by multipolar astrocytes and oligodendrocytes; however, in the cerebellum (Bergmann glia) and retina (Muller cells), they remain as specialized cells (Choi and Kim, 1985; Choi and Lapham, 1980; Stagaard *et al.*, 1991). Bergmann radial glia are unipolar protoplasmic astrocytes that direct neuronal migration during pre- and postnatal periods (Rakic, 1971; Yamada and Watanabe, 2002). Starting at embryonic day 17 (E17), in mice, they migrate to their future location in the cerebellum and direct the migration of Purkinje cells (Altman and Bayer, 1997; Yuasa, 1996). Bergmann glia proliferate once they are in the cerebellum from postnatal day (P) 1 to P 21 in mice (Reichenbach *et al.*, 1995; Shiga *et al.*, 1983). Postnatally, they associate with the inward migrating postmitotic granule cells moving from the external granular layer to the internal granular layer (Rakic, 1971).

Purkinje cells mature in three stages. Initially, they are distributed in multiple layers and are small and fusiform shaped. They then become multipolar and form a single row of cells. Finally, extra processes withdraw, and the dendrites are rearranged in a plane perpendicular to the long axis of the lobule. In the mouse, Purkinje cells stop

dividing at E12 (Miale and Sidman, 1961). At E21, the Purkinje cells are still in several layers (Uzman, 1960); they form a monolayer by P10 (Miale and Sidman, 1961). The dendritic trees develops during the second and third postnatal weeks (Weiss and Pysh, 1978).

In the mouse, matrix cells move from the neuroepithelial surface, across the rhombic lip to the outer pial surface of the developing cerebellum. A layer of proliferating precursor granule cells spreads across the external surface as more precursors migrate across the rhombic lip. The entire surface of the cerebellum is covered by the granule cells between E13 and E16 (Hatten *et al.*, 1982). The cells in the external granule layer migrate inwardly starting at birth. They may migrate a short distance and become cells of the molecular layer, or they may migrate further and become granule cells. Most of the granule cell layer, 81 to 92% is formed after P7, with 50% being formed after P10 (Altman, 1972a; Altman, 1972c). Parallel fiber synapses on Purkinje cells dendrites that are formed during the third postnatal week (Altman, 1972b).

Precise neuronal function requires highly ordered cell proliferation, differentiation, migration and synaptic specificity. Development of the central nervous system depends on both intrinsic and extrinsic factors that orchestrate neuronal migration to form laminae (Hatten, 1999; Rakic, 1971), the compartments in which neurons become differentiated and specialized. During cortical development, postmitotic neuronal precursors use radial glia as a pathway for migration to final adult locations (laminae) (Kriegstein and Noctor, 2004). This applies to cortical regions of the cerebrum as well as the cerebellum. Thus, the molecular control of radial glial migration and differentiation is crucial for the formation of normal cortical architecture and synaptic circuitry.

MITOCHONDRIA

In the second half of the nineteenth century, Rudolf Albrecht von Köllicker, a Swiss anatomist and physiologist, noticed characteristically arranged granules in the sarcoplasm. In 1890, Altmann recognized the ubiquitous nature of “bioblasts” (Altmann,

1890), and in 1989, Carl Benda named the organelle the "mitochondrion", meaning threadlike granules (Benda, 1989). The ultra-structure of mitochondria was described by Palade (1952), and mitochondrial DNA was defined by Nass and Nass (1963). In 1912, Kingsbury suggested that mitochondria serve "as a structural expression of reducing substances concerned in cellular respiration (Luft, 1997)." In 1978, the Nobel Prize in Chemistry was awarded to Peter Mitchell for his contribution to the understanding of biological energy transfer through the formulation of the chemiosmotic theory (Mitchell, 1993). The primary role of mitochondria has been determined to be electron transport, oxidation processes, oxidative phosphorylation and respiratory control, thus, production of energy for the cell.

Mitochondria are thought to have originated from free-living proteobacteria that became symbiotic with precursors to eukaryotic cells (Margulis, 1971). This relationship and the evolution of the oxidative phosphorylation system allowed the efficient metabolism of food, using oxygen, to produce energy. Mitochondria contain two membranes: a smooth outer membrane and a highly folded inner membrane. The outer membrane is selectively permeable to ions and small molecules (up to 10 kD) that can diffuse across the membrane through porin protein channels. In addition, the outer membrane contains voltage-dependent anionic channels (VDAC) that allow the import and export of specific ions, such as Ca^{2+} (Voet and Voet, 2004). The inner membrane is compartmentalized into cristae that increase the surface area of the membrane (Perkins *et al.*, 2001). The cristae are not simple folds but are a complex array of invaginations and tubules of the inner membrane that divide and fuse continuously depending on the amount of mitochondrial activity (Mannella, 2006; Renken *et al.*, 2002). The inner membrane is the site of the electron transport chain which are the proteins that mediate electron transport, oxidative phosphorylation and ATP production (Duchen, 1999). The inner membrane is permeable only to O_2, CO_2, and H_2O, but contains transport proteins that control the movement of molecules such as ATP, ADP, pyruvate, Ca^{2+}, and phosphate across the membrane (Voet and Voet, 2004). This low permeability and tight control permits the generation of an ionic gradient across the inner membrane and

compartmentalization of metabolic functions. The matrix, bounded by the inner membrane, contains soluble enzymes of oxidative metabolism (tricarboxylic acid cycle (TCA) enzymes). The matrix also contains substrates, nucleotide cofactors, inorganic ions, and mitochondrial genetic machinery (Nicholls and Ferguson, 2002). Fig I-19 shows a compilation of the functional components of the mitochondrion.

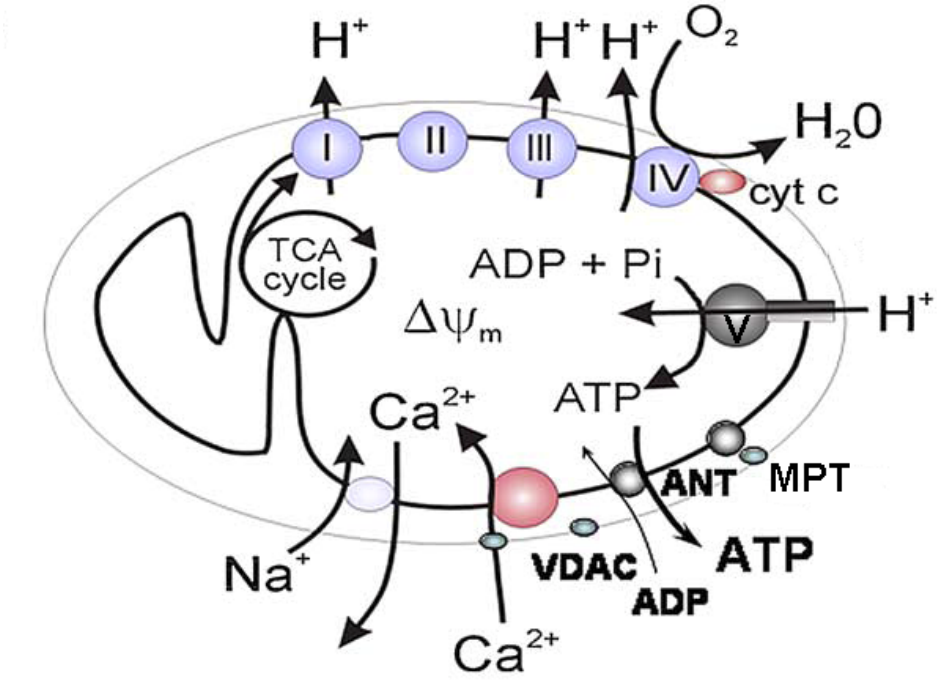

FIG. I-19. The outer membrane is shown containing the VDAC for import and export of Ca^{2+}. The inner membrane is shown containing Complexes I - V of the electron transport chain, Complex V for oxidative phosphorylation, the mitochondrial permeability transition pore (MPT), and the adenine nucleotide translocase (ANT) for exchange of ADP and ATP. H+ ions are shown being pumped across the inner mitochondrial membrane by Complexes I, III, IV, and V. The matrix is shown containing the sites of ADP phosphorylation and the TCA cycle. It is in the matrix where the mitochondrial membrane potential is created. Modified from Das, J. (2006). The role of mitochondrial respiration in physiological and evolutionary adaptation. *BioEssays* 28, 373.

The TCA cycle and electron transport chain are involved in the break down of organic molecules for the production of energy as ATP. Energy sources such as glucose are initially metabolized in the cytoplasm. The products are imported into the matrix of the mitochondria where acetyl-CoA transfers its acetyl group to oxaloacetate to form citrate. The citrate loses two carboxyl groups as CO_2. The energy from these reactions is

transferred in NADH to the process of oxidative phosphorylation to drive ATP synthesis (Voet and Voet, 2004).

Oxidative phosphorylation occurs in the electron transport chain (Fig I-20). This chain couples a chemical reaction between the electron donor, NADH, and the electron acceptor, O_2, to the transfer of H^+ ions across the membrane, to the inner membrane space, through a set of mediating biochemical reactions. These H^+ ions produce ATP as they move back across the membrane (Voet and Voet, 2004). There are four membrane-spanning enzyme systems in the inner membrane. Three of them are proton pumps. In Complex I (NADH dehydrogenase), NADH is oxidized to NAD^+ and two electrons are released and passed on to coenzyme Q (Q, ubiquinone). Complex I contains flavoproteins and non-heme-iron proteins. Coenzyme Q can accept one electron to form a semiquinone (free radical) or two to form a fully reduced ubiquinol form that diffuses across the membrane. Complex I moves four protons (H^+) across the membrane from the matrix to the inner membrane space. Complex II (succinate dehydrogenase) is not a proton pump, but removes electrons from succinate and transfers them to Q (Das, 2006). The succinate is produced in the Krebs cycle and through β-oxidation of fatty acids. In Complex III (ubiquinol cytochrome C reductase), two electrons are removed from Q and transferred to two molecules of cytochrome C. Complex III contains an iron-sulphur protein plus cytochromes b and c_1. Cytochromes are heme proteins which accept electrons by allowing Fe(III) at the center of the heme ring to be reduced to Fe^{2+}. Two more protons are transferred across the membrane, and quinone is reduced to quinol. In Complex IV (cytochrome C oxidase), four electrons are removed from four molecules of cytochrome C and transferred to oxygen (O_2) to produce two molecules of water. Complex IV contains cytochrome a, cytochrome a_3, and copper ions. At the same time, four more protons are moved across the membrane to the inner membrane space. Complexes, I, II and III all contain non-heme iron; complex IV contains copper; Complex III, IV and cytochrome C contain heme (Duchen, 2004).

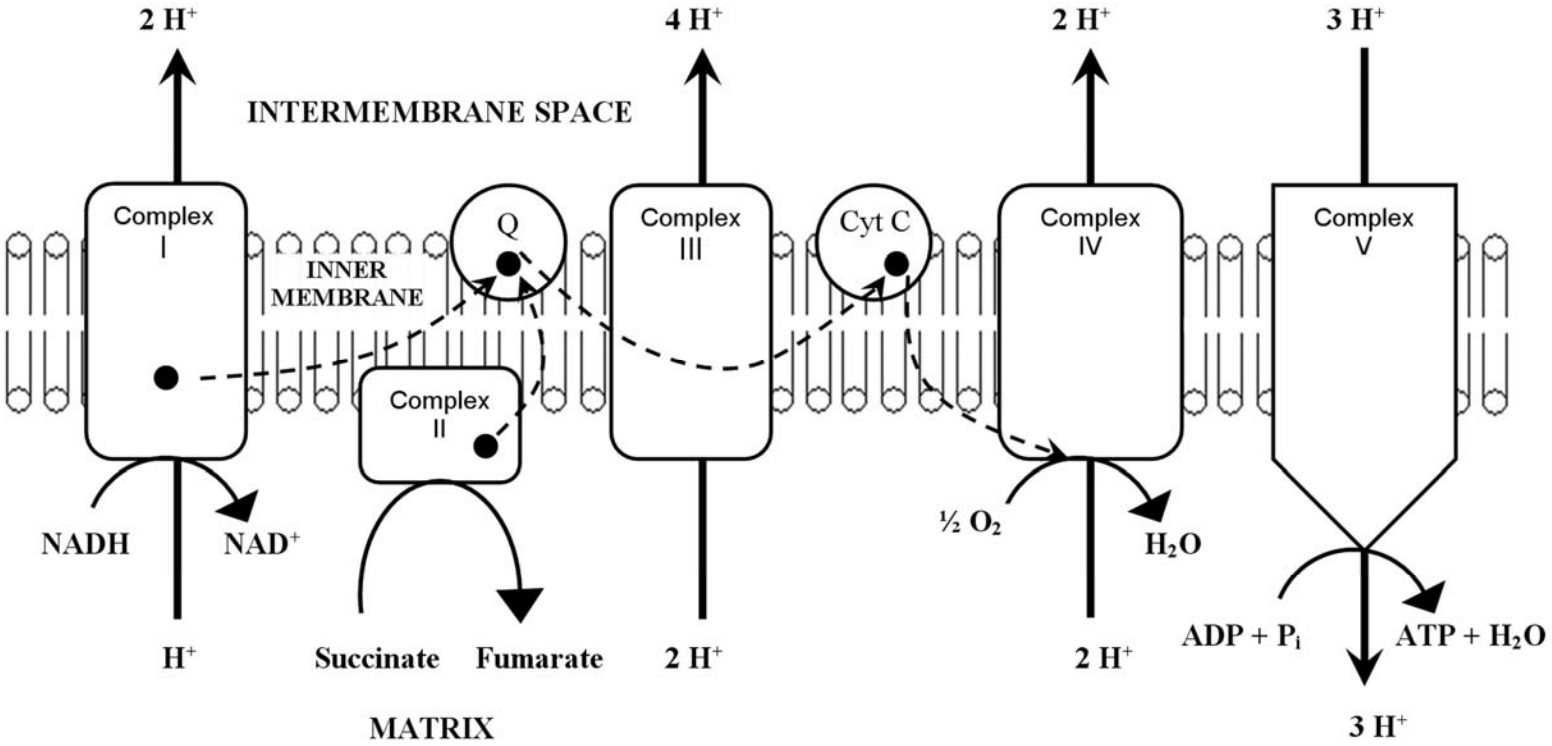

FIG. I-20. Diagram of the mitochondrial electron transport chain. Electrons are transferred between Complexes I and III by the membrane-soluble ubiquinone (Q) and between Complexes III and IV by the peripheral membrane protein cytochrome C (Cyt C). Complex II transfers electrons from succinate to Q. The path of electrons (solid black circles) is shown with dotted arrows. Complexes I, III and IV use the energy from electron transfer to pump protons into the intermembrane space, creating an electrochemical gradient, or mitochondrial membrane potential. Complex V uses the energy stored in the electrochemical gradient to phosphorylate ADP to form ATP.

The protons pumped into the intermembrane space establish an electrochemical proton gradient (proton-motive force). This gradient has two components: 1) a pH gradient due to the acidic property of the protons and 2) an ionic gradient created by the charge of the protons. The ionic gradient is called the mitochondrial membrane potential and is usually 150 – 180 mV negative relative to the cytosol (Duchen, 2004). ATP synthase uses the proton gradient to make ATP by oxidative phosphorylation. ATP synthase forms a channel that returns protons back to the mitochondrial matrix (inward) from the inner membrane space. Their movement depolarizes the mitochondrial membrane potential. During the inward proton movement, ATP synthase phosphorylates ADP, and ATP is released (Stock *et al.*, 1999). Incoming ADP and outgoing ATP are exchanged across the inner mitochondrial membrane by adenine nucleotide translocase (ANT), making ATP available to the rest of the cell.

Although the inner membrane is quite impermeable, because of the need to maintain the electrochemical gradient, there is a proton leak. As protons are leaked, the energy created by electron transport appears as heat rather than ATP. This leak is a major contributor to the body's heat production (Hittelman *et al.*, 1969).

The rate at which the protein complexes function is correlated with the proton gradient. Respiration will run faster when the membrane is depolarized because the energy required to move protons is reduced. It will run slower when the membrane potential increases (hyperpolarizes) (Duchen, 2004). For example, carbonyl cyanide *m*-chlorophenylhydrazone (CCCP) uncouples the process of oxidative phosphorylation and allows the membrane potential to dissipate. This action results in an increase in the respiratory rate (Chen *et al.*, 2002). Similarly, oligomycin blocks the ATP synthase proton channel and prevents the movement of protons back into the matrix. This action increases the membrane potential and slows the respiratory rate (Chen *et al.*, 2002). Mitochondrial membrane potential is maintained by cellular respiration. A drop in membrane potential may occur for several reasons: 1) respiratory inhibition, 2) substrate deprivation, or 3) uncoupling of oxidative phosphorylation (Duchen, 2004).

Although production of ATP is the primary role of mitochondria, they are also involved in cell signaling, differentiation, growth and death (McBride *et al.*, 2006). In addition, mitochondria contribute to glucose homeostasis, calcium regulation, synthesis of steroids and lipids, DNA replication, transcription and translation of proteins, and oxygen sensing (Duchen and Biscoe, 1992; McBride *et al.*, 2006; Rowe *et al.*, 1981).

REACTIVE OXYGEN SPECIES

The demonstration that xanthine oxidase produces O_2^- (McCord and Fridovich, 1968) and that erythrocytes contain an enzyme that efficiently and specifically catalyze the conversion of O_2^- into $H_2O_2 + O_2$ (McCord and Fridovich, 1969) led to the understanding that O_2^- is commonly produced within aerobic biological systems and that there are cellular mechanisms that oxidize this molecule. O_2^- is known as a radical. Radicals, also called free radicals, are atoms or groups of atoms that have one or more unpaired electrons and have high chemical reactivity. A variety of normal biochemical reactions form radicals as necessary intermediates.

Oxygen radicals are known as reactive oxygen species (ROS); although, the term ROS includes both oxygen radicals and non-radicals that are oxidizing agents that may be easily converted to radicals (Halliwell and Gutteridge, 2007). Oxygen has two unpaired electrons in each of two outer orbitals, making oxygen particularly susceptible to radical formation. Sequential reduction of molecular oxygen results in the formation of the following ROS: superoxide anion, peroxide ion, and hydroxyl radical (Halliwell and Gutteridge, 2007). A list of some ROS, both radical and non-radical, is shown in Table I-4.

TABLE I-4
Nomenclature of Reactive Oxygen Species

Free radicals	Non-radicals
Superoxide, $O^{\cdot}{}_2^-$	Hydrogen peroxide, H_2O_2
Hydroxyl, $OH^{\cdot}$	Ozone, O_3
Hydroperoxyl, $HO^{\cdot}{}_2$	Peroxide ion, O_2^{2-}
Peroxyl, $RO^{\cdot}{}_2$	
Alkoxyl, $RO^{\cdot}$	
Carbon dioxide, $CO^{\cdot}{}_2^-$	

ROS are formed primarily in the mitochondria as oxygen is reduced along the electron transport chain during aerobic metabolism. Some non-mitochondrial enzymatic reactions also form ROS intermediates (Saez *et al.*, 1982). In addition, white blood cells produce ROS as defense against pathogens (Bernhagen, 2005). Studies indicate that ROS may be involved in inter- and intracellular signalling (Nemoto *et al.*, 2000). For example, addition of superoxide or hydrogen peroxide to cultured cells results in an increased rate of DNA replication and cell proliferation (Burdon *et al.*, 1989).

Mitochondria produce ATP by oxidative phosphorylation where hydrogen ions are transported across the inner mitochondrial membrane via the electron transport chain. In the chain, electrons are passed through a series of proteins via oxidation-reduction reactions, with each acceptor protein along the chain having a greater reduction potential than the last. The last destination for an electron is an oxygen molecule. Normally, electrons pass from one component of the chain to the other, and oxygen is reduced to water; however, 0.1-2% of electrons that pass through the chain are leaked directly to oxygen, which is prematurely and incompletely reduced to form the superoxide radical, O_2^- (Muller, 2000). This occurs particularly in Complex I (Turrens and Boveris, 1980) and Complex III (Boveris *et al.*, 1976; Han *et al.*, 2001; St-Pierre *et al.*, 2002), although Complex II can also produce the superoxide radical (Zhang *et al.*, 1998).

Despite the beneficial activities associated with ROS, they may also be toxic to cells. When generated in excess or not properly controlled, ROS can cause damage to

macromolecules such as DNA, phospholipids, and proteins. When electron transfer is hindered by high membrane potential, point mutations or respiratory inhibitors such as antimycin A, there may be enhanced leakage of electrons to oxygen, particularly at Complex III. Events such as hypoxia (heart attack and stroke) (Carden and Granger, 2000), extreme heat (Martindale and Holbrook, 2002), exposure to various chemicals and drugs (Munday, 1989), and ionizing radiation (Carugo and Carugo, 2005) generate excess ROS in cells and cause oxidative stress. For example, ROS damage cellular membranes by lipid peroxidation (Gardner, 1989). Peroxidation targets unsaturated fatty acids in the phospholipids of membranes. A chain reaction occurs: hydrogen is removed from the fatty acid by a hydroxyl radical, leaving a carbon-centered radical as part of the fatty acid. The new carbon radical reacts with oxygen to yield the peroxyl radical that then reacts with other fatty acids or proteins. Membrane peroxidation may result in increased membrane rigidity, decreased activity of membrane-bound enzymes (e.g. sodium pumps), altered activity of membrane receptors, and altered permeability (Gardner, 1989). Similarly, ROS may directly attack membrane proteins and induce lipid-lipid, lipid-protein, and protein-protein crosslinking (Davies, 2005), all of which have adversely affect membrane function.

As a defense against oxidative stress and ROS damage, cells contain antioxidants. Antioxidants are any substance that delays, prevents, or removes oxidative damage to a target molecule (Halliwell and Gutteridge, 2007). Antioxidants may be enzymatic or non-enzymatic. Important enzymatic antioxidants include superoxide dismutase, catalase, and glutathione peroxidase. Non-enzymatic antioxidants include ascorbic acid (vitamin C) (Padayatty *et al.*, 2003), glutathione, and vitamin E (tocopherol) (Yoshida *et al.*, 2003). Vitamin E is lipid-soluble and protects membranes inhibiting lipid peroxidation because they scavenge lipid peroxyl radicals ($LO\cdot_2$) faster than the radical can react with adjacent fatty acid side chains or membrane proteins (Mukai *et al.*, 1993; Porter, 1993).

Superoxide dismutase (SOD) catalyzes the conversion of two superoxides into hydrogen peroxide and oxygen. Hydrogen peroxide is significantly less toxic than

superoxide and can be removed by other antioxidants. SOD is associated with metals that are necessary for their function. Zinc (Zn^{2+}) or copper (Cu^{2+}) are bound to SOD (CuZnSOD) in the cytoplasm (Fridovich, 1995a). Manganese (Mn) binds to SOD (MnSOD) in the mitochondria (Fridovich, 1995a). In CuZnSOD, the copper ion catalyzes dismutation by undergoing alternate oxidation and reduction. A copper chaperone delivers copper to the metal-free SOD and ensures that the correct disulphide bridge forms (Furukawa *et al.*, 2004). The Zn^{2+} is not catalytic, but stabilizes the enzyme. Non-biological metals such as mercury cannot replace the Cu^{2+}, but can replace the Zn^{2+}, which results in a functional, but less stable enzyme (Fridovich, 1995a). MnSOD catalyzes essentially the same reactions as CuZnSOD. It requires the presence of bound Mn to be functional; other metal ions can bind, but do not yield a functional enzyme.

Catalase is located in peroxisomes. It catalyses a dismutation reaction where hydrogen peroxide is converted to water and oxygen, thus detoxifying the product of the SOD reaction (Chance *et al.*, 1979). Mammalian catalases contain Fe(III)-heme at the active site (Reid *et al.*, 1981).

Glutathione peroxidases are enzymes that contain selenium at its active site (Brigelius-Flohé, 1999). They degrade H_2O_2 by coupling its reduction to water with oxidation of reduced glutathione, GSH, a thiol-containing tripeptide (glutamyl-cysteinyl-glycine). Cysteine provides an exposed free sulphydryl group (SH) that is highly reactive, thus providing a target for H_2O_2 attack. The reaction oxidizes glutathione (GSSG). Glutathione peroxidases can also act on non-H_2O_2 peroxidases. For example, they catalyze GSH-dependent reduction of fatty acid hydroperoxides. The peroxide group is reduced to an alcohol (Brigelius-Flohé, 1999).

Glutathione reductase converts GSSG back to GSH. Each of the two subunits contain FAD (Thieme *et al.*, 1981). NADPH reduces the FAD, which passes its electrons onto a disulphide bridge. The two –SH groups then interact with GSSG and reduce it to 2GSH, reforming the protein disulphide bridge.

CALCIUM

Calcium function in neurons

Normal neuronal action potentials and synaptic transmission is dependent upon calcium ions (Ca^{2+}). Ca^{2+} is taken into neurons from the extracellular matrix by calcium channels such as voltage gated channels (VGCC), ligand gated channels (LGCC), and transient receptor potential ion channels (TRP) (Bezin *et al.*, 2006; Carafoli, 2004). VGCCs operate when the cell is depolarized by the influx of sodium (Na^{+}) ions (Bear *et al.*, 2001). Following depolarization, VGCCs open and allow Ca^{2+} to move down their concentration gradient and into the cytosol. LGCCs open in response to neurotransmitter binding (Kandel and Siegelbaum, 2000). TRP channels are activated primarily through signal transduction pathways. TRP channels are transported to the plasma membrane by the activity of phospholipase C and di-acyl glycerol (Clapham, 2003).

In addition to action potential propagation and synaptic transmission, Ca^{2+} is a component of intracellular signaling pathways that initiate or control many cellular processes. In neurons, these processes include neurotransmitter release, excitability, neurite outgrowth, synaptogenesis, gene expression, cellular differentiation, plasticity, and cell death and survival (Pietrobon, 2002; 2005).

Maintenance of calcium homeostasis

Normally, intracellular free calcium (Ca^{2+}) levels are around 0.1 μM or less. Total Ca^{2+} is greater, but most is sequestered within the mitochondria, the endoplasmic reticulum (ER) or bound to cytoplasmic proteins. Ca^{2+} concentration outside the cell is typically 1.5 mM (Berridge *et al.*, 2000). Transient increases in free Ca^{2+} regulate many physiological processes, including cell proliferation and neurotransmitter release (Montell, 2005). However, uncontrolled rises in intracellular free Ca^{2+} can lead to cell injury or death (Dubin and Stoppani, 2000).

Low intracellular Ca^{2+} levels are maintained by the coordinated activity of several systems: 1) plasma membrane ATP-dependent Ca^{2+} export proteins, 2) uptake of Ca^{2+} into the ER lumen, 3) uptake of Ca^{2+} by the nucleus, and 4) uptake of Ca^{2+} by

mitochondria, and 5) binding of Ca^{2+} to cytosolic calcium-binding proteins. A summary of the maintenance of Ca^{2+} homeostasis is shown in Fig I-21.

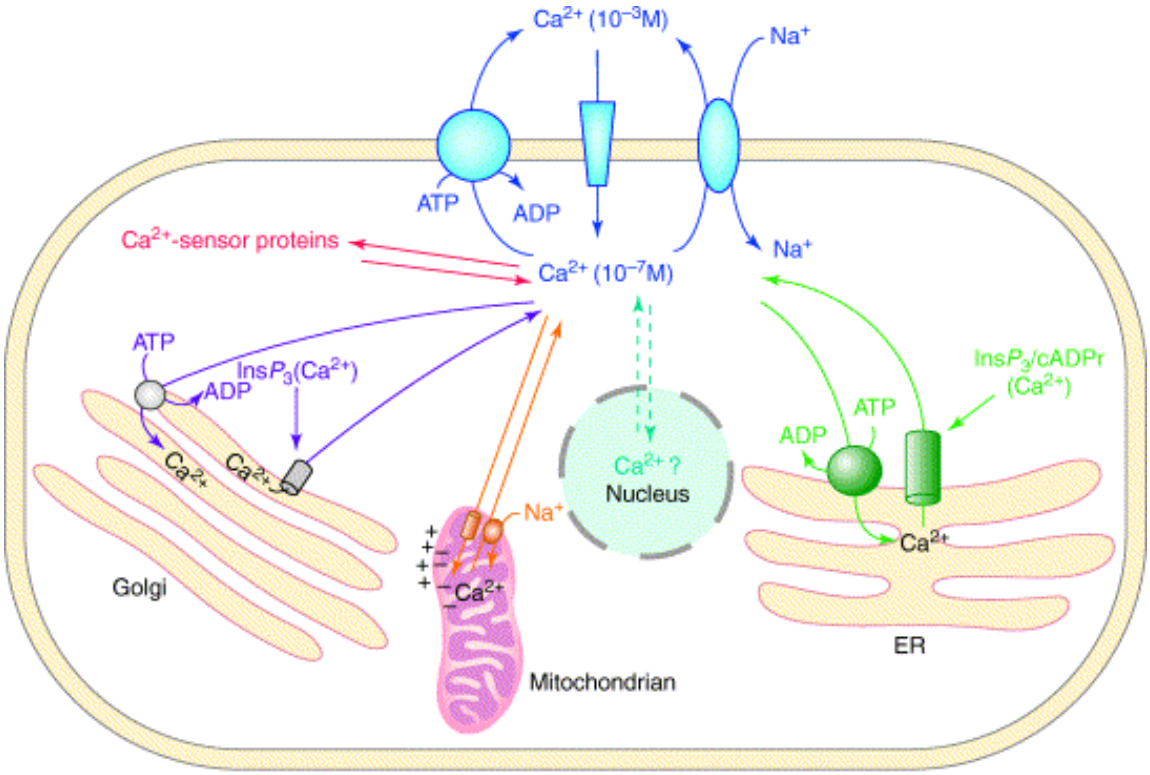

FIG. I-21. Diagram of cellular Ca2+ homeostasis mechanisms. The membrane transporters of Ca2+ in the plasma membrane and in the organelles, as well as the Ca2+ sensor proteins that decipher the Ca2+ before passing it on to enzyme targets, are shown. The Ca2+ channel shown in the plasma membrane is representative of the three types - voltage-gated, ligand-gated, and store operated. Modified from Carafoli, E. (2004). Calcium-mediated cellular signals: a story of failures. *Trends in Biochemical Sciences* 29, 371-379.

Plasma membrane ATP-dependent Ca^{2+}-export proteins function by energy from ATP that drives the Ca^{2+} out of the cell against its concentration gradient (Garcia and Strehler, 1999). Neurons also have Na^{+}/Ca^{2+} exchange transporters. ATP hydrolysis links the export of Ca^{2+} to the entry of Na^{+} down its concentration gradient. Na^{+} is exported by the ATP-dependent sodium pump (Reuter and Porzig, 1995).

The ER can sequester large amounts of Ca^{2+} and quickly release it. This is necessary because rapid intracellular Ca^{2+} mobilization from intracellular stores is

required for Ca^{2+} signaling (Meldolesi, 2001; Meldolesi and Pozzan, 1998). Extracellular signalling molecules bind to cell surface receptors and lead to release of Ca^{2+} from the ER by stimulating synthesis of inositol triphosphate (IP_3). This results in the opening of Ca^{2+} channels in the membrane of the ER, and Ca^{2+} is released into the cytosol (Venkatachalam *et al.*, 2002). This surface receptor binding and subsequent Ca^{2+} release is called calcium induced Ca^{2+} release (CICR) (Berridge *et al.*, 2000; Carafoli, 2004). Ca^{2+} enters the ER via ER Ca^{2+}-ATPase (SERCA) pumps on the ER membrane (Carafoli, 2004). Once inside the ER, much of the Ca^{2+} becomes bound to calreticulin and calsequestrin. These CaBPs regulate the pool of free Ca^{2+} available for release upon stimulation (Meldolesi, 2001).

Much of the nuclear Ca^{2+} uptake and release occurs in close association with the ER because the outer nuclear membrane is continuous with the ER membrane. Ca^{2+} in the ER is mobilized into the nucleus through IP3 receptors and RyRs in the nuclear envelope (Barbara, 2002; Hirose *et al.*, 2008). Nuclei can also regulate Ca^{2+} independent of the SER. The ATP-dependent nuclear Ca^{2+}-ATPase and the IP4-mediated inositol 1,3,4,5-tetrakisphophate receptor transport cytosolic Ca^{2+} into the nucleus (Malviya and Klein, 2006).

If intracellular Ca^{2+} levels increases so much that the ER can no longer transport the excess, the mitochondria become a second line of Ca^{2+} buffering (Gunter *et al.*, 2000; Meldolesi, 2001). Mitochondria are biosensor of Ca^{2+} microdomains. They take up Ca^{2+} from high cytosolic Ca^{2+} areas near active Ca^{2+} channels in the plasma membrane. Mitochondria need a local Ca^{2+} concentration of at least 500 nM to begin to take up Ca^{2+} (Nicholls and Scott, 1980a; Nicholls and Scott, 1980b). This allows a localized initiation of Ca^{2+} signaling, but prevents the newly entered Ca^{2+} from initiating Ca^{2+} signaling in all areas of the cell. This control over cytosolic Ca^{2+} signaling is necessary for regulation of compartmentalized cell functions (Alonso *et al.*, 2006).

The mitochondria have two Ca^{2+} uptake systems, the uniporter and the fast Ca^{2+} uptake. Ca^{2+} efflux is through two ion exchangers coupled with Na^+ or H^+ (Carafoli, 1974; Sparagna *et al.*, 1995). The inner mitochondrial membrane has permeability

transition pores (PTP) that operate at two physiological states. The low conductance confirmation is involved in normal Ca^{2+} regulation through changes in the pH of the mitochondrial matrix (Davidson and Halestrap, 1990; Ichas *et al.*, 1994). The high conductance confirmation results in irreversible changes in the mitochondrial membrane potential. The outer membrane eventually ruptures and apoptosis signaling molecules are released into the cytosol (Ichas and Mazat, 1998; Scarlett and Murphy, 1997).
Free Ca^{2+} within the cell can become bound to cytosolic calcium-binding proteins (CaBPs). One example is calmodulin (Klee and Means, 2002). Calmodulin regulates many enzymes, including calcineurin and nitric oxide synthase (Corti *et al.*, 1999). It also regulates cellular processes such as cytoskeletal assembly (Rozenblum and Gimona, 2008). Calmodulin is rich in methionine residues and is a potential target for oxidative damage. Other cytosolic calcium-binging proteins (CaBPs) include either Ca^{2+} sensors (calmodulin, caldendrin, and calneurons) or buffers (calretinin, calbindin, and parvalbumin) (Baimbridge *et al.*, 1992; Mikhaylova *et al.*, 2006; Seidenbecher *et al.*, 1998).

Negative consequences of altered intracellular Ca^{2+} levels

Oxidative stress can alter Ca^{2+} metabolism and cause a rise in free Ca^{2+}. ROS can damage the ER-Ca^{2+} uptake system and interfere with Ca^{2+} efflux through the plasma membrane by oxidizing –SH groups within the transmembrane channels (Lehotsky *et al.*, 2002). ROS may also cause voltage-gated Ca^{2+} channels in the plasma membrane to open and allow excess Ca^{2+} to enter the cell (Lehotsky *et al.*, 2002). Negative consequences of excess intracellular free Ca^{2+} include disruption of the cytoskeleton, production of more ROS, and disruption of membrane organization.

Polymerization and reorganization of actin, as well as its binding to focal adhesion sites for cell attachment are necessary for proper cell function. High intracellular Ca^{2+} activates calpains (proteinases) that cleave actin-binding proteins and cause the plasma membrane to separate from the cytoskeleton (Dourdin *et al.*, 2001). High calpain activity has been implicated in diseases such as muscular dystrophy

(Bertipaglia and Carafoli, 2007) and Alzheimer's disease (Raynaud and Marcilhac, 2006).

High free Ca^{2+} stimulates eNOS and nNOS (Duchen, 2000); their activity produces intermediates that ultimately cause the formation of superoxide (Baldelli *et al.*, 2008). One of the intermediates, nitric oxide ($NO^{\cdot}$), is toxic in high concentrations and inhibits cytochrome oxidase (Cooper *et al.*, 2008).

Phospholipase A_2 is an enzyme that cleaves membrane phospholipids. It is stimulated by high Ca^{2+} levels. The production of excess free fatty acids and their hydrolysis products results in membrane disorganization (Vanlangenakker *et al.*, 2008). In addition, transglutaminases are activated by Ca^{2+}. These catalyze the crosslinking of proteins within membranes and produce insoluble aggregates (Shin *et al.*, 2008).

Finally, in the process of mitochondrial sequestration of Ca^{2+}, the excess Ca^{2+} can trigger the mitochondrial permeability transition pore (MPT) in the inner membrane to open (Smaili and Russell, 1999). This causes a collapse in the membrane potential as well as the release of cytochrome C and apoptosis inducing factor (AIF) (Duchen, 2000), resulting in the death of the cell.

NEUROTOXICOLOGY

General overview

The nervous system processes, stores, and transmits information. Biochemical and molecular events within the nervous system lead to conscious and unconscious actions or behavior. The nervous system is highly organized, but complex; this results in vulnerability to toxicant exposure. Cell types and functions, structural content, and energy consumption all play a role in the complexity and susceptibility of the nervous system to toxic effects.

Cells within the nervous system are either neurons or glia. They each have a specific function, but also a specific relationship between each other. The maintenance of the relationship between the two cell types is necessary for normal function of the nervous system (Abbott *et al.*, 1992; LoPachin and Aschner, 1999). Although there are

basically only neurons and glia, the brain is heterogeneous in its cellular composition. The cells types and some of the specialized sub-populations of cells within the hippocampus and cerebellum have been discussed previously. These two brain regions alone provide examples of just how diverse and varied neuronal components may be.

There are a number of enzyme systems involved in neurotransmitter production and maintenance that are unique to the nervous system, but vary from cell to cell depending on its function (i.e. nicotinic, muscarinic, cholinergic, dopaminergic functions). The German pathologist, Franz Nissl, observed that administration of particular agents consistently resulted in characteristic injury to neurons of defined areas of the brain (Lowndes *et al.*, 1995). This became known as *pathoclisis*. *Pathoclisis* states that cells in particular regions of the brain, by virtue of unique biochemical or anatomical features, are vulnerable to intoxication by certain classes of xenobiotics and not by others. This is demonstrated by the vulnerability of dopaminergic neurons in the pars compacta of the substantia nigra to 1-methyl-4-phenyl-1,2,3,6-tetrahydropyridine (MPTP) (Langston *et al.*, 1984).

The nervous system relies on aerobic glucose metabolism for energy production and has a very high metabolic rate. Twenty percent of the oxygen consumed by the body and 15 % of the total cardiac output are used to support the brain that is only 1.5 to 2 % of total body weight (Heiss, 1981). Therefore, toxicants that disrupt glucose metabolism and mitochondrial function may significantly affect the nervous system (Nichlas, 1992). The brain has low-levels of antioxidants and is highly composed of polyunsaturated fatty acids. This, along with the high metabolic rate, increases the possibility of oxidative damage (Evans, 1993) upon exposure to certain toxicant.

Xenobiotic metabolism in the brain

Metabolization of xenobiotics occurs primarily by phase I (biotransformation) and phase II (conjugation) enzyme processes. These phases usually result in detoxification and excretion; however, formation of toxic intermediates or products is possible. Phase I metabolism is achieved by monooxygenation, dealkylation, reduction,

aromatization, or hydrolysis. The important enzymes are the cytochrome P-450s and the mixed-function oxygenases. Phase II metabolism involves glucuronyltransferases, sulfotransferases, methyl- and acetyltransferases, and glutathione S-transferases (Parkinson, 2001). Neither Phase I, nor Phase II, enzymes are located homogeneously throughout the brain. Cytochrome P450s (Volk *et al.*, 1991) and glutathione S-transferases (Philbert *et al.*, 1991; Slivka *et al.*, 1987) are found primarily in the neuropil, not in neurons, the exception being the olfactory bulb dorsal root ganglia, and Purkinje and cerebellar granule neurons in mice (Philbert *et al.*, 1991; Slivka *et al.*, 1987). Sulfotransferases are located primarily in catecholaminergic neurons such as those in the human hippocampal pyramidal and nonpyramidal neurons of CA2 and CA3 (Zou *et al.*, 1990). In the rat, methyltransferases are important in the metabolism of adrenergic neurotransmitters (Acquas *et al.*, 1992; Moghrabi *et al.*, 1992), while acetyltransferases are important in the formation of neurotransmitters (Saji and Miura, 1991); these enzymes, therefore, are located in neurons with neurotransmitter function.

Blood-brain barrier

A protective component of the central nervous system (CNS) is the blood-brain barrier (BBB). The BBB is not an absolute barrier to the passage of toxic agent into the CNS. Instead, it is a site of limited permeability compared to other areas of the body. There are four major anatomic and physiologic reasons some toxicants do not readily enter the CNS (Rozman and Klaassen, 2001). First, capillary endothelial cells of the CNS are continuous and contain tight junctions (Fig I-22). There are few or no pores between the cells. However, water, gases, and lipid-soluble molecules can diffuse across endothelial cells. Second, the endothelial cells contain ATP-dependent transporters. The endothelial cells have relatively few pinocytotic vesicles, and vesicular traffic is almost completely restricted to receptor-mediated transport (Gartner and Hiatt, 1997). The multi-drug-resistant (mdr) protein exudes some chemicals back into the blood (Schinkel *et al.*, 1994). Ions are also transported across the blood-brain barrier through ion channels via active transport. Molecules, such as glucose, amino acids, certain vitamins,

and nucleosides, are transferred across the BBB by specific carrier proteins (Gartner and Hiatt, 1997). Third, the capillaries in the CNS are surrounded by protoplasmic astrocyte processes (end-feet). The end-feet cover neurons, the inner surface of the pia, and every blood vessel within the CNS (Fig I-23). Lipid-soluble compounds must traverse the membranes of the endothelial cells as well as those of the astrocyte end-feet (Rozman and Klaassen, 2001). For small to medium-sized water-soluble molecules, the tight junctions of the capillary endothelium and the lipid membranes of the glial cell processes are major barriers. Fourth, the protein concentration in the interstitial fluid of the CNS is much lower than that in other body fluids. This greatly limits the movement of water-insoluble compounds by paracellular transport, which is possible in a largely aqueous medium only when such compounds are bound to proteins (Rozman and Klaassen, 2001).

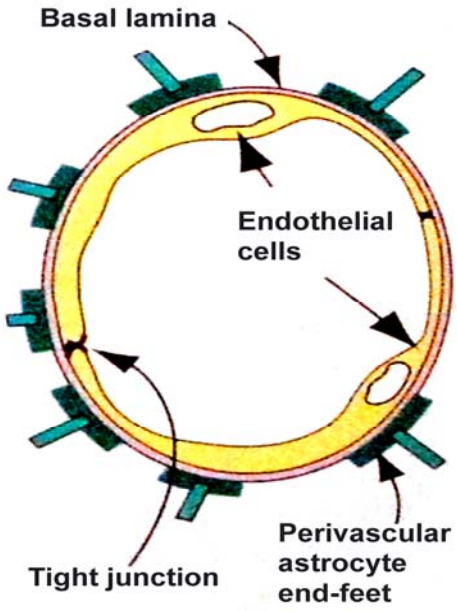

FIG. I-22. Schematic of the tight junctions of the blood-brain barrier. The CNS capillaries are lined by continuous endothelial cell linked by tight junctions. The basal lamina and the astrocytic perivascular end-feet are also components of the blood-brain barrier. Modified from Kierszenbaum, A. L. (2002). Histology and Cell Biology: An Introduction to Pathology. p. 208. St. Louis, Mosby Inc.

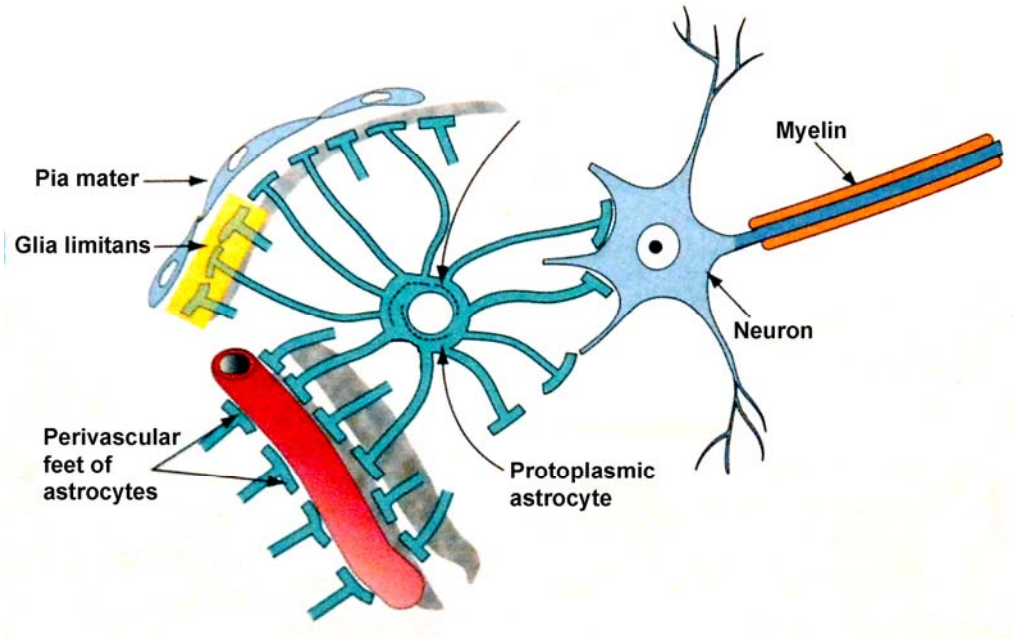

FIG. I-23. Schematic of the blood-brain barrier. Protoplasmic astrocytes in the CNS have cytoplasmic processes with end-feet. The end-feet cover neurons, the inner surface of the pia mater, and the blood vessels. The joined end-feet processes adjacent to the pia mater form the glia limitans. Modified from Kierszenbaum, A. L. (2002). Histology and Cell Biology: An Introduction to Pathology. p. 208. St. Louis. Mosby, Inc.

The effectiveness of the BBB varies from one brain region to another. The cortex, lateral nuclei of the hypothalamus, pineal gland, and posterior lobe of pituitary are more permeable than other areas of the brain. This may be due to the increased blood supply in these areas, a more permeable barrier, or both. In general, however, only the non-protein-bound portion of a toxicant equilibrates rapidly with the brain (Rozman and Klaassen, 2001). Increased lipid solubility increases the rate of penetration of toxicant, whereas ionization decreases it. Some xenobiotics may enter the brain by carrier-mediated processes. Methylmercury combines with cysteine, forming a structure similar to methionine, and is accepted by the large neutral amino acid carrier of the capillary endothelial cells (Clarkson, 1987).

DEVELOPMENTAL NEUROTOXICOLOGY

General overview

Exposure of the developing nervous system to toxicants may have a subtle or a profound affect. Development is characterized by changes in size, biochemistry, physiology, form, and function. These changes are orchestrated by factors that regulate the maternal transcription of genes and translation of proteins, which activate regulatory genes in the embryo, followed by sequential gene activation throughout development. Intercellular and intracellular signaling pathways, essential for normal development, rely on transcriptional, translational, and posttranslational controls. Toxicant exposure may result in alterations at any point in the developmental sequence leading to a life time of consequences for the individual as well as for the general public.

The nervous system is important for coordinating motor and cognitive functions, therefore, toxicants that alter normal functions may cause impairment in muscular movement, senses, learning and memory. Alterations of chemical properties and physiology of neurons and glia during development can impair the intracellular environment, leading to structural abnormalities such as changes in neuron morphology and the intra- and extracellular environments.

Several chemicals are known to be neurotoxic, especially for the developing nervous system. In children, lead exposure causes psychological deficits and learning disabilities (Davis *et al.*, 1990; Hansen *et al.*, 1989; Winneke *et al.*, 1990). Polychlorinated biphenyl (PCB) causes low birth weights, hyperactivity, and altered visual recognition memory (Kimbrough, 1995; Tilson *et al.*, 1990). Substances of abuse, such as nicotine (Fried *et al.*, 1999; Jones, 1973; Strauss, 1997), ethanol (Driscoll *et al.*, 1990), and cocaine (Chiriboga, 1998) are also developmentally neurotoxic. They cause decreased head circumference, delays in fine motor skills and speech development, increased impulsivity, and hypertonic tetraparesis. In addition to environmental toxicants, chemicals such as the prescription drug isotretinoin (Accutane) (Adams and Lammer, 1993) and thalidomide (McBride, 1961) are known to be neurotoxic These chemicals are toxic to the developing animal, as opposed to the adult animal, likely

because of the unique processes that occur during growth and development. Neuronal cell proliferation and subsequent migration, differentiation (including neurite outgrowth and formation of dendritic spines) and maturation are events that must be appropriately timed and occur with precision. Any alteration at any point along this path may have negative consequences to the developing nervous system.

Causes of increased susceptibility to toxicants

As previously mentioned, the brain and nervous system have a high metabolic rate. This is particularly true for the developing nervous system. In late gestation, there is an increase in respiration (Nakai *et al.*, 2000) that is accompanied by an increase in mitochondrial proliferation (Stewart and Hayakawa, 1994). Just following parturition, there is a second increase in respiration that is associated with maturation of the mitochondria and the production of high energy phosphates necessary for fetal adaptation to birth (Nakai *et al.*, 2000). As with the adult animal, toxicants that disrupt energy production and mitochondrial function may be toxic to the nervous system.

The BBB is not fully developed at birth; therefore, some chemicals are more toxic in newborns than to adults. Morphine is three to ten times more toxic to newborns than to adult rats because of the non-developed BBB (Kupferberg and Way, 1963). Lead produces encephalomyelopathy in newborn rats but not in adults, apparently because of differences in the stages of development of the BBB (Pentschew and Garro, 1966).

The placenta provides nutrition for the conceptus, exchanges maternal and fetal blood gases, disposes of fetal excretory material, and maintains pregnancy through complex hormonal regulation. Most of the vital nutrients necessary for the development of the fetus are transported by active transport systems. Vitamins, amino acids, essential sugars, and ions such as calcium and iron are transported from mother to fetus against a concentration gradient (Ginsburg, 1971). In contrast, most toxicants cross the placenta by passive diffusion.

The placenta contains active transport systems that protect the fetus from some xenobiotics. Multi-drug-resistant null (mdr null) fetuses are more susceptible to cleft

palate produced by avermectin (Lankas *et al.*, 1998). The placenta also has some biotransformation capabilities that may prevent some toxic substances from reaching the fetus (Juchau, 1972). As in the brain, increased lipid-solubility increased the rate at which a toxicant will enter the placenta. Under steady-state conditions, the concentrations of a toxic compound in the plasma of the mother and fetus are similar. An increase in the concentration a toxicant in the fetus compared to the mother depends on the ability of the fetus to concentrate the toxicant. For example, the concentration of diphenylhydantoin in the plasma of fetal goats was about half that in the mother, most like due to the differences in plasma protein concentration and the binding affinity of diphenylhydantoin to plasma proteins in the fetus (Shoeman *et al.*, 1972). Different body compositions between mother and fetus may be another reason for differences in toxicant concentration. For example, fetuses have very little fat; therefore lipophilic chemicals such as TCDD accumulate at higher concentrations in the mother than the fetus (Li *et al.*, 1995). In contrast, higher concentration of toxicants such as methylmercury may be found in the fetus compared to the mother because of the immature BBB (Null *et al.*, 1973; Reynolds and Pitkin, 1975).

ARTIFACTS OF CELL CULTURE

Cell culture studies have given much valuable information about mechanisms of metabolism and signal transduction and of regulation of gene expression, proliferation, senescence, and death (Halliwell, 2003). However, cells in culture may behave differently from cells *in vivo* in many ways. Artifacts can affect the interpretation of cell culture studies. The process of cell culture imposes a state of oxidative stress on cells. The culture media can catalyze the oxidation of added compounds, resulting in an observed cellular effect that may in fact be due to ROS produced by the culture media (Halliwell, 2003). Culture media are often deficient in antioxidants (vitamins C and E) and antioxidant precursors (selenium) and contain “free” metal ions, present as contaminants or even added deliberately iron (III) salts are added to Dulbecco’s modified Eagle’s medium). These may present a problem in appropriate interpretation of

studies involving metal exposure, or studies that may be affected by the presence or absence of antioxidants (ROS studies).

Most animal cells are cultured as a monolayer under 95% air:5% CO_2 (152 mmHg); they are also in a hyperoxic environment, which is likely to increase their rates of ROS formation (de Groot and Littauer, 1989). One study showed the intracellular partial pressure of oxygen ($pO_{2)}$ of cultured lung endothelial cells to be 140 mmHg (Kutala *et al.*, 2004). This measurement is significantly higher than physiological levels. Studies involving the production of ROS may be affected by the environmental O_2 levels and again, by the antioxidant status of the system.

Other problems in cell culture studies include the use of proteinases such as trypsin in subculturing and the lack of growth factors, hormones and influences of surrounding cells. Proteinases can alter membrane permeability (Averdunk, 1970) and the proteins involved in adherence of the cells to a surface (Tiruppathi *et al.*, 2002). Changes in these proteins often initiate intracellular signalling (Tiruppathi *et al.*, 2002) of processes within the cell that may affect the results of the parameters being examined. Environmental factors affect the function of all cells. Neurons in culture are often delicate, but in the brain, glia help to protect them (Dhandapani and Brann, 2002).

One must examine potential reactions of compounds with the culture medium, be aware of the absence or presence of compounds that might confound interpretation, and set up adequate controls to mitigate such problems, even when a potential confounding factor cannot be identified. It is essential to be cautious when interpreting data on cells in culture. In addition, whenever possible, one must use a combination of cell culture experimentation in tandem with *in vivo* studies to enhance the validity of the results observed in a culture system.

MERCURY

Historical perspective

Mercury (Hg) is a ubiquitous and hazardous environmental contaminant found in ocean and freshwater fishes, shellfish, and plants (Hall and St. Louis, 2004; Mikac *et*

al., 1985; Westoo, 1973). The organic or methylated form of Hg, methylmercury (MeHg), accounts for most of the Hg to which humans are exposed and is known to have serious neurotoxic effects on both the developing and mature central nervous system (CNS) (Miura, 1998; Spurgeon, 2006).

Historically, MeHg toxicity has been associated with high morbidity and mortality rates. In 1865, George Edwards wrote the first case report on MeHg poisoning. It was not until 1940, that Hunter *et al.* published the first detailed account of four men exposed to MeHg during the manufacturing of seed fungicide. Their symptoms began 3 to 4 months following initial exposure to MeHg and continued to progress after exposure cessation. Initial symptoms were paresthesia of the extremities, followed by ataxia of gate, dysarthria, and impaired peripheral vision. The cardinal signs were constricted visual fields, ataxia, dysarthria, and sensory deficits such as stereognosis and impaired two-point discrimination in the extremities. This array of symptoms became known as Hunter-Russell syndrome (Hunter and Russell, 1954).

In Japan, in May 1956, the first mass outbreak of MeHg poisoning occurred in Minamata City, located in the southwest region of Kyushu Island. Residents in the Minamata Bay area began to notice phenomena such as birds falling from the sky while in flights and fish rotating continuously or floating upside down. Cats exhibited excessive salivation, convulsions, violent rotation movements and abnormal gait, followed by death. Some cats appeared frenzied and would jump into the sea to their death. The symptoms observed in cats were instrumental in determining the etiology of the disease (Harada, 1995).

The source of the epidemic was traced to the Chisso Corporation's factory that used inorganic mercury compounds as a catalyst to synthesize acetaldehyde. The resulting 81.3 tons of waste methylmercury chloride (Irukayama *et al.*, 1977) was released into Minamata Bay with the factory's wastewater, where it bioaccumulated in the fish and was consumed by humans in the area (Clarkson, 2002). Between April and December 1956, 50 cases of Hunter-Russell syndrome were diagnosed. By October 1960, 111 cases were known, and by December 1965, 37 % of those diagnosed had died.

In the Minamata Bay area, over 1700 cases had been recognized by 1981 (Tokuomi *et al.*, 1982). Hunter-Russell syndrome is now known as Minamata disease.

A second outbreak of MeHg poisoning occurred in Niigata, Japan in 1965, this time, due to consumption of contaminated fish from the industrial contamination of the Agano River. By 1974, there were 520 recognized cases (Tsubaki and Irukayama, 1977). Around the same time, during the winter of 1971 – 1972, Minamata disease was identified in Iraq. Planting-wheat treated with MeHg was given, for free, to farmers throughout the country. Instead of planting the wheat, they washed out the red dye, ground it into flour, and used it to make bread. Over 6500 individuals were diagnosed with MeHg poisoning, and over 450 of those died (Bakir *et al.*, 1973).

The most common initial symptoms were paresthesia of the extremities, perioral paresthesia, constricted visual fields, ataxia of the limbs and gait, slow slurred speech that sometimes progressed to anarthria, deafness to high tones, and sensory deficits (Tokuomi, 1960). In addition to the sensory impairments described by Hunter *et al.* (1940), MeHg toxicity victims in Japan experienced impairment of pain and touch sensation, called glove and stocking distribution. Less frequent symptoms included rigidity of the limbs with chorea or arthetosis, mental impairment, emotional lability, depression, and excessive sweating. The most severely affected individuals became comatose and died within a few months of onset of symptoms (Tsubaki and Irukayama, 1977).

Mercury in the environment

Mercury comes from both natural and man-made sources. It is present in the earth's crust and can be released into the air through weathering of rock containing Hg ore or volcanic eruption (WHO, 1990). Mercury is used in the electrical industry in the production of instruments such as thermometers and barometers, fluorescent tubes, and alkaline batteries. It is produced from smelters, combustion of fossil fuel, and from mining and gold refining. Large quantities are used in the chloralkali industry during the production of chlorine and caustic soda through the electrolysis of NaCl solutions. In

addition, dental amalgam filling contain mercury (WHO, 1991). Although mercury is ubiquitous, it has no beneficial biological function (Eisler, 2004).

Although mercury exists in several forms (Hg^0, Hg^+, Hg^{2+}, MeHg, Me_2Hg), MeHg is the form that is most important in human exposure (Massaro, 1996). Mercury in the environment is constantly cycled in six major steps: 1) degassing of mercury from rock, soils, and surface water, or emission from volcanoes and from human activities, 2) movement in gaseous form through the atmosphere, 3) deposition of mercury on land and into surface waters, 4) conversion of the element into insoluble mercury sulfide, 5) precipitation or bioconversion into more volatile or soluble forms such as methylmercury, and 6) re-entry into the atmosphere or bioaccumulation in food chains (Fig I-24). Mercury vapor is a very stable gas with approximate residence time of one year in the atmosphere. Therefore, mercury can be globally distributed from point sources to remote regions of the planet (Clarkson, 2002). Sulfate-reducing bacteria in aquatic environments methylate inorganic and elemental Hg, creating methylmercury (MeHg) (Heyes *et al.*, 2006; Sunderland *et al.*, 2006). MeHg enters marine animals and is passed up the food chain. Most marine fish contain less than 0.5 ppm, but sharks, sailfish, and marlin may have over 1 ppm MeHg (Matthews, 1983). Fish from Minamata Bay were reported to contain up to 40 ppm (Myers and Davidson, 1998). Contaminated areas in Canada have fish with over 10 ppm (Harada *et al.*, 1976). Individuals that eat fish regularly can have hair mercury levels up to 30 ppm or higher (Turner *et al.*, 1980).

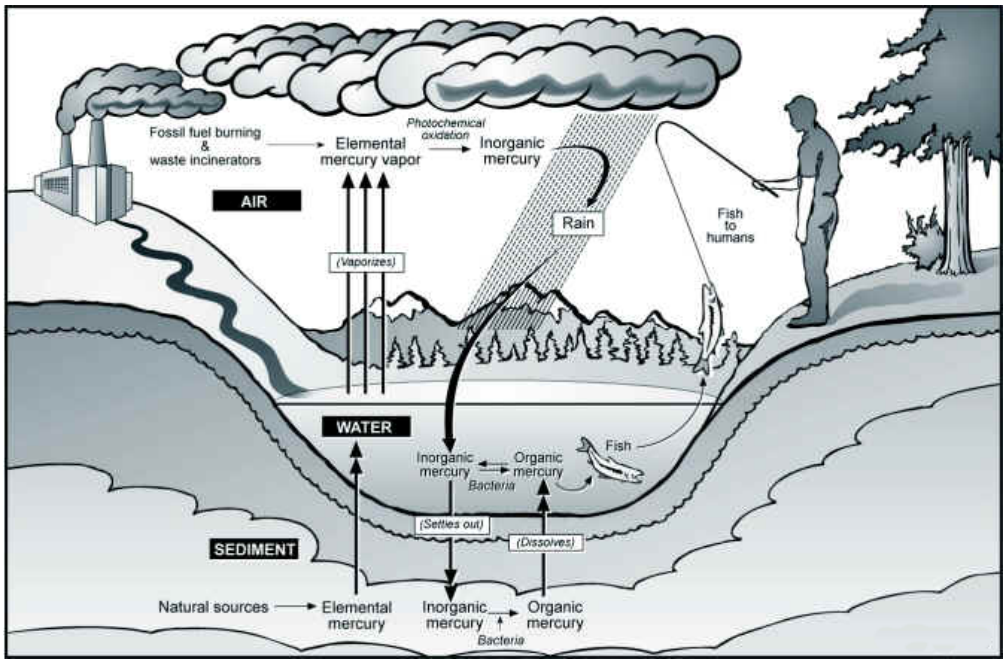

FIG. I-24. Biological mercury cycling. Natural and human activities release mercury vapor into the environment. Elemental mercury vapor undergoes photochemcial oxidation to become inorganic mercury that combines with water vapor and travels back to the earth's surface as rain. In water, inorganic mercury is converted into insoluble mercury sulfide, which is deposited into sediment where it is converted to methylmercury by sulfate reducing bacteria. Methylmercury adsorbs to plankton, which are consumed by higher organisms in the food chain. This pattern continues into small fish and progressively bigger fish, then finally humans. Image by Messenger, L. (1996). http://people.uwec.edu/piercech/Hg/mercury_water/cycling.htm

Absorption, distribution, and excretion

MeHg in the human diet is taken up by the gastrointestinal (GI) tract and rapidly enters the bloodstream (WHO, 1990). About 95% is distributed throughout the body over the next three to four days (Aberg *et al.*, 1969). Blood contains 5% of the absorbed MeHg, and more than 90% of that is attached to hemoglobin (Kershaw *et al.*, 1980). MeHg is metabolized at the rate of 1% of the body burden per day (Clarkson, 2002). The whole body half-life of MeHg in the human is 72 days (Aberg *et al.*, 1969), and 7.4 days in the mouse (Kostyniak, 1980). MeHg dissociates to some degree into the inorganic ionic form of Hg^{2+}. In rats, of total MeHg consumed, the percentage of inorganic Hg^{2+} in the total amount of mercury is approximately 4% in blood, 3% in the brain, 6% in the liver, and 12 to 46% in the kidneys (Magos *et al.*, 1976; Magos and Butler, 1976).

MeHg is excreted from the body in the feces and bile. Of the total mercury excreted, 90% is in the form of MeHg in feces, and 10% is in the form of Hg^{2+} in urine.

MeHg easily crosses the blood-brain barrier; about 10% of the MeHg absorbed through the GI tract accumulates within the brain. Studies in rodents indicate that MeHg is transported as a MeHg-L-Cysteine complex across the blood-brain barrier by a leucine preferring amino acid transporter (Aschner *et al.*, 1991; Kerper *et al.*, 1992). Formation of a MeHg-glutathione complex is another possible mechanism of MeHg transport into the brain (Fujiyama *et al.*, 1994). Once in the brain, MeHg is slowly demethylated to the inorganic (Hg^{2+}) form and becomes permanently trapped within the CNS.

MeHg is not homogeneously distributed throughout the brain, neither is it consistently distributed. One study in rats showed a higher concentration in the cerebellum than the cerebral cortex (Magos *et al.*, 1981); however, other studies have shown no difference in MeHg levels in different regions of the brain (Somjen *et al.*, 1973b). In guinea pigs, the concentration in the cerebellum was lower than in the cerebral cortex (Komsta-Szumska *et al.*, 1983). In macaques, the corpus callosum had the highest concentration of MeHg in the cerebrum, and the dentate nucleus had the highest concentration in the cerebellum (Evans *et al.*, 1977).

Total mercury levels in the body can be measured using hair samples and standard cold-vapor analytical techniques. Hair samples taken from victims of Minamata disease within two months of onset of symptoms (1956) contained mean total mercury levels of 280 – 700 μg/g. By 1968, hair samples from symptomatic individuals contained 10.5 μg/g total mercury and 7.1 μg/g as methylmercury. Again in 1968, the mean value for total mercury in the hair of individuals from the Minamata area with high fish consumption was 9.4 μg/g, whereas the total mercury in the hair of individuals eating small quantities of fish was 7.8 μg/g. The mercury content in hair was higher in males than in females, and higher in persons above 15 years of age, than below (Irukayama *et al.*, 1977). Mercury content was also measured in some autopsy cases of individuals that died within ninety days of exposure. Brain mercury levels in these individuals were 5 – 25 μg/g. The level was 2 μg/g in the brains of individuals that died after two years after

exposure (Irukayama *et al.*, 1977). Current detection limits for assessing mercury hair levels are 0.01 – 0.04 ppm (Gaggi *et al.*, 1996; Lopez-Artiguez *et al.*, 1994). Populations with little or no fish consumption had hair mercury levels of 0.2 – 0.8 ppm (Grandjean *et al.*, 1992b; Smith *et al.*, 1997). In the Seychelles and Faroe Islands, mean levels of mercury in the hair were 6.8 and 4.8 ppm respectively (Cernichiari *et al.*, 1995b; Grandjean *et al.*, 1992b).

The present detection limits for total Hg in the blood is 0.1 – 0.3 ppb (Grandjean *et al.*, 1992b; Mahaffey and Mergler, 1998). In modern non-fish or limited fish-eating populations, the mean total mercury level in blood is 2 ppb (Brune *et al.*, 1991), while the mean total mercury blood levels in high fish-eating populations, such as in the Faroe Islands, is 24 ppb (Grandjean *et al.*, 1992b).

In addition to crossing the blood-brain barrier, MeHg easily crosses the placental barrier in the developing fetus. Methylmercury is easily transported from maternal blood into the fetus. MeHg has a higher affinity for fetal hemoglobin than adult hemoglobin and therefore accumulates in the fetus at 25% higher concentration than in the mother (Amin-Zaki *et al.*, 1976). In rats (Null *et al.*, 1973) and mice (Satoh and Suzuki, 1983), the MeHg concentration was higher in fetal brains than in maternal brains at fetal non-lethal exposure levels. A significant amount of MeHg crosses the placentas of humans as well. High concentrations of MeHg were found in fetal livers and placentas of individuals in the Japanese (Marsh *et al.*, 1977) and Iraqi (Magos *et al.*, 1976) poisonings. Fetal brain mercury levels have been shown to be as much as 5 – 7 times higher than the maternal blood (Cernichiari *et al.*, 1995a).

Infants and newborn animals may also be exposed to MeHg during lactation. MeHg elimination in mice (Greenwood *et al.*, 1978) is accelerated during lactation. Similarly, lactation decreased the biological half-life from sixty-six days to forty-five days in breast-feeding females poisoned in Iraq (Greenwood *et al.*, 1978).

Pathology and clinical signs

Adults

The major target of MeHg is the CNS in both adult and developing organisms; however, the toxic effects and possibly the mechanism of action differ somewhat between the two (Bakir *et al.*, 1980; Counter and Buchanan, 2004). Clinical signs of MeHg exposure in adults in Minamata included concentric constriction of visual fields, sensory disturbances, ataxia, dysarthria, auditory disturbances and tremors (Harada, 1995). Patients with chronic Minamata disease were categorized into one of three groups: 1) gradually progressive, 2) delayed onset, and 3) escalating or progressive with aging. Pathological changes included loss of neurons in the cerebral and cerebellar cortices. The visual, motor, sensory, and auditory cortices were the areas of the cerebral cortex that were most affected. Granule cells were the most affected target in the cerebellum (Harada, 1995; Takeuchi *et al.*, 1962; Tokuomi, 1960). Although the CNS is the primary target, the peripheral nervous system (PNS) is also affected in adults. Damage and demyelination of the dorsal root and sensory nerve fiber have been observed in the PNS (Takeuchi *et al.*, 1962).

Similar symptoms and pathology were observed in individuals exposed to MeHg in Iraq. Numbness in the extremities and perioral area were the first symptoms observed. Some individuals developed symptoms immediately following the consumption of the contaminated bread, while others developed symptoms weeks (16 – 38 days) to months (60 days) later. The severity of symptoms and the delay of onset were correlated with the level of MeHg exposure. Short exposure times resulted in numbness and paresthesia only. Long-term exposure resulted in ataxia, constriction of visual fields, slurred speech, and hearing difficulties (Bakir *et al.*, 1973; Clarkson *et al.*, 1976).

Children

In Japan and Iraq, children exposed to high levels of MeHg *in utero* or during early childhood exhibited symptoms such as congenital cerebral palsy, mental retardation, primitive reflexes, cerebellar ataxia, disturbances in physical development

and nutrition, dysarthria, deformed limbs, hyperkinesias, hypersalivation, and strabismus (Amin-Zaki *et al.*, 1976; Bakir *et al.*, 1973; Harada, 1977; Takeuchi *et al.*, 1979; Tsubaki and Irukayama, 1977). The mothers of affected newborns suffered very mild levels of sensory disturbances, ataxia, limb pain constriction of visual fields and tremors (Harada, 1995). Hair samples from the mothers in Minamata analyzed five to eight years following initial exposure indicated 1.82 – 191 ppm of mercury, whereas, their children's hair samples indicated 5.25 – 110 ppm. Pathological findings upon autopsy of children exposed to MeHg *in utero* included atrophy and hypoplasia of the cortex, abnormal cytoarchitecture, hypoplasia of the corpus callosum, and dysmyelination of the pyramidal tract (Matsumoto *et al.*, 1965).

Mechanisms of toxicity

Mercury and its compounds have an affinity for sulfur and sulphydryl groups. Mercury-containing molecules can bind to sulphydryl-rich proteins during translation, or in enzymes or membranes. This binding may constitute a general mechanism of mercury toxicity. Specific hypotheses for the mechanism of methylmercury toxicity include: 1) disturbances of protein and nucleic acid synthesis, 2) aberrant post-translational protein modification, 3) disturbance of Ca^{2+} homeostasis, and 4) oxidative injury.

Disruption of protein synthesis may be an early indication of MeHg toxicity (Verity *et al.*, 1977; Yoshino *et al.*, 1966). Cerebral and cerebellar slices from rats exposed to MeHg *in vivo* showed decreased incorporation of [^{14}C] leucine prior to the appearance of neurological symptoms (Verity *et al.*, 1977; Yoshino *et al.*, 1966). Similarly, decreased incorporation of [^{14}C] leucine was observed in rat brain slices and synaptosomes exposed to MeHg in culture (Verity *et al.*, 1975). Sarafian *et al*. (1984) showed a decrease in protein synthesis in 50% of isolated neonatal cerebellar cells exposed to 14 μM MeHg. The protein synthesis inhibition occurred independent of RNA synthesis, mitochondrial function, and ATP content. They suggested that the inhibition was due to direct interaction of MeHg with the protein synthetic machinery. MeHg has a high affinity for thiol or sulphydryl (-SH) groups and will form complexes with –SH-

rich compounds, such as the amino acid cysteine. The methylmercury-cysteine complex resembles the amino acid methionine, which is important in the initiation of polypeptide chains (Fig I-25) (Clarkson, 1987). The substitution of the MeHg-cysteine complex with methionine may disrupt translation.

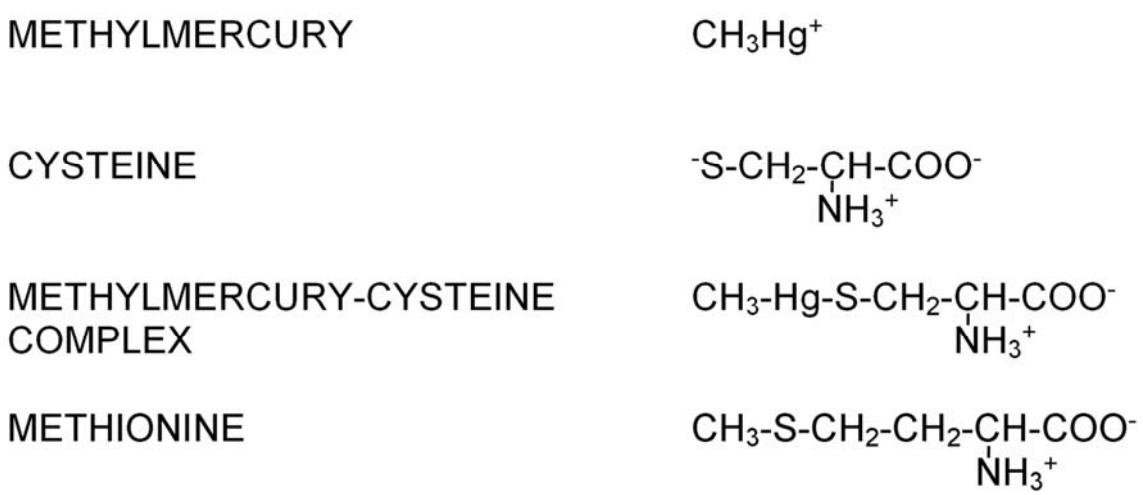

FIG. I-25. Comparison of the methylmercury-cysteine complex structure to methionine. The MeHg-cysteine and methionine structures are similar and could result in the MeHg-cysteine complex mimicking and competing with methionine.

MeHg inhibits DNA and RNA synthesis as well (Brubaker *et al.*, 1973; Chang and Hartmann, 1972; Syversen, 1982). In contrast to the progressive inhibition of DNA synthesis observed with MeHg, Hg^{2+} has been shown to stimulate DNA synthesis prior to the onset of inhibition (Nakada and Imura, 1980).

Studies have revealed that inhibition of DNA, RNA, and protein synthesis, both *in vivo* and *in vitro*, are mediated by at least three separate, possible mechanisms. There is MeHg-inhibition of protein synthesis associated with: 1) selective inhibition of the activities of one or more aminoacyl-tRNA synthetases (post-transcriptional modification) (Cheung and Verity, 1985; Hasegawa *et al.*, 1988); 2) reduction of the ATP/ADP ratio (mitochondrial involvement) (Kuznetsov and Richter, 1987; Kuznetsov *et al.*, 1987); and 3) formation of a complex that can block or interfere with protein synthesis (binding to –SH groups).

Other possibilities of MeHg alterations in post-transcriptional or translational modification have been studied. MeHg (3.0 μM) has been shown to enhance phosphorylation of proteins in cultured cerebellar granule neurons by 300 – 500% after twenty-four hours of exposure (Sarafian and Verity, 1990). However, 1.0 and 5.0 μM MeHg inhibits phosphorylation of intermediate filament proteins in rat cerebral cortex slices. This inhibition was ameliorated by application of 15 μM diselenide (Moretto *et al.*, 2005). Data also indicate that MeHg affects the de-sialylation of neural cell adhesion molecules (NCAMs). NCAMs are molecules whose proper temporal and spatial expression is important during synaptic structuring in neurodevelopment. MeHg inhibits the conversion of embryonic NCAM to the adult form in the cerebella of neonatal mice treated for 4 days beginning at P1 (Reuhl *et al.*, 1994). There is a failure of the embryonic NCAM to be de-sialylnated into the adult form. This failure may alter the stereotypic formation of neuronal contacts and could contribute to the behavioral and morphological disturbances observed following MeHg exposure during early development (Dey *et al.*, 1999). In another study, the amount of detyrosinated tubulin and tubulin-tyrosine ligase in the cytosol of brain cells from rats treated with MeHg (10 mg/kg/day, for 7 days) was decreased, suggesting that MeHg alters cellular activities associated with the tyrosination status of the tubulin (Ishida *et al.*, 1997). Other studies have also indicated a connection between MeHg and tyrosination of tubulin (Falconer *et al.*, 1994; Graff *et al.*, 1997).

Several studies have implicated MeHg in microtubule disruption. MeHg binds to the tubulin dimer SH-groups and depolymerizes the cytoplasmic microtubules, or inhibits their polymerization in mouse glioma cells and fibroblasts (Miura *et al.*, 1984; Sager *et al.*, 1983), resulting in mitotic arrest (Miura *et al.*, 1978; Sager, 1988). Similar findings were demonstrated in the developing rat brain (Rodier *et al.*, 1984; Sager *et al.*, 1984). In addition, tubulin mRNA and protein levels were decreased in mouse glioma cells exposed to 5.0 μM MeHg for three hours. This concentration completely depolymerized the tubules. It is thought that the disruption of the microtubules by MeHg

resulted in the inhibition of the synthesis of tubulin itself through autoregulatory repression in post-transcriptional processes (Miura *et al.*, 1998).

A number of studies have shown that MeHg alters intracellular calcium ion (Ca^{2+}) homeostasis. Studies show that MeHg interacts with voltage-dependent Ca^{2+} channel in the plasma membrane (Atchison, 1986; Shafer *et al.*, 1990). Uptake of extracellular Ca^{2+} into depolarized rat forebrain synaptosomes through voltage-dependent Ca^{2+} channels was depressed by MeHg (70% at 200 μM) and Hg^{2+} (5% at 200 μM) (Atchison *et al.*, 1986). In addition, low-micromolar concentrations of MeHg (0.25 – 1 μM) reduced the amplitude of the current in depolarized cultured neonatal cerebellar granule cells. This reduction was attenuated with the application of various Ca^{2+} channel antagonists, indicating that the alteration in current amplitude was a result of MeHg interaction with the Ca^{2+} channels (Sirois and Atchison, 2000). Later, it was shown that incubation of rat cerebellar granule cells with 0.2 – 5.0 μM MeHg produced an increase in the intracellular Ca^{2+} levels, which could be blocked only through nifedipine- and omega-conotoxin-MVIIC-sensitive pathways, suggesting that L-, N-, and P/Q-type Ca^{2+} channels were involved in entry or mode of action of MeHg (Marty and Atchison, 1997).

MeHg is known to cause release of acetylcholine in the neuromuscular junction (Levesque and Atchison, 1987). This release is thought to be a result of an increase in the free Ca^{2+} within the cell, most likely from mitochondria (Alnaes and Rahamimoff, 1975), smooth endoplasmic reticulum (ER) (Blaustein *et al.*, 1978), influx of extracellular Ca^{2+} (Kirischuk *et al.*, 1996), or the decreased export of intracellular free Ca^{2+} across the plasma membrane (Garcia and Strehler, 1999). Studies suggest that the mitochondria, instead of the ER are a probable source because ruthenium red, which blocks mitochondrial transport of Ca^{2+} via the uptake uniport protein, and N,N-bis (3,4-dimethoxyphenylethyl)-N-methylamine, which inhibits mitochondrial release of Ca^{2+} were more effective at blocking MeHg induced acetylcholine release than inhibitors that block the release of Ca^{2+} from ER (Levesque and Atchison, 1987). Supporting this evidence is a study showing that MeHg blocks the uptake and increases the release of

Ca^{2+} from isolated mitochondria at the same concentrations (10 – 20 μM) that result in spontaneous acetylcholine release from whole neurons (Levesque and Atchison, 1991).

MeHg concentrations of 30 μM cause a moderate increase in intracellular Ca^{2+} levels, inhibit respiration, and cause partial depolarization of the mitochondrial membrane potential in guinea pig cerebral cortical synaptosomes (Kauppinen *et al.*, 1989). Marty and Atchison (1998) showed that 0.5 μM MeHg application for forty-five minutes to rat cerebellar granule cells resulted in decreased viability of the cells, which could be rescued by incubation with the Ca^{2+} chelator 1,2-bis(2-aminophenoxy)ethane-N,N,N′,N′-tetraacetic acid tetrakis(acetoxymethyl)ester (BAPTA; 10 μM).

Most of the Ca^{2+} associated changes that occur upon exposure to MeHg are also related to mitochondria. In addition to the studies previously mentioned, the mitochondria / MeHg relationship has been supported in other studies as well. Sone *et al*. (1977) showed that 10 to 50 nM concentrations of MeHg bind to mitochondrial proteins, inhibit oxidative phosphorylation, cause mitochondrial swelling, and dissipate the mitochondrial membrane potential in isolated mitochondria from rat livers. In neonatal rats receiving injections of MeHg (1.5 mg/kg) every forty-eight hours from postnatal (P) 2 to 50, mitochondria of cortical neurons were condensed, had disrupted cristae, and had accumulation of electron-dense material in the matrix. These observations are consistent with inhibition of mitochondrial respiration (O'Kusky, 1983). MeHg related decreases in the rate of respiration have been observed both *in vitro*, using synaptosomes from rats (Verity *et al.*, 1975) and guinea pig slices (Fox *et al.*, 1975) and *in vivo* in rats (Yoshino *et al.*, 1966).

More recently, MeHg has been implicated in the opening of the permeability transition pore (MTP) in the inner mitochondrial membrane. Dissipation of the mitochondrial membrane potential and opening of the mitochondrial transition pore were observed in cultured rat cerebellar granule cells at MeHg concentrations of 0.2 and 0.5 μM. This effect was delayed by pretreatment of the cells with cyclosporine A (5 μM) (Limke and Atchison, 2002). Opening of the MTP results in the release of molecules < 1.5 kDa, including proapoptotic cytochrome C, thus inducing cell death.

In contrast, MeHg (1.0 mg and 5.0 mg/kg) has been shown to decrease mitochondrial membrane potential and increase mitochondrial Ca^{2+} in acutely isolated cerebellar granule cells from adult mice exposed to MeHg *in vivo*. However, the changes in mitochondrial membrane potential and Ca^{2+} were not associated with increased cell death (Bellum *et al.*, 2007a), but instead with a change in motor coordination and balance (Bellum *et al.*, 2007b). The data from these studies imply that subcellular alterations and abnormal neuronal function resulting in behavioral changes may occur in the absence of cell death.

Reactive oxygen species (ROS) are known to cause oxidative damage in cells. MeHg has been implicated in the elevation of ROS. MeHg induced increase in ROS have been observed in human monocytes (InSug *et al.*, 1997), T-cells (Shenker *et al.*, 1998), and neurons from mice and rats (Ali *et al.*, 1992). In addition, the antioxidant selenium has been shown to be protective against MeHg toxicity (Ganther, 1978; Ganther *et al.*, 1972). MeHg stimulates the rate of ROS production in synaptosomal preparations from the cerebellum of rats and mice (LeBel *et al.*, 1990). In HeLa cells, overexpression of the antioxidant Mn-SOD decreased the toxicity of MeHg (Naganuma *et al.*, 1998). Increased levels of superoxide anion and hydrogen peroxide combined with reductions in the levels of antioxidants such as superoxide dismutase (SOD) and glutathione (GSH) have been observed in cellular fractions of mouse brains following exposure to MeHg (Yee and Choi, 1994). A study by Mori *et al*. (2007) that compared the oxygen consumption, ROS production rates, and antioxidant levels of the cerebrum, cerebellum, and liver of rats exposed to MeHg showed that in control animals, the cerebrum and cerebellum had higher mitochondrial oxygen consumption and ROS productions rates than the liver, and that glutathione peroxidase and superoxide dismutase activities were lower in the cerebrum and cerebellum than the liver. The cerebellum showed the highest oxygen consumption and ROS production rate and the lowest mitochondrial glutathione levels. In the MeHg treated rats, decreased oxygen consumption and increased ROS generation were observed in the cerebellum, but not the liver. Interestingly, this occurred in spite of the fact that the cerebellum contained lower

Hg levels than the liver. The metabolic activity and low defense system of the brain, specifically the cerebellum, may be a cause for the susceptibility of the CNS to MeHg toxicity. In addition, supplementation with succinate substrates increased ROS generation in the cerebellum. This suggests that oxidative stress might affect the complex II-III mediated pathway in the electron transport chain of the cerebellar mitochondria (Mori *et al.*, 2007).

Physiologically, changes in intracellular Ca^{2+}, the production of ROS, and mitochondrial disruption are interrelated. MeHg has been shown to cause changes is each of these parameters individually. Some studies, however, have integrated the three. MeHg (5 μM) decreased mitochondrial function, increased cytosolic and mitochondrial Ca^{2+} concentrations, and increased ROS levels in rat striatal synaptosomes after thirty minutes of exposure (Dreiem and Seegal, 2007). In the same study, the antioxidant Trolox reduced ROS levels, but did not restore mitochondrial function. Similarly, in acutely isolated cerebellar granule cells from mice exposed to MeHg (1.0 μM and 5.0 μM) *in vivo*, Bellum *et al*. (2007a) showed that these cells showed decreased mitochondrial membrane potential, increased mitochondrial Ca^{2+}, and increased rate of ROS production.

Mercury in the CNS interacts with many cellular components, exerting multiple actions at the same time, simultaneously inducing an array of damages and dysfunctions. There are many proposed mechanisms for methylmercury toxicity. Likely, there is not only one mechanism, but many (Fig I-26). The mechanism at work will depend on the exposure level, developmental stage of the organism, local neuronal environmental factors, the species of mercury, etc. Methylmercury is an insidious neurotoxicant with devastating consequence of exposure, and as such, requires complete and well thought out experimental attention.

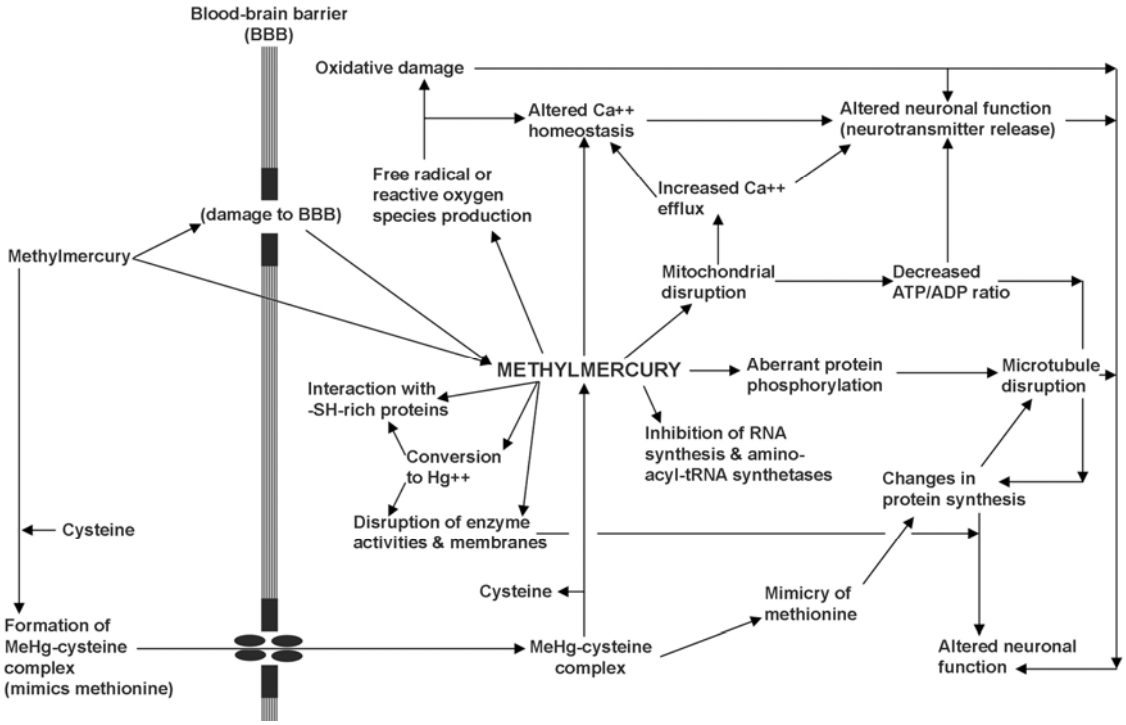

FIG. I-26. Proposed mechanisms of methylmercury neurotoxicity. Modified from Chang, L. W. and Verity, M. A. (1995). Mercury neurotoxicity: Effects and mechanisms: in Handbook of Neurotoxicology (Chang, L. W. and Dyer, R. G. Eds.), p. 41. Marcel Kekker, Inc., New York.

OBJECTIVE OF THIS DISSERTATION

Exposures to chemicals in our environment and the resulting adverse consequences have become important topics of concern in the last century. Recently, concern over exposure to MeHg as a health problem has increased. Headlines in the media such as “Scientists study mercury in the Great Salt Lake: Source and danger of poison to birds, other wildlife remain a mystery” (MSNBC, 2008) and “Autism is linked to mercury poisoning” (Henderson, 2003), have brought the topic of mercury toxicity to the attention of the general public. Appropriate public awareness, toxicity prevention and amelioration of misplaced fear begin with basic scientific research followed by adequate education and subsequent appropriate action.

Although many of the effects of MeHg exposure both in adults and during development are known, the mechanism(s) of toxicity are still unclear. Because it is

impossible to remove MeHg completely from any biological system, and the consumption of fish and associated omega-3 fatty acids are important to human nutrition and health (Domingo, 2007), it is necessary to investigate and understand the mechanisms of toxicity in order to control or minimize the adverse consequences of its exposure and accumulation in the central nervous system.

Scientific literature suggests that mitochondria may be involved in the mechanism(s) of MeHg toxicity. The key function of mitochondria is to provide energy to eukaryotic cells by converting organic materials into adenosine triphosphate (ATP) to fuel cellular processes (Henze and Martin, 2003). In addition, mitochondria are involved in virtually every signaling cascade and metabolic process that has been described, as well as the synthesis and repair of DNA, RNA and proteins (McBride *et al.*, 2006; Pedersen, 1999). Mitochondria are known to respond to calcium ions (Ca^{2+}) and to contribute to the regulation of intracellular Ca^{2+} signaling (McBride *et al.*, 2006). They can sequester intracellular Ca^{2+} to dampen or buffer potentially toxic increases of cytosolic Ca^{2+} (Chang and Reynolds, 2006; Gunter, 1998; Marty and Atchison, 1998). Conversely, mitochondria can be negatively affected by increased levels of cytosolic Ca^{2+} and initiate the death of the cell (Alberdi *et al.*, 2005; Levesque and Atchison, 1991; Sirois and Atchison, 2000). In addition, they are a major generator of reactive oxygen species (ROS). ROS production is an unavoidable by-product of ATP production that occurs through the electron transport chain located in the inner membrane of mitochondria (Alberdi *et al.*, 2005; Chang and Reynolds, 2006; Lemasters *et al.*, 1998). Overproduction of ROS results in cellular membrane and protein damage.

The levels of MeHg exposure commonly used in both *in vivo* and *in vitro* laboratory experiments are significantly higher than those typically found in the blood of environmentally exposed humans. In addition, *in vivo* experiments, historically, have involved acute exposures via drinking water or intraperitoneal injection. We know however, that animals and humans are exposed to chronic levels of MeHg through the ingestion of food (Eto *et al.*, 1999; Futatsuka *et al.*, 2000). Few studies have been conducted that focus on sub-lethal cellular effects of MeHg at chronic environmentally

relevant exposure levels with appropriate routes of exposure. Previous studies in our lab indicate that behavioral changes occur in adult animals exposed to low-levels of MeHg during gestation (Montgomery *et al.*, 2008). Our studies suggest that MeHg can exert its toxic effects at low-levels as well as high.

Many currently conducted mechanistic studies use immortalized or primary cell cultures. However, these types of cells may not function similarly to cells *in vivo*. Cell culture studies of both immortalized neuronal cell lines and primary cultured neurons have shown changes in mitochondrial function and in intracellular Ca^{2+} levels when cells are exposed to high concentrations of methylmercury (Allen *et al.*, 2001; Shanker and Aschner, 2001; Soderstrom and Ebendal, 1995; Wilke *et al.*, 2003). These cells, when exposed to MeHg, may not behave the same way as neurons *in vivo*. As a result, the knowledge gained from these studies may not be applicable to the whole animal or to humans due to both the model systems and the MeHg concentrations used.

Based on current literature we know that: 1) mitochondria, Ca^{2+}, and ROS may be involved in MeHg toxicity, particularly at high MeHg concentrations; 2) there are few to no studies involving chronic low to moderate environmentally relevant concentrations of MeHg exposure; 3) there are few to no studies that provide side-by-side comparison of developmental and adult MeHg exposure; and 4) there has been no validation of *in vitro* culture data using *in vivo* models for MeHg.

Therefore, the **overall objective** of this dissertation is to further elucidate the mechanism of MeHg induced neurotoxicity. Within this overall objective were two sub-objectives: 1) compare the mechanism of MeHg neurotoxicity between animals exposed to MeHg as adults and those exposed during gestation, and 2) develop an *in vitro* model of *in vivo* MeHg exposure.

I hypothesize that chronic exposures to moderate and low levels of methylmercury do not cause cell death, but disrupt neuronal cell function via Ca^{2+} dependent mitochondrial changes in both adult and developing neurons *in vivo*, and that an *in vitro* culture system can be used to model this process.

I have designed three specific aims to test the general hypothesis stated above.

Specific Aim 1: evaluate mitochondrial associated subcellular changes in the cerebellum and hippocampus of young adult mice exposed to methylmercury.

Working Hypothesis for Specific Aim 1: Chronic exposure to moderate and low-levels of methylmercury in young adult mice results in mercury accumulation in the cerebellum and hippocampus. The mercury exposure does not result in neuronal cell death, but instead, results in an increase in mitochondrial membrane potential (initial stress response), an increase in cytosolic basal intracellular Ca^{2+} concentration and an increase in the generation of ROS in neurons.

Specific Aim 2: evaluate mitochondrial associated subcellular changes in the developing cerebellum and hippocampus of mice exposed to methylmercury during gestation.

Working Hypothesis for Specific Aim 2: Chronic exposure to moderate and low-levels of methylmercury *in utero* will result in mercury accumulation in the developing cerebellum and hippocampus. Exposure to mercury does not result in cell death, but instead, causes an increase in MMP, an increase in basal intracellular Ca^{2+} concentration, and an increase in ROS generation in developing neurons. Similar results will be observed at postnatal day (P) 0 and P 10.

Specific Aim 3: develop a neuronal *in vitro* model to assess mitochondrial associated subcellular changes in response to inorganic mercury or methylmercury treatment and determine which of the forms of mercury, organic or inorganic, produces effects *in vitro* that are most similar to those observed in the whole animal.

Working Hypotheses for Specific Aim 3: Chronic exposure to moderate and low-levels of methylmercury and inorganic mercury in undifferentiated human SH-SY5Y neuroblastoma cells will result in mercury accumulation within the cells. The

mercury exposure will not result in cell death, but instead, will result in an increase in MMP, an increase in basal intracellular Ca^{2+} concentration and an increase in the generation of ROS in the SY5Y cells. All changes will be concentration dependent and there will be no difference between inorganic and methylmercury treatments.

The following information was collected for each of the Specific Aims: accumulation of total mercury in the tissues or cells, presence or absence of cell death, MMP, basal intracellular Ca^{2+} concentration, and the rate of production of ROS.

MeHg concentrations used were: *Specific Aim 1* – 0, 1.0, or 5.0 μM, *Specific Aim 2* – 0, 0.1, or 1.0 μM, and *Specific Aim 3* – 0, 0.01, 0.1, and 1.0 μM. In addition, inorganic mercury ($HgCl_2$) was used in *Specific Aim 3* at the same concentrations as those for MeHg (0, 0.01, 0.1, and 1.0 μM $HgCl_2$). MeHg was administered to live animals via oral ingestion in moistened rodent chow.

Mercury levels in tissues / cells was determined by the combustion / trapping / atomic absorption method using a Milestone Direct Mercury Analyzer 80 (DMA 80).

Cell death was determined as follows: Specific Aim 1 and 2 (*in vivo*) – Fluoro-Jade staining and activated caspase 3 immunohistochemistry, and Specific Aim 3 (*in vitro*) – Trypan blue exclusion cell counts, lactate dehydrogenase measurement, and measurement of specific live cell and cell death proteins.

Mitochondrial membrane potential (MMP) was determined using fluorescence microscopy and tetramethyl rhodamine methylester perchlorate (TMRM), a lipophilic potentiometric mitochondrial dye.

Basal Ca^{2+} levels were determined using fluorescence microscopy and calcium green 1-AM (CG), a long-wavelength calcium indicator that exhibits an increase in fluorescence emission intensity upon binding to calcium.

The rate of reactive oxygen species (ROS) production was measured using fluorescence microscopy and 5-(and-6)-chloromethyl-2’7’dichlorodihydrofluorescein diacetate acetyl ester (CM-H_2DCFDA), a compound that is oxidized to fluorescent 2’7’dichlorofluorescein (DCF) by the action of ROS.

CHAPTER II

SUBCELLULAR CHANGES IN CEREBELLAR AND HIPPOCAMPAL GRANULE CELLS OF YOUNG ADULT MICE EXPOSED TO METHYLMERCURY

SUMMARY

Whole animal and cell culture studies indicate that cellular changes associated with high methylmercury (MeHg) exposure include induction of apoptosis typically through the intrinsic apoptotic cascade which includes dissipation of the mitochondrial membrane potential (MMP), increased $[Ca^{2+}]_i$, and increased production of reactive oxygen species (ROS). However, severe human MeHg toxicity epidemiological studies and the bulk of whole animal and cell culture laboratory studies have involved MeHg concentrations that are significantly higher than to what the modern human population is exposed. The number of previous whole animal studies using MeHg concentrations at or near environmentally relevant exposure levels are limited. The purpose of this study was to determine whether adult mice exposed to chronic low-levels of MeHg would exhibit increased cell death and changes in MMP, $[Ca^{2+}]_i$, and ROS similar to the changes known to occur with high MeHg exposure concentrations.

Total Hg accumulation, cell death, changes in MMP, $[Ca^{2+}]_i$, and ROS production were determined in cerebella and hippocampi from C57Bl/6 young adult male and female mice exposed to 0, 0.2, or 1.0 mg/kg body weight MeHg per day in food from postnatal day (P)35 to 40. We observed dose-dependent uptake of MeHg by the cerebellum and hippocampus with brain total Hg concentrations representing 0.04 % of the original MeHg dose. Cell death was determined using Fluoro-Jade B staining and activated caspase 3 immunohistochemistry. Cell death in the cerebellum was increased primarily in the 5.0 mg/kg total dose MeHg treatment compared to controls, in females compared to males, and in the molecular and granule cell layers compared to the

Purkinje cell layer, whereas, no abnormal levels of cell death were observed in the hippocampus.

MMP, $[Ca^{2+}]_i$, and ROS were measured in acutely isolated cerebellar and hippocampal granule cells using fluorescence microscopy. MMP and $[Ca^{2+}]_i$ were increased with MeHg treatment to a greater extent in females than males, but ROS were decreased in females compared to males. MMP increases were greater in the cerebellum than the hippocampus, whereas $[Ca^{2+}]_i$ increases were greater in the hippocampus than in the cerebellum. MeHg treatment had no effect on ROS production, but ROS production was increased in the hippocampus compared to the cerebellum.

The changes observed in MMP, $[Ca^{2+}]_i$, and ROS were related primarily to sex and brain region differences rather than MeHg treatment. Varying combinations of MMP, $[Ca^{2+}]_i$, and ROS changes were indicated, suggesting responses associated with cell cycle regulation, cell proliferation, and cytoprotection through Ca^{2+} sequestering by mitochondria and induction of ROS as signaling molecules. These data indicate that MeHg may alter cellular function, rather than inducing cell death at concentrations near those experienced by modern fish eating populations. More thorough studies are necessary to determine the mechanism by which MeHg acts at environmentally relevant concentrations. Further investigation into the mechanism of action of chronic low-level MeHg exposure is warranted.

INTRODUCTION

Neurotoxic effects of methylmercury (MeHg) exposure have been well documented (Clarkson and Magos, 2006; Takeuchi *et al.*, 1962), and over the last decade, extensive research has been conducted to elucidate the mechanisms involved in MeHg toxicity. Early mechanistic studies were based on the premise that MeHg exposure resulted in apoptosis (Fonfria *et al.*, 2002; Kunimoto, 1994; Li *et al.*, 1998; Nagashima *et al.*, 1996), as was suggested by early epidemiological evidence and post-mortem examinations of individuals poisoned by MeHg in Japan and Iraq (Bakir *et al.*, 1973; Matsumoto *et al.*, 1965; Yoshino *et al.*, 1966). Processes associated with

apoptosis such as changes in intracellular calcium ion concentration ($[Ca^{2+}]_i$) (Orrenius *et al.*, 2003; Smaili *et al.*, 2000), depolarization of the inner mitochondrial membrane (Green and Reed, 1998; Montal, 1998), and increased production of reactive oxygen species (ROS) have all been studied in context of the apoptosis / methylmercury toxicity relationship.

MeHg exposure is known to cause changes in $[Ca^{2+}]_i$, mitochondrial membrane potential (MMP), and production of ROS. MeHg produces increased $[Ca^{2+}]_i$ in cerebrocortical synaptosomes (Kauppinen *et al.*, 1989), cerebellar granule cells (Sarafian, 1993), and NG108-15 neuroblastoma/glial hybrid cells (Hare *et al.*, 1993). MMP is decreased by MeHg exposure in astrocytes (Yin *et al.*, 2007) and rat cerebellar granule cells (Limke and Atchison, 2002). Mitochondrial function is altered by MeHg in rat striatal synaptosome (Dreiem and Seegal, 2007). The production of ROS is increased in rat brain mitochondria (Mori *et al.*, 2007) and C6-glial and B35-neuronal cell lines (Kaur *et al.*, 2007) following exposure to MeHg.

In the above listed studies, and a vast majority of others, MeHg experimentation was conducted at high concentrations for short periods of time, using cultured primary or immortalized cell lines. Typical *in vitro* MeHg experiments have used MeHg exposure concentrations ranging from 2.0 to 100.0 μM (Kauppinen *et al.*, 1989; Limke and Atchison, 2002; Sarafian, 1993; Yin *et al.*, 2008). Exposure time periods typically have been 30 min and 1 hour, with exposure time periods ranging from 15 min to 24 hours (Dreiem and Seegal, 2007; Kauppinen *et al.*, 1989; Kaur *et al.*, 2007; Limke and Atchison, 2002). In addition, cultured primary or immortalized cells lines may or may not respond to MeHg in the same manner as cells in the whole animal.

Other than epidemiological studies associated with severe MeHg poisoning such as in Japan (Tsubaki and Irukayama, 1977) or Iraq (Clarkson *et al.*, 1976), or those involving high fish-eating populations as in the Faroe Islands (Myers and Davidson, 1998) and the Seychelles (Cernichiari *et al.*, 1995b), far fewer MeHg studies have been conducted *in vivo*, compared to *in vitro*. As in cell culture studies, most MeHg studies in whole animals have involved relatively high doses that are not environmentally relevant

to modern fish-eating populations. Exposure times and concentrations for MeHg whole animal studies typically have included 2.5 mg/kg daily for 14 days (Yee and Choi, 1994), 1.0 to 3.0 mg/kg for up to 26 months (Weiss *et al.*, 2005), and 6.43 mg/kg daily for 14 days (Farina *et al.*, 2005).

The general human population is exposed to MeHg primarily through the diet and the consumption of both saltwater and freshwater fish. The average human daily intake of MeHg, which includes both fish eating and non-fish eating populations, is 2.4 μg/day (International Programme on Chemical Safety, 1990). A number of high fish-eating communities have been identified where individual intake of MeHg exceeds 200 μg/day (International Programme on Chemical Safety, 1990). The maximum possible daily intake of MeHg from food stuffs in any population is estimated to be 1800 μg/day (International Programme on Chemical Safety, 1990). Assuming the average body weight of an adult individual to be 67 kg, reported daily MeHg intake values translate to 0.036 μg/kg per day for average intake, 2.99 μg/kg per day for individuals in high fish-eating communities, and 26.9 μg/kg per day as the maximum daily intake. Comparing the lowest exposure level for average human populations to the lowest exposure levels used in most MeHg laboratory studies, MeHg concentrations used in the laboratory studies are typically 28,000 times higher than what the average consumer would experience. The highest MeHg exposure level in humans of 26.9 μg/kg per day maximum compared to 6.43 mg/kg daily for laboratory studies (Farina *et al.*, 2005), the experimental MeHg exposure level is 239 times higher than would be maximally experienced by a human individual.

In addition to the high MeHg exposure levels used in most whole animal laboratory studies, the administration of MeHg in most previous studies is not provided through environmentally relevant routes of exposure. Examples of routes of MeHg exposure in whole animal experiments include intraperitoneal injection (Yee and Choi, 1994), drinking water (Weiss *et al.*, 2005), water through an oral catheter, also called gavage, (Mori *et al.*, 2007), and brain microdialysis (Faro *et al.*, 1997). The absorption, distribution, and metabolism of toxicants vary depending on the route of exposure, such

as oral, dermal, inhalational, or by injection. For each specific route of exposure, the vehicle in which the toxicant is carried may also affect the absorption, distribution, and metabolism. For example, MeHg ingested orally in water may not be absorbed in the same manner as MeHg ingested in food, or MeHg ingested orally in food, administered by oral gavage in one bolus, may not be absorbed in the same manner as MeHg ingested in that same quantity of food consumed over an eight to twelve hour time period. Bellum *et al.* (2007c) showed that MeHg administered in food at a single time point was absorbed by the gastrointestinal (GI) tract and transported into the brain to a greater degree than was MeHg administered at a single time point by intraperitoneal injection. Similarly, Bellum *et al.* (2007c) also showed that a specific quantity of MeHg administered over a five-day period was absorbed by the GI tract and transported into the brain to a greater degree than was the same quantity of MeHg administered orally at a single time point.

Current scientific literature suggests that the cerebellum and hippocampus are important brain regions associated with MeHg toxicity. MeHg is known to specifically target and cause cell death in cerebellar granule cells in adult rats, cats, mice, monkeys, and humans (Bellum *et al.*, 2007a; Eto, 1997; Garman *et al.*, 1975; Miller *et al.*, 1985; Syversen *et al.*, 1981). Cerebellar symptoms associated with MeHg toxicity include ataxia, tremor, posture disorders, and uncoordinated movement (Evans *et al.*, 1975; Harada, 1995; Weiss *et al.*, 2005). Other symptoms associated with MeHg toxicity include learning and memory deficits and depression in humans and mice (Grandjean *et al.*, 1999a; Montgomery *et al.*, 2008; Onishchenko *et al.*, 2007; Yokoo *et al.*, 2003). The hippocampus has been shown to be associated with learning and memory and depression in humans and rodents (Campbell and Macqueen, 2004; Shors, 2004; Zola-Morgan *et al.*, 1986). In addition, MeHg is known to cause reduction in neurogenesis, decreases in cell cycle regulator genes, and altered biogenic monoamines in the hippocampus of rats (Burke *et al.*, 2006; Falluel-Morel *et al.*, 2007; Falluel-Morel *et al.*, 2006; Sano *et al.*, 1987). Therefore, the cerebellum and hippocampus were selected for analysis in the present study.

Clearly, mitochondria, Ca^{2+}, and ROS are involved in MeHg toxicity and apoptotic cell death. However, the dose, route of exposure, or experimental model organism in most MeHg studies have not been relevant to human populations. It is the objective of this study to determine whether MeHg exposure in a whole animal model, at or near exposure levels seen in humans, would produce MMP, $[Ca^{2+}]_i$, and ROS effects similar to those described at high MeHg concentrations. We hypothesized that low-level MeHg exposure in young adult mice would result in effects similar to those described in the literature for higher concentrations of MeHg: a dose-dependent increase in total Hg accumulation, cell death, a dose-dependent decrease in MMP, and dose-dependent increases in basal $[Ca^{2+}]_i$ and production of reactive oxygen species. To test this hypothesis, male and female C57Bl/6 mice were exposed to 0.2 or 1.0 mg/kg body weight MeHg per day for five days from postnatal (P) day 35 to 39 via their food. The selected MeHg concentrations ranged from 0.2 mg/kg per day, which is near maximum human consumption, to 1.0 mg/kg per day, which is a value that has been used in current MeHg studies (Weiss *et al.*, 2005). P35 to 39 were selected as exposure time points because the mouse brain is considered to be fully developed by P35, and P35 to P39 have been used in previous MeHg studies (Bellum *et al.*, 2007b; Bellum *et al.*, 2007c). At P40, total Hg levels were measured in cerebellar and hippocampal samples. Sections from cerebella and hippocampi were stained with Fluoro-Jade B or immunolabeled with anti-activated caspase 3 to determine the presence of cell death via apoptosis or by other means. Neurons from cerebella and hippocampi were acutely isolated and examined for changes in MMP, $[Ca^{2+}]_i$, and ROS. Results of this study will provide MeHg toxicity data that can be used for human risk assessment. These data will be helpful in establishing an appropriate minimum exposure level (reference dose) for MeHg in humans.

MATERIALS AND METHODS

Chemicals

Methylmercuric chloride, 95% (MeHg) was purchased from Alfa Aesar (Ward Hill, MA). DOLT-2, DORM-2, and DOLT-3 were purchased from the National Research Council Canada (NRCC), Institute for Environmental Chemistry (Ottawa, Canada). Fluoro-Jade® B was purchased from Millipore (Temecula, Ca). Affinity-Purified Rabbit Anti-human/mouse Activated Caspase 3 was purchased from R&D Systems Inc. (Minneapolis, MN). Biotynilated affinity purified Goat Anti-Rabbit IgG (H+L) was purchased from Vector Laboratories, Inc. (Burlingame, CA). Permount® was purchased from (Fisher Scientific). DPX Mounting Medium was purchased from Electron Microscopy Sciences (Fort Washington, PA). Minimum Essential Medium Eagle (spinner modification with Earle's salts and $NaHCO_3$, without calcium chloride and L-glutamine (SMEM)), Minimum Essential Medium Eagle (with Earle's Salts and L-glutamine, without sodium bicarbonate (MEM)), deoxyribonuclease I from bovine pancreas (DNase I), poly-D-lysine hydrobromide >300,000 kD, L-alanyl-L-glutamine, *tertiary*-butyl hydroperoxide (*t*BHP), Hank's Balanced Salt Solution (modified with $NaHCO_3$ and without phenol red (HBSS)), protease type IX (bacterial from *Bacillus polymyxa*), carbonyl cyanide 3-chloro-phenylhydrazone (CCCP), and thapsigargin were purchased from Sigma-Aldrich, Inc. (St. Louis, MO). Fetal bovine serum (FBS) was purchased from Gemini (Woodland, CA). Anti-NeuN clone A60 IgG1was purchased from Chemicon. Tetramethylrhodamine methyl ester perchlorate (TMRM), Calcium Green™-1 AM, 5-(and 6)-chloromethyl-2'7'-dichlorodihydrofluorescein diacetate acetyl ester (CM-H_2DCFDA), Pluronic® F-127, ProLong® Gold Antifade with DAPI, and Alexa Fluor® 488 donkey anti-rabbit IgG (H+L) were purchased from Invitrogen/Molecular Probes (Eugene, OR). Lab-Tek 2-well chambered coverglasses were purchased from Nunc Inc. (Naperville, IL).

Animals

All animal procedures were carried out in accordance with guidelines described in the *Guide for the Care and Use of Laboratory Animals* (NRC, 1996). Adult male and female C57Bl/6 mice, originally obtained from The Jackson Laboratory (Bar Harbor, MA), were housed at the Laboratory Animal Research and Resource building, Texas A&M University, at constant temperature (21 - 22°C) and humidity (45 – 55%) with a 12-hour light/dark photoperiod. Breeding animals were provided rodent chow and distilled water *ad libitum*. Mice were bred and the offspring weaned at postnatal day (P) 30; the offspring were used for experimentation.

Treatment

MeHg stock solution (1.0 mg/mL) was prepared in distilled water, sterilized by filtration, and stored at 4°C. Working MeHg solutions were prepared from the 1.0 mg/mL stock solution, diluted in sterile distilled water, and stored at 4°C. For each experiment, six male and six female mice were assigned to control (distilled water), 0.2 mg/kg, or 1.0 mg/kg body weight MeHg. Experimental mice were housed individually. Litters were divided such that only one male and one female mouse from a single litter was used for any one experiment; the litter was the statistical unit of measure (EPA, 2000; OECD, 2007). Experimental mice were weaned at P25. The feeding and MeHg administration procedures used in this study have been used successfully in previously published experiments (Bellum *et al.*, 2007a; Bellum *et al.*, 2007b; Bellum *et al.*, 2007c). Dry rodent chow and distilled drinking water were provided *ad libitum*. Starting at P30 and continuing through P34 (a total of 5 days), mice were trained to consume all of 2.0 g of moistened rodent chow in a 12-hour time period. Dry rodent chow was provided *ad libitum* only during the 12 hours of light. During the 12 hours of dark, the dry chow was removed and replaced with 2.0 g of rodent chow that was moistened with distilled water to achieve a crumbled texture. The feeding dish and cage were examined each morning to ensure that each mouse was consistently consuming all of the moistened chow provided. Beginning at P35 and continuing to P39 (five days), MeHg was added to

the moistened rodent chow (distilled water for controls). Distilled drinking water was provided to all animals *ad libitum*. All experimental procedures were carried out on P40, 24 hours following final MeHg administration. Total Hg content in the rodent chow was analyzed as described in the following section to identify any potential Hg exposure to the animals other than what was intentionally administered.

Body, cerebellar, and hippocampal weights

Body, cerebellar, and hippocampal formation (both sides) weights were measured at P40 at the time of tissue collection. Mean and standard error of the mean were calculated and data were analyzed by two-way analysis of variance (ANOVA) to determine main effects and interactions associated with sex and MeHg treatment.

Mercury accumulation

Total Hg was measured to determine the amount of total Hg transported into the cerebellum and hippocampus. Mice were anesthetized with isoflurane and decapitated. The whole brain was removed and the cerebellum and hippocampus dissected, weighed, rapidly frozen in powdered dry ice, and stored at -20°C. Cerebellar and hippocampal tissues were freeze-dried for 48 hours and total Hg content was measured in the Trace Element Research Laboratory at Texas A&M University, by combustion/ trapping / atomic absorption (Salvata and Pirola, 1994) on a Milestone Direct Mercury Analyzer 80, DMA 80 (Milestone Inc., Shelton, CT) equipped with an autosampler and dual cell detector. The DMA 80 was calibrated using a calibration blank and a series of seven aliquots of certified reference standard ranging from 1 to 750 ng Hg. The calibration line was verified using an independent CRM standard (NRCC DOLT-2) and a blank nickel boat. Samples were weighed to the nearest 0.00001 g and placed into the DMA 80 in pre-combusted nickel boats. A method blank, two certified reference materials (DORM-2 and DOLT-3), a spiked sample, and a duplicate sample were included at the beginning and end of each sample run to determine changes in an individual run from beginning to end, differences from one run to the next, and differences between duplicate samples

within a run. The DMA 80 has a detection limit of 0.005 ng Hg and a working range of up to 1000 ng Hg (Milestone, Inc. Shelton, CT). Total Hg accumulation (ng Hg / g wet sample weight) was determined for the cerebellum and hippocampus from each of four to six male and female mice for each treatment group.

Total Hg concentrations, as total Hg content (ng Hg) per unit volume of wet brain (w. w.) tissue (ng/g), was calculated by dividing the total Hg measured in each sample by the measured wet brain tissue weight for that sample. Total Hg concentration values were analyzed by three-way ANOVA to determine main effects and interactions associated with sex, cerebellar and hippocampal brain regions, and MeHg treatment. Significant differences, as indicated by three-way ANOVA, were followed with Tukey's Honest Significant Difference (HSD) and Student's t post hoc tests, as appropriate, to determine differences among all treatments. The average amount of MeHg provided in the original dose was calculated by multiplying the MeHg dose administered (mg/kg) by five days of exposure, multiplied by the average body weight of the mice. The percentage of Hg accumulated in the cerebellum and hippocampus compared to the amount of MeHg provided in the original dose was calculated by dividing the average amount of total Hg measured in brain samples by the amount of MeHg provided in the original dose and multiplying by 100.

Fluoro-Jade B staining

To detect dying neurons, cells were stained with Fluoro-Jade B, an anionic fluorochrome that selectively stains cell bodies, dendrites, axons, and axon terminal of degenerating neurons, but does not stain healthy neurons, myelin, vascular elements or neuropil (Schmued *et al.*, 1997a; Schmued *et al.*, 1997b). Mice were anesthetized by intraperitoneal injection of 150.0 g/kg ketamine and 15.0 mg/kg xylazine. Once anesthetized, the mice were fixed by transcardial perfusion with 50 mL Tyrode's saline (room temperature) followed by 300 mL cold 4% phosphate buffered paraformaldehyde. Whole perfused mouse bodies were wrapped in foil and kept at 4°C for 24 hours to allow for greater fixation of brain tissue. Brains were removed, immersed in cold 4%

phosphate buffered paraformaldehyde for 48 hours, and then cryoprotected by immersion in cold 20% sucrose in 0.1 M PBS for 48 to 72 hours, or until the brain settled to the bottom of the sucrose solution. Once cryoprotected, brains were rapidly frozen in powdered dry ice and stored at -70°C.

Serial sagittal sections (15 μm), through whole frozen brains, were cut with a SLEE cryostat (Slee, Mainz, Germany), mounted onto gelatin-coated slides, and stored at -70°C. Every seventh section was used for Fluoro-Jade B staining to ensure that no labeled cell was counted twice. Sections from testes of non-treated adult mice and sections of brains from P20-P60 leaner mouse cerebella were used as negative (Fluoro-Jade B dye was excluded from the staining protocol) and positive controls, because both testes and leaner mouse cerebella exhibit a predictable and reliable pattern of cell death as revealed by Fluoro-Jade staining.. The leaner mouse exhibits extensive cell death in the cerebellum from P20-P60 and is therefore a good positive control (Frank *et al.*, 2003; Lau *et al.*, 2004). Leaner mice carry an autosomal recessive mutation in the CACNA1A gene coding for the α_{1A} pore-forming subunit of Ca_V 2.1 voltage-gated calcium channel (P/Q-type) (Herrup and Wilczynski, 1982). This mutation results in extensive cerebellar granule cell death that begins around P10 and continues into adulthood (Herrup and Wilczynski, 1982; Lau *et al.*, 2004). Frozen sections were dried for 1 hour at 50°C, cooled for 10 min, and then stained as described by Schmued and Hopkins (2000). Dried sections were placed in a 1% sodium hydroxide in 80% alcohol solution for 5 min, followed by 70% alcohol for 5 min, distilled water for 2 min, and then immersed and gently shaken in 0.06% potassium permanganate in distilled water for 10 min. Sections were rinsed twice in distilled water, for 1 min each, and then transferred to and shaken gently in 0.0004% Fluoro-Jade B in 0.1% acetic acid and distilled water for 20 min. Sections were then washed with distilled water three times, for 1 min each, and then rapidly dried by blowing cool air onto the slides with an air-gun for approximately 20 min. Dried slides were immersed in xylene twice, for 5 min each, and then coverslipped with DPX mounting media.

Fluoro-Jade B-positive cells were viewed with a Zeiss Axioplan 2 microscope (Carl Zeiss, Thornwood, NY) using a fluorescein isothiocyanate (FITC) filter and equipped with a Color AxioCam camera. Fluoro-Jade B positive cells were counted in each of the ten lobules of the cerebellar vermis and distinguished among the molecular, Purkinje, and granule cell layers. Positive cells also were counted in the dentate gyrus and hippocampus proper of the hippocampal formation. In the dentate gyrus, positive cells were distinguished among the granular and subgranular zones, and the hilus. Positive cells in the pyramidal cell layer of the hippocampus proper were distinguished between the CA1 and CA3 regions. Slides were coded to blind the investigator as to the treatment and gender of the sections during data collection.

Positive cell counts from each region, using a minimum of four sections per animal (six male and six female per treatment), were averaged to obtain the positive counts for each individual animal. Data from the dentate gyrus, hippocampus proper, and cerebellum were analyzed independently by three-way ANOVA to determine main effects and interactions associated with sex, brain region, and MeHg treatment. Differences, as indicated by three-way ANOVA, were analyzed by Tukey's HSD or Student's t post hoc tests, as appropriate, to determine differences among all treatments or brain regions.

Activated caspase 3 immunohistochemistry

Caspase 3 is activated in the process of apoptosis (Burke *et al.*, 2006). Activated caspase 3 immunohistochemistry was used to detect neurons dying by apoptosis. Whole brain fixed/frozen sections adjacent to those used for Fluoro-Jade B staining were used for activated caspase 3 analysis (see Fluoro-Jade B section for tissue and slide preparation procedures). Frozen sections were dried at room temperature for 1 hour, and then permeabilized by immersed in 0.3% Triton-X in 0.1 M phosphate buffered saline (PBS) for 1 hour, followed by three washes in 0.1 M PBS for 10 min each. Washed slides were immersed in 1% hydrogen peroxide in 0.1 M PBS for 5 min, followed by two washes in 0.1 M PBS for 5 min each with gently agitation. Sections were transferred

to 5% normal goat serum in 0.1 M PBS for 1 hour, and then into anti-activated caspase 3 primary antibody (1:25000) in 2% normal goat serum and 0.1 M PBS over night at 4°C (approximately 16 hours). Following application of the primary antibody, sections were rinsed in 0.1 M PBS three times, for 10 min each, and then immersed in biotynilated secondary antibody (1:400) in 0.1 M PBS for 2 hours. Sections were then washed in 0.1 M PBS three times, for 10 min each, followed by immersion in Streptavidin horseradish peroxidase (1:5000) in 0.1 M PBS for 2 hours. Sections were rinsed in 0.1 M PBS once, for 10 min, and then in 0.05 M Tris-HCl buffer (pH 7.6) twice, for 10 min each. Finally, sections were placed in 0.024% diaminobenzadine (DAB) (5.0 µL of 30% hydrogen peroxide, 150.0 mg of 5% nickel ammonium sulfate, 1.0 mL of 6.2 mg DAB per 500 µL, and 24.0 mL of 0.05 M Tris-HCl buffer, at pH 7.6) for 20 min, and then washed in 0.05 M Tris-HCl buffer (pH 7.6) for 5 min, followed by two washes in 0.1 M PBS for 5 min each. Stained slides were dehydrated in a graded series of ethanols (EtOH) and counterstained with a dilute solution of eosin (0.1%) in 95% EtOH. Alcohol dehydration was as follows: 5 min in 70% EtOH, 5 min in 80% EtOH, 4 dips in Eosin in 95% EtOH, 5 min in 95% EtOH, 5 min in 95% EtOH, 5 min in 100% EtOH, and 5 min in 100% EtOH. Following dehydration, tissue was cleared by immersion in xylene two times for 5 min each, and then coverslipped with Permount® mounting media. Activated caspase 3 positive cells were counted and the data analyzed as described for Fluoro-Jade B. As with Fluoro-Jade B, sections from testes of non-treated adult mice and sections of brains from P20-P60 leaner mouse cerebella were used as negative (activated caspase 3 antibody was excluded from the protocol) and positive controls.

Acute isolation of cerebellar granule and hippocampal neurons

Acutely isolated neurons were prepared as described by Oberdoerster (2001) and Bellum *et al.* (2007a). This isolation method yields more than 90% viable cells as demonstrated using 0.08% Trypan blue exclusion and has been used successfully in other published experiments (Bellum *et al.*, 2007a). Cell isolations and subsequent MMP, $[Ca^{2+}]_i$, and ROS imaging were carried out in batches containing one animal from

each treatment group, all of the same gender. Batch experiments allow comparison of data from one day to the next. Mice were anesthetized with isoflurane, and then decapitated. Whole brains were removed and cerebella and hippocampi dissected and placed in SMEM (without Ca^{2+} and Mg^{2+}, with 2.5 mM L-alanyl-L-glutamine). All solutions were cold and on ice unless otherwise specified. Tissues were chopped into ~ 1 mm pieces with a scalpel blade, and then placed in dissociation media (DM), consisting of SMEM, 1.5 U/mL protease, and 2.5 mM L-alanyl-L-glutamine. Neurons were isolated in DM by mechanical disruption on a stir-plate. Each of five stir-cycles included stirring with a stir-bar for 10 min, followed by a 2 min rest period to allow large tissue pieces to sediment. After each stir-cycle, approximately 80% of the DM/cell solution was carefully removed, so as not to disturb large settled pieces of brain tissue, and then combined with growth media (MEM, sodium bicarbonate, L-alanyl-L-glutamine, 10% FBS) and kept on ice. Fresh DM, to replace the removed media, was added to each beaker before beginning the next stir-cycle. DNase I (80 U/mL working concentration) was added during the second stir-cycle. Cell solutions were centrifuged at 1100 x g for 10 minutes and the supernatant discarded. Cell pellets were reconstituted in growth media at 37°C and plated onto chambered coverslips coated in 2.5% gelatin and 1x poly-D-lysine. Prior to use, chambered coverslips were coated with gelatin for 10 min and then in 1x poly-D-lysine overnight (approximately 12 hours) at 4°C. The poly-D-lysine was removed and the coverslips rinsed in warmed (37°C) HBSS a few minutes before the cells were added. The coverslips were not allowed to dry. Each individual isolated cell sample was divided and plated onto three separate coverslips, one for each analysis: MMP, basal $[Ca^{2+}]_i$, and ROS. Plated cells were incubated at 37°C (5% CO_2) for 30 min to allow cells to attach to the coverslip surface.

Identification and validation of acutely isolated cells as neurons

NeuN and DAPI staining of isolated cells were used to identify neurons for subsequent analysis. NeuN is a marker for neurons. In the cerebellum, NeuN is specific for granule cells (Weyer and Schilling, 2003), and in the hippocampus, NeuN is specific for neurons in the granular and subgranular zone and for pyramidal cells of the CA1 and CA3 regions (Domoráková *et al.*, 2006). NeuN intensely labels the nucleus and lightly labels the cytoplasm of neurons (Domoráková *et al.*, 2006; Mullen *et al.*, 1992). DAPI is a fluorescent stain that binds strongly to DNA and is used to identify the nucleus of cells (Robinson *et al.*, 2008). After isolation and a 30 min incubation of plated cells, the growth medium was removed and the cerebellar and hippocampal cells were fixed in 4% paraformaldehyde for 15 min. Cells were then washed in 0.1 M PBS twice for 1 min each, and then permeabilized with 0.3% Triton-X for 5 min. Cells were washed in 0.1 M PBS twice for 3 min each, and then immersed in 5% normal goat serum in 0.1 M PBS for 1 hour. Cells were then placed into NeuN primary antibody (1:2000) (Mullen *et al.*, 1992; Weyer and Schilling, 2003) in 2% normal goat serum and 0.1 M PBS over night (approximately 16 hours) at 4°C. Following incubation in the primary antibody, cells were washed twice for 3 min each, and then immersed in Biotynilated Goat Anti-mouse AF594t secondary antibody (1:400) for 2 hours. Finally, the cells were washed in 0.1 M PBS twice for 3 min each, and then coverslipped with ProLong® Antifade with DAPI (Turville *et al.*, 2008). The DAPI within the ProLong® Antifade solution enters the nuclei of the cells and binds to the nucleic acids during the coverslip drying period. Cells were imaged using a Zeiss Axioplan 2 microscope (Carl Zeiss, Thornwood, NY) with Texas Red and DAPI filters, and equipped with a Color AxioCam camera.

Mitochondrial membrane potential

Tetramethylrhodamine methyl ester (TMRM) was used to detect changes in MMP (Barhoumi *et al.*, 2004). TMRM is a lipophilic potentiometric mitochondrial dye that accumulates in mitochondria in proportion to the membrane potential (Scaduto Jr and Grotyohann, 1999). TMRM dye stock solution (1.0 mM) was prepared in 100%

methanol and stored in desiccant at -20°C. TMRM working solution (150.0 nM) was prepared from the 1.0 mM stock solution in HBSS just before use. The methanol concentration in the working solution was 0.015%. HBSS was used in the TMRM working solution instead of growth media to prevent the TMRM dye from binding to proteins within the medium and inhibiting movement of dye into the cells. After cell isolation and a 30 min incubation, the growth medium was removed from the acutely isolated cerebellar and hippocampal neuronal cultures and replaced with a 150.0 nM solution of TMRM in HBSS for 20 min at 37°C. The TMRM solution was replaced with HBSS for imaging. Three negative controls (HBSS and cells with no dye, HBSS with no cells and no dye, and HBSS with dye, but no cells) and a positive control (HBSS and cells with dye and 20.0 μM CCCP) were included. CCCP was used to determine that the observed fluorescence was associated with the mitochondrial membrane and not other non-specific TMRM fluorescence (Julian *et al.*, 2005). CCCP is a lipid-soluble weak acid that uncouples oxidative phosphorylation in the inner mitochondrial membrane. It enters the mitochondria in a protonated form, discharges the pH gradient, then leaves the mitochondria as an anion, depolarizing the mitochondrial membrane (Lim *et al.*, 2001). When CCCP is co-administered to cells with TMRM, the CCCP-induced depolarization of the inner mitochondrial membrane results in release of accumulated TMRM from mitochondria into the cytosol, and a decrease in fluorescence occurs.

Fluorescent mitochondrial images were collected over a 10 min time period at 63x using a Zeiss Axiovert 200M microscope equipped with a Cy3 filter set (excitation: 560/40 nm, dichroic FT 585; emission: BP 630/75 nm) and SlideBook™ 4.1.0 software from Intelligent Imaging Innovations Inc. (3I, Denver, CO). Image retrieval and MMP fluorescent data collection were performed using Simple PCI and Imaging System Software (v5.0.0.1503, Compix Inc.). Relative MMP values of individual mitochondria from a minimum of ten cells from each animal were measured and averaged to give the MMP value for each of six individual animals from each sex, brain region, and treatment group. Mitochondria were identified as fluorescent, round or oblong-shaped, punctate fluorescence objects within the granule cells.

MMP data were calculated as percentage of control within each batch (one control and one of each treated sample analyzed at the same time) to allow comparison of data from one day to the next. MMP data were analyzed by three-way ANOVA to determine main effects and interactions associated with sex, brain region and MeHg treatment. Differences, as indicated by ANOVA, were analyzed by Tukey's HSD or Student's t post hoc tests, as appropriate, to determine differences among all treatments or brain regions.

Basal intracellular Ca^{2+}

Calcium Green™-1 AM was used to measure the relative concentration of basal intracellular Ca^{2+} (Gilroy and Jones, 1992). Calcium Green™-1 AM is a long-wavelength Ca^{2+} indicator that exhibits an increase in fluorescence emission intensity upon binding to Ca^{2+} (Eberhard and Erne, 1991). The dye is in the AM ester form, which enhances cell permeability and is non-fluorescent in the absence of Ca^{2+} (Lee *et al.*, 1999). Upon binding to Ca^{2+}, the dye exhibits an approximately 100-fold increase in emission intensity, which enables detection of changes in Ca^{2+} concentration within a large dynamic range (Lee *et al.*, 1999). Calcium Green™-1 AM stock solution (2.0 mM) was prepared in DMSO (19.37 µL DMSO to 50.0 µg dye) and stored in desiccant at -20°C for up to two weeks. Working solutions of Calcium Green™-1 AM (1.0 µM) were prepared just before use in 0.01% Pluronic® F-127 and HBSS. The DMSO concentration in the working solution was 0.05%. HBSS was used in the Calcium Green™-1 AM working solution instead of growth media to prevent the Calcium Green™-1 AM dye from binding to proteins within the medium and inhibiting movement of dye into the cells. After cell isolation and a 30 min incubation, the growth medium was removed and replaced with a 1.0 µM solution of Calcium Green™-1 AM in 0.01% Pluronic® F-127 and HBSS for 20 min at room temperature. Incubation of the cells with Calcium Green™-1 AM dye at room temperature prevented compartmentalization of the dye into cellular organelles. The Calcium Green™-1 AM solution was removed and replaced with HBSS for 20 min to allow de-esterification of

the dye. The AM ester of the molecule, which enhances the movement of the dye into the cell, must be removed by endogenous esterases for the dye to fluoresce when bound to Ca^{2+}.

Three negative controls (HBSS and cells with no dye, HBSS with no cells and no dye, and HBSS with dye, but no cells) and a positive control (HBSS and cells with dye and thapsigargin) were included. Thapsigargin is an inhibitor of sarco-endoplasmic reticulum Ca^{2+} ATPases and raises cytosolic free Ca^{2+} by blocking the ability of the cell to pump Ca^{2+} into the endoplasmic reticulum (ER) (Treiman *et al.*, 1998). ER-store depletion can secondarily activate plasma membrane Ca^{2+} channels, allowing an influx of Ca^{2+} into the cytosol (Barhoumi *et al.*, 2006). When thapsigargin is co-administered to cells with Calcium Green™-1 AM, the thapsigargin-induced increase in cytosolic free Ca^{2+} causes a dramatic increase in fluorescence. Fluorescent Ca^{2+} images were collected and analyzed as described for MMP, with the exception that the FITC filter set (excitation: BP 470/20, dichroic FT493; emission: BP 505-530 nm) was used. Relative $[Ca^{2+}]_i$ values from a minimum of ten cells from each animal were measured and averaged to give the value for each of six individual animals from each sex, brain region, and treatment group. $[Ca^{2+}]_i$ data were calculated as percentage of control within each batch (one control and one of each treated sample analyzed at the same time) to allow comparison of data from one day to the next. $[Ca^{2+}]_i$ data were analyzed by three-way ANOVA to determine main effects and interactions associated with sex, MeHg treatment, and brain region. Differences, as indicated by three-way ANOVA, were analyzed by Tukey's HSD and Student's t post hoc tests, as appropriate, to determine differences among all treatments or brain regions.

Reactive oxygen species

5-(and 6)-chloromethyl-2'7'-dichlorodihydrofluorescein diacetate acetyl ester (CM-H_2DCFDA) was used to determine the relative rate of ROS production over time (Bellum *et al.*, 2007a) (Oyama *et al.*, 1994). CM-H_2DCFDA is a non-fluorescent compound that is oxidized to highly fluorescent 2',7'-dichlorofluorescein (DCF) by the

action of ROS (LeBel *et al.*, 1992). The attached chloromethyl (CM) group allows the dye to passively diffuse into cells. Subsequent oxidation of the dye molecule by endogenous esterases traps the derivatives within the cell where they can react with ROS. The CM-H_2DCFDA stock solution (2.0 mM) was prepared in DMSO (43.268 µL DMSO to 50 µg dye) and stored in desiccant at -20°C for up to two weeks. Working solutions of CM-H_2DCFDA (1.0 µM) were prepared just before use in 0.01% Pluronic® F-127 and HBSS. DMSO concentration in the working solution was 0.05%. HBSS was used in the CM-H_2DCFDA working solution instead of growth media to prevent the CM-H_2DCFDA dye from binding to or reacting with proteins within the medium and inhibiting movement of dye into the cells. After the isolation and 30 min incubation, the growth medium was removed and replaced with a 1.0 µM solution of CM-H_2DCFDA in 0.01% Pluronic® F-127 and HBSS for 5 min at room temperature. Incubation of the cells with CM-H_2DCFDA dye at room temperature prevented compartmentalization of the dye into cellular organelles. The CM-H_2DCFDA was removed and replaced with HBSS for imaging. Three negative controls (HBSS and cells with no dye, HBSS with no cells and no dye, and HBSS with dye, but no cells) and a positive control (HBSS and cells with dye and *tertiary*-butyl hydroperoxide (*t*BHP)) were included (Drahota *et al.*, 2005). *t*BHP is a lipophilic, membrane-permeant oxidant (Elliott *et al.*, 1992) that reacts with iron in heme-proteins and produces alkoxyl radicals (Kim *et al.*, 2005b). When *t*BHP is co-administered to cells with CM-H_2DCFDA dye, the *t*BHP-induced increase in ROS causes an increase in fluorescence. Fluorescent images were collected every 2.5 min for 30 min, as described for MMP and $[Ca^{2+}]_i$, using the FITC filter set. The relative amount and rate of ROS production was calculated using a minimum of five cells from each animal.

ROS data were calculated as percentage of control within each batch (one control and one of each treated sample analyzed at the same time) to allow comparison of data from one day to the next. A three-way MANOVA with repeated measures for ROS reading time was used to assess between- and within-subject differences and interactions associated with sex, brain region, and MeHg treatment. The condition of sphericity was

analyzed. The condition of sphericity was not met in any of the ROS data analyzed; therefore, the Greenhouse-Geisser adjusted univariate analysis was used for subsequent within-subject analyses (Grieve, 1984).

Statistical analyses

All data were represented as mean (*M*) ± standard error of the mean (*SEM*). Detailed descriptions of statistical analyses have been described within the text for each experiment. In brief, data for MMP, $[Ca^{2+}]_i$, and ROS were calculated as percentage of control to normalize batch differences. A three-way MANOVA with repeated measures for ROS reading time, followed by the Greenhouse-Geisser adjusted univariate test was used to assess differences among sex, brain regions, and MeHg treatment for ROS. All other experiments were analyzed using a two- or three-way ANOVA and Tukey's HSD or Student's t post hoc tests, as appropriate, to determine main effects and interactions for sex, brain regions, and MeHg treatment. For all experiments, $\alpha = 0.05$, and all data were analyzed using JMP 7.0.2 statistical software from the SAS Institute Inc. (Cary, NC).

RESULTS

General observations

Over the course of the study, mice appeared healthy with no obvious changes in movement or behavior. Data are represented as (*M* = mean, *SEM* = standard error of the mean). Body, cerebellar, and hippocampal weight for young adult mice were analyzed by two-way ANOVA to determine differences and interactions associated with sex and MeHg treatment. Two-way ANOVA for body weights indicated a main effect for sex, $F(1, 78) = 56$, $p < 0.0001$. Student's t post hoc analysis indicated that male mice (*M* = 19.3 g, *SEM* = 0.2) weighed more than female mice (*M* = 16 g, *SEM* = 0.20). No body weight differences were indicated among MeHg treatments. There was no difference in the weight of cerebella (*M* = 0.054 g, *SEM* = 0.0008) or hippocampi (*M* = 0.027 g, *SEM*

= 0.0008) between sexes or among MeHg treatment groups as analyzed by two-way ANOVA.

Mercury accumulation

Total mercury (Hg) concentrations presented as total Hg content (ng Hg) per unit volume of wet brain (w. w.) tissue (ng/g), were calculated by dividing the total Hg measured in each sample by the measured wet brain tissue weight for that sample. Total Hg concentration values were analyzed by three-way ANOVA for differences and interactions associated with sex, cerebellar and hippocampal brain regions, and MeHg treatment. Analysis indicated a main effect for MeHg treatment, F (2, 34) = 332, $p <$ 0.0001. There was no difference in total Hg concentration between sexes or between cerebellar or hippocampal brain regions. Tukey's HSD post hoc analysis indicated that total Hg concentration was increased in the 5.0 mg/kg total dose treatment (M = 980.0 ng/g, *SEM* 52.0) compared to the 1.0 mg/kg total dose treatment (M = 170.0 ng/g, *SEM* = 7.0) and controls (M = 0.71 ng/g, *SEM* = 0.14), and that Hg accumulation was increased in the 5.0 mg/kg treatment compared to controls (Table II-1). The average amount of MeHg provided in the original dose was calculated to be 0 for controls, 17,500 ng for 0.2 mg/kg per day, and 87,500 ng for 1.0 mg/kg per day (Hg dose mg/kg multiplied by five days of exposure, and then also multiplied by an average measured mouse body weight of 17.5 g). The percentage of Hg accumulated in the cerebellum and hippocampus compared to the amount of MeHg provided in the original dose was calculated by dividing the average amount of total Hg measured in brain samples divided by the amount of MeHg provided in the original dose and multiplying by 100. The percentage of total Hg accumulated in cerebellar and hippocampal regions of the brain were 0.04 % for the 1.0 mg/kg total dose MeHg treatment, and 0.05 % for the 5.0 mg/kg total dose MeHg treatment (Table II-1). Hg content for a method blank, two certified reference materials, a spiked sample, and a duplicate sample were analyzed to determine changes in an individual run from beginning to end, differences from one run to the next, and differences between duplicate samples within a run. No intra-run, between-run, or

between-duplicate sample differences were observed (data not shown). The recovery rate for certified reference materials and spiked samples ranged from 92 to 99% (data not shown). Total Hg content in the rodent chow was analyzed to identify potential Hg exposure other than what was intentionally administered. Total Hg levels in the rodent chow were below the level of detection for the analysis used (< 0.005 ng, data not shown).

TABLE II-1

Total Mercury Accumulation in Cerebella and Hippocampi of Young Adult Mice Following Exposure to 0, 1.0, or 5.0 mg/kg Total Dose Methylmercury Divided Over Five Days

	Total Hg Accumulation in Cerebella and Hippocampi Combined		
	Hg (ng)	Hg / w.w. (ng/g)	% Original Dose
Controls	0.029 (0.0050)	0.71 (0.14)	NA
1.0 mg/kg	7.0 (0.71)	170 (7.0) *	0.040
5.0 mg/kg	39 (3.7)	980 (52) *†	0.045

Data are represented as mean (standard error of the mean).
Hg (ng) = total Hg content measured in both cerebella and hippocampi
Hg / w.w. (ng/g) = total Hg content measured divided by the wet tissue weights of cerebella and hippocampi
% Original Dose = total Hg content measured in cerebella and hippocampi expressed as a percentage of the entire MeHg dose administered to the whole animal
Total Hg concentration was analyzed by three-way ANOVA to determine differences associated with sex, brain region, and MeHg treatment, followed by Tukey's HSD post hoc test. Both MeHg treatments were significantly increased compared to controls (*). The 5.0 mg/kg MeHg treatment was increased compared to the1.0 mg/kg treatment (†). No differences in total Hg concentration were observed between sexes or between cerebellar and hippocampal brain regions.
Three-way ANOVA: F (2, 34) = 332, $p < 0.0001$, $\alpha = 0.05$.

Fluoro-Jade B and activated caspase 3

The number of Fluoro-Jade B positive dying cells in the dentate gyrus was analyzed by three-way ANOVA to determine differences and interactions associated with sex, dentate gyrus cell layer, and MeHg treatment. Data indicated differences in the number of dying cells among the cell layers of the dentate gyrus, F (2, 87) = 42, $p <$ 0.0001, but no differences in sex or MeHg treatment (Fig II-1). Tukey's HSD post hoc analysis indicated that the hilar region exhibited fewer dying cells compared to the granular and subgranular layers, and that the granular layer exhibited fewer dying cells than the subgranular layer. An interaction between cell layers and MeHg treatment also was observed, F (4, 87) = 3.56, p = 0.0098, indicating that the differences in the number of dying cells among the cell layers of the dentate gyrus were greater in controls than in MeHg treated mice. No differences were observed in the number of Fluoro-Jade B positive dying cells among sexes, cell layers, or MeHg treatments in the hippocampus proper (CA1 and CA3 pyramidal cells) when analyzed by three-way ANOVA.

Similar cell death results were observed in the dentate gyrus when analyzed by positive labeling for activated caspase 3 (Fig II-1). The number of activated caspase 3 positive dying cells in the dentate gyrus was analyzed by three-way ANOVA. Data indicated differences in the number of dying cells among the cell layers of the dentate gyrus, F (2, 87) = 34, $p < 0.0001$, but no differences in sex or MeHg treatment. Tukey's HSD post hoc analysis indicated that the hilar region exhibited fewer activated caspase 3-positive cells compared to the granular and subgranular layers, and that the granular layer exhibited fewer activated caspase 3-positive cells than the subgranular layer. An interaction between cell layers and MeHg treatment also was observed, F (4, 87) = 2.5, p = 0.0490, indicating that the differences in the number of dying cells among the cell layers of the dentate gyrus were greater in controls than in MeHg treated mice. Similar to the results indicated by Fluoro-Jade B staining, no differences were observed in the number of activated caspase 3 positive dying cells among sex, cell layer, or MeHg treatment in the hippocampus proper when analyzed by three-way ANOVA.

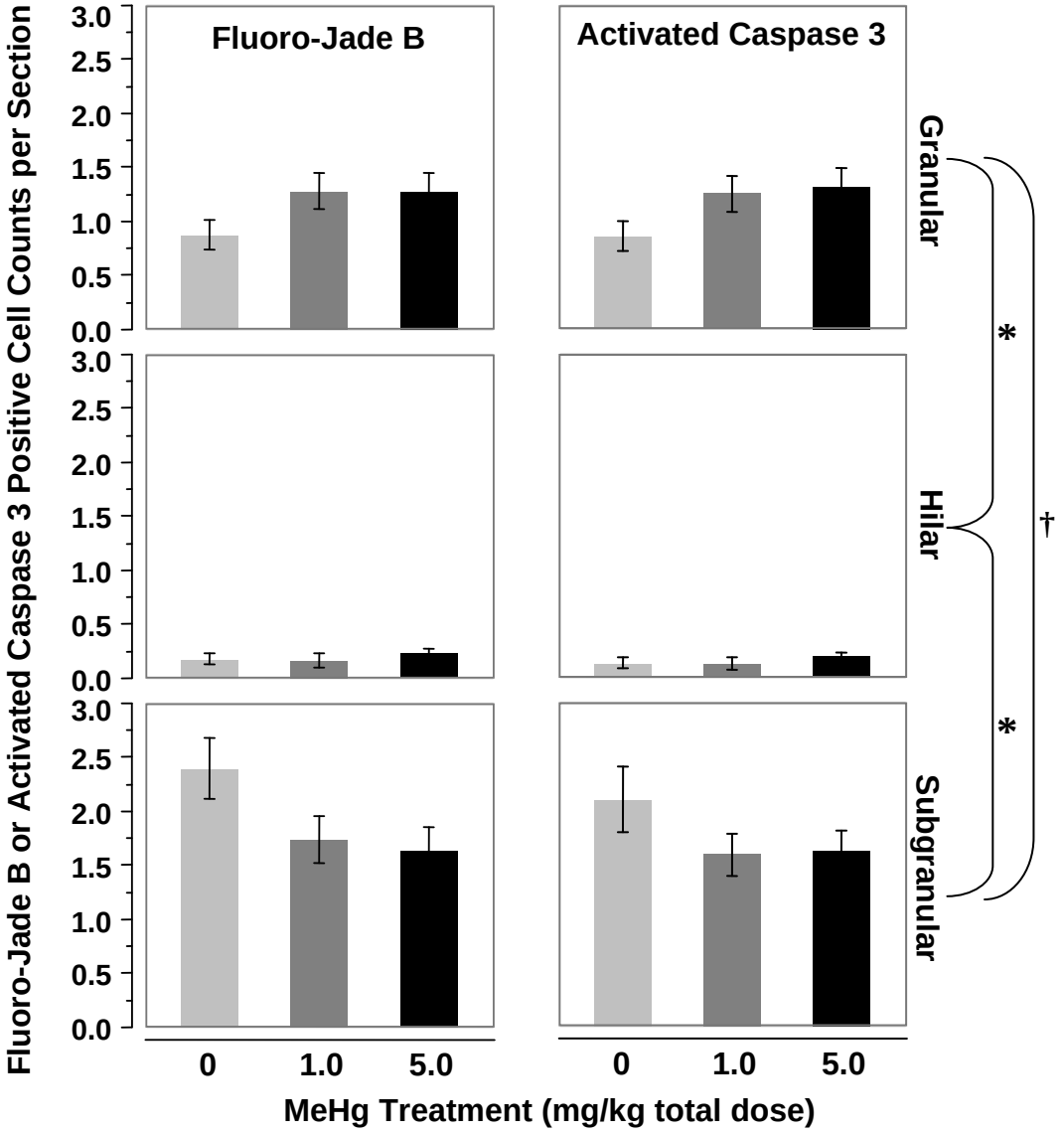

FIG. II-1. Fluoro-Jade B and activated caspase 3 positive cell counts in the granular, hilar, and subgranular cell layers of the dentate gyrus of young adult mice treated with 0, 1.0, or 5.0 mg/kg total dose MeHg divided over five days. There was a difference in the number of dying cells among cell layers of the dentate gyrus for both the Fluoro-Jade B (F (2, 87) = 42, $p < 0.0001$) and activated caspase 3 (F (2, 87) = 34, $p < 0.0001$) methods when analyzed by three-way ANOVA. Tukey's HSD post hoc analysis indicated that the subgranular and granular layers exhibited more dying cells than the hilar region (*), and the subgranular layer exhibited more dying cells than the granular layer (†). No difference was observed in the number of Fluoro-Jade B or activated caspase 3 positive dying cells between sexes or among treatments. An interaction in the number of dying cells between cell layers and MeHg treatments was observed (Fluoro-Jade B: F (4, 87) = 3.56, $p = 0.0098$; activated caspase 3: F (4, 87) = 2.5, $p = 0.0490$) indicating that the differences in the number of dying cells among the dentate gyrus cell layers was greater in controls than in MeHg treated mice. Data are represented as mean ± standard error of the mean. $\alpha = 0.05$ for all statistical analyses.

The number of Fluoro-Jade B positive dying cells was analyzed by three-way ANOVA to determine differences associated with sex, cell layers of the cerebellum, and MeHg treatment. Data indicated an overall effect, F (17, 846) = 38.6, $p < 0.0001$, with main effects exhibited for sex, F (1, 846) = 8, $p = 0.0048$, cell layer, F (2, 846) = 46, $p < 0.0001$, and MeHg treatment, F (2, 846) = 38, $p < 0.0001$ (Fig II-2). An interaction among sex, cell layer, and MeHg treatment also was observed, F (4, 846) = 4.42, $p = 0.0015$, indicating that the MeHg treatment differences were greater in females than males and greater in the molecular layer than the granule and Purkinje cell layers. Tukey's HSD post hoc analysis indicated that the molecular and granule cell layers had more dying cells than the Purkinje cell layer for both males and females at all MeHg treatment concentrations. The molecular layer exhibited more dying cells than the granule cell layer for female control and 5.0 mg/kg total dose MeHg treated cerebella, and for male control cerebella. The Student's t-test post hoc analysis indicated that Fluoro-Jade positive dying cells were increased in female control molecular, granule, and Purkinje cell layers compared to those same layers in control male cerebella. Increased numbers of dying cells in females compared to males were observed only in the molecular layer of 5.0 mg/kg treated mice. Tukey's HSD post hoc analysis for treatment differences indicated that Fluoro-Jade B positive dying cells were increased in the 5.0 mg/kg MeHg treatment compared to controls in all cerebellar cell layers in both males and females. The 1.0 mg/kg total dose MeHg treatment exhibited increases in the number of dying cells compared to controls in the granule cell layer of male mice only. Fluoro-Jade B positive dying cells were also analyzed by three-way ANOVA to determine differences associated with sex, cerebellar forebrain / hindbrain, and MeHg treatment for each of the cell layers, independently. No difference was observed in the number of dying cells between the forebrain and hindbrain regions of the cerebellum in any of the three cerebellar cell layers in male or female mice.

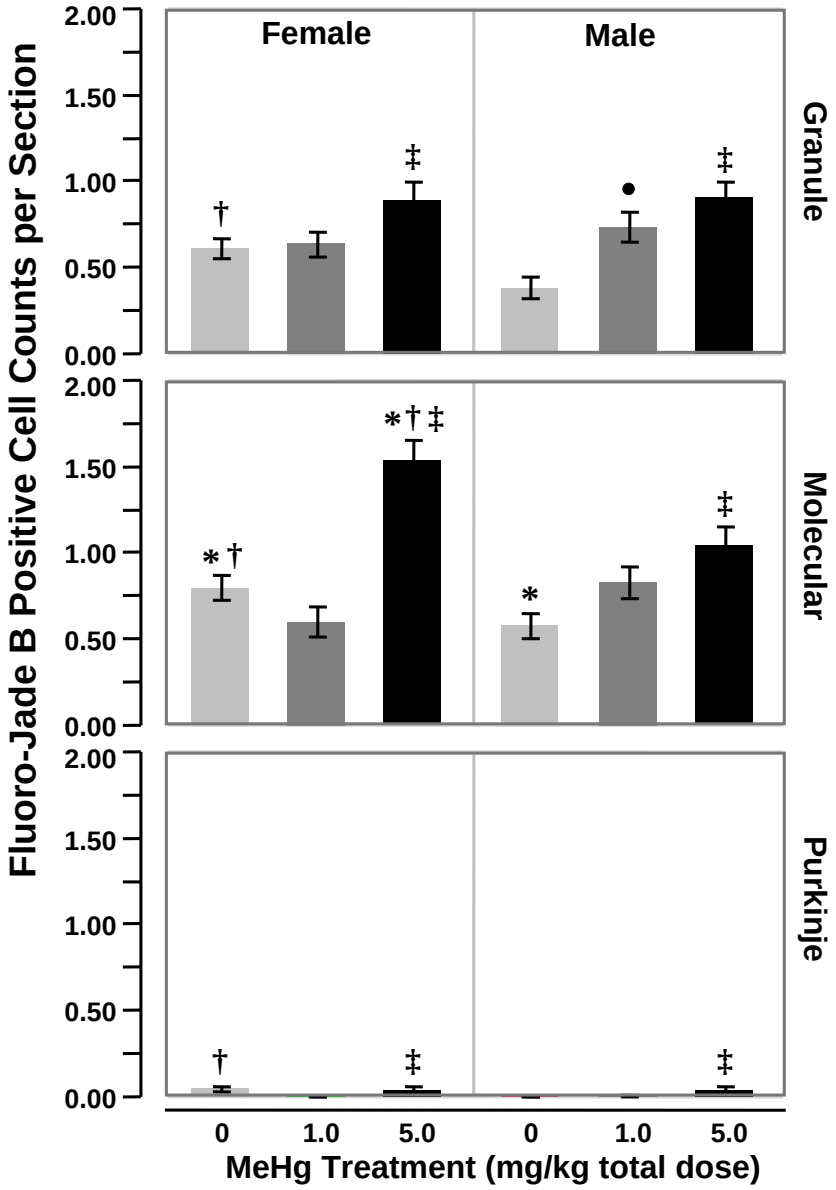

FIG. II-2. Fluoro-Jade B positive cell counts in the granular, molecular, and Purkinje cell layers of the cerebellum of female and male young adult mice treated with 0, 1.0, or 5.0 mg/kg total dose MeHg divided over five days. Main effects were indicated for sex, F (1, 846) = 8, p = 0.0048, cell layer, F (2, 846) = 46, $p < 0.0001$, and MeHg treatment, F (2, 846) = 38, $p < 0.0001$. Tukey's HSD post hoc analysis indicated more dying cells in the molecular layer than the granule cell layer for 0 and 5.0 mg/kg MeHg treated females and for control males (*). Dying cells were increased in females compared to males in controls for the molecular, granule, and Purkinje cell layers, and in the 5.0 mg/kg MeHg treatment molecular layer (†). Increased dying cells were observed in the 5.0 mg/kg MeHg treatment compared to controls in all three cell layers for both males and females (‡). Dying cells were increased in the 1.0 mg/kg MeHg treatment compared to controls in the male granule cell layer (•). An interaction in the number of dying cells for sex, cell layer, and MeHg treatment was observed indicating that MeHg treatment differences were greater in females than males and greater in the molecular layer than the granule and Purkinje cell layers, F (4, 846) = 4.42, p = 0.0015. Data are represented as mean ± standard error of the mean. $\alpha = 0.05$ for all statistical analyses.

Results in the cerebellum for activated caspase 3 were similar to those observed for Fluoro-Jade B staining. Three-way ANOVA, used to determine differences associated with sex, cell layers of the cerebellum, and MeHg treatment, indicated an overall effect, F (17, 846) = 30.0, $p < 0.0001$ (Fig II-3). Main effects were indicated for sex, F (1, 846) = 17, $p < 0.0001$, cell layer, F (2, 846) = 30, $p < 0.0001$, and MeHg treatment, F (2, 846) = 33, $p < 0.0001$. An interaction among sex, cell layer, and MeHg treatment also was observed, F (4, 846) = 4.15, $p = 0.0025$, indicating that the MeHg treatment differences were greater in female mice compared to male mice, and greater in the molecular layer than the granule and Purkinje cell layers. Tukey's HSD post hoc analysis indicated that the molecular and granule cell layers exhibited increased dying cells compared to the Purkinje cell layer in both male and female mice for all MeHg treatments, including controls. In addition, the molecular layer exhibited increased dying cells compared to the granule cell layer in the female control mice and in mice treated with a total dose of 5.0 mg/kg MeHg. Student's t-test post hoc analysis indicated increased numbers of dying cells in female mice compared to male mice for all control cell layers and for both the 1.0 and 5.0 mg/kg treated molecular layers. Tukey's HSD post hoc analysis for treatment differences indicated that the number of dying cells in the male molecular and granule cell layers exhibited increased dying cells in the 1.0 and 5.0 mg/kg total dose MeHg treatments compared to controls, and that there were increased numbers of dying cells in the female molecular layer for the 5.0 mg/kg MeHg treatment compared to controls. As with Fluoro-Jade B analysis, a three-way ANOVA was performed to determine differences associated with sex, rostral and caudal regions of the cerebellar vermis, and MeHg treatment for each of the cell layers, independently. Analysis indicated no differences in the number of dying cells between the rostral and caudal regions of the cerebellar vermis in any of the three cerebellar cell layers for male or female mice.

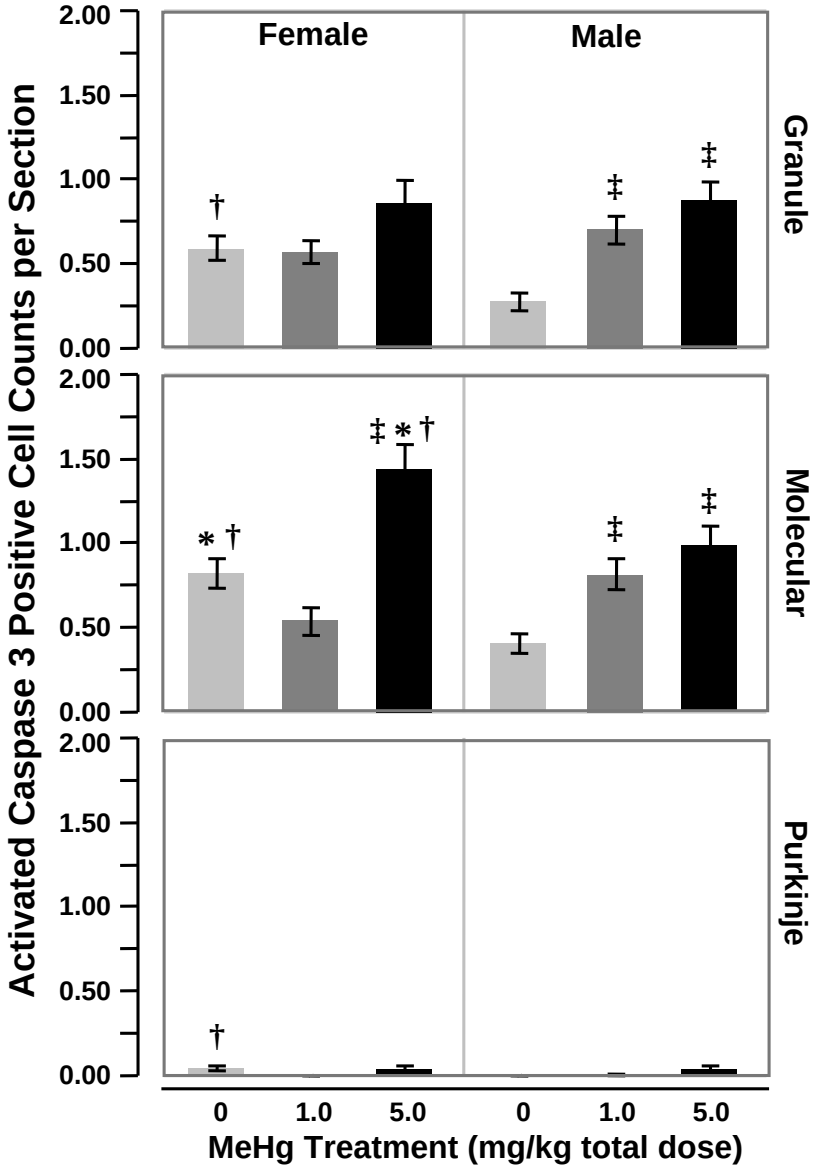

FIG. II-3. Activated caspase 3 positive cell counts in the granular, molecular, and Purkinje cell layers of the cerebellum of female and male young adult mice treated with 0, 1.0, or 5.0 mg/kg total dose MeHg divided over five days. When analyzed by three-way ANOVA, main effects were indicated for sex, F (1, 846) = 17, $p < 0.0001$, cell layer, F (2, 846) = 30, $p < 0.0001$, and MeHg treatment, F (2, 846) = 33, $p < 0.0001$. Tukey's HSD post hoc analysis indicated that dying cells were increased in the molecular layer compared to the granule cell layer in female control and 5.0 mg/kg MeHg treatments (*). Increased numbers of dying cells were observed in females compared to males for all control cell layers and for the 5.0 mg/kg MeHg treated molecular layer (†). In females, the 5.0 mg/kg MeHg treated molecular layer exhibited increased numbers of dying cells compared to controls (‡). In males, the 1.0 and 5.0 mg/kg MeHg treated molecular and granule cell layers exhibited increased numbers of dying cells compared to controls (‡). An interaction in the number of dying cells for sex, cell layer, and MeHg treatment was observed indicating that MeHg treatment differences were greater in females than males and greater in the molecular layer than the granule and Purkinje cell layers, F (4, 846) = 4.15, $p = 0.0025$. Data are represented as mean ± standard error of the mean. $\alpha = 0.05$ for all statistical analyses.

Identification and validation of acutely isolated cells as neurons

Examples of neurons isolated from cerebella and hippocampi of young adult mice are shown in Fig II-4. Double fluorescence imaging using NeuN to label nuclei and cytoplasm of neurons and DAPI to label nuclei of all cells showed the isolation procedure used in this study yielded predominantly more neurons than other cell types. All nuclei were labeled with DAPI (blue) and nuclei and some cytoplasm of neurons were labeled with NeuN (red). Granule cells were distinguished from other neurons based on their small cell size (5 – 8 μm).

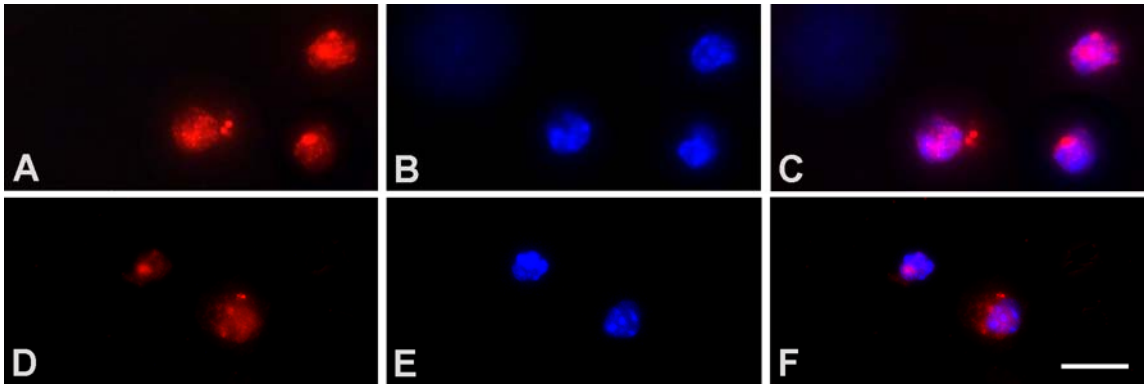

FIG. II-4. NeuN and DAPI double-labeled cells isolated from the cerebellum and hippocampus of young adult control mice. A, B, and C are cells from the cerebellum. D, E, and F are cells from the hippocampus. A and D show cells labeled with NeuN; B and E show cells labeled with DAPI; C and F are overlay images of cell labeled with NeuN and DAPI. Granule cells were distinguished from other neurons based on their small size (5 – 8μm). The majority of isolated cells were double-labeled granule cells. Scale bar = 10 μm.

Mitochondrial membrane potential

Membrane potential (MMP) of the inner mitochondrial membrane of isolated cerebellar and hippocampal granule cells was analyzed using TMRM dye and fluorescence microscopy to determine whether *in vivo* treatment with MeHg altered mitochondrial function. Images of fluorescent mitochondria in hippocampal granule cells are shown in Fig II-5. Analysis by three-way ANOVA indicated an overall difference, F (11, 61) = 6.66, $p < 0.0001$, with between-subject differences among MeHg treatments, F (2, 61) = 12, $p < 0.0001$. Tukey's HSD post hoc analysis indicated that MMP was increased in female cerebellar granule cells exposed to a total dose of 1.0

mg/kg MeHg compared to controls. MMP also was increased in female hippocampal cells exposed to a total dose of 5.0 mg/kg MeHg compared to the 1.0 mg/kg MeHg treatment and controls. In males, Tukey's HSD post hoc analysis for MeHg treatment indicated that male cerebellar granule cells exposed to 5.0 mg/kg MeHg exhibited increased MMP compared to controls (Fig II-6). No between-subject differences were observed between sexes or between cerebellar and hippocampal brain regions; however, an interaction was observed among sex, brain region, and MeHg treatment, F (2, 61) = 7.2, p = 0.0015, indicting that the increased MMP associated with MeHg treatment was greater in females than males, and greater in the cerebellum than the hippocampus. CCCP was added to isolated control granule cells (positive method control) to verify that the method used to measure changes in MMP was, in fact, measuring changes in MMP. CCCP uncouples oxidative phosphorylation within mitochondria which results in decreased MMP. Addition of CCCP to control cells incubated with TMRM resulted in a dramatic decrease in the fluorescence intensity of mitochondria indicating depolarization of the mitochondrial membrane (data not shown); no auto-fluorescence was observed in samples without TMRM dye, nor in samples without cells that contained TMRM dye (negative controls, data not shown).

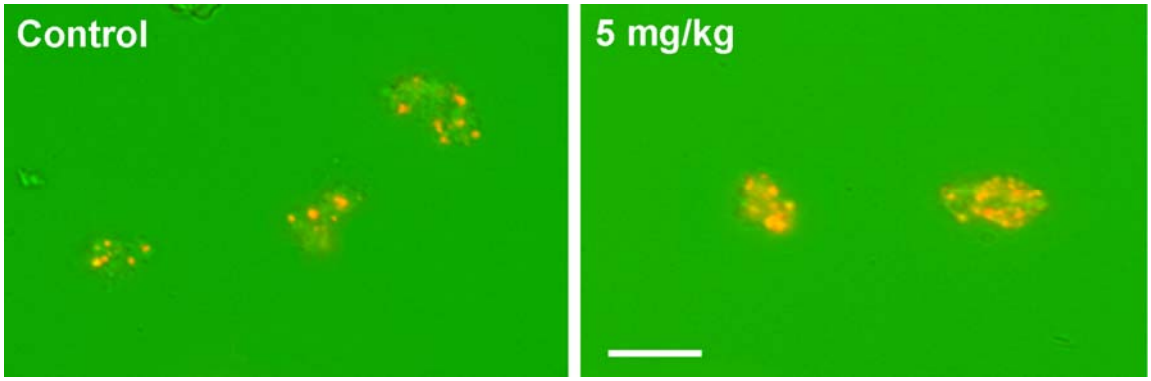

FIG. II-5. Representative images of young adult isolated female hippocampal granule cells treated with 0 or 5.0 mg/kg total dose MeHg divided over five days. Cells were acutely isolated, incubated with 150 nM TMRM for 20 min, and imaged by fluorescence microscopy. Mitochondria accumulated TMRM and appeared as individual red dots within the granule cells. Fluorescence intensity is relative to mitochondrial membrane potential. Mitochondria in 5.0 mg/kg total dose MeHg treated female hippocampal cells exhibited increased fluorescence compared to mitochondria in control cells indicating that MMP was increased in treated cells compared to controls. Scale bar = 10 µM.

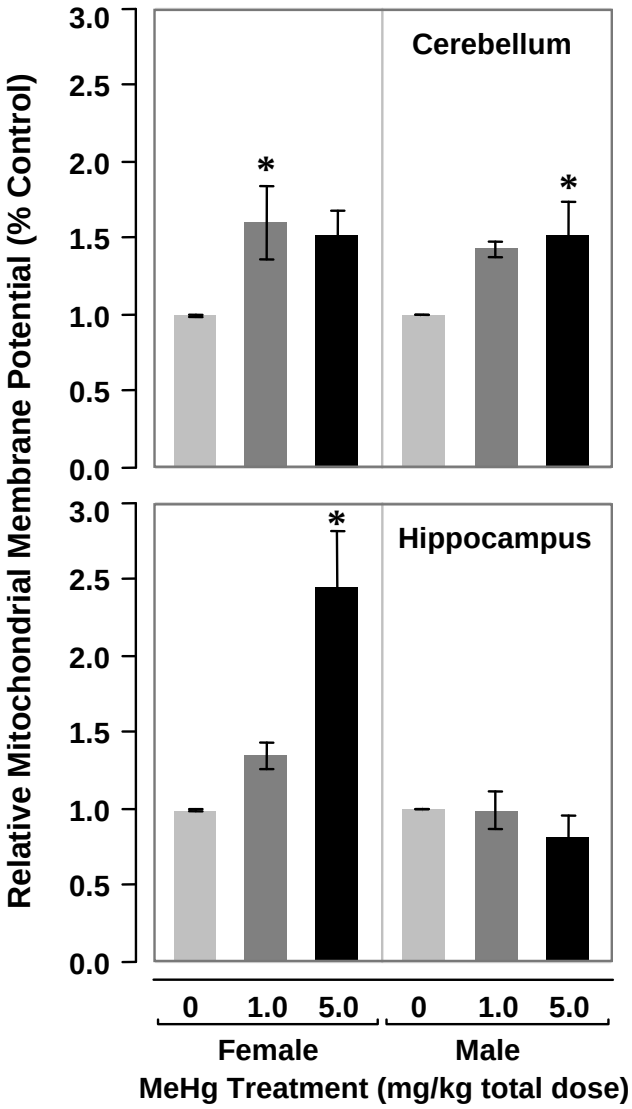

FIG. II-6. Relative mitochondrial membrane potential (MMP) in isolated cerebellar and hippocampal granule cells from young adult mice treated with 0, 1.0, of 5.0 mg/kg total dose MeHg divided over five days. Cells were incubated with 150.0 nM TMRM for 20 min and imaged by fluorescence microscopy. Data were collected for individual mitochondria within the isolated granule cells. Analysis by three-way ANOVA indicated between-subject differences for MeHg treatment, F (2, 61) = 12, $p < 0.0001$, but not for sex and brain regions. An interaction was indicted among sex, brain region, and MeHg treatment, F (2, 61) = 7.2, $p = 0.0015$. Cerebellar granule cells from females treated with 1.0 mg/kg MeHg exhibited increased MMP compared to controls (*). MMP also was increased in female hippocampal granule cells treated with 5.0 mg/kg MeHg compared to 1.0 mg/kg MeHg treated cells and controls (*). For males, MMP was increased in cerebellar granule cells treated with 5.0 mg/kg MeHg compared to controls (*). The observed interaction indicated that differences in MMP associated with MeHg treatment were greater in females than males and greater in the cerebellum than the hippocampus. Data are represented as mean ± standard error of the mean and as % control to eliminate experimental various from day to day; $\alpha = 0.05$ for all statistical analyses.

Basal intracellular Ca^{2+}

Calcium ion homeostasis was examined by measuring $[Ca^{2+}]_i$ in isolated cerebellar and hippocampal granule cells from male and female young adult mice treated with 0, 1.0, or 5.0 mg/kg MeHg for five days. Representative images of fluorescent Ca^{2+} in isolated female hippocampal granule cells from control and mice treated with a total dose of 5.0 mg/kg MeHg treated mice are shown in Fig. 7. Analysis by three-way ANOVA indicated an overall effect, F (11, 60) = 6.75, $p < 0.0001$, with no between-subject differences, but with interactions between brain region and MeHg treatment, F (2, 60) = 4, $p = 0.0247$, and between sex and MeHg treatment, F (2, 60) = 13, $p < 0.0001$. Tukey's HSD post hoc analysis indicated that $[Ca^{2+}]_i$ was increased in the 5.0 mg/kg MeHg treated female hippocampus compared to controls, increased compared to similarly treated male hippocampi, and increased compared to 5.0 mg/kg MeHg treated female cerebellar granule cells. These data and the exhibited interaction indicated that the increase in $[Ca^{2+}]_i$ in the 5.0 mg/kg MeHg treatment were greater in females than males, and greater in the hippocampus than the cerebellum (Fig. 8). Thapsigargin was added to isolated control cerebellar and hippocampal granule cells as a method control to validate the measurement of changes in $[Ca^{2+}]_i$. Thapsigargin is an inhibitor of sarco-endoplasmic reticulum Ca^{2+} ATPases and raises cytosolic free Ca^{2+} by blocking the ability of the cell to pump Ca^{2+} into the endoplasmic reticulum (Treiman *et al.*, 1998). Addition of thapsigargin to isolated control cerebellar and hippocampal granule cells (positive method control) resulted in a substantial increase in the fluorescence within the cells, indicating an increase in $[Ca^{2+}]_i$; no auto-fluorescence was observed in samples without Calcium Green-1, nor in samples without cells that contained Calcium Green-1 (negative controls), indicating minimal atmospheric and/or photo-oxidation (data not shown).

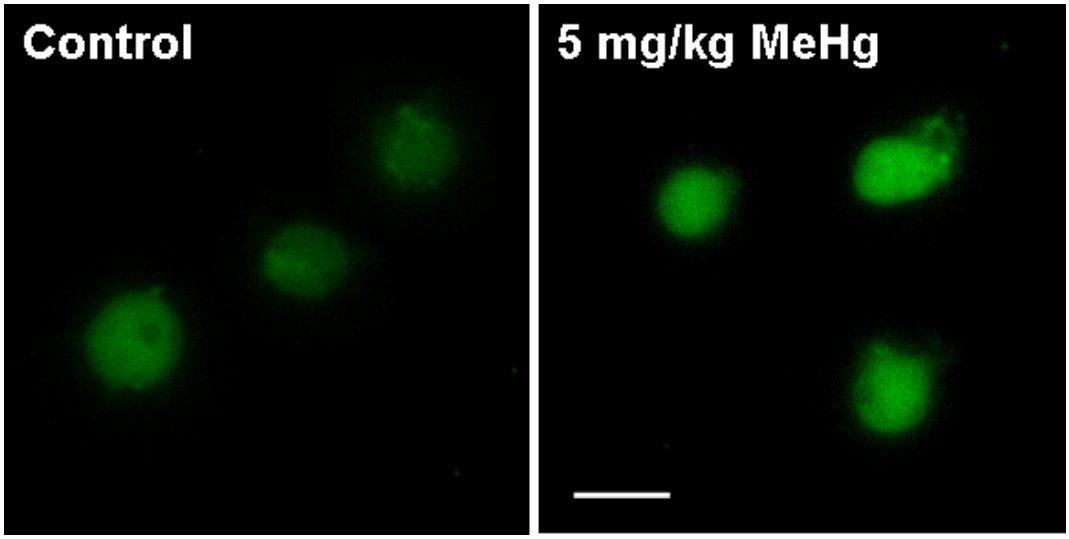

FIG. II-7. Representative images of isolated hippocampal granule cells from a female young adult mouse treated with 0 or 5.0 mg/kg total dose MeHg divided over five days. Free $[Ca^{2+}]i$ bound to Calcium Green-1 dye is green when examined by fluorescence microscopy. Granule cells from the 5.0 mg/kg MeHg treated female hippocampus exhibited increased intensity of green color indicating that the MeHg treated hippocampal cells contained higher levels of free $[Ca^{2+}]i$ than did control hippocampal cells. Scale bar = 10 μm.

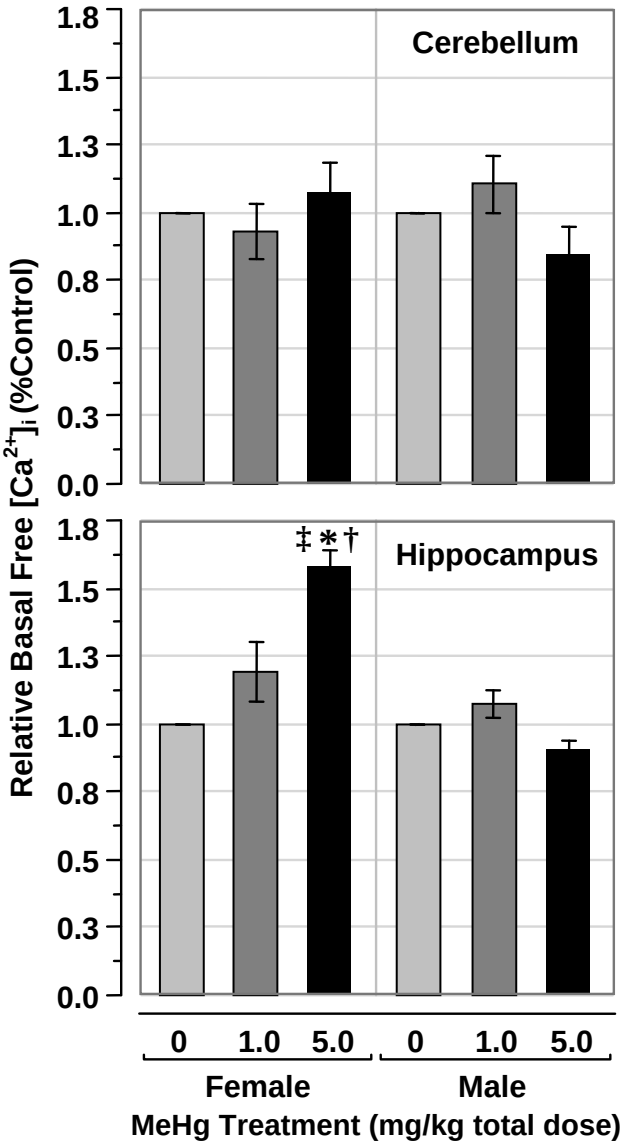

FIG. II-8. Relative basal intracellular free Ca^{2+} ($[Ca^{2+}]_i$) in isolated cerebellar and hippocampal neurons from young adult male and female mice treated with 0, 1.0, or 5.0 mg/kg total dose MeHg divided over five days. Analysis by three-way ANOVA, F (11, 60) = 6.75, $p < 0.0001$, indicated an overall difference, but no between-subject differences associated with sex, brain region, and MeHg treatment. However, interactions were indicated between sex and MeHg treatment, F (2, 60) = 4, $p = 0.0247$, and between brain regions and MeHg treatment, F (2, 60) = 13, $p < 0.0001$. Tukey's HSD post hoc analysis indicated that female hippocampal granule cells treated with 1.0 mg/kg MeHg exhibited higher $[Ca^{2+}]$i than controls (*). In addition, female hippocampal granule cells treated with 5.0 mg/kg MeHg also exhibited higher $[Ca^{2+}]_i$ than similar treated male hippocampal granule cells (†) and female cerebellar granule cells treated with 5.0 mg/kg MeHg (‡). The interactions suggested by three-way ANOVA and specific differences suggested by Tukey's HSD post hoc analyses indicated that the differences in $[Ca^{2+}]_i$ observed in the 5.0 mg/kg MeHg treatment were greater in females than males, and greater in the hippocampus than the cerebellum. Data are represented as mean ± standard error of the mean and as % control to eliminate experimental variation from day to day; $\alpha = 0.05$ for all statistical analyses.

Reactive oxygen species

The rate of generation and the level of ROS in isolated cerebellar and hippocampal granule cells from mice treated with 0, 1.0, or 5.0 mg/kg MeHg divided over five days was measured by fluorescence microscopy and imaging of the fluorescence of the dye CM-H_2DCFDA every 2.5 min for 30 min. Data for the rate of ROS generation were analyzed by three-way MANOVA with repeated measures for ROS reading time to determine between-subject differences associated with sex, brain region, and MeHg treatment. Analysis indicated no between-subject differences or interactions in the rate of ROS production for sex, brain regions, or MeHg treatment. Data did not meet the condition of sphericity; therefore data were analyzed by the Greenhouse-Geisser adjusted univariate analysis to determine within-subject differences (Grieve, 1984). Adjusted univariate analysis for the rate of ROS production indicated within-subject interactions between ROS reading time and sex, F (2, 122) = 3.74, p = 0.0259, and between ROS reading time and MeHg treatment, F (4, 122) = 3.98, p = 0.0043. Within-subject differences in both sex, and MeHg treatment, did not occur until reading time point twelve. These with-subject interactions indicated that the rate of ROS production was increased in males compared to females, and increased in controls compared to the 1.0 and 5.0 mg/kg MeHg treatments over the 30 minutes of reading time (Fig II-9).

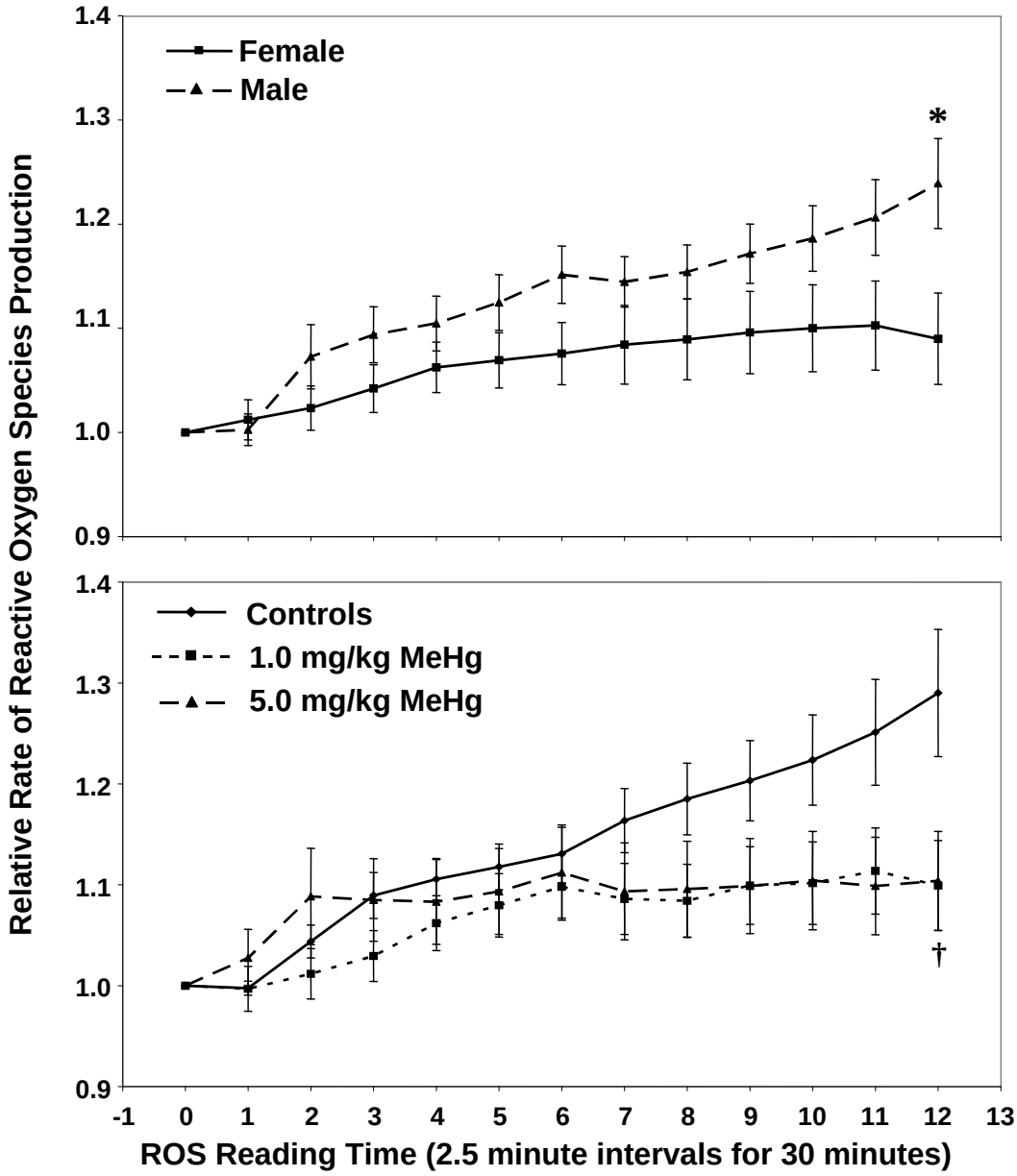

FIG. II-9. Relative rate of reactive oxygen species (ROS) production in isolated granule cells from the cerebellum and hippocampus of young adult mice exposed to 0, 1.0, or 5.0 mg/kg total dose MeHg divided over five days. The rate of ROS production were measured in isolated granule cells from the cerebellum and hippocampus every 2.5 min for 30 min. Data were analyzed by three-way MANOVA with repeated measures for ROS reading time. No between-subject effects were indicated for sex, brain region (cerebellum and hippocampus), or MeHg treatment. Data were further analyzed by adjusted univariate analysis to determine with-subject differences. Data indicated within-subject interactions between ROS reading time and sex, and between ROS reading time and MeHg treatment, that occurred at reading time point twelve. The rate of ROS production was increased in males compared to females (*), and decreased in the 1.0 and 5.0 mg/kg MeHg treatments compared to controls (†). Within subject interactions: reading time and sex, F (2, 122) = 3.74, p = 0.0259, and reading time and MeHg treatment F (4, 122) = 3.98, p = 0.0043; $\alpha = 0.05$.

In addition to the rate of ROS generation, the relative amount of ROS produced was analyzed by three-way MANOVA with repeated measures for ROS reading time to determine between-subject differences and interactions associated with sex, brain region, and MeHg treatment. Analysis indicated between-subject differences in brain region, F (1, 60) = 10.3, p = 0.0021, and sex, F (1, 60) = 7.89, p = 0.0067. In addition, between-subject interactions were indicated for brain region and sex, F (1, 60) = 10.95, p = 0.0016, and for brain region and MeHg treatment, F (2, 60) = 4.36, p = 0.017. The indicated between-subject interactions suggested that the level of production of ROS is increased in males compared to females, and increased in the hippocampus compared to the cerebellum (Fig II-10). Data did not meet the condition of sphericity; therefore data were analyzed by the Greenhouse-Geisser adjusted univariate analysis to determine within-subject differences and interactions (Grieve, 1984). Adjusted univariate analysis for the level of ROS produced indicated within-subject interactions between ROS reading time and sex, F (2, 105) = 1.43, p = 0.0035, and between ROS reading time and MeHg treatment, F (4, 105) = 4.43, p = 0.0037. Within-subject differences in sex began at reading time six and continued to reading time twelve. Within-subject differences in MeHg treatment began at reading time seven and continued to reading time twelve. These within-subject interactions suggested that the level of ROS production was higher in males than females, and higher in controls than MeHg treatments over the 30 minutes of reading time (Fig II-10). *Tertiary* butyl hydroperoxide (*t*BHP) was added to isolated control cerebellar and hippocampal granule cells as a method control to validate the measurement of changes in $[Ca^{2+}]_i$. *t*BHP penetrates the cell membrane and react with heme-proteins to produce alkoxyl radicals. Addition of *t*BHP to isolated control granule cells (positive control) resulted in a dramatic increase in the fluorescence within the cells indicating an increase in the level of ROS; no auto-fluorescence was observed in samples without CMH_2DCFDA dye, nor in samples without cells that contained CMH_2DCFDA (negative control), indicating minimal atmospheric and/or photo-oxidation (data not shown).

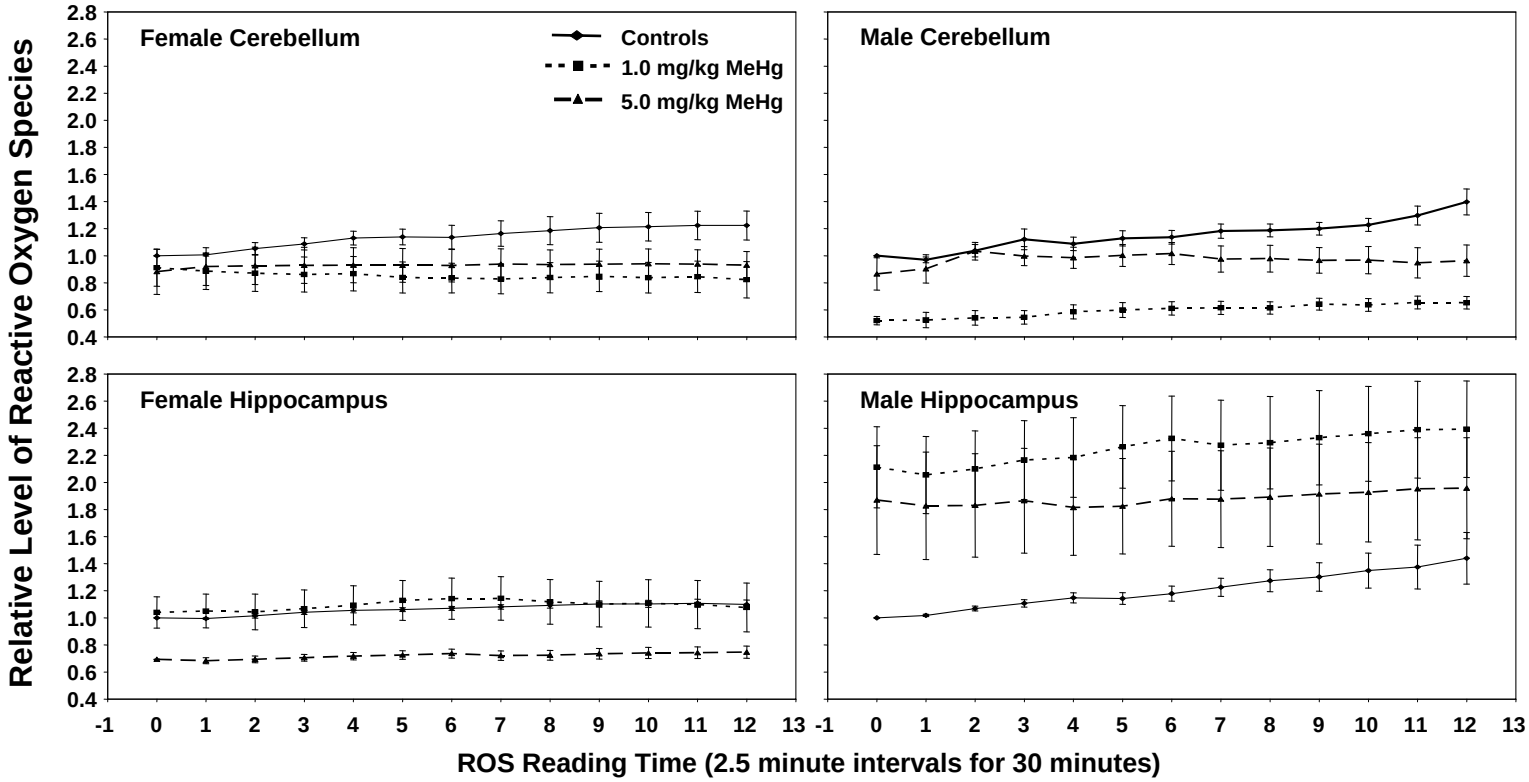

FIG. II-10. Relative level of reactive oxygen species (ROS) in isolated granule cells from cerebella and hippocampi of young adult mice exposed to 0, 1.0, or 5.0 mg/kg total dose MeHg divided over five days. The level of ROS were measured in isolated granule cells from the cerebellum and hippocampus every 2.5 min for 30 min. Data were analyzed by three-way MANOVA with repeated measures for ROS reading time. Between-subject effects were indicated for brain region (cerebellum and hippocampus) and sex. Between-subject interactions were indicated for brain region and sex, and for brain region and MeHg treatment. Level of ROS was greater in males than females, and greater in the hippocampus than the cerebellum. Data were further analyzed by adjusted univariate analysis to determine with-subject differences. Data indicated within-subject interactions between ROS reading time and sex, and between ROS reading time and MeHg treatment. Differences in males and females began at reading time six. Differences among MeHg treatments began at reading time seven. Between-subject effect: brain region, F (1, 60) = 10.3, p = 0.0021, and sex, F (1, 60) = 7.89, p = 0.0067. Between-subject interactions: brain region and sex, F (1, 60) = 10.95, p = 0.0016, brain region and MeHg treatment, F (2, 60) = 4.36, p = 0.017. Within subject interactions: reading time and sex, F (2, 105) = 1.43, p = 0.0035, and reading time and MeHg treatment, F (4, 105) = 4.43, p = 0.0037; $\alpha = 0.05$.

DISCUSSION

As hypothesized, total Hg accumulated in brain tissue, and cell death and $[Ca^{2+}]_i$ increased with MeHg exposure. However, MMP was increased and no differences in ROS were indicated with MeHg exposure. Total Hg accumulated in cerebella and hippocampi in a dose-dependent manner in both male and female mice exposed to MeHg in their food. No difference in the accumulation of total Hg was observed between males and females, or between the cerebellum and the hippocampus. A study by Vahter *et al*. (1995) using *Macaca fascicularis* monkeys given 50 μg/kg body weight MeHg for eighteen months showed evenly distributed total Hg throughout the brain. Similarly, in pigs given a single oral dose of 5.0 mg/kg MeHg (Platonow, 1968), and in mice given 2.0 mg/kg MeHg for five days (Somjen *et al.*, 1973a), no differences were observed in total Hg concentration in the cerebral cortex (4.1 ppm for pigs and 3.1 μg/kg w. w. for rats) and the cerebellum (4.0 ppm for pigs and 3.2 μg/kg w. w. for rats). This same study by Somjen et al. (1973a) reported the percentage of total Hg in all brain tissue compared to the total dose administered to be 0.02 to 0.12 %, which corresponds to our 0.04 to 0.05 % values for the percentage of total Hg in brain tissue compared to the total dose administered.

Fluoro-Jade B staining and activated caspase 3 immunohistochemistry were used to detect the presence of dying cells. Patterns of positively identified dying cells for Fluoro-Jade B and activated caspase 3 were similar in the dentate gyrus of the hippocampus. Although, the three-way ANOVA indicated an overall difference in cell death in the dentate gyrus, post hoc analysis showed increased numbers of dying cells in the granular and subgranular zones compared to the hilar region. The subgranular zone of the dentate gyrus is an area of neurogenesis in the adult hippocampus and will naturally contain greater numbers of dying cells than non-proliferating regions (Eriksson *et al.*, 1998; Gage *et al*.,1998). The data showed an interaction effect in the number of dying cells between cell layers and MeHg treatments, suggesting that the differences in the number of dying cells among regions of the dentate gyrus were decreased in the MeHg treated mice compared to controls. A decrease in cell death in the subgranular or

granular zone may be connected to decreased neurogenesis. MeHg has been shown to decrease cell proliferation and alter cell cycle regulation (Faustman *et al.*, 2002; Mendoza *et al.*, 2002) in developing neurons. This interaction may represent an affect of MeHg on the process of neurogenesis in the subgranular zone, but the low sample size (n = 6) may not be powerful enough to show significant main effects.

Cell death in the cerebellum was increased in females compared to males, in the 5.0 mg/kg total MeHg treatment compared to controls, and in the molecular and granule cell layers compared to the Purkinje cell layer. MeHg is known to cause cell death, particularly in granule cells of the cerebellum of adult humans and animals and in cultured cells (Bakir *et al.*, 1980; Fonfria *et al.*, 2002; Kunimoto, 1994). In the present study, both the granule and molecular layers exhibited increased numbers of dying cells, specifically in the high MeHg treatment group. In support of our findings, literature indicates that cerebellar degeneration associated with high exposure to MeHg involves significant cell death in the granule cell layer, although increased cell death is usually observed in basket and stellate cells of the molecular layer as well (Chang, 1977; Takeuchi *et al.*, 1962). Purkinje cells, however, are preserved upon MeHg exposure (Sager *et al.*, 1984). Although no extensive research in sex differences associated with MeHg-induced cell death exists, a study by Magos *et al.* (1981) revealed that female rats developed more intensive coordination disorders and had more extensive damage in the granular layer of the cerebellum than males with similar MeHg treatment. In contrast, Evans *et al.* (1977) showed that female macaques accumulated Hg within the brain and had neurological signs of MeHg toxicity similarly to male macaques exposed to the same MeHg treatment. Conflicting data on male and female differences in cell death caused by MeHg exposure could be due to species or MeHg concentration differences. As in the current study, Evans *et al.* (1977) used a rodent model, and a somewhat higher MeHg concentration (10 mg/kg total) compared to the present study, whereas Magos *et al.* (1981) used a primate model and higher MeHg concentrations for a longer period of time. Cell death in the present study was observed primarily in the 5.0 mg/kg total MeHg treatment, however, the 1.0 mg/kg total MeHg treatment resulted in increased cell death

in the male granule and molecular cell layers. No literature is available at this time to corroborate the sex difference in cell death observed at lower concentrations. However, Carrillo *et al*. (1992) and Taskiran *et al.* (1997) have reported sex-related differences in antioxidant defenses in the rat brain, with catalase activity being higher in females than males. In addition, liver mitochondria from female rats exhibit higher expression of antioxidant enzymes compared to males (Borrás *et al.*, 2003). Estrogen also is known to exert protective affects by acting as a scavenger of ROS or inducing the synthesis of protective molecules via activation of estrogen receptors (Behl *et al.*, 1995). These protective aspects associated with cells from females may play a role in the decrease in cell death observed in the 1.0 mg/kg total MeHg treated cerebella.

Literature suggests that MeHg exposure decreases MMP (Dreiem and Seegal, 2007), which result in increases in ROS (InSug *et al.*, 1997) that increases $[Ca^{2+}]_i$ (Marty and Atchison, 1998; Ueha-Ishibashi *et al.*, 2004) in dying cells. Our data suggest that changes in MMP, basal $[Ca^{2+}]_i$, and ROS associated with both the 1.0 and 5.0 mg/kg total MeHg treatment concentrations may be indicative of cellular activities other than apoptosis. Our data indicated increased cell death in the 5.0 mg/kg total MeHg treatment, but the typically reported pattern of MMP, $[Ca^{2+}]_i$, and ROS changes was not observed.

The present study indicated that MMP and basal $[Ca^{2+}]_i$ were increased with MeHg treatment to a greater extent in females than males, but that ROS were decreased in females compared to males. As stated previously, females exhibit increased antioxidant defenses compared to males (Behl *et al.*, 1995; Borrás *et al.*, 2003; Carrillo *et al.*, 1992; Taskiran *et al.*, 1997). The process of activating the proteins necessary for these antioxidant defenses may involve increased transcription and translation, both of which would result in increased mitochondrial activity.

We observed that MMP increases were greater in the cerebellum than the hippocampus, whereas $[Ca^{2+}]_i$ increases were greater in the hippocampus than in the cerebellum. $[Ca^{2+}]_i$ in the granule cells of the cerebellum may be held at a stable level by sequestration of Ca^{2+} in the mitochondria. One of the roles of mitochondria is to aid in

the maintenance of $[Ca^{2+}]_i$ homeostasis (Nicholls *et al.*, 2007). Mitochondrial Ca^{2+} uptake is primarily driven by the electrochemical gradient established by the MMP. Energized mitochondria will move Ca^{2+} from the cytosol into the matrix in proportion to the MMP, thus preventing an even greater increase in cell death.

Data also indicted that MeHg treatment had no effect on ROS production, but ROS production was increased in the hippocampus compared to the cerebellum. Studies indicate that ROS play a role in cell cycle progression and cell proliferation. Metabolic by-products of fatty acids have been shown to be stimulatory to cell proliferation (Bégin, 1987). These by-products are a result of oxidation by ROS. The observed increase in ROS production in the hippocampus compared to the cerebellum may be associated with neurogenesis which occurs in the subgranular layer of the hippocampus.

The hippocampus in the present study exhibited decreased cell death with MeHg treatment, in addition to the decreased MMP and increased ROS compared to the cerebellum. Studies show that TNFα induces cytoprotection by inducing the production of free radicals from mitochondria, which stimulates cytoprotective mechanisms. The short-term generation of ROS results in a modest and temporal membrane depolarization (Lacerda *et al.*, 2006). MeHg exposure may exert stress upon hippocampal cells, leading to the production of cytoprotective ROS produced in association with a decrease in MMP over a short period of time.

MMP, Ca^{2+}, and ROS have many functions in neurons other than induction of apoptosis. Neurons exhibit $[Ca^{2+}]_i$ oscillations that may be associated with synaptic strengthening among neurons in the same domain (Singer, 1993; Stryker *et al.*, 1990). In neuronal spines and dendrites, $[Ca^{2+}]_i$ changes are mediated by the NMDA receptor which is crucial for the generation of long-term potentiation (LTP) associated with learning and memory (Alford *et al.*, 1993; Collingridge and Bliss, 1995). $[Ca^{2+}]_i$ changes in neurons initiate signaling pathways that trigger gene transcription (Bailey *et al.*, 1996; Martin *et al.*, 1997). Mitochondria are involved in more than energy production and induction of apoptosis (Green and Reed, 1998). They function in xenobiotic metabolism and glucose sensing (Maechler, 2002), as well as steroid

hormone synthesis and lipid metabolism (Brookes *et al.*, 2004). In addition, ROS are involved not only in damage of membranes by lipid peroxidation (Gardner, 1989) and the crosslinking of proteins (Davies, 2005), but are important for cell signaling (Brookes and Darley-Usmar, 2002; Brookes *et al.*, 2002) and cell proliferation (Burdon *et al.*, 1989).

In summary, we observed dose-dependent uptake of MeHg by the cerebellum and hippocampus. Cell death occurred primarily in the 5.0 mg/kg total MeHg treated cerebellum, but was also observed in the 1.0 mg/kg total MeHg treated male cerebellum. The changes observed in MMP, $[Ca^{2+}]_i$, and ROS were related primarily to sex and brain region differences rather than MeHg treatment. There were varying combinations of MMP, $[Ca^{2+}]_i$, and ROS changes that suggested responses associated with cell cycle regulation, cell proliferation and cytoprotection through Ca^{2+} sequestering by mitochondria, and induction of ROS as signaling molecules. It appears as though exposure to 1.0 mg/kg MeHg divided over five days does not cause cell death and changes in MMP, $[Ca^{2+}]_i$, and ROS in neurons similar to MeHg exposure concentrations at or greater than 5.0 mg/kg divided over five days or more, as indicated by current scientific literature. In addition, total MeHg exposure concentrations of 1.0 mg/kg divided over five days result in an increase in cell death, but the changes in MMP, $[Ca^{2+}]_i$, and ROS are different than what are observed with MeHg exposure concentrations of 5.0 mg/kg divided over five days. No thorough studies have been conducted to determine the mechanism by which MeHg acts at environmentally relevant concentrations. Therefore, based on the data for low-level MeHg exposure in the current study, further investigation into the mechanism of action of low-level MeHg exposure is warranted.

CHAPTER III

SUBCELLULAR CHANGES IN CEREBELLAR AND HIPPOCAMPAL GRANULE CELLS OF MOUSE PUPS EXPOSED TO METHYLMERCURY DURING GESTATION

SUMMARY

Neuropathology observed in children exposed to high levels of methylmercury (MeHg) during gestation or early development includes generalized brain atrophy and abnormal cytoarchitecture of the cerebral and cerebellar cortices. Recent epidemiological research from the Faroe Islands and Brazil suggests that chronic low levels of MeHg in the diets of pregnant females and young children may have a negative affect on motor function, attention, memory, and language development. High levels of MeHg exposure are known to cause changes in $[Ca^{2+}]_i$, mitochondrial membrane potential (MMP), and production of reactive oxygen species (ROS). However, little is known regarding cell death, MMP, $[Ca^{2+}]_i$, and ROS production in neurons from developing fetuses and infants exposed to low levels of MeHg. The purpose of this study was to determine whether developing mice prenatally exposed to MeHg at chronic low levels would exhibit cell death and changes in MMP, $[Ca^{2+}]_i$, and ROS similar to those known to occur with high MeHg exposure concentrations.

Total Hg accumulation, cell death, changes in MMP, $[Ca^{2+}]_i$, and ROS production were determined in cerebella and hippocampi from C57Bl/6 male and female mouse pups at postnatal day (P) 0 and 10 exposed to a total dose of 0, 0.1, or 1.0 mg/kg dam body weight MeHg in food divided over gestational days (G)8 to 18. We observed dose-dependent uptake of MeHg by the cerebellum and hippocampus with decreased MeHg concentrations in the brains of mice at P10 compared to P0. Cell death was determined using Fluoro-Jade B staining and activated caspase 3 immunohistochemistry. No MeHg treatment-associated cell death was observed in cerebella or hippocampi.

MMP, $[Ca^{2+}]_i$, and ROS were measured in acutely isolated cerebellar and hippocampal granule cells using fluorescence microscopy. MMP was decreased in the 1.0 mg/kg MeHg treated P0 cerebella, but increased in the 0. 1 MeHg treated P10 cerebella. MMP was increased in female P10 hippocampi with 0.1 mg/kg MeHg treatment. $[Ca^{2+}]_i$ was increased in the 0.1 and 1.0 mg/kg MeHg treated P0 cerebella, and in the 1.0 mg/kg MeHg treated P10 cerebella. $[Ca^{2+}]_i$ was increased in male P10 hippocampi with 1.0 mg/kg MeHg treatment. At both P0 and P10, ROS were increased in MeHg treated cerebella compared to controls, but decreased or similar to controls in MeHg treated hippocampi.

The hypothesized pattern of increased cell death, decreased MMP, increased $[Ca^{2+}]_i$, and increased ROS which is typical with high MeHg and other toxicant exposures that initiate apoptosis, was not indicated for any MeHg treatment in the cerebellum or hippocampus at P0 or P10. Our data suggest that chronic low levels of MeHg exposure during development may cause mitochondrial dysfunction, oxidative stress, and changes in Ca^{2+} homeostasis that may result in abnormal cellular function, proliferation and/or migration rather than death of neurons. More thorough studies are necessary to determine the mechanism by which MeHg acts at environmentally relevant concentrations. Low-levels of MeHg may affect neuronal function. Therefore, further developmental whole animal investigation is warranted at chronic low-level MeHg concentrations.

INTRODUCTION

Methylmercury (MeHg) poisoning was first observed on a large scale in Minamata, Japan in 1956. Adults exposed to MeHg through consumption of fish and shellfish taken from the Minamata Bay in Japan exhibited visual and sensory disturbances and ataxia, along with pathological changes including massive loss of neurons in the visual, sensory, and motor cortices of the cerebral cortex and granule cells of the cerebellum (Harada, 1995; Takeuchi *et al.*, 1962). Children exposed to MeHg, both *in utero* and during early postnatal development, suffered a more severe array of

symptoms than were observed in adult victims. Mental retardation, primitive reflexes, alterations in physical development, and cerebral palsy were the most common side effects among surviving neonates and children (Harada, 1977). The immature blood-brain barrier and the extensive proliferation, migration, and differentiation of neurons and glia during CNS development predispose the developing fetus and neonate to increased risk of MeHg neurotoxicity (Rodier *et al.*, 1984; Sager, 1988; Sager *et al.*, 1984). Neuropathology observed in children exposed to MeHg included generalized brain atrophy, abnormal cytoarchitecture of the cerebral and cerebellar cortices, hypoplasia of the corpus callosum, and dysmyelination of the pyramidal tract (Matsumoto *et al.*, 1965).

Recent epidemiological research from the Faroe Islands (Grandjean *et al.*, 1997; Steuerwald *et al.*, 2000) and Brazil (Grandjean *et al.*, 1999b) suggests that MeHg in the diets of pregnant females and young children may have a negative affect on motor function, attention, memory, and language development. Two areas of the brain associated with these functions are the cerebellum and the hippocampus (Mangina and Sokolov, 2006). Although the cerebellum is typically associated with motor function (Marr, 1969), studies over the last twenty years have indicated that the cerebellum plays a significant, although not clearly understood, role in cognitive function (Schmahmann, 1997; Schmahmann and Sherman, 1997).

Developmental exposure to MeHg is known to inhibit cell proliferation and decrease cell cycle regulators in the cerebellum and hippocampus of rats (Burke *et al.*, 2006). Also in rats exposed to MeHg *in utero*, hippocampal and cerebellar size, DNA synthesis, cyclin mRNA, and proteins D1, D3 and E are decreased (Falluel-Morel *et al.*, 2007). Other affects of *in utero* MeHg exposure on the hippocampus and cerebellum include spontaneous release of noradrenaline (Gasso *et al.*, 2000), neuronal degeneration (Wakabayashi *et al.*, 1995), and alterations in the central dopaminergic and serotonergic systems (Castoldi *et al.*, 2006).

In primary cultures of mouse cerebellar granule cells, MeHg exposure results in abnormal cell migration (Kunimoto and Suzuki, 1997), inhibition of cell proliferation,

decrease in cell cycle regulators (Burke *et al.*, 2006), disruption of glutamate transport, (Fonfria *et al.*, 2005), decreased glutathione (Fonnum and Lock, 2004), reduced cellular antioxidant status, altered intracellular calcium ion homeostasis (Sirois and Atchison, 2000), increased reactive oxygen species (ROS) (Ali *et al.*, 1992), and impaired mitochondrial function (Mori *et al.*, 2007). Similar results have been observed in cultured cortical neurons exposed to MeHg (Kauppinen *et al.*, 1989; LeBel *et al.*, 1990; Mundy and Freudenrich, 2000; O'Kusky, 1983).

MeHg exposure is known to cause changes in $[Ca^{2+}]_i$, mitochondrial membrane potential (MMP), and ROS production. MeHg produces increased $[Ca^{2+}]_i$ in cerebrocortical synaptosomes (Kauppinen *et al.*, 1989), cerebellar granule cells (Sarafian, 1993), and NG108-15 neuroblastoma/glial hybrid cells (Hare *et al.*, 1993). MMP is decreased by MeHg exposure in astrocytes (Yin *et al.*, 2007) and rat cerebellar granule cells (Limke and Atchison, 2002). Mitochondrial function is altered by MeHg in rat striatal synaptosomes (Dreiem and Seegal, 2007). MeHg exposure results in increased production of ROS in rat brain mitochondria (Mori *et al.*, 2007) as well as in C6-glial and B35-neuronal cell lines (Kaur *et al.*, 2007).

Mitochondria, Ca^{2+}, and ROS are important in normal neuronal function. Neurons exhibit $[Ca^{2+}]_i$ oscillations that may be associated with synaptic strengthening among neurons in the same domain (Singer, 1993; Stryker *et al.*, 1990). In neuronal spines and dendrites, $[Ca^{2+}]_i$ changes, mediated by NMDA receptors, are crucial for the generation of long-term potentiation (LTP) (Alford *et al.*, 1993; Collingridge and Bliss, 1995). Synaptic strengthening and LTP are believed to be important in learning and memory. $[Ca^{2+}]_i$ changes in neurons initiate signaling pathways that trigger gene transcription (Bailey *et al.*, 1996; Martin *et al.*, 1997). Mitochondria are involved not only in energy production. Mitochondria function in the induction of apoptosis (Green and Reed, 1998) xenobiotic metabolism, glucose sensing (Maechler, 2002), steroid hormone synthesis, and lipid metabolism (Brookes *et al.*, 2004). Abnormal mitochondrial function has been implicated in diseases such as Leigh syndrome, spastic paraplegia, and Charcot-Marie Tooth, which result from alterations in the mitochondrial

respiratory chain or mitochondrial migration (DiMauro and Schon, 2008). ROS are not only harmful byproducts of cellular respiration that can cause damage to membranes by lipid peroxidation (Gardner, 1989) and the crosslinking of proteins (Davies, 2005), but are important signalling molecules within the cell (Brookes and Darley-Usmar, 2002; Brookes *et al.*, 2002) and function in cell proliferation (Burdon *et al.*, 1989) and cytoprotection (Piantadosi and Zhang, 1996).

The known associations of MeHg exposure with such important neuronal processes such as cell proliferation and migration suggests the mechanism(s) of MeHg developmental neurotoxicity may involve mitochondrial functions, Ca^{2+} homeostasis, and/or oxidative stress. However, most whole animal studies to date have used relatively high exposure levels of MeHg and routes of exposure that are not environmentally relevant to modern fish-eating populations (Grandjean *et al.*, 1992a; Mielke *et al.*, 2006*;* Spurgeon, 2006). Typical MeHg concentrations used in previous *in vivo* studies range from 2.5 mg/kg body weight per day to 6.43 mg/kg per day for up to one month, and are administered via intraperitoneal injection or through drinking water (Burke *et al.*, 2006; Castoldi *et al.*, 2006; Farina *et al.*, 2005; Weiss *et al.*, 2005; Yee and Choi, 1994). The general population is exposed to MeHg primarily through the diet, mainly saltwater and/or freshwater fish. The average human daily intake of MeHg is about 2.4 µg (International Programme on Chemical Safety, 1990), although some populations with high daily fish consumption may average 20 - 100 µg per day (WGMF, 1980). Maximum consumption rates are estimated to be 1800 µg per day (International Programme on Chemical Safety, 1990; UNEP, 2002). A daily MeHg intake of 3 – 7 µg/kg body weight (50 – 125 µg/g mercury in hair) for adults represents a 5% risk of neurological damage (International Programme on Chemical Safety, 1990). In addition, hair mercury (Hg) levels above 10 – 20 µg/g (0.6 – 1.2 µg/kg body weight daily MeHg) in adult females have been shown to correlate with neurological deficits in their children (Grandjean *et al.*, 1998; Grandjean *et al.*, 1997).

The design of the present study is based on the following known information about MeHg developmental toxicity: 1) the developing central nervous system is highly

susceptible to MeHg toxicity; 2) the cerebellum and hippocampus are specifically targeted; 3) mitochondrial function, Ca^{2+} homeostasis, and ROS are affected by MeHg exposure and are associated with developmental cell proliferation and migration; and 4) current MeHg developmental exposure studies use MeHg concentrations that are higher than or administered differently than what commonly occurs in human populations.

The purpose of this study was to determine whether chronic low levels of MeHg administered during gestation, at or near exposure levels seen in humans, would produce similar effects observed at higher MeHg exposure levels. We hypothesized that total mercury (Hg) would accumulate, cell death would increase, mitochondrial membrane potential would decrease, and $[Ca^{2+}]_i$ and ROS production would decrease in a dose-dependent manner upon exposure to MeHg. To test this hypothesis, we exposed pregnant C57Bl/6 mice to a total dose of 0.1 or 1.0 mg/kg MeHg via their food divided over gestational days (G) 8 to 18 (parturition). Treatment days were selected based on the high susceptibility of the developing rodent brain to neurotoxicants beginning at G8, due to the start of neurulation (Rice and Barone, 2000). We examined the cerebellum and hippocampus from pups at P0 (day of birth) or P10 for total Hg accumulation, cell death, mitochondrial function, basal $[Ca^{2+}]_i$, and production of ROS. Sections from cerebella and hippocampi from mouse pups at P0 and P10 were stained with Fluoro-Jade B or immunolabeled with anti-activated caspase 3 antibody to determine the presence of cell death via apoptosis or by other means. Neurons from cerebella and hippocampi were acutely isolated and examined for changes in MMP, $[Ca^{2+}]_i$, and the production of ROS. This study will further the knowledge base of MeHg toxicity in relation to human exposure levels, enhance the understanding of MeHg toxicity as seen in young children, and provide information to aid in establishing an appropriate MeHg minimum exposure level, reference dose.

MATERIALS AND METHODS

Chemicals

Methylmercuric chloride, 95% (MeHg) was purchased from Alfa Aesar (Ward Hill, MA). DOLT-2, DORM-2, and DOLT-3 were purchased from the National Research Council Canada (NRCC), Institute for Environmental Chemistry (Ottawa, Canada). Fluoro-Jade® B was purchased from Millipore (Temecula, Ca). Affinity-Purified Rabbit Anti-human/mouse Caspase 3 Active was purchased from R&D Systems Inc. (Minneapolis, MN). Biotynilated Goat Anti-Rabbit IgG (H+L), affinity purified was purchased from Vector Laboratories, Inc. (Burlingame, CA). Permount® was purchased from (Fisher Scientific). DPX Mounting Medium was purchased from (Electron Microscopy Sciences, Fort Washington, PA). Minimum Essential Medium Eagle (spinner modification with Earle's salts and $NaHCO_3$, without calcium chloride and L-glutamine (SMEM)), Minimum Essential Medium Eagle (with Earle's Salts and L-glutamine, without sodium bicarbonate (MEM)), deoxyribonuclease I from bovine pancreas (DNase I), poly-D-lysine hydrobromide >300,000 kD, L-alanyl-L-glutamine, *tertiary*-Butyl hydroperoxide (*t*BHP), Hank's Balanced Salt Solution (modified with $NaHCO_3$ and without phenol red (HBSS)), protease type IX (bacterial from *Bacillus polymyxa*), carbonyl cyanide 3-chloro-phenylhydrazone (CCCP), and thapsigargin were purchased from Sigma-Aldrich, Inc. (St. Louis, MO). Fetal bovine serum (FBS) was purchased from Gemini (Woodland, CA). Anti-NeuN clone A60 IgG1was purchased from Chemicon. Tetramethylrhodamine methyl ester perchlorate (TMRM), Calcium Green™-1 AM, 5-(and 6)-chloromethyl-2'7'-dichlorodihydrofluorescein diacetate acetyl ester (CM-H_2DCFDA), Pluronic® F-127, ProLong® Gold Antifade with DAPI, and Alexa Fluor® 488 donkey anti-rabbit IgG (H+L) were purchased from Invitrogen/Molecular Probes (Eugene, OR). Lab-Tek 2-well chambered coverglasses were purchased from Nunc Inc. (Naperville, IL).

Animals

All animal procedures were carried out in accordance with guidelines described in the *Guide for the Care and Use of Laboratory Animals* (NRC, 1996). Adult male and female C57Bl/6 mice, originally obtained from The Jackson Laboratory (Bar Harbor, MA), were housed at the Laboratory Animal Research and Resource building, Texas A&M University, at constant temperature (21 - 22°C) and humidity (45 – 55%) with a 12-hour light/dark photoperiod.

Treatment

MeHg stock solution (1.0 mg/mL) was prepared in sterile distilled water, and then sterilized by filtration and stored at 4°C. Working MeHg solutions were prepared from the 1.0 mg/mL stock solution, diluted in sterile distilled water, and stored at 4°C. All animals were provided distilled drinking water *ad libitum*. Each evening, one male mouse was placed in a cage containing 3 to 5 female mice. Twelve hours later, the male mouse was removed and the female mice were checked for vaginal plugs. Female mice containing plugs were weighed, separated, and housed individually for seven days. During the seven days, the individually housed female mice were trained to consume all of 3.0 g of moistened rodent chow in a 12-hour time period. The feeding and MeHg administration procedures used in this study have been used successfully in previously published experiments (Bellum *et al.*, 2007a; Bellum *et al.*, 2007b; Bellum *et al.*, 2007c). Dry rodent chow was provided *ad libitum* only during the 12 hours of light. During the 12 hours of dark, dry chow was removed and replaced with 3.0 g of rodent chow that was moistened with distilled water to achieve a crumbled texture. The feeding dish and cage were examined each morning to ensure that each mouse was consistently consuming all of the moistened chow provided. On the seventh day, the individually housed female mice were re-weighed. A female mouse was considered pregnant if the body weight had increased at least 1.8 g since mating. Pregnant dams were assigned to control (distilled water) or a total dose of 0.1 or 1.0 mg/kg body weight MeHg. MeHg treatment began on gestational day (G) 8 and continued through G18. The feeding

regimen continued as described previously, but 0.01mg/kg or 0.1 mg/kg MeHg was added to the food of treated pregnant female mice daily. Treatment days were selected based on the high susceptibility of the developing rodent brain to neurotoxicants beginning at G8, due to the start of neurulation (Rice and Barone, 2000). All experimental procedures were conducted on postnatal day (P) 0 (+ 1 day) or P10 (± 1 day). Litters were divided such that only one male and one female from a single litter were used for any one experiment per postnatal day age; the litter is the statistical unit of measure (EPA, 2000; OECD, 2007).

Mercury accumulation

Total mercury (Hg) was measured to determine the amount of Hg transported into the cerebellum and hippocampus. Male and female mice, three to six for each treatment, at both P0 and P10 were anesthetized with isoflurane and decapitated. The whole brain was removed and the cerebellum and hippocampus dissected, weighed, rapidly frozen in powdered dry ice, and stored at -20°C. Cerebellar and hippocampal tissues were freeze-dried for 48 hours and total Hg content was measured in the Trace Element Research Laboratory at Texas A&M University, by combustion / trapping / atomic absorption (Salvata and Pirola, 1994) on a Milestone Direct Mercury Analyzer 80, DMA 80 (Milestone Inc., Shelton, CT) equipped with an autosampler and dual cell detector. The DMA 80 was calibrated using a calibration blank and a series of seven aliquots of certified reference standard ranging from 1 to 750 ng Hg. The calibration line was verified using an independent CRM standard (NRCC DOLT-2) and a blank nickel boat. Samples were weighed to the nearest 0.00001 g and placed into the DMA 80 in pre-combusted nickel boats. A method blank, two certified reference materials (DORM-2 and DOLT-3), a spiked sample, and a duplicate sample were included at the beginning and end of each sample run. The DMA 80 has a detection limit of 0.005 ng Hg and a working range of up to 1000 ng Hg (Milestone, Inc. Shelton, CT). Total Hg accumulation was determined for the cerebellum and hippocampus from each male and female mouse for each age and treatment group. Measured total Hg content (ng Hg) for

each sample was divided by the measured wet weight (w.w.) of that sample to determine the total Hg concentration in the brain tissue (ng Hg / g w.w.). In addition, total Hg concentrations were measured in cerebella and hippocampi from MeHg treated dams ten days following parturition. Total Hg concentrations were calculated as were for P0 and P10 pups.

Three-way analysis of variance (ANOVA), followed by Tukey's HSD or Student's t post hoc tests, as appropriate, were used to determine between-subject differences and interactions in total Hg concentration (ng Hg / g w.w.) associated with sex, brain region, and MeHg treatment at P0 and P10, independently. Two-way ANOVA, followed by Tukey's HSD or Student's t post hoc tests, as appropriate, were used to determine between-subject differences and interactions in total Hg concentrations (ng Hg / g w.w.) associated with brain region and MeHg treatment in MeHg treated dams.

Fluoro-Jade B staining

To detect dying neurons, cells were stained with Fluoro-Jade B, an anionic fluorochrome that selectively stains cell bodies, dendrites, axons, and axon terminals of degenerating neurons, but does not stain healthy neurons, myelin, vascular elements or neuropil (Schmued *et al.*, 1997a; Schmued *et al.*, 1997b). P0 mice were anesthetized by intraperitoneal injection of 150.0 g/kg ketamine and 15.0 mg/kg xylazine and decapitated. The whole head was fixed by immersion in 4% phosphate buffered paraformaldehyde for 72 hours at 4°C, and then cryoprotected by immersion in 20% sucrose in 0.1 M PBS for 48 to 72 hours, or until the head settled to the bottom of the sucrose solution. Once cryoprotected, whole heads were rapidly frozen in powdered dry ice and stored at -70°C. P10 mice were anesthetized by intraperitoneal injection of 150.0 mg/kg ketamine and 15.0 mg/kg xylazine. Once anesthetized, they were fixed by transcardial perfusion with 6 mL Tyrode's saline (room temperature) followed by 6 mL cold 4% phosphate buffered paraformaldehyde. The brain was removed, immersed in cold 4% phosphate buffered paraformaldehyde for 48 hours, and then cryoprotected by

immersion in 20% sucrose in 0.1 M PBS for 48 to 72 hours, or until the brain settled to the bottom of the sucrose solution. Once cryoprotected, brains were rapidly frozen in powdered dry ice and stored at -70°C.

Serial sagittal sections (15 μm), through whole frozen heads (P0) or brains (P10), were cut with a SLEE cryostat (Slee, Mainz, Germany), mounted on gelatin-coated slides, and stored at -70°C. Every seventh section was used for Fluoro-Jade B staining to ensure that no labeled cell was counted twice. Sections from testes of non-treated adult mice and sections of cerebella from P20 to P60 leaner mice were used as negative (Fluoro-Jade B dye was excluded from the staining protocol) and positive controls. Leaner mice carry an autosomal recessive mutation in the CACNA1A gene coding for the α_{1A} pore-forming subunit of Ca_V 2.1 voltage-gated calcium channel (P/Q-type) (Herrup and Wilczynski, 1982). This mutation results in extensive cerebellar granule cell death that begins around P10 and continues into adulthood (Herrup and Wilczynski, 1982; Lau *et al.*, 2004). Frozen sections were dried for 1 hour at 50°C, cooled for 10 min, and then stained as described by Schmued and Hopkins (2000). Dried sections were placed in a 1% sodium hydroxide in 80% alcohol solution for 5 min, followed by 70% alcohol for 5 min, distilled water for 2 min, and then immersed and gently shaken in 0.06% potassium permanganate in distilled water for 10 min. Sections were rinsed in distilled water twice for 1 min each, and then transferred to and shaken gently in 0.0004% Fluoro-Jade B in 0.1% acetic acid and distilled water for 20 min. Sections were then washed again with distilled water three times for 1 min each, and then rapidly dried by blowing cool air onto the slides with an air-gun for approximately 20 min. Dried slides were immersed in xylene twice for 5 min each, and then coverslipped with DPX mounting media. Fluoro-Jade B-positive cells were viewed with a Zeiss Axioplan 2 microscope (Carl Zeiss, Thornwood, NY) using a fluorescein isothiocyanate (FITC) filter and equipped with a Color AxioCam camera. Fluoro-Jade B positive cells were counted in the cerebellar vermis and in the dentate gyrus and hippocampus proper of the hippocampal formation. At P0 and P10, within the cerebellar vermis, positive cells were distinguished between the rostral and caudal cerebellum and among the external

germinal, molecular, Purkinje, and granule cell layers. At P0 and P10, positive cells in the pyramidal cell layer of the hippocampus proper were distinguished between the CA1 and CA3 regions. Demarcations of regions in the dentate gyrus were not visible at P0. Positive cells in the developing P0 dentate gyrus, regardless of location, were counted as a group. At P10, positive cells in the dentate gyrus were distinguished among the granular and subgranular zones, and the hilus. Slides were coded to blind the investigator as to the treatment and gender of the sections during data collection.

Fluoro-Jade positive cell counts were collected from cerebella and hippocampi from male and female mice (three to six individuals in each group) at P0 and P10 using a minimum of four sections per animal. Data from the four sections were averaged to obtain the positive cell counts for each individual animal. Data from the dentate gyrus of P0 pups were analyzed by two-way ANOVA to determine between-subject differences and interactions associated with sex and MeHg treatment. Data from the dentate gyrus of P10 pups were analyzed by three-way ANOVA to determine between-subject differences and interactions associated with sex, cell layer of the dentate gyrus, and MeHg treatment. Data from the hippocampus proper of P0 and P10 pups were analyzed by three-way ANOVA to determine between-subject differences and interactions associated with sex, pyramidal cell region, and MeHg treatment. Data from pups at P0 and P10 were analyzed by three-way ANOVA to determine between-subject differences and interactions associated with sex, cerebellar cell layer, and MeHg treatment. Data from pups at P0 and P10 were analyzed by three-way ANOVA to determine between-subject differences and interactions associated with sex, rostral and caudal cerebellar vermis, and MeHg treatment for each cerebellar cell layer, independently. Differences, as indicated by three-way ANOVA, were analyzed by Tukey's HSD or Student's t post hoc tests, as appropriate, to determine differences among all treatments or brain regions.

Activated caspase 3 immunohistochemistry

Caspase 3 is activated in the process of apoptosis (Burke *et al.*, 2006). Activated caspase 3 immunohistochemistry was used to detect neurons dying by apoptosis. Fixed and frozen brain sections adjacent to those for Fluoro-Jade B staining were used for activated caspase 3 analysis (see Fluoro-Jade B section for tissue and slide preparation procedures). Frozen sections were dried at room temperature for 1 hour, and then immersed in 0.3% Triton-X in 0.1 M phosphate buffered saline (PBS) for 1 hour, followed by three washes in 0.1 M PBS for 10 min each. Washed slides were immersed in 1% hydrogen peroxide 0.1 M PBS for 5 min, followed by two washes in 0.1 M PBS for 5 min each with gentle agitation. Sections were transferred to 5% normal goat serum in 0.1 M PBS for 1 hour, and then into anti-activated caspase 3 primary antibody (1:25000) in 2% normal goat serum and 0.1 M PBS over-night at 4°C (approximately 16 hours). Following application of the primary antibody, sections were rinsed in 0.1 M PBS three times for 10 min each, and then immersed in the biotynilated secondary antibody (1:400) in 0.1 M PBS for 2 hours. Sections were then washed in 0.1 M PBS three times for 10 min each, followed by immersion in Streptavidin horseradish peroxidase (1:5000) in 0.1 M PBS for 2 hours. Sections were rinsed in 0.1 M PBS for 10 min, and then in 0.05 M Tris-HCl buffer (pH 7.6) twice for 10 min each. Finally, sections were placed in 0.024% diaminobenzadine (DAB) (5.0 µL of 30% hydrogen peroxide, 150.0 mg of 5% nickel ammonium sulfate, 1.0 mL of 6.2 mg DAB per 500 µL, and 25.0 mL of 0.05 M Tris-HCl buffer, pH 7.6) for 20 min, and then washed in 0.05 M Tris-HCl buffer (pH 7.6) for 5 min, followed by two washes in 0.1 M PBS for 5 min each. Stained slides were dehydrated in a graded series of ethanols (EtOH) and counterstained with eosin. Alcohol immersions were as follows: 5 min in 70% EtOH, 5 min in 80% EtOH, 4 dips in eosin in 80% EtOH, 5 min in 95% EtOH, 5 min in 95% EtOH, 5 min in 100% EtOH, and 5 min in 100% EtOH. Following dehydration, tissue was cleared by immersion in xylene two times for 5 min each, and then coverslipped with Permount® mounting media. Activated caspase 3 positive cells were counted and the data analyzed as described for Fluoro-Jade B. As with Fluoro-Jade B, sections from

testes of non-treated adult mice and sections of P20 to P60 leaner mouse cerebella were used as negative (activated caspase 3 antibody was excluded from the protocol) and positive controls.

Acute isolation of cerebellar granule and hippocampal neurons

Acutely isolated neurons were prepared as described by Oberdoerster (2001) and Bellum *et al.* (2007a). This isolation method yields more than 90% viable cells as demonstrated using 0.08% Trypan blue exclusion (Bellum *et al.*, 2007a). Cell isolations and subsequent MMP, Ca^{2+}, and ROS imaging were carried out in batches containing cells obtained from one animal from each treatment group, all of the same age and gender. Mice were anesthetized with isoflurane, and then decapitated. Whole brains were removed and cerebella and hippocampi dissected and placed in SMEM (with 2.5 mM L-alanyl-L-glutamine). All solutions were cold and on ice unless otherwise specified. Tissues were chopped into ~ 1 mm pieces with a razor or scalpel blade, and then placed in dissociation media (DM), consisting of SMEM, 1.5 U/mL protease, and 2.5 mM L-alanyl-L-glutamine. Neurons were isolated in DM by mechanical disruption by trituration with a 10 mL glass serological pipette. Each of four trituration-cycles involved ten triturations followed by a 1 min rest period to allow large tissue pieces to sediment. After each cycle, approximately 80% of the DM/cell solution was carefully removed, so as not to disturb large settled pieces of brain tissue, and then combined with growth media (MEM, sodium bicarbonate, L-alanyl-L-glutamine, 10% FBS) and kept on ice. The removed media was replaced with fresh DM before beginning the next trituration cycle. DNase I (80 U/ml) was added during the second cycle. Cell solutions were centrifuged at 1100 g for 10 minutes and the supernatant discarded. Cell pellets were reconstituted in growth media at 37°C and plated onto 2.5% gelatin and 1x poly-D-lysine-coated chambered coverslips. Chambered coverslips were coated with 2.5% gelatin for 10 min and then in 1x poly-D-lysine overnight (approximately 12 hours) at 4°C. The poly-D-lysine was removed and the coverslips rinsed in warmed (37°C) HBSS a few minutes before the cells were added. The HBSS was removed before the cells in

growth media were plated. Each individual sample was divided and plated onto three separate coverslips, one for each analysis: MMP, basal $[Ca^{2+}]_i$, and ROS. Plated cells were incubated at 37°C (5% CO_2) for 30 min to allow cells to attach to the coverslip surface.

Identification and validation of acutely isolated cells as neurons

NeuN and DAPI staining of isolated cells were used to identify neurons for subsequent analysis. NeuN is a marker for neurons. In the cerebellum, NeuN is specific for granule cells (Weyer and Schilling, 2003), and in the hippocampus, NeuN is specific for neurons in the granular and subgranular zone and for pyramidal cells of the CA1 and CA3 regions (Domoráková *et al.*, 2006). NeuN intensely labels the nucleus and lightly labels the cytoplasm of neurons (Domoráková *et al.*, 2006; Mullen *et al.*, 1992). DAPI is a fluorescent stain that binds strongly to DNA and is used to identify the nucleus of cells (Robinson *et al.*, 2008). After isolation and 30 min incubation of plated cells, growth medium was moved and the cerebellar and hippocampal cells were fixed in 4% paraformaldehyde for 15 min. Cells were then washed in 0.1 M PBS twice for 1 min each, and then permeabilized with 0.3% Triton-X for 5 min. Cells were washed in 0.1 M PBS twice for 3 min each, and then immersed in 5% normal goat serum in 0.1 M PBS for 1 hour. Cells were then placed into NeuN primary antibody (1:2000) (Mullen *et al.*, 1992; Weyer and Schilling, 2003) in 2% normal goat serum and 0.1 M PBS over night (approximately 16 hours) at 4°C. Following application of the primary antibody, cells were washed twice for 3 min each, and then immersed in Biotynilated Goat Anti-mouse AF594t secondary antibody (1:400) for 2 hours. Finally, the cells were washed in 0.1 M PBS twice for 3 min each, and then coverslipped with ProLong® Antifade with DAPI (Turville *et al.*, 2008). Cells were imaged using a Zeiss Axioplan 2 microscope (Carl Zeiss, Thornwood, NY) with Texas Red and DAPI filters, and equipped with a Color AxioCam camera.

Mitochondrial membrane potential

Tetramethylrhodamine methyl ester (TMRM) was used to detect changes in mitochondrial membrane potential (MMP) (Barhoumi *et al.*, 2004). TMRM is a lipophilic potentiometric mitochondrial dye that accumulates in mitochondria in proportion to the membrane potential (Scaduto Jr and Grotyohann, 1999). TMRM dye stock solution (1.0 mM) was prepared in 100% methanol and stored in desiccant at -20°C. TMRM working solution (150.0 nM) was prepared from the 1.0 mM stock solution in HBSS just before use. The methanol concentration in the working solution was 0.015%. HBSS was used in the TMRM working solution instead of growth media to prevent the TMRM dye from binding to proteins within the medium and inhibiting movement of dye into the cells. After cell isolation and a 30 min incubation, growth media was removed from the acutely isolated cerebellar and hippocampal neuronal cultures and replaced with a 150.0 nM solution of TMRM in HBSS for 20 min at 37°C. The TMRM solution was replaced with HBSS for imaging. Three negative controls (HBSS and cells with no dye, HBSS with no cells and no dye, and HBSS with dye and no cells) and a positive control (HBSS and cells with dye and 20 μM CCCP) were included. CCCP was used to determine that the observed fluorescence was associated with the mitochondrial membrane and not other non-specific TMRM fluorescence (Julian *et al.*, 2005). CCCP is a lipid-soluble weak acid that uncouples oxidative phosphorylation in the inner mitochondrial membrane. It enters the mitochondria in a protonated form, discharges the pH gradient, then leaves the mitochondria as an anion, depolarizing the mitochondrial membrane (Lim *et al.*, 2001). When CCCP is co-administered to cells with TMRM, the CCCP-induced depolarization of the inner mitochondrial membrane results in release of accumulated TMRM from mitochondria into the cytosol, and a decrease in fluorescence occurs.

Fluorescent mitochondrial images were collected over a 10 min time period at 63x using a Zeiss Axiovert 200M microscope equipped with a Cy3 filter set (excitation: 560/40 nm, dichroic FT 585; emission: BP 630/75 nm) and SlideBook™ 4.1.0 software from Intelligent Imaging Innovations Inc. (3I, Denver, CO). Image retrieval and MMP

fluorescent data collection were performed using Simple PCI and Imaging System Software (v5.0.0.1503, Compix Inc.). Relative MMP values of individual mitochondria from a minimum of ten cells from each animal were measured and averaged to give the MMP value for each of three individual animals from each treatment, brain region, sex, and age group. Mitochondria were identified as fluorescent round or oblong-shaped punctate fluorescence objects within the granule cells.

MMP data were calculated as percentage of control within each batch (one control and one of each treated sample, at a single age, analyzed at the same time) to control for inter-analysis variation and allow comparison of data from one day to the next. MMP data were analyzed by three-way ANOVA to determine significant between-subject differences associated with sex, brain region (cerebellum and hippocampus), and MeHg treatment. Differences, as indicated by three-way ANOVA, were analyzed by Tukey's HSD or Student's t post hoc tests, as appropriate to determine differences among all brain regions, ages, and MeHg treatments.

Basal intracellular Ca^{2+}

Calcium Green™-1 AM was used to measure the relative concentration of basal intracellular Ca^{2+} (Gilroy and Jones, 1992). Calcium Green™-1 AM is a long-wavelength Ca^{2+} indicator that exhibits an increase in fluorescence emission intensity upon binding to Ca^{2+} (Eberhard and Erne, 1991). The dye is in the AM ester form, which enhances cell permeability and is non-fluorescent in the absence of Ca^{2+} (Lee *et al.*, 1999). Upon binding to Ca^{2+}, the dye exhibits an approximately 100-fold increase in emission intensity, which enables detection of changes in Ca^{2+} concentration within a large dynamic range (Lee *et al.*, 1999). Calcium Green™-1 AM stock solution (2.0 mM) was prepared in 100% DMSO and stored in desiccant at -20°C for up to two weeks. Working solutions of Calcium Green™-1 AM (1.0 μM) were prepared just before use in 0.01% Pluronic® F-127 and HBSS. The final DMSO concentration in the working solution was 0.05%. HBSS was used in the Calcium Green™-1 AM working solution instead of growth media to prevent the Calcium Green™-1 AM dye from binding to

proteins within the medium and inhibiting movement of dye into the cells. After the cell isolation and 30 min incubation, growth media was removed and replaced with a 1.0 μM solution of Calcium Green™-1, AM in 0.01% Pluronic® F-127 and HBSS for 20 min at room temperature. Incubation of the cells with Calcium Green™-1 AM dye at room temperature prevents compartmentalization of the dye into cellular organelles. The Calcium Green™-1 AM solution was removed and replaced with HBSS for 20 min to allow de-esterification of the dye; the AM ester of the molecule, which enhances the movement of the dye into the cell, must be removed by endogenous esterases for the dye to fluoresce when bound to Ca^{2+}. Three negative controls (HBSS and cells with no dye, HBSS with no cells and no dye, and HBSS with dye, but no cells) and a positive control (HBSS and cells with dye and thapsigargin) were included. Thapsigargin is an inhibitor of sarco-endoplasmic reticulum Ca^{2+} ATPases and raises cytosolic free Ca^{2+} by blocking the ability of the cell to pump Ca^{2+} into the endoplasmic reticulum (ER) (Treiman *et al.*, 1998). ER-store depletion can secondarily activate plasma membrane Ca^{2+} channels, allowing an influx of Ca^{2+} into the cytosol (Barhoumi *et al.*, 2006). When thapsigargin is co-administered to cells with Calcium Green™-1 AM, the thapsigargin-induced increase in cytosolic free Ca^{2+} causes a dramatic increase in fluorescence.

Fluorescent Ca^{2+} images were collected and analyzed as described for MMP, with the exception that the FITC filter set (excitation: BP 470/20, dichroic FT493; emission: BP 505-530 nm) was used. Relative $[Ca^{2+}]_i$ values from a minimum of ten cells from each animal were measured and averaged to give the Ca^{2+} value for each of three individual animals from each treatment, brain region, sex, and age group. $[Ca^{2+}]_i$ data were calculated as percentage of control within each batch (one control and one of each treated sample, at a single age, analyzed at the same time) to control for inter-analysis variation and allow comparison of data from one day to the next. $[Ca^{2+}]_i$ data were analyzed by three-way ANOVA to determine significant between-subject differences associated with sex, brain region, and MeHg treatment. Differences, as indicated by three-way ANOVA, were analyzed by Tukey's HSD or Student's t post hoc

tests, as appropriate, to determine differences among brain regions, ages, and MeHg treatments.

Reactive oxygen species

5-(and 6)-chloromethyl-2'7'-dichlorodihydrofluorescein diacetate acetyl ester (CM-H_2DCFDA) was used to determine the relative amount and rate of ROS production over time (Bellum *et al.*, 2007a; Oyama *et al.*, 1994). CM-H_2DCFDA is a non-fluorescent compound that is oxidized to highly fluorescent 2',7'-dichlorofluorescein (DCF) by the action of ROS (LeBel *et al.*, 1992). The chloromethyl (CM) group on the dye allows the dye to passively diffuse into cells. Subsequent oxidation of the dye molecule by endogenous esterases traps its derivatives within the cell where they can react with ROS. CM-H_2DCFDA stock solution (2.0 mM) was prepared in DMSO and stored in desiccant at -20°C for up to two weeks. Working solutions of CM-H_2DCFDA (1.0 μM) were prepared just before use in 0.01% Pluronic® F-127 and HBSS. The DMSO concentration in the working solution was 0.05%. HBSS was used in the CM-H_2DCFDA working solution instead of growth media to prevent the CM-H_2DCFDA dye from binding to or reacting with proteins within the medium and inhibiting movement of dye into the cells. After the isolation and 30 min incubation, the growth medium was removed and replaced with a 1.0 μM solution of CM-H_2DCFDA in 0.01% Pluronic® F-127 and HBSS for 5 min at room temperature. Incubation of the cells with CM-H_2DCFDA dye at room temperature prevents compartmentalization of the dye into cellular organelles. The CM-H_2DCFDA was removed and replaced with HBSS for imaging. Three negative controls (HBSS and cells with no dye, HBSS with no cells and no dye, and HBSS with dye, but no cells) and a positive control (HBSS and cells with dye and *tertiary*-butyl hydroperoxide (*t*BHP) were included (Drahota *et al.*, 2005). *t*BHP is a lipophilic, membrane-permeant oxidant (Elliott *et al.*,1992). It reacts with iron in heme-proteins and produces alkoxyl radicals (Kim *et al.*,2005b). When *t*BHP is co-administered to cells with CM-H_2DCFDA dye, the *t*BHP-induced increase in ROS causes an increase in fluorescence. Fluorescent images were collected every 2.5 min for

30 min as described for MMP and $[Ca^{2+}]_i$ using the FITC filter set. The relative rate of ROS production was calculated using a minimum of five cells from each animal.

ROS data were calculated as percentage of control within each batch (one control and one of each treated sample, at a single age, analyzed at the same time) to control for inter-analysis variation and allow comparison of data from one day to the next. A three-way MANOVA with repeated measures for reading time was used to assess between- and within-subject differences and interactions associated with sex, brain region, and MeHg treatment. The condition of sphericity was analyzed to determine the appropriate univariate analysis test. The condition of sphericity was not met in any of the ROS data analyzed. Therefore, the Greenhouse-Geisser adjusted univariate test was used for repeated measures analysis of reading time (Grieve, 1984).

Statistical analysis

All data were represented as mean ± standard error of the mean (SEM). Detailed descriptions of statistical analyses have been described within the text for each experiment. In brief, data for MMP, $[Ca^{2+}]_i$, and ROS were calculated as percentage of control to normalize batch differences. A three-way MANOVA adjusted univariate-repeated measures for time was used to assess differences among brain regions, gender, and MeHg treatment for ROS. All other experiments were analyzed using a three-way ANOVA and Tukey's HSD or Student's t post hoc tests, as appropriate, for brain regions, sex, and MeHg treatment. For all experiments, $\alpha = 0.05$ (JMP 7.0.2, SAS Institute Inc., Cary, NC).

RESULTS

General observations

Over the course of the study, pregnant female mice and offspring appeared healthy with no obvious changes in movement or behavior. Data are represented as (*M* = mean, *SEM* = standard error of the mean). Body, cerebellar, and hippocampal weights for mouse pups at P0 and P10 were analyzed by two-way ANOVA to determine

differences and interactions associated with sex and MeHg treatment. Two-way ANOVA for body, cerebellar, and hippocampal weights in pups at P0 and P10 indicted no differences or interactions in sex or MeHg treatment for body (for P0, M = 1.4 g, SEM = 0.05; for P10, M = 6.2 g, SEM = 0.15), cerebellar (for P0, M = 0.0092 g, SEM = 0.0004; for P10, M = 0.036 g, SEM = 0.0007), or hippocampal (for P0, M = 0.010 g, SEM = 0.0005; for P10, M = 0.025 g, SEM = 0.0006) weights. Body, cerebellar, and hippocampal weights for adult female mice, ten days following parturition, were analyzed by one-way ANOVA to determine differences in MeHg treatments. One-way ANOVA for body, cerebellar, and hippocampal weights in previously-pregnant dams indicated no differences in MeHg treatments for body (M = 30.0, SEM = 0.87), cerebellar (M = 0.053, SEM = 0.0005), or hippocampal weights (M = 0.030, SEM = 0.002).

Mercury (Hg) accumulation

Total Hg concentration, presented as total Hg content (ng Hg) per unit volume of wet brain weight (w. w.) tissue (ng/g), was calculated by dividing the total Hg measured in each sample by the wet brain tissue weight for that sample. Total Hg concentration values were analyzed by three-way ANOVA, at P0 and P10, for differences and interactions in total Hg concentration associated with sex, cerebellar and hippocampal brain regions, and MeHg treatment. Data for mice at P0 indicated an overall effect, F (11, 36) = 13, $p < 0.0001$, with total Hg concentrations increased in the 1.0 mg/kg MeHg treatment (M = 300 ng/g, SEM = 39) compared to the 0.1 mg/kg MeHg treatment (M = 18 ng/g, SEM = 1.7) and compared to controls (M = 1.8 ng/g, SEM = 0.60), (Table III-1). No differences were observed in total Hg concentration between sexes or cerebellar and hippocampal brain regions. Data from P10 mice indicated an overall effect, F (11, 51) = 9.1, $p < 0.0001$, with total Hg concentration increased in the 1.0 mg/kg MeHg treatment (M = 29 ng/g, SEM = 15) compared to the 0.1 mg/kg MeHg treatment (M = 5.2 ng/g, SEM = 3.1) and compared to controls (M = 4.1 ng/g, SEM = 0.56), (Table III-1). Total Hg concentration was evaluated by Student's t-test post hoc analysis to compare total Hg

concentration between P0 and P10 pup brains at each MeHg treatment. Data indicated that total Hg concentration was increased in the P10 pup brains compared to the P0 pup brains in the controls, F (1, 42) = 7.7, p = 0.0081. However, the P0 pup brains exhibited increased total Hg concentration compared to P10 pup brains for both the 0.1 mg/kg, F (1, 31) = 70, $p < 0.0001$, and 1.0 mg/kg, F (1, 32) = 92, $p < 0.0001$, MeHg treatments. Hg content (ng Hg) per unit volume of wet brain weight (w. w.) tissue (ng/g) also was calculated for previously pregnant female mice ten days following parturition. Analysis by two-way ANOVA for differences associated with brain region and treatment indicated an overall effect, F (5, 12) = 33, $p < 0.0001$, with total Hg concentration in adult female brains increased in the 1.0 mg/kg MeHg treatment (M = 55 ng/g, SEM = 8.8) compared to the 0.1 mg/kg MeHg treatment (M = 4.9 ng/g, SEM = 0.28) and compared to controls (M = 0.81 ng/g, SEM = 0.12) (Table III-1). No difference in total Hg concentration was observed between cerebellar and hippocampal brain regions. However, two-way ANOVA showed an interaction effect between MeHg treatment and brain regions, F (2, 12) = 6.1, p = 0.015, indicating that treatment differences were greater in the hippocampus than in the cerebellum of previously pregnant adult female mice. Hg content for a method blank, two certified reference materials, a spiked sample, and a duplicate sample were analyzed to determine changes within individual runs from beginning to end, from one run to the next, and between duplicate samples within a run. No intra-run, between-run, or between-duplicate sample differences were observed (data not shown); recovery rate for certified reference materials and spiked samples ranged from 92 to 99% (data not shown). Total Hg content in the rodent chow was analyzed to identify potential Hg exposure other than what was intentionally administered. Total Hg levels in rodent chow were below the level of detection for the analysis used (< 0.005 ng, data not shown).

Fluoro-Jade B and activated caspase 3

P0 cerebella

The number of Fluoro-Jade B positive dead cells in the cerebellum of mice at P0 was analyzed by three-way ANOVA to determine between-subject differences and interactions associated with sex, cerebellar cell layer, and MeHg treatment. Data indicated a main effect for cerebellar cell layer, F (3, 56) = 39.1, $p < 0.0001$. Differences in Fluoro-Jade positive dead cell counts, as determine by Tukey's HSD post hoc analysis, were as follows: Purkinje cell layer = external germinal cell layer < molecular cell layer < granule cell layer (Fig III-1). Differences were not observed between sexes or among MeHg treatments in cerebella from mice at P0. Fluoro-Jade positive dead cell count data for cerebella from mice at P0 were analyzed by three-way ANOVA to determine between-subject differences and interactions associated with sex, rostral and caudal cerebellum, and MeHg treatment for each cerebellar cell layer, independently. Differences were not observed in Fluoro-Jade positive dead cells for sex, rostral and caudal cerebellum, and MeHg treatment for the different cell layers of cerebella from mice at P0.

TABLE III-1

Total Mercury Concentration in Cerebella and Hippocampi of Adult Female Mice and Their Pups at Postnatal Days 0 and 10 Following Exposure to 0, 0.1, or 1.0 mg/kg Total Dose of Methylmercury Divided Over Gestational Days 8 to 18

	Total Hg Concentration in Both Cerebella and Hippocampi (Hg/w.w., ng/g)		
	Controls	0. 1 mg/kg	1.0 mg/kg
0	1.8 (0.6)	18 (1.7) †	300 (39) * †
10	4.1 (0.56) ‡	5.2 (3.1)	29 (15) *
Dams	0.81 (0.12)	4.9 (0.28)	55 (8.8) *

Data are represented as mean (standard error of the mean).
Hg / wet weight (w.w.) as ng/g = total Hg content measured divided by the wet tissue weights in cerebella and hippocampi. Total Hg concentration was analyzed by three-way ANOVA to determine differences associated with sex, brain region, and MeHg treatment, followed by Tukey's HSD or Student's t post hoc tests, $\alpha = 0.05$. Total Hg concentration was increased in the 1.0 mg/kg MeHg treatment compared to the 0.1 mg/kg MeHg treatment and controls for pups at both P0 and P10 (*). No differences were observed between sexes or between cerebellar and hippocampal brain regions for P0 or P10 pups. P0 three-way AVOVA: overall F (11, 36) = 13, $p < 0.0001$, and P10 three-way ANOVA: overall F (11, 51) = 9.1, $p < 0.0001$; $\alpha = 0.05$. Total Hg concentration was increased in the P0 pups (†) compared to the P10 pups in both the 0.1 and 1.0 mg/kg MeHg treatments, whereas the P10 pups exhibited increased total Hg concentration compared to P0 control pups (‡). One-way ANOVA for 0.1 mg/kg, F (1, 31) = 70, $p < 0.0001$, for 1.0 mg/kg, F (1, 32) = 92, $p < 0.0001$, and for controls, F (1, 42) = 7.7, $p = 0.0081$; $\alpha = 0.05$. Total Hg concentration in cerebella and hippocampi from previously pregnant female mice was measured ten days following parturition and analyzed by two-way ANOVA for brain region and MeHg treatment differences. Data indicated that total Hg concentration was increased in the 1.0 mg/kg MeHg treatment (*) compared to the 0.1 mg/kg MeHg treatment and controls. No differences were observed between cerebellar and hippocampal brain regions. Two-way ANOVA: overall F (5, 12) = 33, $p < 0.0001$; $\alpha = 0.05$.

The number of activated caspase 3 positive dying cells in the cerebellum of mice at P0 was analyzed by three-way ANOVA to determine between-subject differences and interactions associated with sex, cerebellar cell layer, and MeHg treatment. Main effects were observed for treatment, F (2, 48) = 3.56, p = 0.04, and cerebellar cell layer, F (3, 48) = 12.09, $p < 0.0001$. Tukey's HSD post hoc analysis indicated that the 1.0 mg/kg total dose MeHg treatment exhibited increased numbers of activated caspase 3 positive cells than did controls in the Purkinje cell layer (Fig III-2). No treatment differences were observed in any of the other cerebellar cell layers. Data also indicated that the granule and external germinal cell layers exhibited increased numbers of activated caspase 3 positive cells compared to the molecular and Purkinje cell layers in controls. In the 0.1 mg/kg MeHg treatment, only the granule cell layer exhibited increased numbers of activated caspase 3 positive cells compared to the molecular and Purkinje cell layers (Fig III-2). No differences were observed in the number of activated caspase 3 positive cells among the cell layers for the 1.0 mg/kg MeHg treatment. Three-way ANOVA for sex, anterior and posterior cerebellum, and MeHg treatments for each of the P0 cerebellar cell layers showed main effects for anterior/posterior region in the granule cell layer, F (1, 24) = 5.03, p = 0.03, and for MeHg treatment in the Purkinje cell layer, F (2, 24) = 6.30, p = 0.01. Student's t post hoc analysis indicated that activated caspase 3 positive cells were increased in the posterior cerebellum compared to the anterior cerebellum in the granule cell layer (Fig III-3). Tukey's HSD post hoc analysis indicated that activated caspase 3 positive cells were increased in the 1.0 and 0.1 mg/kg MeHg treatments compared to the Purkinje cell layer in age-matched and sex-matched control mice (Fig III-3).

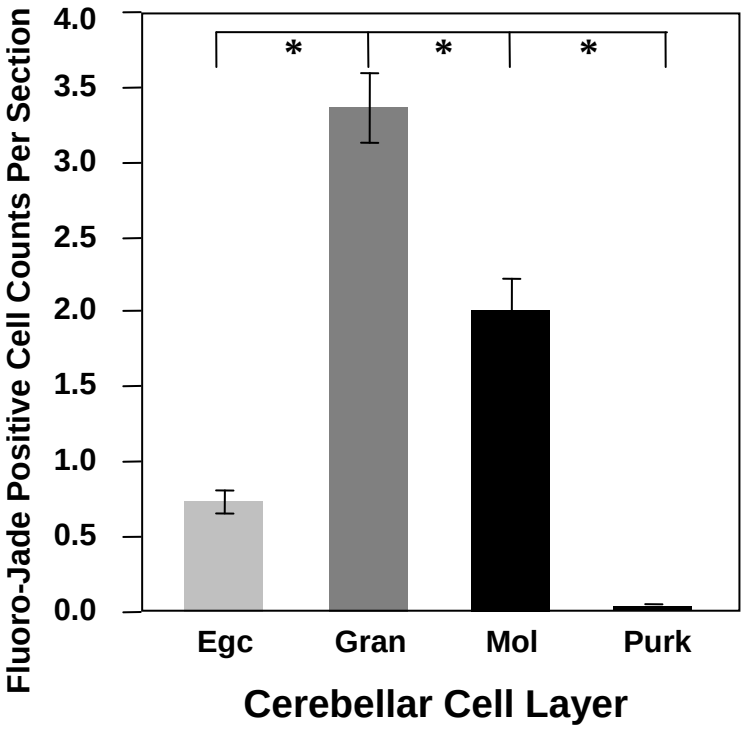

FIG. III-1. Fluoro-Jade positive cell counts in the cerebellum of mice at postnatal day 0 following exposure to 0, 0.1, or 1.0 mg/kg total dose MeHg divided over gestational days 8 to 18. The number of Fluoro-Jade positive cells was different among all cerebellar cell layers (*). The number of Fluoro-Jade positive cell counts were ordered as follows: granule cell layer (Gran) > molecular (Mol) > external germinal layer (Egc) > Purkinje cell layer (Purk). Analysis indicated no differences associated with sex or MeHg treatment. Data are presented as mean ± standard error of the mean and were analyzed by three-way ANOVA and Tukey's HSD post hoc analysis, F (3, 56) = 39.1, $p < 0.0001$, $\alpha = 0.05$.

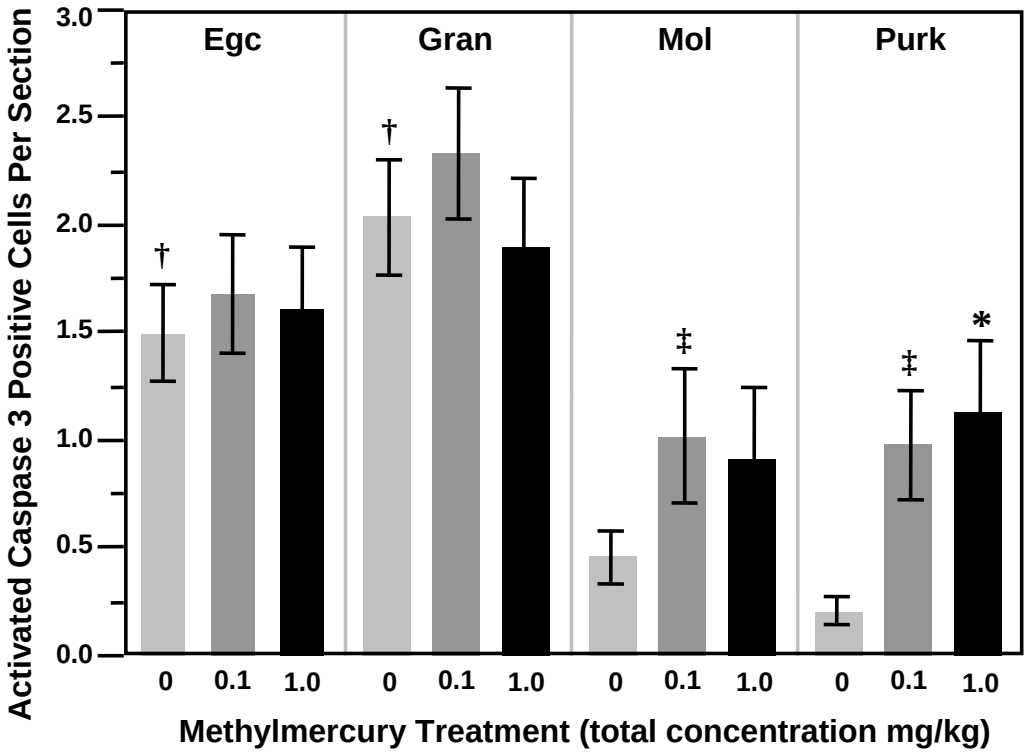

FIG. III-2. The number of activated caspase 3 positive cells in the layers of the cerebellum of mice at postnatal day 0 following exposure to 0, 0.1, or 1.0 mg/kg total dose MeHg divided over gestational days 8 to 18. Cerebellar cell layers are represented as: Egc (external germinal cell layer), Gran (granule cell layer), Mol (molecular cell layer), and Purk (Purkinje cell layer). Main effects were indicated for MeHg treatment and cerebellar cell layer. The number of activated caspase 3 positive cells was increased in the 1.0 mg/kg treatment compared to controls in the Purkinje cell layer (*). No MeHg treatment differences were observed in any of the other cell layers. The number of activated caspase 3 positive cells was increased in the granule and external germinal cell layers compared to the molecular and Purkinje cell layers in control cerebella (†). The molecular and Purkinje cell layers exhibited decreased numbers of activated caspase 3 positive cells compared to the granule cell layer in 0.1 mg/kg MeHg treated cerebella (‡). No differences were indicated for sex. Data are presented as mean ± standard error of the mean and were analyzed by three-way ANOVA and Tukey's HSD post hoc analysis. MeHg treatment, F (2, 48) = 3.56, $p = 0.04$, and cerebellar cell layer, F (3, 48) = 12.09, $p < 0.0001$, $\alpha = 0.05$.

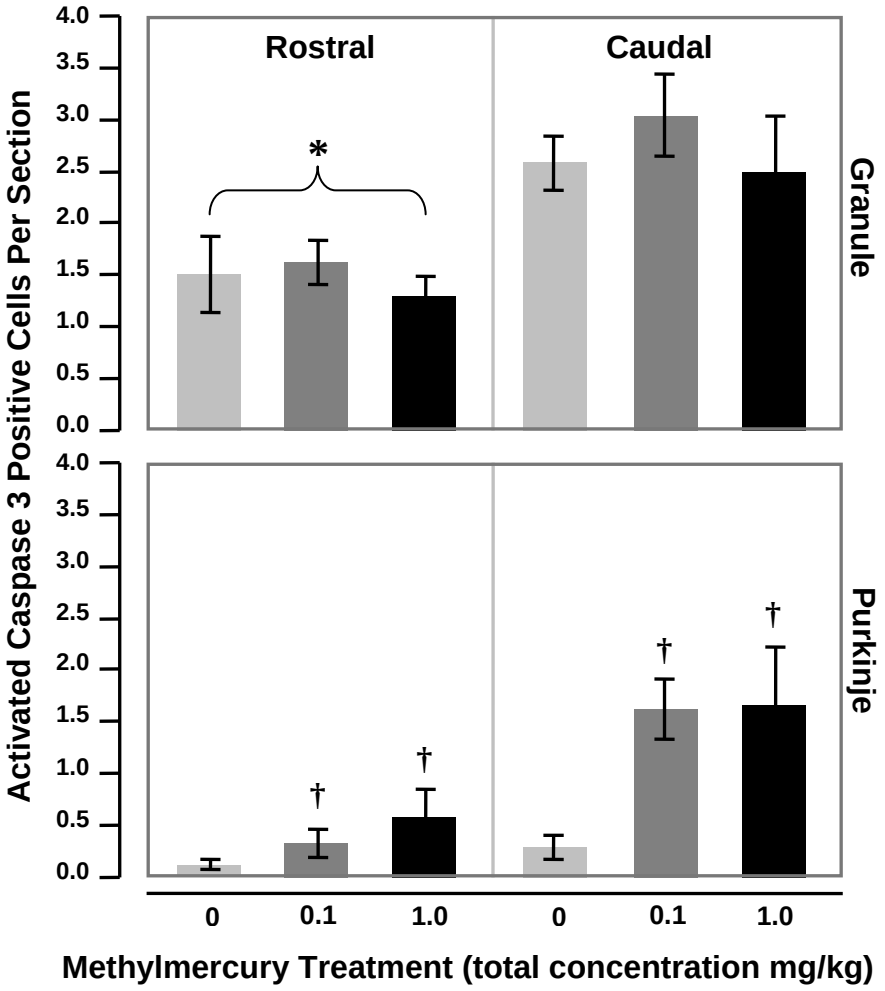

FIG. III-3. The number of activated caspase 3 positive cells in the cerebellum of mice at postnatal day 0 following exposure to 0, 0.1, or 1.0 mg/kg total dose MeHg divided over gestational days 8 to 18. Data indicated that the number of activated caspase 3 positive cells in the granule cell layer of the rostral cerebellum was decreased compared to those in the granule cell layer of the caudal cerebellum (*). The number of activated caspase 3 positive cells was increased in 0.1 and 1.0 MeHg treated cerebella compared to controls (†). No differences were indicated for sex. Data are presented as mean ± standard error of the mean and were analyzed by three-way ANOVA and Tukey's HSD post hoc or Student's t analysis. Granule cell layer, F (1, 24) = 5.03, p = 0.03, and Purkinje cell layer, F (1, 24) = 6.30, p = 0.01, α = 0.05.

P10 cerebella

The number of Fluoro-Jade positive dying cells in the cerebellum of mice at P10 was analyzed by three-way ANOVA to determine between-subject differences and interactions associated with sex, cerebellar cell layer, and MeHg treatment. Data indicated main effects for MeHg treatment, F (2, 48) = 4.3, p = 0.02, and cerebellar cell layers, F (3, 48) = 24.13, $p < 0.0001$. Tukey's HSD post hoc analysis indicated that Fluoro-Jade positive cells were increased in the 0.1 total dose MeHg treatment compared to the 1.0 MeHg treatment in the external germinal cell layer (Fig III-4). No treatment differences were observed in any of the other cerebellar cell layers. Data also indicated increased numbers of Fluoro-Jade positive dying cells for controls in the molecular layer compared to the external germinal cell layer. Both the molecular and external germinal cell layers exhibited increased numbers of Fluoro-Jade positive cells compared to the Purkinje cell layer in controls. In the 0.1 mg/kg MeHg treatment, increased numbers of Fluoro-Jade positive cells were observed in the molecular layer compared to the granule and external granule cell layers, and in all three of these layers compared to the Purkinje cell layer. In the 1.0 mg/kg MeHg treatment, increased numbers of Fluoro-Jade positive cells were observed in the molecular and granule cell layers compared to the external germinal cell layer, and in all three of these layers compared to the Purkinje cell layer (Fig III-4). Three-way ANOVA was used to determine between-subject differences and interactions in the number of Fluoro-Jade positive dying cells associated with sex, cerebellar lobule, and MeHg treatment for each cerebellar cell layer, independently. Main effects were indicated for MeHg treatment, F (2, 96) = 8.89, p = 0.0003, and cerebellar lobule, F (9, 96) = 2.15, p = 0.05 in the external granule cell layer only. Tukey's HSD post hoc analysis indicated decreased numbers of Fluoro-Jade positive dying cells in the 1.0 mg/kg MeHg treatment compared to controls in lobule IV/V and IX of the external germinal layer of P10 cerebella (Fig III-5). Data also indicated that lobules III and IV/V exhibited increased numbers of Fluoro-Jade positive dying cells compared to lobule VII in the external germinal layer of control P10 cerebella (Fig III-5).

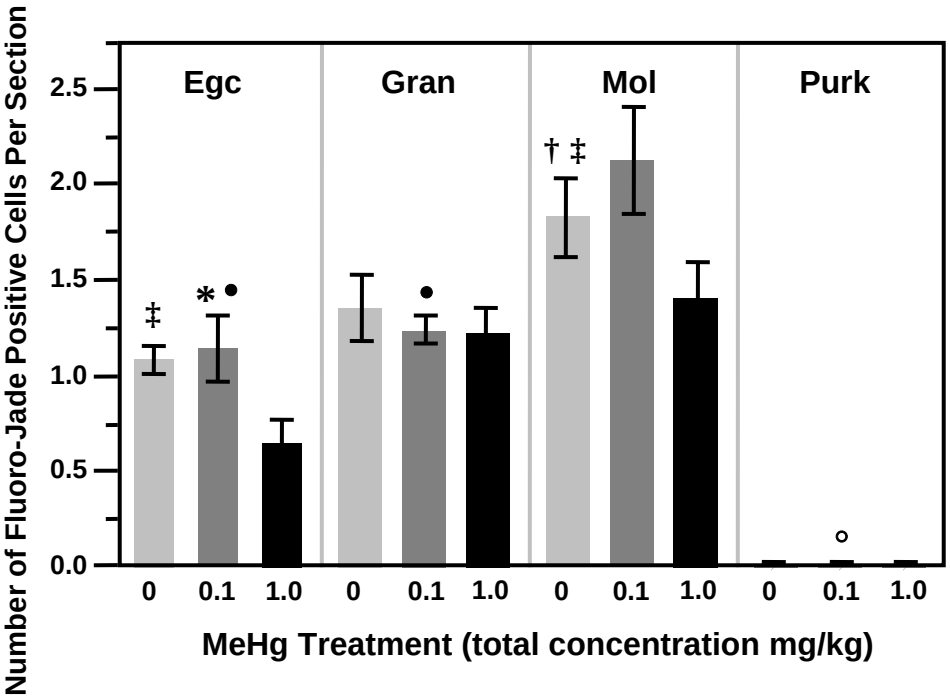

FIG. III-4. The number of Fluoro-Jade positive cells in the layers of the cerebellum of mice at postnatal day 10 following exposure to 0, 0.1, or 1.0 mg/kg total dose MeHg divided over gestational days 8 to 18. Cerebellar cell layers are represented as: Egc (external germinal cell layer), Gran (granule cell layer), Mol (molecular cell layer), and Purk (Purkinje cell layer). Analysis indicated differences in cerebellar cell layers and MeHg treatments. The number of Fluoro-Jade positive dying cells was increased in the 0.1 MeHg treatment compared to the 1.0 MeHg treatment in the external germinal cell layer (*). No MeHg treatment differences were observed in any of the other cerebellar cell layers. Fluoro-Jade positive cell numbers were increased in the molecular layer controls compared to the external germinal layer controls (†). The molecular layer controls and the external germinal layer controls both exhibited increased numbers of Fluoro-Jade positive cells compared to Purkinje cell layer controls (‡). The number of Fluoro-Jade positive cells in 0.1 mg/kg MeHg treated cerebella was decreased in the external germinal layer and granule cell layer compared to the molecular layer (•). The number of Fluoro-Jade positive cells in 0.1 mg/kg MeHg treated cerebella was decreased in the Purkinje cell layer compared to the molecular, granule, and external germinal cell layers (°). No differences were indicated for sex. Data are presented as mean ± standard error of the mean and were analyzed by three-way ANOVA and Tukey's HSD post hoc analysis. MeHg treatment, F (2, 48) = 4.3, p = 0.02, and cerebellar cell layers, F (9, 48) = 24.13, p < 0.0001, $\alpha = 0.05$.

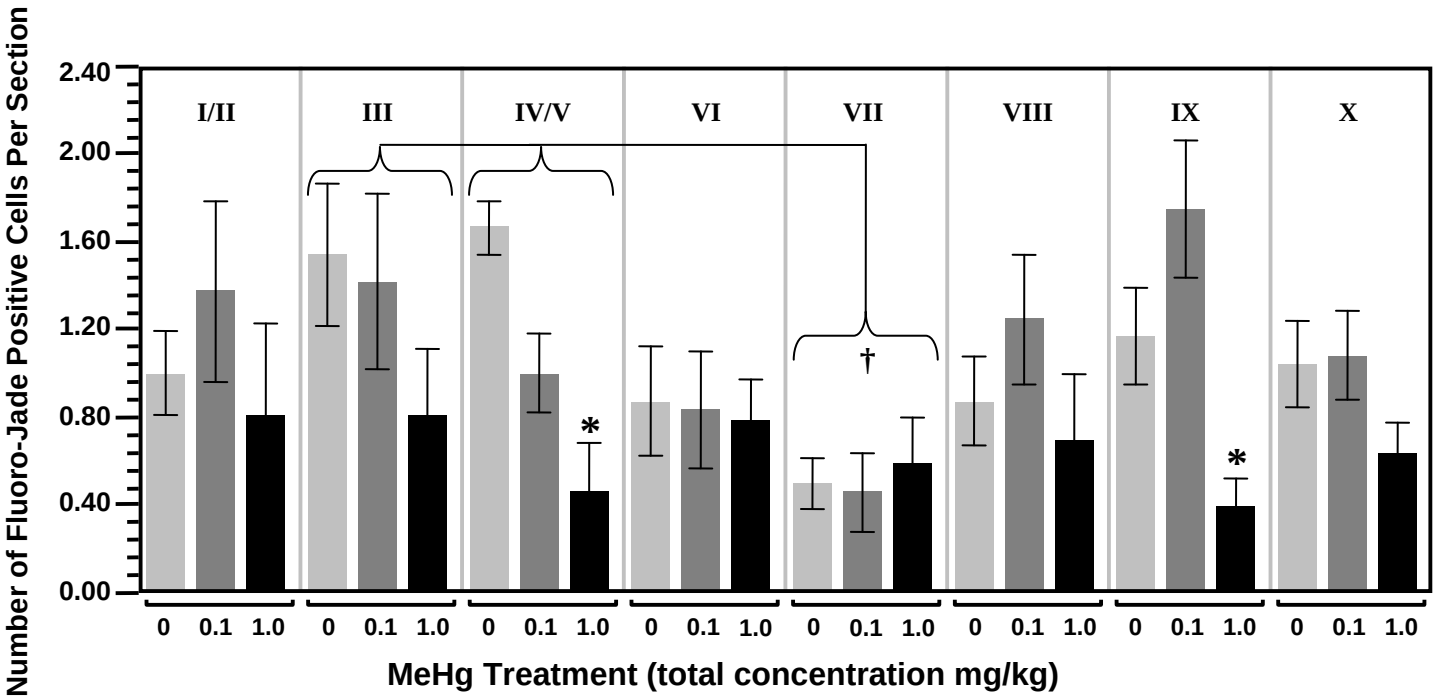

FIG. III-5. The number of Fluoro-Jade positive cells in the cerebellum of mice at postnatal day 10 following exposure to 0, 0.1, or 1.0 mg/kg total dose MeHg divided over gestational days 8 to 18. Roman numerals identify the cerebellar lobules. Analysis indicated differences in MeHg treatments and cerebellar lobules in the external germinal cell layer. No differences were observed in any of the other cerebellar cell layers. No differences were observed for sex. Data indicated decreased numbers of Fluoro-Jade positive dying cells in the 1.0 mg/kg MeHg treatment compared to controls in cerebellar lobules IV/V and IX of the external germinal layer (*). Data also indicated that lobule VII exhibited decreased numbers of Fluoro-Jade positive cells compared to lobules III and IV/V in the external germinal layer of control cerebella (†). Data are presented as mean ± standard error of the mean and were analyzed by three-way ANOVA and Tukey's HSD post hoc analysis. MeHg treatment, F (2, 96) = 8.89, p = 0.0003, and cerebellar lobule, F (9, 96) = 2.15, p = 0.05, α = 0.05.

The number of activated caspase 3 positive cells in the cerebellum of P10 mice was analyzed by three-way ANOVA to determine between-subject differences and interactions associated with sex, cerebellar cell layer, and MeHg treatment. Main effects were indicated for sex, F (1, 48) = 9.74, p = 0.003, and for cerebellar cell layer, F (3, 48) = 6.43, p = 0.0009. Student's t post hoc analysis indicated no differences in the numbers of activated caspase 3 positive cells in females compared to males in any of the cell layers of the P10 cerebellum (Fig III-6). For P10 female and male cerebella, Tukey's HSD post hoc analysis indicated that activated caspase 3 positive cells were increased in the molecular, granule and external germinal cell layers compared to the Purkinje cell layer (Fig III-6). Three-way ANOVA was used to determine between-subject differences and interactions in the number of activated caspase 3 positive cells associated with sex, cerebellar lobule, and MeHg treatment for each cerebellar cell layer, independently. No differences were observed in the number of activated caspase 3 positive cells between males and females, among MeHg treatments, or among lobules in any of the cerebellar cell layers.

P0 hippocampi

The number of Fluoro-Jade and activated caspase 3 positive cells in the dentate gyrus, CA1, and CA3 regions of the hippocampus of mice at P0 was analyzed by three-way ANOVA to determine between-subject differences and interactions associated with sex, hippocampal region, and MeHg treatment. Analysis indicated no differences in sex, hippocampal region, or MeHg treatment in P0 hippocampi for the Fluoro-Jade or the activated caspase 3 experiments.

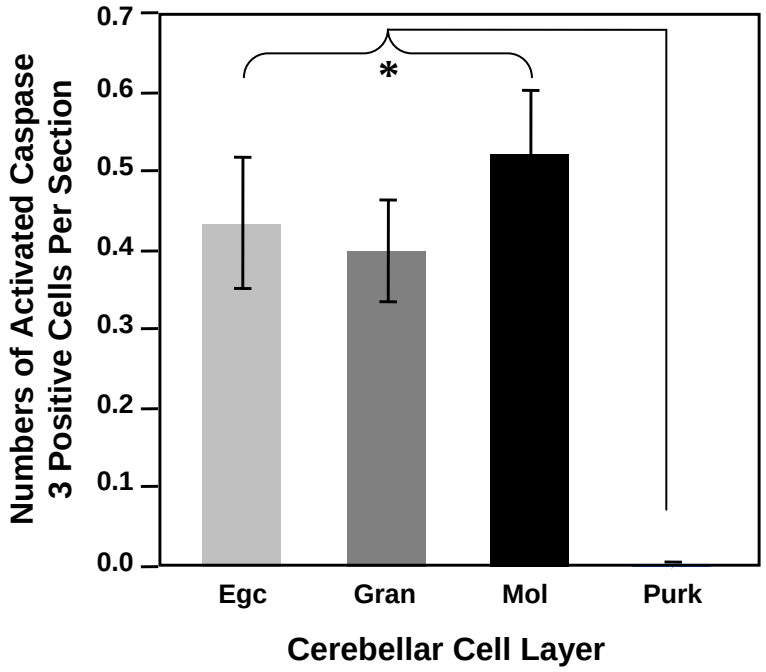

FIG. III-6. The number of activated caspase 3 positive cells in the cerebellum of mice at postnatal day 10 following exposure to 0, 0.1, or 1.0 mg/kg total dose MeHg divided over gestational days 8 to 18. Cerebellar cell layers are represented as: Egc (external germinal cell layer), Gran (granule cell layer), Mol (molecular cell layer), and Purk (Purkinje cell layer). Analysis indicated differences in sex and cerebellar cell layer. No differences were observed in MeHg treatments. Data indicated increased numbers of activated caspase 3 positive cells in the external germinal, granule, and molecular cell layers compared to the Purkinje cell layer of P10 male and female cerebella (*). Although a main effect was indicated for sex, Student's t post hoc analysis indicated no differences in the number of activated caspase 3 positive cells between males and females in any of the cell layers. Data are presented as mean ± standard error of the mean and were analyzed by three-way ANOVA and Tukey's HSD or Student's t post hoc analysis. Sex, F (1, 48) = 9.74, p = 0.003, and cerebellar cell layer, F (3, 48) = 6.43, p = 0.0009, $\alpha = 0.05$.

P10 hippocampi

The number of Fluoro-Jade positive cells in the dentate gyrus and the hippocampus proper was analyzed by three-way ANOVA to determine between-subject differences and interactions associated with sex, cell layer, and MeHg treatment. Data indicated a main effect for cell layer in the dentate gyrus, F (2, 36) = 4.10, p = 0.03. Tukey's HSD post hoc analysis indicated increased numbers of Fluoro-Jade positive dying cells in the granule and subgranular cell layers compared to the hilar region of the dentate gyrus from mice at P10 (Fig III-7). Analysis by three-way ANOVA also

indicated a main effect for region (CA1 and CA3) in the hippocampus proper, F (1, 24) = 5.13, p = 0.03. Student's t post hoc analysis indicated increased numbers of Fluoro-Jade positive dying pyramidal cells in the CA3 region compared to the CA1 region of the hippocampus proper from mice at P10 (Fig III-8). No main effects were observed for sex or MeHg treatment in either the dentate gyrus or the hippocampus proper for Fluoro-Jade analysis. The number of activated caspase 3 positive cells in the dentate gyrus and the hippocampus proper was analyzed by three-way ANOVA to determine between-subject differences and interactions associated with sex, cell layer/region, and MeHg treatment. No between-subject main effects were observed in either the dentate gyrus or the hippocampus proper for activated caspase 3 positive cells in mice at P10.

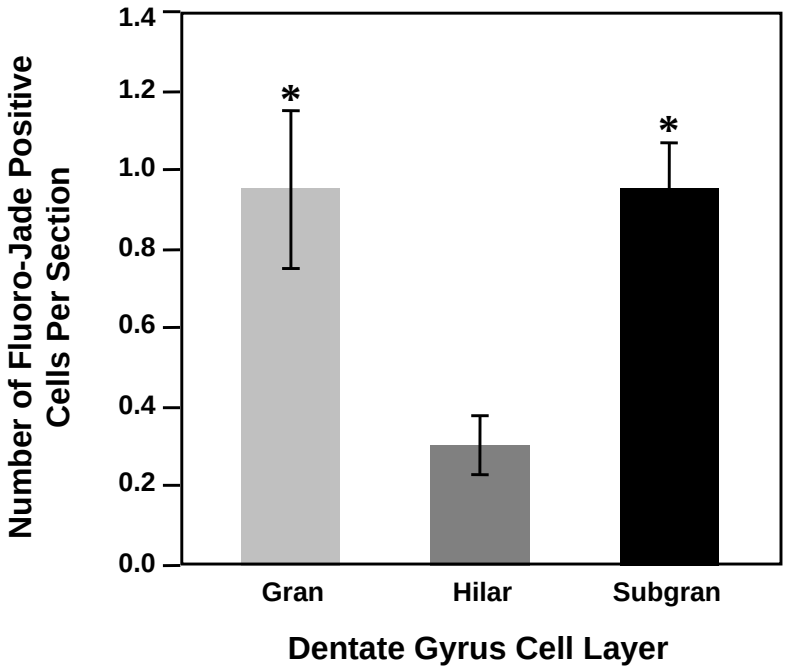

FIG. III-7. The number of Fluoro-Jade positive cells in the dentate gyrus of the hippocampus of mice at postnatal day 10 following exposure to 0, 0.1, or 1.0 mg/kg total dose MeHg divided over gestational days 8 to 18. Dentate gyrus cell layers are represented as: Gran (granule cell layer), Hilar (hilar region), and Subgran (subgranular layer). Data indicated increased numbers of Fluoro-Jade positive cells in the granule and subgranular cell layers compared to the hilar region of the P10 dentate gyrus (*). No differences were indicated for sex or MeHg treatment. Data are presented as mean ± standard error of the mean and were analyzed by three-way ANOVA and Tukey's HSD post hoc analysis. F (2, 36) = 4.10, p = 0.03, α = 0.05.

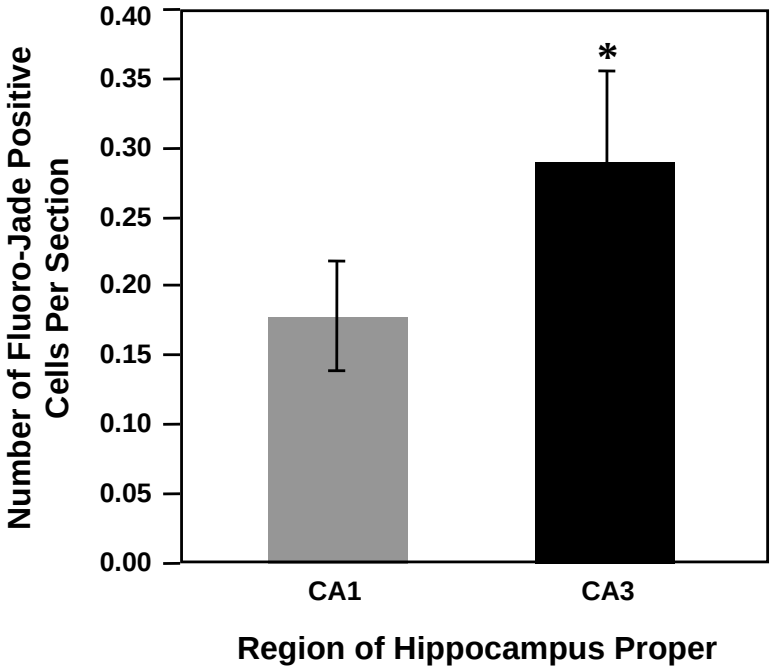

FIG. III-8. The number of Fluoro-Jade positive pyramidal cells in the hippocampus proper of mice at postnatal day 10 following exposure to 0, 0.1, or 1.0 mg/kg total dose MeHg divided over gestational days 8 to 18. Data indicated increased numbers of Fluoro-Jade positive pyramidal cells in the CA3 region compared to the CA1 region of the hippocampus proper of P10 mice hippocampi (*). No differences were observed in MeHg treatments or sex. Data are presented as mean ± standard error of the mean and were analyzed by three-way ANOVA and Student's t post hoc analysis. F (1, 24) = 5.13, p = 0.03, α = 0.05.

Identification and validation of acutely isolated cells as neurons

Examples of neurons isolated from cerebella and hippocampi of mice at P0 are shown in Fig III-9. Double fluorescence imaging using NeuN to label nuclei and cytoplasm of neurons and DAPI to label nuclei of all cells showed the isolation procedure used in this study yielded predominantly more neurons than other cell types. All nuclei were labeled with DAPI (blue), and nuclei and some cytoplasm of neurons were labeled with NeuN (red). Granule cells were distinguished from other neurons based on their small cell size (5 – 8 μm).

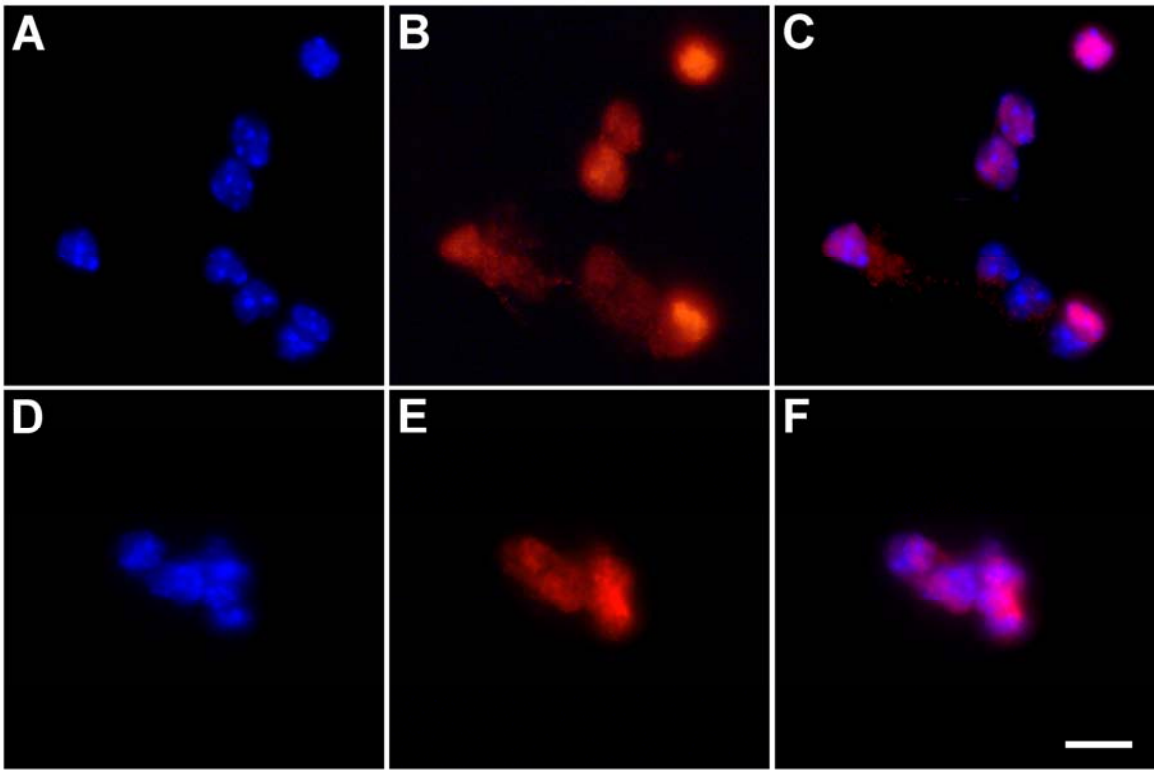

FIG. III-9. NeuN and DAPI double-labeled cells isolated from the cerebellum and hippocampus of mouse pups at postnatal day 0. Panels A, B, and C are cells from the cerebellum. Panels D, E, and F are cells from the hippocampus. Panels A and D show cells labeled with DAPI; B and E show cells labeled with NeuN; C and F are overlay images of NeuN and DAPI. Granule cells were distinguished from other neurons based on their small size (5 - 8 μm). The majority of isolated cells were double-labeled granule cells. Scale bar = 5 μm.

Mitochondrial membrane potential

Membrane potential (MMP) of the inner mitochondrial membrane of isolated cerebellar and hippocampal granule cells was measured using TMRM dye and fluorescence microscopy to determine whether treatment with MeHg from gestational day 8 to 18 would alter mitochondrial function in mouse pups at P0 and P10. Relative MMP for pups at P0 was analyzed by three-way ANOVA for differences and interactions in sex, brain regions, and MeHg treatment. Analysis indicated main effects for MeHg treatment, F (2, 36) = 3.99, p = 0.0273, but not for sexes or cerebellar and hippocampal brain regions. In addition, an interaction was indicated between MeHg treatment and brain region, F (2, 36) = 12.26, $p < 0.0001$. Tukey's HDS post hoc analysis indicated decreased MMP in the 1.0 mg/kg total dose MeHg treatment compared to controls (Fig III-10). The interaction observed for MeHg treatment and structure indicated that treatment differences were greater for the cerebellum than for the hippocampus.

Relative MMP for pups at P10 was analyzed by three-way ANOVA to determine differences associated with sex, brain region, and MeHg treatment. Data indicated main effects for MeHg treatment, F (2, 48) = 30.79, $p < 0.0001$, and interactions between MeHg treatments and brain region, F (2, 48) = 3.98, p = 0.0251, and among sex, MeHg treatments, and brain region, F (2, 48) = 9.83, p = 0.0003. Tukey's HSD post hoc analysis indicated that MMP was increased in the 0.01 mg/kg MeHg treatment compared to the 1.0 mg/kg MeHg treatment and controls. The interactions indicated for sex, brain region, and MeHg treatment suggested that MeHg treatment differences were greater in females than males, and greater in the cerebellum than the hippocampus (Fig III-11). CCCP was added to isolated control granule cells (positive method control) to verify that the method used to measure changes in MMP was, in fact, measuring changes in MMP. CCCP uncouples oxidative phosphorylation within mitochondria which results in decreased MMP. Addition of CCCP to control cells incubated with TMRM resulted in a dramatic decrease in the fluorescence intensity of mitochondria indicating depolarization of the mitochondrial membrane (data not shown); no auto-fluorescence was observed in

samples without TMRM dye, nor in samples without cells that contained TMRM dye (negative controls, data not shown).

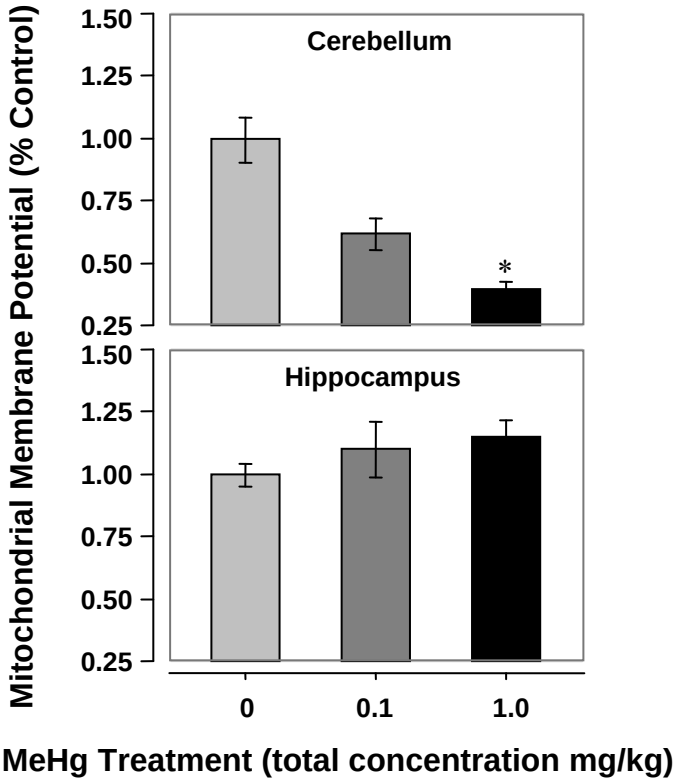

FIG. III-10. Relative mitochondrial membrane potential for cerebella and hippocampi of mice at postnatal day 0 exposed to 0, 0.1, or 1.0 mg/kg total dose MeHg divided over gestational days 8 to 18. Cells were incubated with 150 nM TMRM for 20 min and imaged by fluorescence microscopy. Data were collected for individual mitochondria within the isolated granule cells. Analysis by three-way ANOVA indicated differences in MeHg treatment, but not in sex and brain region. However, an interaction was indicated for MeHg treatment and brain region. Tukey's HDS post hoc analysis indicated decreased MMP in the 1.0 mg/kg MeHg treatment compared controls (*). The indicated interaction suggested that observed MeHg treatment differences were greater in the cerebellum than the hippocampus. Data are represented as percentage of control and mean ± standard error of the mean. Three-way ANOVA for MeHg treatment, F (2, 36) = 3.99, p = 0.0273, and interaction F (2, 36) = 12.26, $p < 0.0001$; $\alpha = 0.05$.

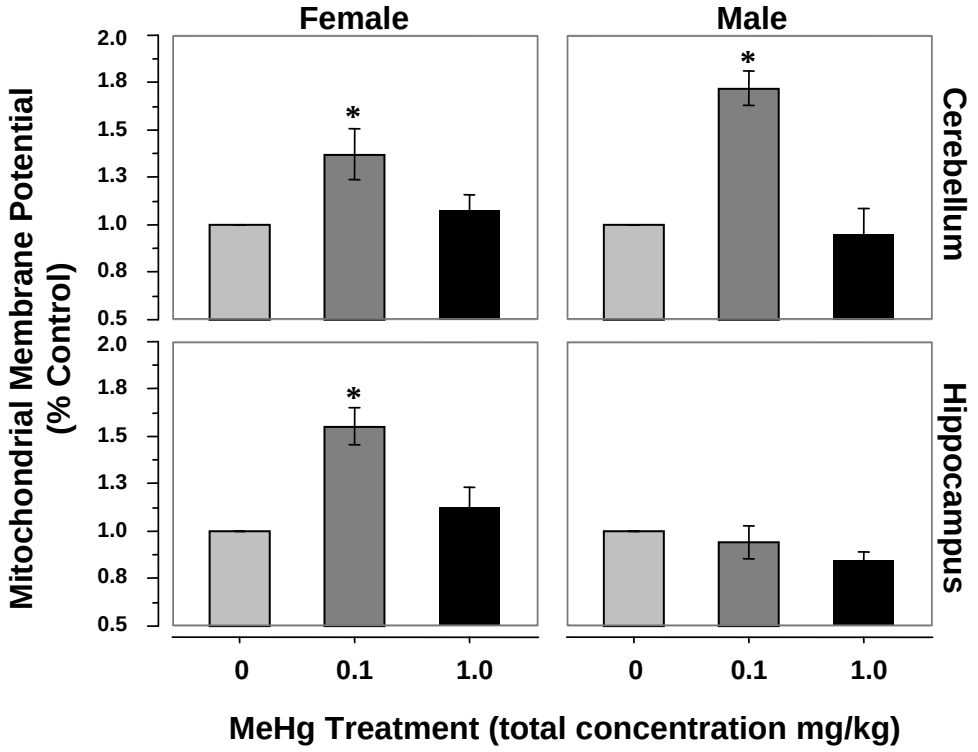

FIG. III-11. Relative mitochondrial membrane potential for cerebella and hippocampi of mice at postnatal day 10 exposed to 0, 0.1, or 1.0 mg/kg total dose MeHg divided over gestational days 8 to 18. Analysis by three-way ANOVA indicated differences in MeHg treatment, but not in sex and brain region. However, an interaction was indicated for MeHg treatment and brain region, and for sex, MeHg treatment and brain region. Tukey's HDS post hoc analysis indicated increased MMP in the 0.1 mg/kg MeHg treatment compared to the 1.0 mg/kg MeHg treatment and controls (*). The indicated interaction suggested that observed MeHg treatment differences were greater in the cerebellum than the hippocampus, and greater in females than males. Data are represented as percentage of control and mean ± standard error of the mean. Three-way ANOVA for MeHg treatment, F (2, 48) = 30.79, $p < 0.0001$, and MeHg treatment and brain region interaction F (2, 48) = 3.98, $p = 0.0251$, and sex, MeHg treatment, and brain region interaction F (2, 48) = 9.83, $p = 0.0003$; $\alpha = 0.05$.

Basal free intracellular Ca^{2+}

Calcium ion homeostasis was examined by measuring $[Ca^{2+}]_i$ in isolated cerebellar and hippocampal granule cells from male and female mice at P0 and P10 following exposure to 0, 0.1, and 1.0 mg/kg total dose MeHg divided over G8 to G18. Relative $[Ca^{2+}]_i$ data from pups at P0 were analyzed by three-way ANOVA to determine differences associated with sex, brain region, and MeHg treatment. Data indicated a main effect for MeHg treatment, F (2, 36) = 10.39, p = 0.0003, but not for sex or brain region. In addition, an interaction was indicated for MeHg treatment and brain region, F (2, 36) = 11.68, p = 0.0001. Tukey's HSD post hoc analysis indicated that $[Ca^{2+}]_i$ was increased in both the 0.1 and 1.0 mg/kg MeHg treatments compared to controls (Fig III-12). The indicated interaction between MeHg treatment and brain region suggested that the observed differences in MeHg treatment were greater in the cerebellum than the hippocampus (Fig III-12).

Relative $[Ca^{2+}]_i$ data from pups at P10 were analyzed by three-way ANOVA to determine differences associated with sex, brain region, and MeHg treatment. Representative images of isolated cerebellar and hippocampal granule cells incubated with Calcium Green-1 dye are shown in Fig III-13. Data indicated a main effect for MeHg treatment, F (2, 44) = 31.97, $p < 0.0001$, and an interaction among sex, brain region, and MeHg treatment, F (2, 44) = 11.05, p = 0.0001. Tukey's HSD post hoc analysis indicated that basal $[Ca^{2+}]_i$ was increased in the 1.0 mg/kg MeHg treatment compared to the 0.1 mg/kg MeHg treatment and controls (Fig III-14). The indicated interaction suggested that the observed MeHg treatment differences were greater in females than males, and greater in the cerebellum than the hippocampus (Fig III-14). Thapsigargin was added to isolated control cerebellar and hippocampal granule cells as a method control to validate the measurement of changes in $[Ca^{2+}]_i$. Thapsigargin is an inhibitor of sarco-endoplasmic reticulum Ca^{2+} ATPases and raises cytosolic free Ca^{2+} by blocking the ability of the cell to pump Ca^{2+} into the endoplasmic reticulum (Treiman *et al.*, 1998). Addition of thapsigargin to isolated control cerebellar and hippocampal granule cells (positive method control) resulted in a substantial increase in the

fluorescence within the cells, indicating an increase in $[Ca^{2+}]_i$; no auto-fluorescence was observed in samples without Calcium Green-1, nor in samples without cells that contained Calcium Green-1 (negative controls), indicating minimal atmospheric and/or photo-oxidation (data not shown).

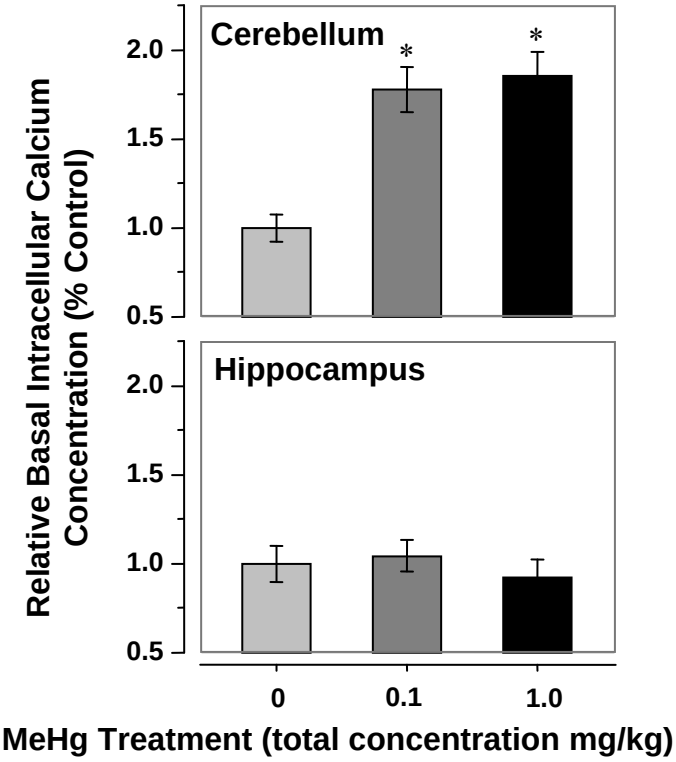

FIG. III-12. Relative basal intracellular calcium ion concentration $[Ca^{2+}]_i$ for cerebella and hippocampi of mice at postnatal day 0 exposed to 0, 0.1, or 1.0 mg/kg total dose MeHg divided over gestational days 8 to 18. Analysis by three-way ANOVA indicated differences in MeHg treatment, but not in sex and brain region. However, an interaction was indicated between MeHg treatment and brain region. Tukey's HDS post hoc analysis indicated increased $[Ca^{2+}]_i$ in the 0.1 and 1.0 mg/kg MeHg treatments compared to controls (*). The indicated interaction suggested that observed MeHg treatment differences were greater in the cerebellum than the hippocampus. Data are represented as percentage of control and mean ± standard error of the mean. Three-way ANOVA for MeHg treatment, F (2, 36) = 10.39, p = 0.0003, and MeHg treatment and brain region interaction F (2, 36) = 11.68, p = 0.0001, α = 0.05.

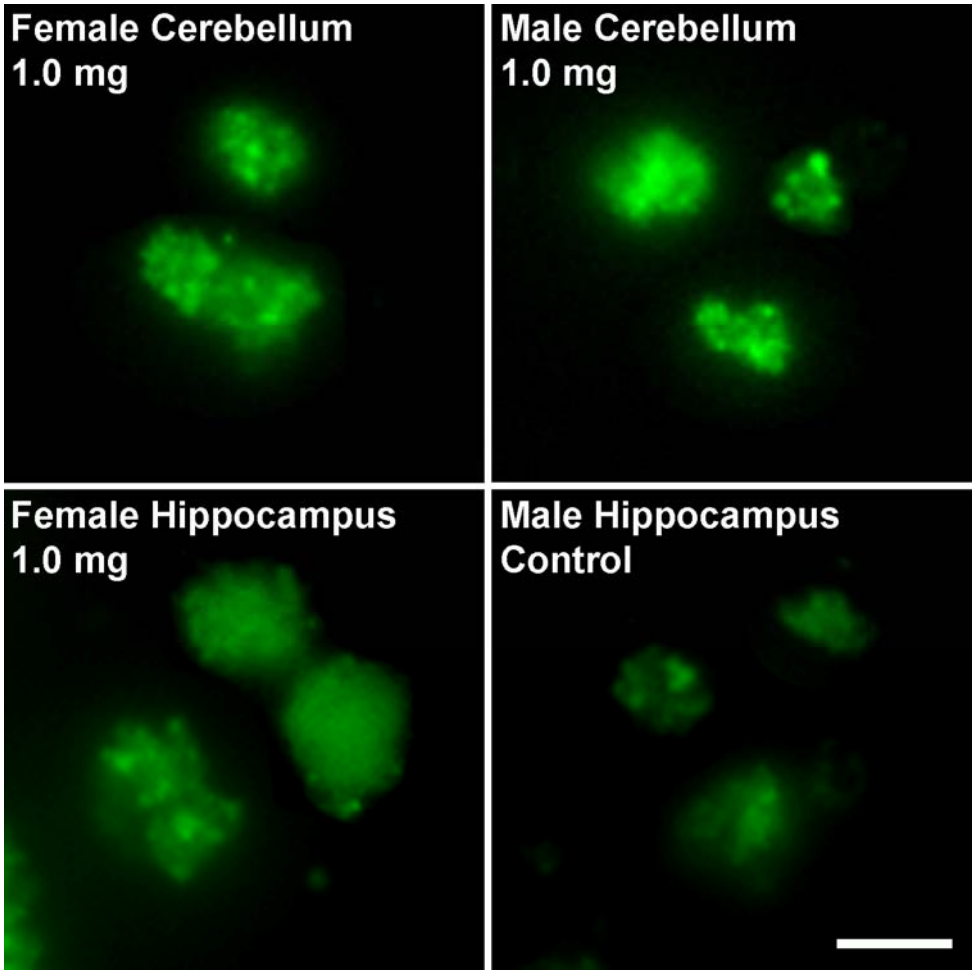

FIG. III-13. Representative images of isolated granule cells from postnatal day 10 male and female hippocampi and cerebella. Free intracellular Ca^{2+} binds to Calcium Green-1 dye within the cell and appears fluorescent green. Cells from cerebella and hippocampi treated with 1.0 mg/kg total dose MeHg exhibited increased fluorescence compared to controls. The increased fluorescence indicated an increased level of intracellular Ca^{2+} in the MeHg treated cells compared to controls. Scale bar is 10 μm.

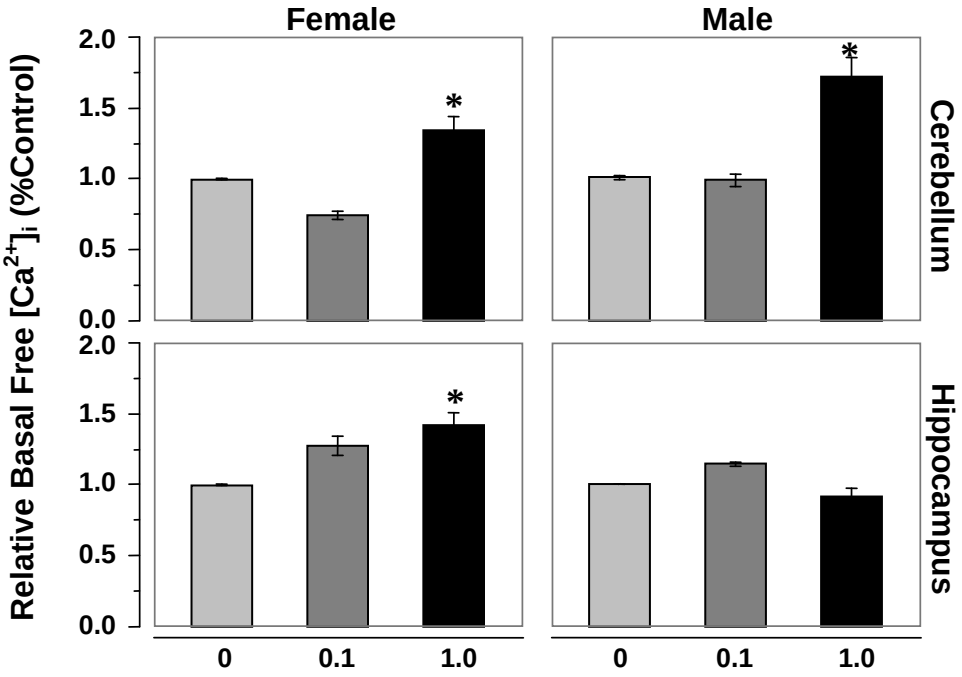

FIG. III-14. Relative basal intracellular calcium ion concentrations $[Ca^{2+}]_i$ for cerebella and hippocampi of mice at postnatal day 10 exposed to 0, 0.1, or 1.0 mg/kg total dose MeHg divided over gestational days 8 to 18. Analysis by three-way ANOVA indicated differences in MeHg treatment, but not in sex and brain region. However, an interaction was indicated between sex, MeHg treatment, and brain region. Tukey's HDS post hoc analysis indicated increased $[Ca^{2+}]_i$ in the 1.0 mg/kg MeHg treatment compared to the 0.1 mg/kg MeHg treatment and controls (*). The indicated interaction suggested that the observed MeHg treatment differences were greater in females than males, and greater in the cerebellum than the hippocampus. Data are represented as percentage of control and mean ± standard error of the mean. Three-way ANOVA for MeHg treatment, F (2, 44) = 31.97, $p < 0.0001$, and MeHg treatment and brain region interaction F (2, 44) = 11.05, $p = 0.0001$, $\alpha = 0.05$.

Reactive oxygen species

The rate of generation of and the level of ROS in isolated cerebellar and hippocampal granule cells from mouse pups at P0 and P10 exposed to 0, 0.1, and 1.0 mg/kg total dose MeHg divided over gestational days 8 to 18 was measured by fluorescence microscopy and imaging of the fluorescence of the dye CM-H_2DCFDA every 2.5 min for 30 min. Data for the rate of generation of ROS for mice at P0 were analyzed by three-way MANOVA with repeated measures for ROS reading time to determine between-subject differences and interactions associated with sex, brain region, and MeHg treatment. No between-subject effects were indicated. Data did not meet the condition of sphericity, therefore, within-subject data were analyzed using the Greenhouse-Geisser adjusted univariate analysis (Grieve, 1984). No within-subject differences were indicated in cerebella or hippocampi from mice at P0. Although there was no difference in the rate at which ROS were produced in mice at P0, data were subsequently analyzed to determine if there were differences in the relative amount of ROS produced. Relative amount of ROS produced in cells isolated from cerebella and hippocampi from mice at P10 were analyzed by three-way MANOVA with repeated measures for ROS reading time to determine between-subject differences and interactions associated with sex, brain region, and MeHg treatment. Data indicated a between-subject interaction effect between brain region and MeHg treatment, F (2, 72) = 6.49, p = 0.0502. The indicated interaction suggests that MeHg treatment effects are greater in the cerebellum than in the hippocampus (Fig III-15). Data did not meet the condition of sphericity, therefore, within-subject data were analyzed using the Greenhouse-Geisser adjusted univariate analysis. No within-subject effects were indicated for the amount of ROS produced in cerebella and hippocampi of P0 mice.

FIG. III-15. Relative level of reactive oxygen species produced in granule cells isolated from cerebella and hippocampi of mouse pups at postnatal day 0 exposed to 0, 0.1, or 1.0 mg/kg total dose MeHg divided over gestational days 8 to 18. The amount of ROS produced was measured over a 30 min time period at intervals of 2.5 min. ROS data were analyzed by three-way MANOVA with repeated measures for reading time. Analysis indicated a between-subject interaction effect of brain regions and MeHg treatments. Although no between-subject differences were indicated for MeHg treatment, the brain region and MeHg treatment interaction suggested that the MeHg treatments differed more in the cerebellum than in the hippocampus (*). The condition of sphericity was not met; therefore with-in subject differences were analyzed by the Greenhouse-Geisser adjusted univariate analysis. No with-in subject differences were observed in the amount of ROS produced. Three-way MANOVA interaction, F (2, 72) = 6.49, p = 0.0502, $\alpha = 0.05$.

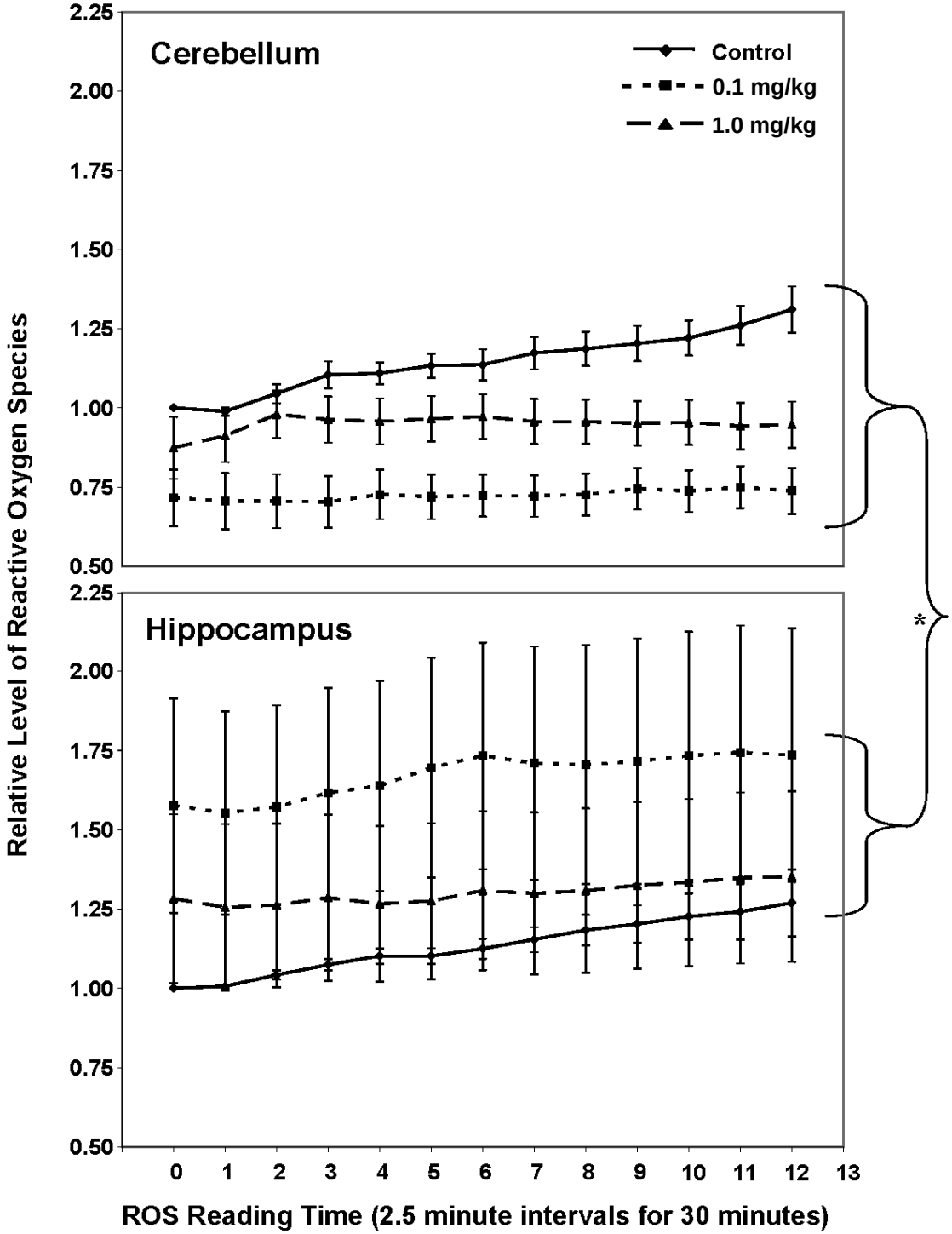
Cerebellum
Control
0.1 mg/kg
1.0 mg/kg
Hippocampus
Relative Level of Reactive Oxygen Species
2.25
2.00
1.75
1.50
1.25
1.00
0.75
0.50
0 1 2 3 4 5 6 7 8 9 10 11 12 13
ROS Reading Time (2.5 minute intervals for 30 minutes)
*

Data for the rate of generation of ROS for mice at P10 were analyzed by three-way MANOVA with repeated measures for ROS reading time to determine between-subject differences and interactions associated with sex, brain region, and MeHg treatment. No between-subject differences were indicated. Data did not meet the condition of sphericity, therefore, within-subject data were analyzed using the Greenhouse-Geisser adjusted univariate analysis (Grieve, 1984). No within-subject differences were indicated for cerebella or hippocampi from mice at P10. Although there was no difference in the rate at which ROS were produced in mice at P10, data were subsequently analyzed to determine if there were differences in the relative amount of ROS produced. Relative amount of ROS produced in cells isolated from cerebella and hippocampi from mice at P10 were analyzed by three-way MANOVA with repeated measures for ROS reading time to determine between-subject differences and interactions associated with sex, brain region, and MeHg treatment. Data indicated a between-subject interaction effect between brain region and MeHg treatment, F (2, 56) = 4.65, p = 0.0147. The indicated interaction suggested that MeHg treatment effects were greater in the cerebellum than in the hippocampus (Fig III-16). Data did not meet the condition of sphericity, therefore, within-subject data were analyzed using the Greenhouse-Geisser adjusted univariate analysis (Grieve, 1984). No within-subject effects were indicated for the amount of ROS produced in cerebella and hippocampi of P10 mice. *Tertiary* butyl hydroperoxide (*t*BHP) was added to isolated control cerebellar and hippocampal granule cells as a method control to validate the measurement of changes in ROS. *t*BHP penetrates the cell membrane and reacts with heme-proteins to produce alkoxyl radicals. Addition of *t*BHP to isolated control granule cells (positive control) resulted in a dramatic increase in the fluorescence within the cells indicating an increase in the level of ROS; no auto-fluorescence was observed in samples without CMH_2DCFDA dye, nor in samples without cells that contained CMH_2DCFDA (negative control), indicating minimal atmospheric and/or photo-oxidation (data not shown).

FIG. III-16. Relative amount of reactive oxygen species produced in granule cells isolated from cerebella and hippocampi of mouse pups at postnatal day 10 exposed to 0, 0.1, or 1.0 mg/kg total dose MeHg divided over gestational days 8 to 18. The amount of ROS produced was measured over a 30 min time period at intervals of 2.5 min. ROS data were analyzed by three-way MANOVA with repeated measures for reading time. Analysis indicated a between-subject interaction effect between brain regions and MeHg treatment. Although no between-subject differences were indicated for MeHg treatment, the brain region and MeHg treatment interaction suggested that the MeHg treatments differed more in the cerebellum than in the hippocampus (*). The condition of sphericity was not met; therefore with-in subject differences were analyzed by the Greenhouse-Geisser adjusted univariate analysis. No with-in subject differences were observed in the amount of ROS produced. Three-way MANOVA interaction, F (2, 56) = 4.65, p = 0.0147, $\alpha = 0.05$.

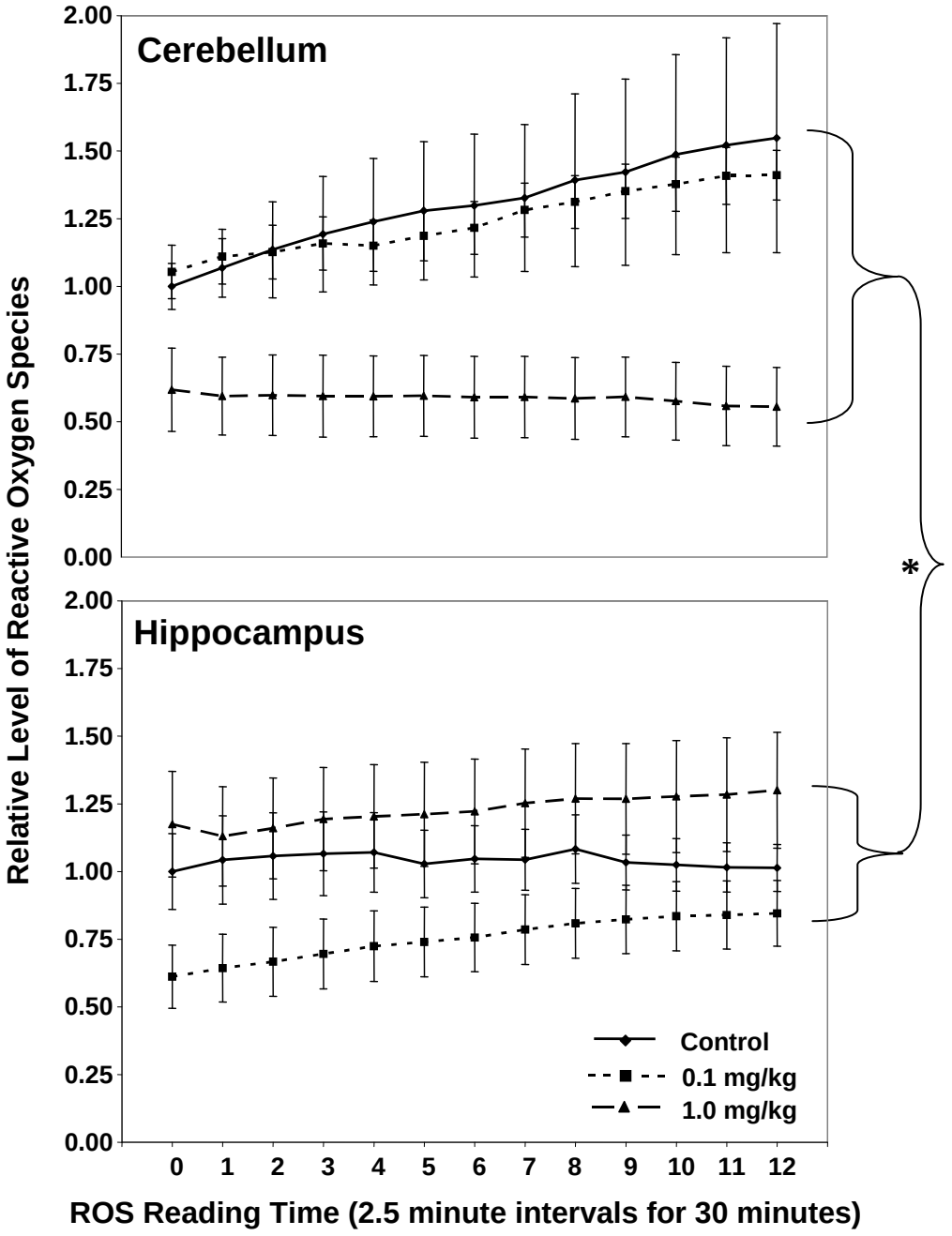
Cerebellum
Hippocampus
Relative Level of Reactive Oxygen Species
2.00
1.75
1.50
1.25
1.00
0.75
0.50
0.25
0.00
0 1 2 3 4 5 6 7 8 9 10 11 12
ROS Reading Time (2.5 minute intervals for 30 minutes)
Control
0.1 mg/kg
1.0 mg/kg
*

DISCUSSION

Total Hg in the cerebellum and hippocampus of mouse pups exposed to MeHg from G8 to G18 was measured. As hypothesized, total Hg accumulated in cerebella and hippocampi of P0 and P10 mice in a dose-dependent manner. Although some literature suggests there may be sex differences in the metabolism and biotransformation of MeHg (Nielsen and Andersen, 1991; Rahola *et al.*, 1973; Thomas *et al.*, 1987), no sex differences were observed in accumulation of total Hg within cerebella or hippocampi of P0 or P10 MeHg mice that were exposed to MeHg prenatally. In support of Hg accumulation data in the present study, similar results were shown by Stern *et al.* (2001); mice prenatally exposed to MeHg accumulated total Hg in a dose-dependent manner, with no gender differences. In addition, Stern *et al*. (2001) showed that the concentration of total Hg in the brains of prenatally exposed pups decreased significantly between P4 and P12. In the present study, total Hg concentrations in the brains of mice at P10 were significantly lower than mice at P0 for both treatment concentrations. Background total Hg levels in controls ranged from 0.3635 ng/g wet weight (w. w.) to 0.9311 ng/g w.w. The background levels in the present study fall below what has been reported for mammalian brain tissue. Background levels in non-treated monkeys were reported as 1.4 – 2.3 ng/g w.w. (Lind *et al.*, 1988).

Fluoro-Jade B staining and activated caspase 3 immunohistochemistry were used to detect the presence of dying cells. Dying cells were detected in both the cerebellum and hippocampus of mice at P0 and P10. With Fluoro-Jade staining of cerebella at P0, dying cells were greatest in the granule cell layer, followed by the molecular, then the external germinal, and finally the Purkinje cell layer. Similarly, the number of dying cells in the cerebellum of mice at P0 as analyzed by activated caspase 3 were increased in the granule and external germinal cell layers compared to the molecular and Purkinje cells layers, with no influence from MeHg treatment observed. Apoptotic cell death is known to occur normally in the various layers of the developing cerebellum (Cowan *et al.*, 1984). As many as 20 to 30 percent of proliferating cells, and 8 to 15 percent of postmitotic cells undergo apoptosis in the granule cell and external granule cell layers

during the third trimester of human cerebellar development (Nat *et al.*, 2001). Similar apoptotic cell death occurs in the rat cerebellum from P0 to P21 (Altman, 1972a; Altman, 1972b). Therefore, our cell death data is consistent with known patterns of cell death in the normal developing rodent cerebellum.

However, P0 mice exposed to a total dose of 1.0 mg/kg MeHg exhibited increased numbers of activated caspase 3 positive cells compared to age- and sex-matched controls in the Purkinje cell layer, and the increase was greater in the posterior cerebellum than the anterior cerebellum. Increases in the number of activated caspase 3 positive cells in the caudal cerebellum also were observed in the granule cell layer. This pattern of positively identified cells was not observed with Fluoro-Jade staining. Studies have shown that caspase 3 is activated in Bergmann glia during the process of glial differentiation and granule cell and Purkinje cell migration (Oomman *et al.*, 2006). Bergmann glia are located in the same area of the cerebellum as Purkinje cells. In addition, glial stem cell production and migration, the dispersal of the external granule cell layer, and the ascent and settling of Purkinje cells begins first in the posterior cerebellum (G18 in the rat) and shifts to the anterior cerebellum (G22 in the rat) (Altman and Bayer, 1997). The cells identified by activated caspase 3 in the P0 pups, in fact, may be Bergmann glia as opposed to Purkinje cells, and the difference in the number of activated caspase 3 positive cells in the rostral versus caudal cerebellum may be a result of the delayed development of the rostral compared to the caudal cerebellum.

MeHg is known to be cytotoxic to glia in culture at concentrations of 1.0 μM or greater and to induce gliosis at concentrations as low as 1.0 nM (Monnet-Tschudi *et al.*, 1996). In addition, Bergmann glia take up MeHg in whole animals (Takeuchi *et al.*, 1989), and abnormal Bergmann glia have been shown to adversely affect neuronal migration (Rakic and Sidman, 1973). Dual labeling with GFAP and anti-activated caspase 3 would be appropriate to determine if the activated caspase 3 identified cells are Bergmann glia as opposed to Purkinje cells. Our data indicate that MeHg may affect glia, and subsequently neuronal migration, as opposed to causing neuronal death in the developing cerebellum.

The number of dying cells also was determined for cerebella from P10 mouse pups using both Fluoro-Jade B staining and detection by anti-activated caspase 3. Fluoro-Jade B analysis indicated increased numbers of dying cells in the molecular layer compared to the external germinal and granule cell layers, with the Purkinje cell layer exhibiting decreased numbers of Fluoro-Jade positive cells compared to all other layers in mice at P10. Beginning around P10 in mice, significant numbers of cells begin migrating from the external germinal layer to the molecular layer (basket and stellate cells) and the granule cell layer (granule cells) (Altman, 1972a; Altman, 1972b). During migration, within the molecular layer, stationary basket and stellate cells as well as vertically migrating granule cells can be observed (Altman, 1972a; Altman, 1972b). During the migration and settling processing, some cells will die. Therefore, it is not unusual to observe increased numbers of dying cells in the molecular layer around P10 in rodents.

The external germinal layer of P10 mice was the only cerebellar layer that exhibited a MeHg treatment effect on cell death, with the 1.0 mg/kg total dose MeHg treatment exhibiting decreased numbers of Fluoro-Jade positive cells, specifically in lobules IV/V and IX. The external germinal cell layer reaches maximal thickness by P10 in rats, and is composed of proliferating and differentiating stem cells (Altman, 1972a). Typically, increased numbers of dying cells can be observed in areas of high cell proliferation (Cowan *et al.*, 1984). In the case of our data, we observed decreased numbers of dying cells in the 1.0 mg/kg MeHg treated external germinal cell layer. These results may be explained by a decrease in cell proliferation rate, thus a decrease in the number of observed dying cells, or no difference in cell proliferation rate, and an actual decrease in the rate of cell death. Analysis of the cells using bromodeoxyuridine (BrdU) and terminal deoxynucleotidyl transferase biotin-dUTP nick end labeling (TUNEL), BrdU and activated caspase 3, or BrdU and Fluoro-Jade double labeling would aid in determining possible correlations between the rate of cell death and the rate of cell proliferation. In addition, volume measurements and total cell counts of the cells in the external germinal layer might be helpful in determining cell death and

proliferation associations. We also observed a decrease in the number of Fluoro-Jade positive cells in cerebellar lobule VII in all treatments. Literature suggests that granule cells are generated in lobules I and X prior to P11 in the rat, and that granule cells are generated last in lobules VI, VII, and VIII (Altman and Bayer, 1997). The decrease in the number of Fluoro-Jade positive cells observed in lobule VII in the present study may be a result of different developmental stages among the cerebellar lobules.

Cell death associated with MeHg exposure was not indicated in the hippocampus of P0 or P10 treated pups. MeHg is known to target granule cells of the cerebellum. Although literature suggests the hippocampus may be affected by MeHg (Burke *et al.*, 2006; Falluel-Morel *et al.*, 2007; Falluel-Morel *et al.*, 2006), significant amounts of cell death have not been observed in this brain location. In addition, the hippocampus develops more fully at an earlier time point that does the cerebellum (Supèr and Soriano, 1994). Because of the time point in development selected for the present study, P0 and P10, any cell death that occurred at an earlier time point in hippocampal development that would be comparable to the developmental stage of the cerebellum at P0 or P10 would have been missed.

Cell death in the hippocampus was increased in the granule and subgranule layers of the dentate gyrus compared to the hilar region. These data are consistent with literature suggesting that cell proliferation in the hilar region decreases significantly postnatally, while proliferation in the granule and subgranule layers remains high (Bayer, 1980). High cell proliferation rates would result in increased numbers of dying cells (Cowan *et al.*, 1984). In addition, increased cell death was observed in the CA3 region compared to the CA1 region in the present study. In contrast to these data, a study by Ferrer, (1990) suggests that cell death is increased in the CA1 region compared to the CA3 region from P5 to P10 in rats, and that there is increased cell death along the CA2/CA3 border. The border between the CA2 and CA3 region is not distinct and represents a transition from CA3-type cells to CA1-type cells (Boss *et al.*, 1987; Ferrer *et al.*, 1990). The increased number of Fluoro-Jade positive cells observed in the present study may be a result of counting CA2/CA3 border cells as cells within the CA3 region.

The combination of these border cells with the CA3 cells could result in an apparent increase in CA3 dying cells compared to cells of CA1.

Mitochondrial membrane potential (MMP) was measured in cerebella and hippocampi of mouse pups at P0 and P10. As hypothesized, a dose-dependent decrease in MMP was observed in cerebella of P0 mouse pups, but no difference was observed in MMP among MeHg treatments for the hippocampus. At P10 however, MMP was increased, rather than decreased, but only in the 0.1 mg/kg total dose MeHg treatment. In addition, no difference in MMP was indicated for the male P10 hippocampus. Our data suggest that MeHg may have a short-term immediate affect on developing neurons that results in dissipation of the mitochondrial membrane electrochemical gradient, but a latent affect, specifically at very low concentrations (0.1 mg/kg total dose), that results in increased mitochondrial activity. Mitochondrial activity is often increased in response to cellular stress as mitochondria are recruited to provide energy for the upregulation of cytoprotective mechanisms or as cytoprotective mechanisms act on the mitochondria to prevent apoptosis (Kirchhoff *et al.*, 2002; Peart and Headrick, 2007; Polla *et al.*, 1996).

Increases in $[Ca^{2+}]_i$ may be toxic to a cell and trigger the cell to die. However, transient increases in $[Ca^{2+}]_i$ are necessary signaling mechanisms in normal cellular function. As hypothesized, we observed increased $[Ca^{2+}]_i$ in the cerebellum of mice at P0 exposed to 0.1 and 1.0 mg/kg total dose MeHg; however, we observed no changes in $[Ca^{2+}]_i$ within cells from the hippocampus. Because the increased $[Ca^{2+}]_i$ in cerebella at P0 is accompanied by decreased MMP, the signal may likely to be one leading to cell death. However, no MeHg induced cell death was indicated for P0 cerebella. For P10 mice, $[Ca^{2+}]_i$ was increased in the high (1.0 mg/kg) MeHg treatment in cerebella and female hippocampi, but no change in $[Ca^{2+}]_i$ was indicated for the male hippocampus. Comparing MMP and $[Ca^{2+}]_i$ for P10 mouse pups, when MMP was decreased, there was no change in $[Ca^{2+}]_i$, and when $[Ca^{2+}]_i$ was increased, there was no change in MMP. Similarly however, neither MMP nor $[Ca^{2+}]_i$ were altered in P10 male hippocampi. There is also no indication that MeHg associated changes in MMP or $[Ca^{2+}]_i$ are associated with an increase in cell death. Therefore the changes in MMP and $[Ca^{2+}]_i$ may

be associated with processes other than apoptosis, such as cellular development, proliferation, migration, or cytoprotection.

We hypothesized a dose-dependent increase in the level of ROS produced in the cerebellum and hippocampus. Instead, at P0, there were no between-subject differences in ROS level, but an interaction was observed between MeHg treatment and cerebellar and hippocampal brain regions. ROS levels were ranked from highest to lowest as controls, 1.0 mg/kg, and 0.1 mg/kg for the cerebellum, but were inverted as 0.1 mg/kg, 1.0 mg/kg, and controls for the hippocampus. Similarly at P10, an interaction was indicated with ROS levels ranked highest to lowest as controls, 0.1 mg/kg, and 1.0 mg/kg MeHg in the cerebellum, compared to 1.0 mg/kg, controls, and 0.1mg/kg MeHg in the hippocampus. High levels of ROS can result in lipid and protein oxidation and permanent damage to membranes (de Groot and Littauer, 1989). Low-levels of ROS may indicate that mitochondria are less energetic. Cells may function abnormally if mitochondria are not metabolizing substrate at a rate equal to the cell's needs. Current data suggests that transient increases in ROS levels are important signals in cytoprotection (Martindale and Holbrook, 2002; Thannickal and Fanburg, 2000).

The purpose of our study was to determine whether low levels of MeHg, at or near exposure levels seen in humans, would produce similar effects observed at higher MeHg exposure levels. A summary of these results are located in Table III-2. As hypothesized, total Hg accumulated in the brains in a dose-dependent manner, and the concentration of MeHg dropped in mice from P0 to P10. We expected to see MeHg associated cell death in both the cerebellum and hippocampus, but instead, observed no cell death, or slight decreases in cell death with MeHg treatment. The hypothesized pattern of increased cell death, decreased MMP, increased $[Ca^{2+}]_i$, and increased ROS, which is typical with high MeHg exposure and exposure to other toxicants that initiate apoptosis, was not indicated for any MeHg treatment in the cerebellum or hippocampus at P0 or P10. Our data indicated, very clearly, that chronic low-levels of MeHg exposure during gestation do not result in effects observed for high MeHg concentrations. Instead, our data suggested mitochondrial dysfunction, oxidative stress, and changes in Ca^{2+}

homeostasis that may result in abnormal cellular function, proliferation and/or migration rather than death of neurons.

Published literature suggests that neuronal dysfunction may be of particular importance in diseases such as Alzheimer's (Mattson *et al.*, 2008; Wojda *et al.*, 2008), Parkinson's (Sugrue and Tatton, 2001), mood disorders (Campbell and Macqueen, 2004), and autism (Bauman and Kemper, 2005; Monnet-Tschudi *et al.*, 2006), all of which are becoming increasingly more prevalent in society. MeHg exposure in today's human population, although low, is chronic and measurable. The United States Environmental Protection Agency (U.S. E.P.A.) has set the reference dose (RfD) for MeHg at 0.1 μg/kg body weight per day. RfD is considered to be a concentration at which a chemical can be consumed on a daily basis over a lifetime without expectation of adverse effects. However, no MeHg behavioral or functional neuronal developmental studies have been conducted at or near the reference dose to determine whether developing and infant young are truly unaffected by this level of MeHg exposure. Our data indicate that low-levels of MeHg may affect neuronal function, and therefore suggest that further developmental whole animal investigation is warranted at chronic low MeHg concentrations.

TABLE III-2

Summary of Cell Death, Mitochondrial Membrane Potential (MMP), Intracellular Ca^{2+} Concentration (Ca^{2+}), and Level of Reactive Oxygen Species Production (ROS) in Cerebella (Ce) and Hippocampi (Hc) of Mouse Pups at Postnatal Day (P) 0 and 10 Following Exposure to 0 (C), 0.1, or 1.0 mg/kg Total Dose Methylmercury (MeHg) Divided Over Gestational Days 8 to 18

Postnatal Day	Cerebellum / Hippocampus	[MeHg] mg/kg	Cell Death	MMP	Ca^{2+}	ROS High to low
P0	Ce	0.1	no	NC	Incr	C, 1.0, 0.1
		1.0	no	Decr	Incr	
	Hc	0.1	no	NC	NC	0.1, 1.0, C
		1.0	no	NC	NC	
P10	Ce	0.1	no	Incr	NC	C, 0.1, 1.0
		1.0	no	NC	Incr	
	Hc	0.1	no	Incr(F), NC(M)	NC	1.0, C, 0.1
		1.0	no	NC	Incr(F), NC(M)	

NC = no change compared to controls
Decr = decreased compared to controls
Incr = increased compared to controls
(F) or (M) indicates change in female or male specifically
If sex is not designated, then no differences in sex were indicated.
High to low = ROS levels were ranked from highest to lowest mean.

CHAPTER IV

SUBCELLUAR CHANGES IN HUMAN SY5Y NEUROBLASTOMA CELLS EXPOSED TO METHYLMERCURY AND MERCURIC CHLORIDE

SUMMARY

High exposure levels of methylmercury (MeHg) cause the death of cerebellar and cerebral neurons in both adult and developing individuals. Increased apoptosis has been observed in cultured cerebellar granule cells and immortalized neurons exposed to MeHg *in vitro.* Mitochondrial dysfunction, alterations in Ca^{2+} homeostasis, and production of reactive oxygen species (ROS) have been implicated in the process of apoptosis, as well as with exposure to high concentrations of MeHg. The vast majority of MeHg *in vitro* experimentation has been conducted at high concentrations for short periods of time and in non-human cultured cell lines. Few studies have involved the use of SH-SY5Y (SY5Y) cells, a nearly diploid human neuroblastoma cell line, making this cell line genetically similar to "normal" human cells. The purpose of our study was to develop a human cell culture model for chronic low-level MeHg exposure by using a cell line known to be sensitive to the affects of MeHg, to examine parameters known to be associated with MeHg toxicity in whole animals and humans, and to compare the action of low levels of the organic and inorganic forms of mercury (Hg) which are both known to be present in the brains of humans exposed to MeHg.

We exposed human neuroblastoma SY5Y cells to 0, 0.01, 0.1, or 1.0 μM MeHg or $HgCl_2$ for 24, 48, or 72 hours and examined the cells for total Hg accumulation, cell death, mitochondrial function, basal $[Ca^{2+}]_i$, and production of reactive oxygen species (ROS). Both MeHg and $HgCl_2$ exposure resulted in a concentration-dependent accumulation of total Hg, and MeHg exposure resulted in higher levels of total Hg in the cells compared to $HgCl_2$ exposure. Total Hg uptake in all treated cells increased over time. The uptake of total Hg in the lower exposure concentrations did not increase as

rapidly as did higher concentrations, and the uptake of total Hg in the $HgCl_2$ exposed cells did not increase as rapidly as in the MeHg exposed cells. Cell death was determined based on three assays: Trypan blue exclusion, lactate dehydrogenase activity, and cytotoxicity. The highest (1.0 μM) concentrations of MeHg and $HgCl_2$ resulted in cell death, and the proportion of cells dying was increased with longer exposure times. Cell death was increased with 1.0 μM MeHg treatment compared to 1.0 μM $HgCl_2$ treatment. Mitochondrial membrane potential (MMP), $[Ca^{2+}]_i$, and production of ROS were measured by fluorescence microscopy or microplate assays. Both MeHg and $HgCl_2$ treatments resulted in decreased MMP in SY5Y cells. However, $HgCl_2$-induced depolarization of mitochondria did not occur until 48 hours, compared to 24 hours for MeHg. In addition, 0.01 and 0.1 μM $HgCl_2$-induced depolarization of mitochondria that began at 48 hours continued at 72 hours, whereas only the 1.0 μM MeHg-induced depolarization of mitochondria continued at 72 hours. MeHg treatments were associated with increased MMP at 24 hours in the lowest exposure group (0.01 μM), but this increase was followed at 48 hours by a dramatic decrease in MMP, and then a return to control levels at 72 hours. There was no difference in $[Ca^{2+}]_i$ between MeHg and $HgCl_2$. $[Ca^{2+}]_i$ was increased at 24 hours, was decreased at 48 hours, and returned to control levels at 72 hours in the 1.0 μM treated cells. The rate of ROS production was decreased over time for all treatment concentrations. Decreased rates of ROS production were indicated for the 0.01 μM $HgCl_2$ and the 1.0 μM MeHg treatments compared to controls at 24 hours, and for the 1.0 μM MeHg treatment compared to controls at 48 hours.

The low concentrations used in the present study (0.01, 0.1, and 1.0 μM) do not appear to result in mitochondrial, Ca^{2+}, and ROS-induced apoptosis. It appears that stimulation of mechanisms of cytoprotection, or those involved in cell proliferation or migration may be an early response of neurons exposed to low levels of MeHg. The potential to induce cytoprotective genes may play a role in determining which individuals (cells and whole organisms) exhibit negative effects at low levels of MeHg exposure and those which do not. Proliferation and migration of neurons in developing young is time-dependent, and alterations in the timing or rate of these events could

significantly alter normal brain development. Non-apoptotic changes in mitochondrial activity, $[Ca^{2+}]_i$, and ROS, specifically at very low MeHg concentrations, have not been previously indicated in current scientific literature, and further studies of these effects and associated mechanisms are warranted. Understanding the mechanism(s) of low-level MeHg toxicity is necessary for the protection of developing young.

INTRODUCTION

Methylmercury (MeHg) is a particularly neurotoxic pollutant ubiquitously found in the environment. Humans are chronically exposed to low-levels of MeHg primarily through consumption of contaminated fish. The deleterious effects of MeHg in humans have been well documented. Adults exposed to high concentrations of MeHg exhibit auditory, motor, and sensory disturbances, while individuals exposed to high levels of MeHg during gestation or early postnatal development show signs of mental retardation and cerebral palsy (Harada, 1977; Takeuchi *et al.*, 1962). Epidemiological studies over the last twenty years have shown that low levels of MeHg exposure in pregnant human females can produce poor motor coordination, decreased attention, and abnormal memory and language development in their children (Grandjean *et al.*, 1997; Grandjean *et al.*, 1999b; Steuerwald *et al.*, 2000). Although the signs and symptoms of MeHg neurotoxicity are known, the mechanisms of MeHg neurotoxicity remain unclear.

Granule cells in the cerebellum and neurons of the cerebral cortex are particularly sensitive to MeHg toxicity. Human studies have shown that high exposure levels of MeHg cause the death of cerebellar and cerebral neurons in both adult and developing individuals (Harada, 1977; Matsumoto *et al.*, 1965; Takeuchi, 1977). Increased apoptosis and necrosis also have been observed in cultured cerebellar granule cells and immortalized neurons exposed to MeHg *in vitro* (Castoldi *et al.*, 2000; Fonfria *et al.*, 2002; Gatti *et al.*, 2004; Toimela and Tähti, 2004; Vendrell *et al.*, 2007).

Mitochondrial dysfunction, alterations in Ca^{2+} homeostasis, and production of reactive oxygen species (ROS) have been implicated in the process of apoptosis (Alberdi *et al.*, 2005; Brookes *et al.*, 2004; Kakkar and Singh, 2007; Smaili *et al.*, 2003;

Waterhouse, 2003), as well as in MeHg toxicity. Studies in adult mice have shown that MeHg exposure causes increases in reactive oxygen species (ROS), abnormal mitochondrial function (Mori *et al.*, 2007; Yee and Choi, 1994) and alterations in intracellular calcium ion ($[Ca^{2+}]_i$) homeostasis (Bellum *et al.*, 2007a) in neurons of the central nervous system (CNS). MeHg affects on mitochondrial membrane potential (MMP) (Bondy and McKee, 1991; InSug *et al.*, 1997; Limke and Atchison, 2002), production of ROS (Ceccatelli *et al.*, 2007; Mori *et al.*, 2007; Yin *et al.*, 2007), and $[Ca^{2+}]_i$ signaling (Hare *et al.*, 1993; Levesque and Atchison, 1991; Marty and Atchison, 1998) have been described for both primary cells and immortalized cell lines in culture.

MeHg exposure produces increases in $[Ca^{2+}]_i$ in cerebrocortical synaptosomes (Kauppinen *et al.*, 1989), cerebellar granule cells (Sarafian, 1993), and NG108-15 neuroblastoma/glial hybrid cells (Hare *et al.*, 1993). MMP is decreased by MeHg exposure in astrocytes (Yin *et al.*, 2007) and rat cerebellar granule cells (Limke and Atchison, 2002); and mitochondrial function is altered by MeHg in rat striatal synaptosomes (Dreiem and Seegal, 2007). The production of ROS is increased by exposure to MeHg in rat brain mitochondria (Mori *et al.*, 2007) and C6-glial and B35-neuronal cell lines (Kaur *et al.*, 2007). In these studies, and the vast majority of others, MeHg exposure occurred at high concentrations for short periods of time, using cultured primary or immortalized cell lines, which may or may not respond to MeHg in the same manner as cells in the whole animal.

Much of the published MeHg *in vitro* experimentation has been conducted at high concentrations for short periods of time and result in cell death. Typical *in vitro* experiments have used MeHg exposure concentrations ranging from 2.0 to 100.0 μM (Kauppinen *et al.*, 1989; Limke and Atchison, 2002; Sarafian, 1993; Yin *et al.*, 2008). Exposure time periods have most commonly been 30 min and 1 hour, with exposure time periods ranging from 15 min to 24 hours (Dreiem and Seegal, 2007; Kauppinen *et al.*, 1989; Kaur *et al.*, 2007; Limke and Atchison, 2002; Sarafian, 1993). These exposure scenarios do not reflect the typical low dose chronic human MeHg exposure.

Nor do they consider the possibility that MeHg may exert subcellular changes that affect neuronal function, without the gross display of cell death.

The observation that MeHg targets neurons for cell death *in vivo* suggests that neuronal cell cultures would be a prime candidate to develop an *in vitro* model to study MeHg toxicity. The majority of neuronal cell lines used for MeHg studies include NB-1 human neuroblastoma (Kunimoto *et al.*, 1992; Kunimoto and Suzuki, 1995; Pramanik *et al.*, 2002), PC12 (Miura *et al.*, 1999), N1E-115 mouse neuroblastoma (Miura *et al.*, 1999; Uki and Narahashi, 1996), Neuro-2a mouse neuroblastoma (Repetto *et al.*, 1993), NBP2 murine neuroblastoma (Prasad, 1991), and Nb2a-AB-1 mouse neuroblastoma cells (Sager and Syversen, 1984). These cell lines display genetic abnormalities such as polyploidy or are not species specific for humans.

Few studies have involved the use of SH-SY5Y (SY5Y) human neuroblastoma cells. SY5Y cells are a nearly diploid subclone of the SK-N-SH human neuroblastoma cell line, making this cell line genetically similar to "normal" human cells. SY5Y cells are a third generation neuroblastoma, cloned from the SK-N-SH cell line isolated from a metastatic bone tumor of a four-year old girl in 1970 (Biedler *et al.*, 1973). The SY5Y cells possess two X chromosomes and lack a Y chromosome, making them genetically female. The cells posses an abnormal chromosome 1, where there is an additional copy of the 1q segment, also referred to as trisomy 1q. SY5Y cells have been used to model dopaminergic pathogenesis (Takahashi *et al.*, 1994) because it expresses dopaminergic phenotypes such as the presence of tyrosine β-hydroxylase activity (Chen *et al.*, 1998; Shaul *et al.*, 2003), dopamine transporters (Manáková *et al.*, 2004), and dopamine metabolism (Legros *et al.*, 2004). SY5Y cells have low levels of choline acetyltransferase, a cholinergic neurotransmitter (Biedler and Spengler, 1976). They are morphologically similar to neuroblasts in culture and can be differentiated by exposure to nerve growth factor, taking on a neuronal cell morphology (Perez-Polo *et al.*, 1979). SY5Y cells have been used to study neurotoxicants such as organophosphates (Ehrich, 1995; Yang and Tiffany-Castiglioni, 2007) and polycyclic aromatic hydrocarbons (PCBs) (Magi *et al.*, 2005; Ndountse and Chan, 2009). SY5Y cells also have been used

to characterize various effects of MeHg (Kim *et al.*, 2007; Sanfeliu *et al.*, 2001) and inorganic mercury (Toimela and Tähti, 2004). MeHg studies using SY5Y cells have shown depletion of cellular reduced glutathione (GSH) pools (Sanfeliu *et al.*, 2001), inhibition of differentiation (Kim *et al.*, 2007), down-regulation of selenoprotein W associated with depletion of GSH (Kim *et al.*, 2005a), and increased cell death, with SY5Y cells being more sensitive to MeHg toxicity than either glioma or retinal epithelial cells (Toimela and Tähti, 2004).

A confounding aspect in determining the mechanism(s) of MeHg toxicity stems from the ability of MeHg to demethylate within the brain, resulting in the presence of the divalent form of mercury (Hg^{2+}) (Aschner and Clarkson, 1987; Berlin *et al.*, 1975; Charleston *et al.*, 1995; Syversen, 1974). The inherent differences in hydrophilic divalent cations and lipophilic organic molecules suggest that the mechanisms of action of the two forms of mercury would be different. Hare and Atchison, (1992) showed that both forms of Hg resulted in mitochondrial and plasma membrane depolarization, but that the inorganic form produced depolarization at lower concentrations than the methyl form. Other comparisons between the two forms of Hg include increased inhibition of protein synthesis by MeHg compared to Hg^{2+} in sarcoma cells (Nakada *et al.*, 1980), but similar effects on glutathione oxidation in mouse brain mitochondria (Franco *et al.*, 2007).

The objective of the present study was based on the following known information about MeHg toxicity: 1) MeHg exposure in humans causes neuronal cell death by apoptosis, 2) cell death by apoptosis involves mitochondrial disruption, altered Ca^{2+} homeostasis, and increased production of ROS, 3) apoptosis, mitochondrial disruption, altered Ca^{2+} homeostasis, and increased production of ROS have been shown to occur in neuronal cell lines exposed to MeHg, 4) mitochondrial, Ca^{2+}, and ROS changes associated with MeHg have not previously been studied in the sensitive human neuroblastoma cell line, SH-SY5Y, 5) studies involving side-by-side comparison of MeHg and Hg^{2+} are limited. The purpose of our study was to develop a human cell culture model for chronic low-level MeHg exposure toxicity by using a cell line known

to be sensitive to the affects of MeHg, to examine parameters known to be associated with MeHg toxicity in whole animals and humans, and to compare the action of the organic and inorganic forms of Hg which are both known to be present in the brains of humans exposed to MeHg. We hypothesized that: 1) there would be a dose-dependent increase in the uptake of total Hg and in cell death in the SY5Y cells, 2) MMP would decrease, and basal $[Ca^{2+}]_i$ and the level of ROS production would increase in a dose-dependent manner associated with the presence of cell death, 3) cell death and associated changes in MMP, Ca^{2+}, and ROS production would be greater in SY5Y cells exposed to MeHg compared to those exposed to Hg^{2+} in the form of $HgCl_2$, and 4) changes in MMP, Ca^{2+}, and ROS production would occur at Hg concentrations that did not result in cell death. To determine whether changes in MMP, Ca^{2+}, and ROS production occur at Hg concentrations that do not result in cell death, we selected exposure concentrations ranging from those known to cause cell death with MeHg at 24 hours (1.0 μM) to those in which cell death has not been observed (0.01 μM) or documented.

To test these hypotheses, we exposed human neuroblastoma SY5Y cells to 0, 0.01, 0.1, or 1.0 μM concentrations of MeHg or $HgCl_2$ for 24, 48, or 72 hours and examined the cells for total Hg accumulation, cell death, mitochondrial function, basal $[Ca^{2+}]_i$, and production of ROS. Exposure time periods of 24, 48, and 72 hours were selected to allow at least one division period for the cells, with a maximum of 72 hours to eliminate the necessity of splitting the cells. At each time point, the amount of total Hg in the cells was measured. Cell death was determined based on three assays: Trypan blue exclusion, lactate dehydrogenase activity, and a cytotoxicity assay. MMP, basal $[Ca^{2+}]_i$, and the level of ROS production were measured by fluorescence microscopy or microplate assays.

MATERIALS AND METHODS

Materials

Methylmercuric chloride, (MeHg), 95%, was purchased from Alfa Aesar (Ward Hill, MA). Human SH-SY5Y human neuroblastoma cells were purchased from

American Type Culture Collection (ATCC, Rockville, MD). Mercuric chloride, ($HgCl_2$), >99.5%, Dulbecco's Modified Eagle's Medium (DMEM), Nutrient Mixture F-12 Ham (F-12), Puck's saline solution with EDTA (Puck's EDTA, no Ca^{2+}, no Mg^{2+}, with 5.4 mM KCl, 1.37 mM NaCl, 4.2 mM $NaHCO_3$, 5.5 mM glucose, and 0.5 mM Na_2 EDTA), poly-D-lysine hydrobromide >300,000 kD, *tertiary*-butyl hydroperoxide (*t*BHP), Hank's Balanced Salt Solution (HBSS, modified with $NaHCO_3$ and without phenol red), carbonyl cyanide 3-chloro-phenylhydrazone (CCCP), thapsigargin, and Janus Green B were purchased from Sigma-Aldrich, Inc. (St. Louis, MO). Fetal bovine serum (FBS) was purchased from Gemini (Woodland, CA). B27 serum-free supplement was purchased from Invitrogen (Carlsbad, CA). DOLT-2, DORM-2, and DOLT-3 were purchased from the National Research Council Canada (NRCC), Institute for Environmental Chemistry (Ottawa, Canada). The Cytotoxicity Detection Kit (LDH) was purchased from Roche Applied Science (Germany). The MultiTox-Fluor Multiplex Cytotoxicity Assay was purchased from Promega (Madison, WI). Tetramethylrhodamine, methyl ester perchlorate (TMRM), Calcium Green™-1 AM, 5-(and 6)-chloromethyl-2',7'-dichlorodihydrofluorescein diacetate acetyl ester (CM-H_2DCFDA), and Pluronic® F-127 were purchased from Invitrogen/Molecular Probes (Eugene, OR). Lab-Tek 2-well chambered coverglasses were purchased from Nunc Inc. (Naperville, IL).

Cell cultures

SY5Y cells, passage numbers 55 to 65 were routinely maintained in T-75 flasks in DMEM/F12 (1:1) supplemented with 10% fetal bovine serum (FBS) in a humidified, 37°C, 5% CO_2 environment. No antibiotics or fungicides were used in the stock cell preparations or those used for experimentation. Experimental cells were detached by application of Puck's EDTA for 5 min at 37°C, plated in DMEM/F12 supplemented with 1x B27, and allowed to attach and grow for 24 hours before treatment. Cells used for total Hg accumulation analysis were seeded in 150 mm x 25 mm round gridded polystyrene culture dishes (BD Falcon, San Jose, CA) at 70,000, 50,000, and 30,000

cells per cm^2 for experiments conducted at 24, 48, and 72 hours, respectively. Cells used for all other experiments were seeded at 30,000 cells per cm^2. Treatments included 0, 0.01, 0.1, or 1.0 μM methylmercury (MeHg) or inorganic mercury ($HgCl_2$) for 24, 48, or 72 hours. MeHg and $HgCl_2$ stock solutions (100 μM) were prepared in distilled / deionized water, filtered, and stored at 4°C. Working MeHg and $HgCl_2$ solutions were prepared from the 100 μM stock solution in growth media just before use.

Mercury accumulation

Total mercury (Hg) was measured to determine the amount of total Hg accumulated within the SY5Y cells. Three independently processed samples were collected for each time point and treatment (n = 3). Following MeHg or $HgCl_2$ exposure, the treatment medium was removed and the cells and plate rinsed with 4 mL Puck's plus EDTA. The Puck's plus EDTA solution was removed and added to the treatment medium. The treatment/EDTA solution was centrifuged at 1000 g for 5 min to pellet any floating cells. Puck's plus EDTA (5 mL) was added to the plate of cells and incubated for 5 min at 37°C to release the cells. The dislodged cells in Puck's plus EDTA were added to the previously pelleted cells. The total volume of cell-containing solution for each sample was 5 mL. 0.5 mL of the cell-containing solution was removed and added to 4.5 mL DMEM/F12 for counting. The cell suspension was mixed at a ratio of 4:1 with 0.4 % Trypan blue solution and incubated for 5 min. The viable (clear) and dead (blue) cells were counted using a hemacytometer and an inverted-phase contrast microscope (Nikon, Model TMS, Tokyo, Japan) (Costa *et al.*, 2007). The remaining cell solution was centrifuged at 1000 g for 5 min, the supernatant removed, and the pellet frozen at -20°C. The frozen pellet of cells was freeze-dried and total Hg content was measured in the Trace Element Research Laboratory at Texas A&M University, by combustion / trapping / atomic absorption (Salvata and Pirola, 1994) on a Milestone Direct Mercury Analyzer 80 (DMA 80) equipped with an autosampler and dual cell detector. The DMA 80 was calibrated using a calibration blank and a series of seven aliquots of certified reference standard ranging from 1 to 750 ng Hg. The calibration line was verified with

an independent CRM standard (NRCC DOLT-2) and a blank nickel boat. Samples were weighed to the nearest 0.00001 g and placed into the DMA 80 in pre-combusted nickel boats. A method blank, two certified reference materials (DORM-2 and DOLT-3), a spiked sample, and a duplicate sample were included at the beginning and end of each sample run. The DMA 80 has a detection limit of 0.005 ng Hg and a working range of up to 1000 ng Hg (Milestone, Inc. Shelton, CT).

Trypan blue exclusion

The Trypan blue dye exclusion assay was performed to determine the number of living and dead cells. The experiment was conducted three times; each experiment included four replicates for each toxicant, treatment, and time point. Cells (30,000 cells per cm^2) were plated in 24-well polystyrene, cell culture treated plates (BD Falcon, San Jose, CA). Following MeHg or $HgCl_2$ exposure, the cells were released by incubation with Puck's plus EDTA for 5 min at 37°C. 0.5 mL of the cell solution was removed and added to 4.5 mL DMEM/F12 for counting. The cell suspension was mixed at a ratio of 4:1 with 0.4 % Trypan blue solution and incubated for 5 min. The viable (clear) and dead (blue) cells were counted using a hemacytometer and an inverted-phase contrast microscope (Nikon, Model TMS, Tokyo, Japan). The average of four counts per replicate was used for data analysis.

Lactate dehydrogenase

The activity of lactate dehydrogenase released into the culture medium was measured to evaluate plasma membrane integrity, which is compromised in dead cells. The experiment was conducted three times; each experiment included seven replicates for each toxicant, treatment, and time point. LDH release was measured with the Roche Cytotoxicity Detection Kit (LDH) (Kondo *et al.*, 1993). Cells (30,000 cells per cm^2) were plated in 24-well polystyrene, cell culture treated plates (BD Falcon, San Jose, CA). After 24 hours of treatment with MeHg or $HgCl_2$, the medium was removed and centrifuged at 1100 g for 5 min to remove floating cells. The supernatant was transferred

into 96-well polystyrene, cell culture treated plates (BD Falcon, San Jose, CA) and incubated with the LDH dye solution and catalyst mixture (included in the kit). Degree of color change was measured in a BioTek® Synergy 4™ microplate reader with Gen5™ data analysis software (Winooski, VT) at absorbance 490 nm. Once released from dying cells, LDH breaks down at 37°C after 24 hours. Therefore, LDH release was measured every 24 hours in the 48 and 72 hour treatment samples. LDH release values at 24 and 48 were summed to attain the value for the total amount LDH released over the 48 hour exposure time. LDH release values at 24, 48, and 72 hours were summed to attain the value for the total amount of LDH released over the 72 hour exposure time. Media used for analysis was replaced with fresh MeHg or $HgCl_2$-treated media in the 48 and 72 hour treatment samples, and the cells were allowed to grow for the next 24-hour time period.

Cytotoxicity assay

A cytotoxicity assay was conducted to determine the relative number of live and dead cells following treatment with 0, 0.01, 0.1, or 1.0 μM MeHg or $HgCl_2$ for 24, 48, or 72 hours. The MultiTox-Fluor Assay measures live-cell protease activity that is restricted to intact viable cells and is measured using a fluorogenic, cell-permeant, peptide substrate (glycyl-phenylalanyl-amino-fluorocoumarin, GF-AFC) (AFC). A second, fluorogenic cell-impermeant peptide substrate (bis-alanyl-alanyl-phenylalanyl-rhodamine 110, bis-AAF-R110) (R110) was used to measure dead-cell protease activity, which is released from cells that have lost membrane integrity (Niles *et al.*, 2006). The experiment was conducted three times; each experiment included six replicates of each toxicant, treatment, and time point. Cells were plated in 96-well polystyrene, cell culture treated plates (BD Falcon, San Jose, CA) at 30,000 cells per cm^2. Following MeHg or $HgCl_2$ exposure, live cell substrate (AFC) or dead cell substrate (R110) was added to each well and incubated for 30 min at 37°C. Plates were analyzed on a BioTek® Synergy 4™ microplate reader with Gen5™ data analysis software (Winooski, VT) at

fluorescence settings of excitation/emission 400/505 nm for live cells (AFC), and excitation/emission 485/520 for dead cells (R110).

Mitochondrial membrane potential

Tetramethylrhodamine methyl ester (TMRM) was used to detect changes in mitochondrial membrane potential (MMP) (Barhoumi *et al.*, 2004) in SY5Y cells treated with 0, 0.01, 0.1, or 1.0 μM MeHg or $HgCl_2$ for 24, 48, or 72 hours. TMRM is a lipophilic potentiometric mitochondrial dye that accumulates in mitochondria in proportion to the membrane potential (Scaduto Jr and Grotyohann, 1999). TMRM dye stock solution (1.0 mM) was prepared in 100% methanol and stored with desiccant at -20°C. TMRM working solution (150.0 nM) was prepared from the 1.0 mM stock solution in HBSS just before use. The methanol concentration in the working solution was 0.015%. HBSS was used in the TMRM working solution instead of growth medium to prevent the TMRM dye from binding to proteins within the medium and inhibiting movement of dye into the cells. Cells were plated in 2-well chambered coverslips coated with gelatin and 1x poly-D-lysine. Cells were treated and analyzed in batches consisting of a control and one of each toxicant at each treatment concentration to control variability from day to day and allow comparison of data from one day to the next.

Following treatment with MeHg or $HgCl_2$, media was removed and replaced with a 150.0 nM solution of TMRM in HBSS for 20 min at 37°C. The TMRM solution was replaced with HBSS for imaging. Three negative controls (HBSS and cells with no dye, HBSS with no cells and no dye, and HBSS with dye, but no cells) and a positive control (HBSS and cells with dye and 20 μM CCCP) were included. CCCP was used to determine that the observed fluorescence was associated with the mitochondrial membrane and not other non-specific fluorescence (Julian *et al.*, 2005). CCCP is a lipid-soluble weak acid that uncouples oxidative phosphorylation in the inner mitochondrial membrane. It enters the mitochondria in a protonated form, discharges the pH gradient, then leaves the mitochondria as an anion, depolarizing the mitochondrial membrane (Lim *et al.*, 2001). When CCCP is co-administered to cells with TMRM, the CCCP-

induced depolarization of the inner mitochondrial membrane results in release of accumulated TMRM from mitochondria into the cytosol, and a decrease in fluorescence occurs.

Fluorescent mitochondrial images were collected over a 10 min time period at 20x using an Olympus 1X-70 microscope with a Hamamatsu ORCA-ER camera at excitation/emission 488/520 nm. Image retrieval and MMP analysis were performed using Simple PCI and Imaging System Software (v5.0.0.1503, Compix Inc.). The relative MMP values of individual mitochondria from a minimum of ten cells per sample were measured and averaged to give the value for each individual sample. Mitochondria were identified as fluorescent round or oblong-shaped punctate fluorescent objects within the SY5Y cells. MMP data were calculated as percentage of control within each batch.

Basal intracellular Ca^{2+}

Calcium Green™-1 AM was used to measure the relative concentration of basal intracellular calcium ions ($[Ca^{2+}]_i$) (Gilroy and Jones, 1992) in SY5Y cells treated with 0, 0.01, 0.1, or 1.0μM MeHg or $HgCl_2$ for 24, 48, or 72 hours. Calcium Green™-1 AM is a long-wavelength Ca^{2+} indicator that exhibits an increase in fluorescence emission intensity upon binding to Ca^{2+} (Eberhard and Erne, 1991). The dye is in the AM ester form, which enhances cell permeability and is non-fluorescent in the absence of Ca^{2+} (Lee *et al.*, 1999). Upon binding to Ca^{2+}, the dye exhibits an approximately 100-fold increase in emission intensity, which enables detection of changes in Ca^{2+} concentration within a large dynamic range (Lee *et al.*, 1999). Calcium Green™-1 AM stock solution (2 mM) was prepared in 100% DMSO and stored with desiccant at -20°C for up to two weeks. Working solutions of Calcium Green™-1 AM (1.0 μM) were prepared just before use in 0.01% Pluronic® F-127 in HBSS. The final DMSO concentration in the working solution was 0.05%. HBSS was used in the Calcium Green™-1 AM working solution instead of growth media to prevent the Calcium Green™-1 AM dye from binding to proteins within the medium and inhibiting movement of dye into the cells.

The experiment was conducted three times; each experiment included eight replicates of each toxicant, treatment, and time point. Cells were plated at a density of 30,000 cells per cm^2 in 48-well polystyrene, cell culture treated plates (BD Falcon, San Jose, CA). Following MeHg or $HgCl_2$ exposure, the medium was removed and replaced with a 1.0 µM solution of Calcium Green™-1, AM in 0.01% Pluronic® F-127 and HBSS for 20 min at room temperature. Calcium Green™-1 was removed and replaced with HBSS for 20 min to allow de-esterification of the dye. The AM ester of the molecule, which enhances the movement of the dye into the cell, must be removed by endogenous esterases for the dye to fluoresce when bound to Ca^{2+}. Three negative controls (HBSS and cells with no dye, HBSS with no cells and no dye, and HBSS with dye, but no cells) and a positive control (HBSS and cells with dye and thapsigargin) were included. Thapsigargin is an inhibitor of sarco-endoplasmic reticulum Ca^{2+} ATPases and raises cytosolic free Ca^{2+} by blocking the ability of the cell to pump Ca^{2+} into the endoplasmic reticulum (ER) (Treiman *et al.*, 1998). ER-store Ca^{2+} depletion can secondarily activate plasma membrane Ca^{2+} channels, allowing an influx of Ca^{2+} into the cytosol (Barhoumi *et al.*, 2006). When thapsigargin is co-administered to cells with Calcium Green™-1 AM, the thapsigargin-induced increase in cytosolic free Ca^{2+} causes a dramatic increase in fluorescence. Plates were analyzed on a BioTek® Synergy 4™ microplate reader (Winooski, VT) at fluorescence settings of excitation 485/20 and emission 528/20 to determine relative $[Ca^{2+}]_i$. Following $[Ca^{2+}]_i$ analysis, Janus Green dye was used to determine the relative number of cells within each well. This value was used to normalize the $[Ca^{2+}]_i$ data among wells. Janus Green B (diethylsafraninazodimethylaniline chloride) is a basic histological stain (Rieck *et al.*, 1993). By staining the cells attached to the surface of the individual wells, and then measuring the absorbance of the Janus Green dye within the wells, we were able to determine a relative value for the cell number that could be used to normalize the data for each well. HBSS was removed from the wells and replaced with 100% ethanol (EtOH) for 90 sec. The EtOH was removed and the wells were allowed to dry for 3 min. Janus Green dye (1 mg/mL in 0.1 M phosphate buffered saline) was added to each well

for 1 min, and then removed and the wells rinsed twice with HBSS. To extract the accumulated dye from the cells, 100% EtOH was added to each well and mixed by pipetting twice. The absorbance was measured at 654 nm in a BioTek® Synergy 4™ microplate reader (Winooski, VT). $[Ca^{2+}]_i$ readings for each well were normalized to the relative cell number absorbance value for the same well. Normalized $[Ca^{2+}]_i$ data were calculated as percentage of control for each plate to eliminate inter-run variability and allow comparison of one experiment to another.

Reactive oxygen species

5-(and 6)-chloromethyl-2'7'-dichlorodihydrofluorescein diacetate acetyl ester (CM-H_2DCFDA) was used to determine the relative rate of ROS production over time (Bellum *et al.*, 2007a; Oyama *et al.*, 1994) in SY5Y cells exposed to 0. 0.01, 0.1, and 1.0 μM MeHg or $HgCl_2$ for 24, 48, or 72 hours. CM-H_2DCFDA is a non-fluorescent compound that is oxidized to highly fluorescent 2',7'-dichlorofluorescein (DCF) by the action of ROS (LeBel *et al.*, 1992). The chloromethyl (CM) group on the dye allows the dye to passively diffuse into cells. Subsequent oxidation of the dye molecule by endogenous esterases traps the metabolites within the cell where they can react with ROS. CM-H_2DCFDA stock solution (2 mM) was prepared in 100% DMSO and stored withn desiccant at -20°C for up to two weeks. Working solutions of CM-H_2DCFDA (1.0 μM) were prepared just before use in 0.01% Pluronic® F-127 in HBSS. The final DMSO concentration in the working solution was 0.05%. The experiment was conducted three times; each experiment included eight replicates of each toxicant, treatment, and time point. Cells were plated at a density of 30,000 cells per cm^2 in 48-well polystyrene, cell culture treated plates (BD Falcon, San Jose, CA). Following MeHg or $HgCl_2$ exposure, the medium was removed and replaced with a 1 μM solution of CM-H_2DCFDA in 0.01% Pluronic® F-127 in HBSS for 5 min at room temperature. The CM-H_2DCFDA was removed and replaced with HBSS for plate-reader analysis. Three negative controls (HBSS and cells with no dye, HBSS with no cells and no dye, and HBSS with dye, but no cells) and a positive control (HBSS and cells with dye and

tertiary-butyl hydroperoxide (*t*BHP) were included) (Drahota *et al.*, 2005). *t*BHP is a lipophilic, membrane-permeant oxidant (Elliott *et al.*, 1992). It reacts with iron in heme-proteins and produces alkoxyl radicals (Kim *et al.*, 2005b). When *t*BHP is co-administered to cells with CM-H_2DCFDA dye, the *t*BHP-induced increase in ROS causes an increase in fluorescence. Fluorescence data were collected every 2.5 min for 30 min at excitation 485/20 and emission 528/20 to determine the relative rate of ROS production (Bellum *et al.*, 2007a) and the amount of ROS produced. Following ROS analysis, Janus Green dye was used to determine the relative number of cells within the well. Janus Green dye procedures are described in the basal intracellular Ca^{2+} section. This value was used to normalize the $[Ca^{2+}]_i$ data among wells. ROS readings for each well were normalized to the relative cell number absorbance value for the same well. Normalized ROS data were calculated as percentage of control for each plate to eliminate inter-run variability and allow comparison of one experiment to another.

Statistical analysis

All data are represented as mean ± standard error of the mean (SEM). All data, except Hg accumulation data, were calculated as percentage of control to eliminate inter-run variability and to normalize data collected at different days and times. A three-way MANOVA with repeated measures for reading time was used to assess between- and within-subject differences in the rate of ROS production associated with exposure time, toxicant, and treatment concentration. The condition of sphericity was analyzed for all ROS data. The condition of sphericity was not met in any of the ROS data analyzed; therefore the Greenhouse-Geisser adjusted univariate test was used for repeated measures analysis of ROS production over reading time (Grieve, 1984). All other data were analyzed by three-way ANOVA and Tukey's honest significant difference (HSD) or Student's t post hoc tests, as appropriate, to determine main effects and interactions associated with exposure time, toxicant, and treatment concentrations. In cases where the experiment was conducted three times, each experiment was statistically analyzed individually, and then the three were compared to each other to determine similarity

between experiments. Data from one of the three experiments has been presented as representative results. For all experiments, $\alpha = 0.05$ (JMP 7.0.2, SAS Institute Inc., Cary, NC).

RESULTS

Mercury accumulation

Total mercury (Hg) incorporated into SY5Y cells exposed to 0, 0.01. 0.1, or 1.0 μM MeHg or $HgCl_2$ for 24, 48, or 72 hours was measured, and then analyzed by three-way ANOVA to determine differences and interactions associated with treatment time, toxicant, and treatment concentration. Total Hg incorporated is reported as ng Hg per g of freeze dried cell volume. The freeze dried cell volume consisted of the entire Hg treated cell population within the growth chamber. Between-subject factors were time (24, 48, or 72 hours), toxicant (MeHg or $HgCl_2$), and treatment (0, 0.01, 0.1, and 1.0 μM). Data are represented as *M* = mean and *SEM* = standard error of the mean. Analysis indicated a main effect for treatment, $F(3, 54) = 28.3$, $p < 0.0001$ (Table IV-1). Tukey's HSD post hoc analysis indicated that the 0.1 (*M* = 46000 ng/g, *SEM* = 10000) and 1.0 μM (*M* = 310000 ng/g, *SEM* = 81000) treatments accumulated more total Hg than did the 0.01 μM treatment (*M* = 4900 ng/g, *SEM* = 490) and controls (*M* = 250 ng/g, *SEM* = 45). The 1.0 μM treatment accumulated more total Hg than did the 0.1 μM treatment. In addition, interactions were indicated for time and treatment, $F(3, 54) = 69.15$, $p < 0.0001$, for toxicant and treatment, $F(3, 54) = 15.11$, $p < 0.0001$, and for time, toxicant, and treatment, $F(3, 54) = 62.44$, $p < 0.0001$. These interactions suggested that the observed differences in treatment were greater for the MeHg toxicant compared to the $HgCl_2$ toxicant, and that the treatment differences increased over exposure time (Table IV-1).

Trypan blue exclusion

The number of dead and total SY5Y cells following exposure to 0, 0.01. 0.1, or 1.0 μM MeHg or $HgCl_2$ for 24, 48, or 72 hours was counted using the Trypan blue

exclusion assay and a hemacytometer. Live cells exclude Trypan blue, while Trypan blue accumulates within dead and dying cells with damaged plasma membranes. The experiment was conducted three times using a sample size of four for each experiment. Data from each experiment were independently analyzed by three-way ANOVA to determine differences and interactions associated with treatment time, toxicant, and treatment concentration. Analysis of live and dead cell count data indicated similar results for all three experiments. Data reported are representative of one of the three experiments conducted. Analysis of the number of dead cells indicated main effects for time, F (2, 72) = 6.29, p = 0.003, and for treatment concentration, F (3, 72) = 3.55, p = 0.019 (Fig IV-1). Data for dead cells also indicated an interaction effect between time and treatment concentration, F (3, 72) = 3.11, p = 0.0092. Tukey's HSD post hoc analysis for dead cells indicated that the number of dead cells was increased in the 1.0 μM MeHg treatment compared to controls at 24, 48, and 72 hours. The number of dead cells was increased in the 1.0 μM $HgCl_2$ treatment compared to controls at 72 hours. The number of dead cells was increased in the 1.0 μM MeHg treatment compared to the 1.0 μM $HgCl_2$ treatment at 24 and 48 hours. Data also indicated that there were more dead cells in all treatment concentrations at 72 hours compared to 24 hours. The dead cell time and treatment concentration interaction suggested that the observed treatment effect increased with exposure time. Analysis of the number of total cells indicated a main effect for exposure time, F (2, 72) = 25.04, $p < 0.0001$. Tukey's HSD post hoc analysis indicated that the total number of cells was increased at 72 hours compared to 48 hours, and increased at 72 and 48 hours compared to 24 hours (Fig IV-1). No main effects for total cell counts were indicated for toxicant or treatment concentration.

Lactate dehydrogenase

LDH activity was measured for SY5Y cells following exposure to 0, 0.01, 0.1 or 1.0 μM MeHg or $HgCl_2$ for 24, 48, or 72 hours. LDH is released from dying cells when the plasma membrane is damaged. LDH activity was measured in media as a relative representation of cell death. The relative cell number was determined for each well. Each

LDH value per well was normalized by the relative cell number determined for that same well. The LDH experiment was conducted three times with a sample size of eight for each experiment. Data from each experiment were independently analyzed by three-way ANOVA to determine differences and interactions associated with treatment time, toxicant, and treatment concentration. Analysis of LDH data indicated similar results for all three experiments. Data reported are representative of one of the three experiments conducted. Analysis of LDH dead cell data indicated a main effect for treatment, F (3, 136) = 37.77, $p < 0.0001$, and interaction effects between time and treatment, F (3, 136) = 2.78, $p = 0.0141$, between toxicant and treatment, F (3, 136) = 28.81, $p < 0.0001$, and among time, toxicant and treatment, F (3, 136) = 3.05, $p = 0.0079$ (Fig IV-2). Tukey's HSD post hoc analysis indicated that LDH was increased in the 1.0 μM $HgCl_2$ and 1.0 μM MeHg treatments at 24, 48, and 72 hours. LDH also was increased in the 1.0 μM MeHg treatment compared to the 1.0 μM $HgCl_2$ at 24, 48, and 72 hours. The interaction effects suggested that LDH levels increased with increased exposure time and with increased treatment concentration. Student's t post hoc test indicated that LDH levels were higher in cells treated with MeHg than in those treated with $HgCl_2$ (Fig IV-2).

TABLE IV-1

Mean Total Mercury Concentration in SY5Y Cells Following Exposure to 0, 0.01, 0.1, or 1.0 µM MeHg or $HgCl_2$ for 24, 48, or 72 Hours

Treatment Concentration (µM)	Total Hg (ng/g) for Exposure Time and Toxicant					
	24		48		72	
	M	H	M	H	M	H
0	346	346	338	338	141	141
0.01	5781	2689	6791	2748	7890	2907
0.1	76386*	6298*	83321*	5904*	98517*	5878*
1.0	206035*	33416*	876250*†	49045*†	650156*†	50170*†

Total Hg concentration data were analyzed by three-way ANOVA for exposure time (24, 48, or 72 hours), toxicant (MeHg or $HgCl_2$), and treatment concentration (0, 0.01, 0.1, or 1.0 µM) differences. Total Hg concentration is reported as mean ng/g (ng total Hg/g of freeze dried cells). The freeze dried cells used for total Hg measurement consisted of the entire cell population within the growth chamber. Analysis indicated a main effect for treatment concentration. Tukey's HSD post hoc analysis indicated that total Hg concentration in the 0.1 and 1.0 µM treatments was increased compared to the total Hg concentration in the 0.01 µM treatment and controls (*). The total Hg concentration the 1.0 µm treatment was increased compared to the total Hg concentration in the 0.1 µM treatment (†). Interaction effects were indicated for time and treatment, for toxicant and treatment, and for time, toxicant, and treatment. The interactions suggested that the observed differences in treatment were greater in the MeHg toxicant compared to the $HgCl_2$ toxicant, and that the treatment differences increased over exposure time. Three-way ANOVA main effect for treatment, $F\ (3, 54) = 28.3$, $p < 0.0001$; interactions for time and treatment, $F\ (3, 54) = 69.15$, $p < 0.0001$, for toxicant and treatment, $F\ (3, 54) = 15.11$, $p < 0.0001$, and for time, toxicant and treatment, $F\ (3, 54) = 62.44$, $p < 0.0001$; $\alpha = 0.05$.

FIG. IV-1. The number of dead and total SY5Y cells following treatment with 0, 0.01, 0.1, or 1.0 μM MeHg or $HgCl_2$ for 24, 48, or 72 hours. Dead and live cells were distinguished by Trypan blue exclusion. Data from three experiments were analyzed independently by three-way ANOVA to determine differences associated with exposure time, toxicant, and treatment concentration. Analysis indicated similar results for all three experiments. Graphical data are representative of one of the three experiments conducted. Data were analyzed by Tukey's HSD or Student's t post hoc tests when appropriate. Panel A: for dead cells, mains effects for time and treatment, and an interaction for time and treatment were indicated. Dead cells were increased in the 1.0 μM MeHg treatment compared to controls at 24, 48 and 72 hours (*). Dead cells were increased in the 1.0 μM $HgCl_2$ treatment compared to controls at 72 hours (*). The number of dead cells was increased in the 1.0 μM MeHg treatment compared to the 1.0 μM $HgCl_2$ treatment at 24 and 48 hours (†). The interaction effect suggested that the number of dead cells in all treatments was increased at 72 hours compared to those treatments at 24 hours. Panel B: for total number of cells, a main effect was indicated for exposure time. The total number of cells were increased at 72 hours compared to 48 hours, and at 72 and 48 hours compared to 24 hours (‡). Data represented as percentage of control and as mean ± standard error of the mean. Three-way ANOVA dead cell count main effect for time, F (2, 72) = 6.29, p = 0.003, and for treatment, F (3, 72) = 3.55, p = 0.019; interaction effect for time and treatment, F (3, 72) = 3.11, p = 0.0092. Three-way ANOVA total cell count main effect for time, F (2, 72) = 25.04, $p < 0.0001$. $\alpha = 0.05$.

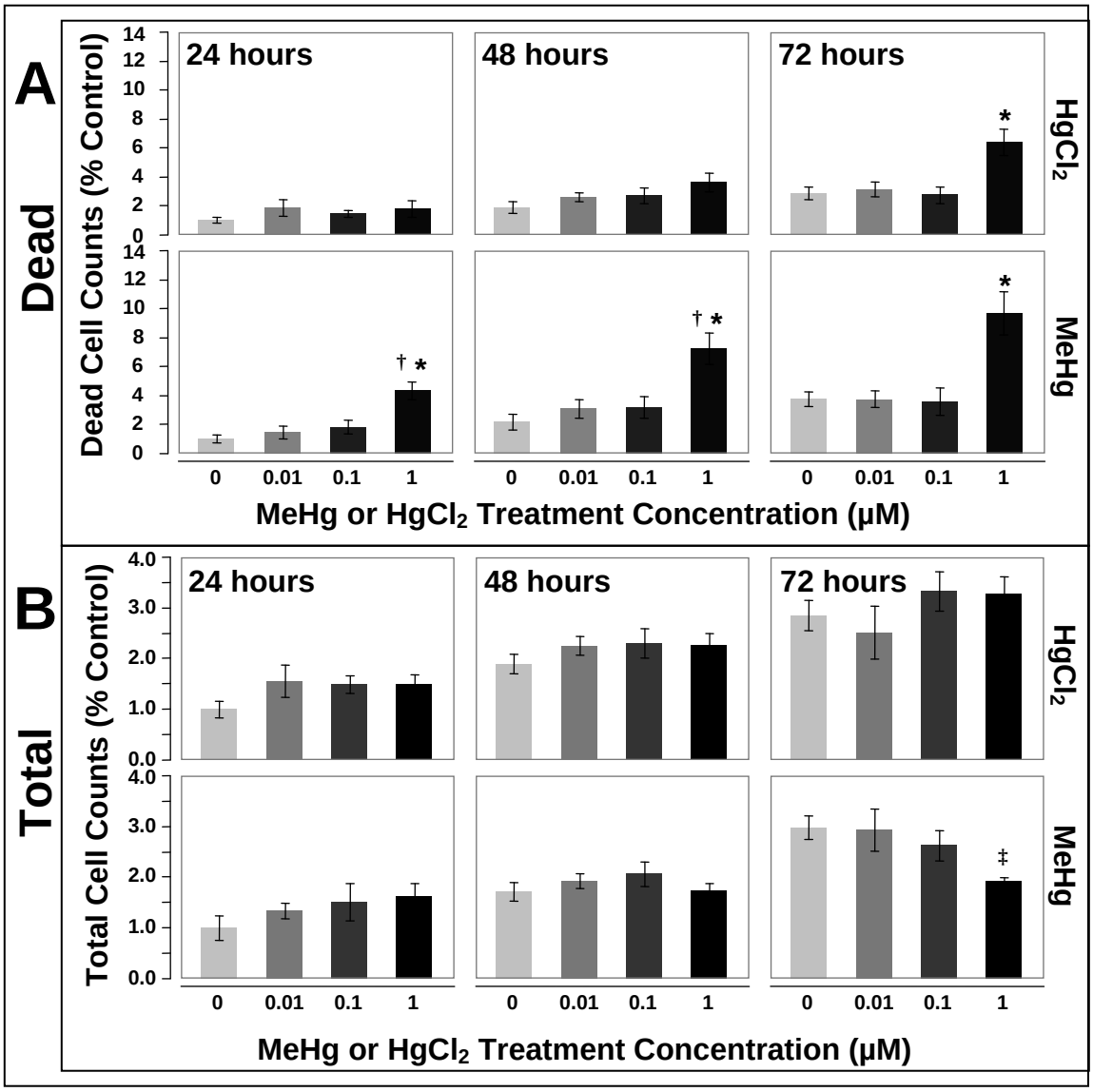
A
Dead
Dead Cell Counts (% Control)
24 hours
48 hours
72 hours
HgCl2
MeHg
0
2
4
6
8
10
12
14
0
0.01
0.1
1
*
† *
MeHg or HgCl2 Treatment Concentration (μM)
B
Total
Total Cell Counts (% Control)
0.0
1.0
2.0
3.0
4.0
‡

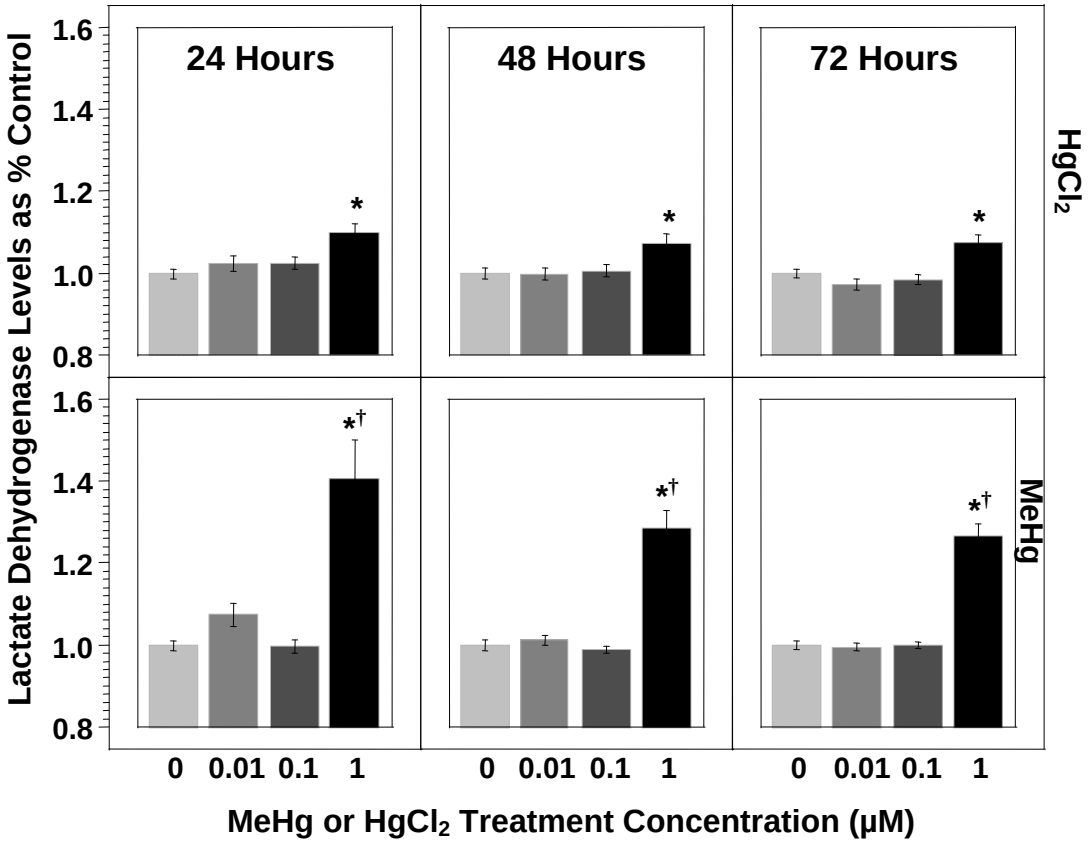

FIG. IV-2. Lactate dehydrogenase (LDH) levels in SY5Y cells exposed to 0, 0.01, 0.1, or 1.0 µM MeHg or $HgCl_2$ for 24, 48, or 72 hours. LDH levels represent the relative amount of cell death. Data from three experiments were analyzed independently by three-way ANOVA to determine differences associated with exposure time, toxicant, and treatment concentration. Analysis indicated similar results for all three experiments. Graphical data are representative of one of the three experiments conducted. Data were analyzed by Tukey's HSD or Student's t post hoc analyses when appropriate. Analysis indicated a main effect for treatment, and interactions for time and treatment, for toxicant and treatment, and for time, toxicant and treatment. LDH was increased in the 1.0 µM $HgCl_2$ and MeHg treatments at 24, 48, and 72 hours (*). LDH also was increased in the 1.0 µM MeHg treatment compared to the 1.0 µM $HgCl_2$ at 24, 48, and 72 hours (†). The interaction effects suggested that LDH levels increased with increased exposure time, with increased treatment concentration, and were higher in cells treated with MeHg than in those treated with $HgCl_2$. LDH values were normalized by values for relative cell number. Data are shown as percentage of control and mean ± standard error of the mean. Three-way ANOVA main effect for treatment, F (3, 136) = 37.77, $p < 0.0001$; interaction effects for time and treatment, F (3, 136) = 2.78, $p = 0.0141$, for toxicant and treatment, F (3, 136) = 28.81, $p < 0.0001$, and for time, toxicant and treatment, F (3, 136) = 3.05, $p = 0.0079$. $\alpha = 0.05$.

Cytotoxicity

Relative numbers of live and dead cells were measured in SY5Y cells following exposure to 0, 0.01, 0.1 or 1.0 μM MeHg or $HgCl_2$ for 24, 48, or 72 hours. The live cell indicator protein is retained within live cells, while the dead cell indicator protein is released into the medium when the plasma membrane is damaged. The relative cell number was determined for each well. The live and dead cell values from each well were normalized by the relative cell number measured for that same well. The cytotoxicity experiment was conducted three times with a sample size of six for each experiment. Data from each experiment were independently analyzed by three-way ANOVA to determine differences and interactions associated with treatment time, toxicant, and treatment concentration. Analysis of cytotoxicity data indicated similar results for all three experiments. Data reported are representative of one of the three experiments conducted. Analysis of dead cells indicated a main effect for treatment, F (3, 119) = 16.49, $p < 0.0001$, and interactions between time and treatment, F (3, 119) = 95.10, $p < 0.0001$, between toxicant and treatment, F (3, 199) = 9.18, $p < 0.0001$, and among time, toxicant and treatment, F (3, 119) = 84.90, $p < 0.0001$ (Fig IV-3). Tukey's HSD post hoc analysis indicated that the number of dead cells in the 1.0 μM MeHg treatment was increased compared to all other MeHg and $HgCl_2$ treatments and controls at 24 and 48 hours. The number of dead cells also was increased in the 1.0 μM $HgCl_2$ treatment compared to the 0.01 and 0.1 μM $HgCl_2$ treatments and controls at 48 hours. The number of dead cells was decreased in the 1.0 μM MeHg treatment compared to controls at 72 hours. The interaction among time, treatment, and toxicant indicated that the number of dead cells increased over time, and that exposure to MeHg resulted in a greater increase in cell death than exposure to $HgCl_2$. Analysis of live cells indicated a main effect for treatment, F (3, 120) = 17.57, $p < 0.0001$, and interactions between time and treatment, F (3, 120) = 5.78, $p < 0.0001$, between toxicant and treatment, F (3, 120) = 12.67, $p < 0.0001$, and among time, toxicant and treatment, F (3, 120) = 3.95, $p = 0.0012$. Tukey's HSD post hoc analysis indicated that the number of live cells was decreased in the 1.0 μM MeHg treatment compared to all other MeHg and $HgCl_2$

treatments and controls at 24, 48, and 72 hours. The interaction among time, treatment, and toxicant indicated that the number of live cells decreased over time as the treatment concentration increased, and that the MeHg treatments resulted in decreased numbers of live cells compared to the $HgCl_2$ treatments (Fig IV-3).

Mitochondrial membrane potential

Membrane potential (MMP) of the inner mitochondrial membrane of SY5Y cells was measured using TMRM dye and fluorescence microscopy to determine whether exposure to 0, 0.01, 0.1 or 1.0 μM MeHg or $HgCl_2$ for 24, 48, or 72 hours would alter mitochondrial function. Representative images of SY5Y cells incubated with TMRM are shown in Fig IV-4. SY5Y cells were incubated with 150.0 nM TMRM for 20 min and imaged by fluorescence microscopy. Data were collected for individual mitochondria within a minimum of ten SY5Y cells from each of four replicate experiments. The mitochondrial data from a single experiment were averaged and represent a sample size of one. Relative MMP data for SY5Y cells was analyzed by three-way ANOVA to determine differences and interactions associated with treatment time, toxicant, and treatment concentration. Analysis indicated a main effect for treatment, F (3, 72) = 32.46, $p < 0.0001$, and interactions between time and treatment, F (3, 72) = 12.52, $p < 0.0001$, and between toxicant and treatment, F (3, 72) = 4.46, $p = 0.0062$ (Fig IV-5). Tukey's HSD post hoc analysis indicated that MMP was decreased in the 1.0 μM treatment compared to the 0.01 and 0.1 μM treatments and controls, and that MMP was increased in the 0.01 μM treatment compared to the 0.1 and 1.0 μM treatments and controls. Tukey's HSD post hoc analysis by toxicant and exposure time indicated that MMP was decreased in the 1.0 μM MeHg treatment compared to controls at 24, 48, and 72 hours. MMP was decreased in the 0.01 and 0.1 μM MeHg treatments compared to controls at 48 hours. However, MMP was increased in the 0.01 MeHg treatment compared to the 0.1 and 1.0 μM MeHg treatments and controls at 24 hours.

FIG. IV-3. Relative number of live and dead SY5Y cells following exposure to 0, 0.01, 0.1, or 1.0 μM MeHg or $HgCl_2$ for 24, 48, or 72 hours. Cells were analyzed using the MultiTox-Fluor Multiplex Cytotoxicity plate reader assay. Data from three experiments were analyzed independently by three-way ANOVA to determine differences associated with exposure time, toxicant, and treatment concentration. Analysis indicated similar results for all three experiments. Graphical data are representative of one of the three experiments conducted. Data were analyzed by Tukey's HSD or Student's t post hoc analyses when appropriate. For live and dead cells, data indicated a main effect for treatment, and interactions for time and treatment, for toxicant and treatment, and for time, toxicant and treatment. The number of live cells was decreased in the 1.0 μM MeHg treatment compared to all other MeHg and $HgCl_2$ treatments and controls at 24, 48, and 72 hours (*). The interaction among time, treatment, and toxicant indicated that the number of live cells decreased over time as the treatment concentration increased, and that the MeHg treatments resulted in decreased numbers of live cells compared to the $HgCl_2$ treatments. The number of dead cells in the 1.0 μM MeHg treatment was increased compared to all other MeHg and $HgCl_2$ treatments and controls at 24 and 48 hours (†). The number of dead cells also was increased in the 1.0 μM $HgCl_2$ treatment compared to the other $HgCl_2$ treatments and controls at 48 hours (†). The number of dead cells was decreased in the 1.0 μM MeHg treatment compared to controls at 72 hours (‡). The interaction among time, treatment, and toxicant indicated that the number of dead cells increased over time, and are increased with exposure to MeHg compared to exposure to $HgCl_2$. Live and dead cell values were normalized by values for relative cell number. Data are shown as percentage of control and mean ± standard error of the mean. Three-way ANOVA live cell main effect for treatment, F (3, 120) = 17.57, $p < 0.0001$, and interactions for time and treatment, F (3, 120) = 5.78, $p < 0.0001$, for toxicant and treatment, F (3, 120) = 12.67, $p < 0.0001$, and for time, toxicant and treatment, F (3, 120) = 3.95, $p = 0.0012$. Three-way ANOVA dead cell main effect for treatment, F (3, 119) = 16.49, $p < 0.0001$, and interactions for time and treatment, F (3, 119) = 95.10, $p < 0.0001$, for toxicant and treatment, F (3, 199) = 9.18, $p < 0.0001$, and for time, toxicant and treatment, F (3, 119) = 84.90, $p < 0.0001$. $\alpha = 0.05$.

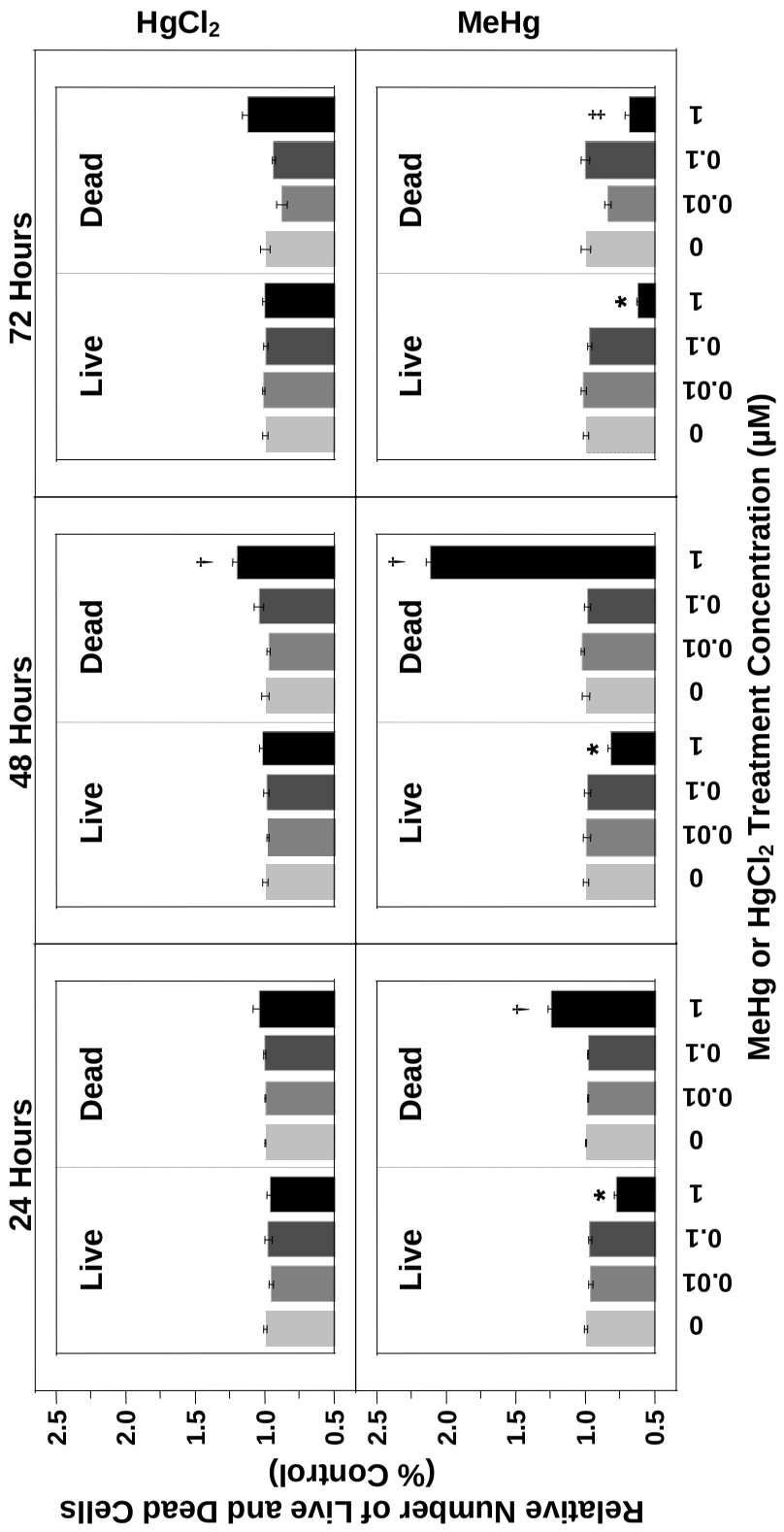
HgCl2
MeHg
24 Hours
48 Hours
72 Hours
Live
Dead
Relative Number of Live and Dead Cells
(% Control)
2.5
2.0
1.5
1.0
0.5
0
0.01
0.1
1
MeHg or HgCl2 Treatment Concentration (μM)

For cells exposed to $HgCl_2$, MMP was decreased in the 0.01 and 0.1 μM $HgCl_2$ treatment compared to controls at 48 and 72 hours. MMP was decreased in the 1.0 μM $HgCl_2$ treatment compared to controls at 72 hours. The indicated interactions suggested that MMP decreased with increased exposure time, and was decreased in the MeHg treatments compared to the $HgCl_2$ treatments (Fig IV-5). CCCP was added to control SY5Y cells (positive method control) to verify that the method used to measure changes in MMP was, in fact, measuring changes in MMP. CCCP uncouples oxidative phosphorylation within mitochondria, which results in decreased MMP. Addition of CCCP to control cells incubated with TMRM resulted in a dramatic decrease in the fluorescence intensity of mitochondria indicating depolarization of the mitochondrial membrane (data not shown); no auto-fluorescence was observed in samples without TMRM dye, nor in samples without cells that contained TMRM dye (negative controls, data not shown).

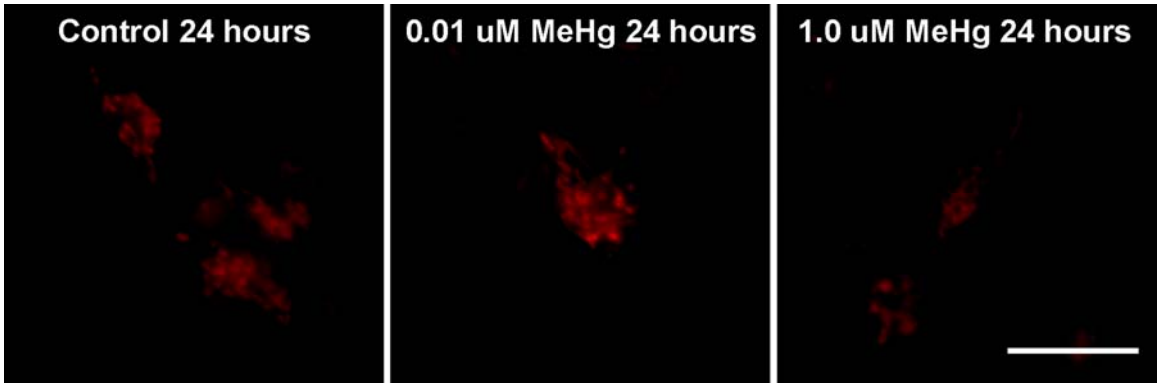

FIG. IV-4. Representative images of SY5Y cells following exposure to 0.01 or 1.0 μM MeHg for 24 hours. Cells exhibited fluorescent mitochondria following incubation with 150.0 nM TMRM dye for 20 min. Active mitochondria exposed to TMRM appeared as red circles or tubes. Fluorescence intensity is proportional to mitochondrial membrane potential. Mitochondria in the 0.01 μM MeHg treated SY5Y cells exhibited increased fluorescence compared to controls. Mitochondria in the 1.0 μM MeHg treated SY5Y cells exhibited decreased fluorescence compared to both the 0.01 μM MeHg treated cells and controls. Scale bar = 25 μm.

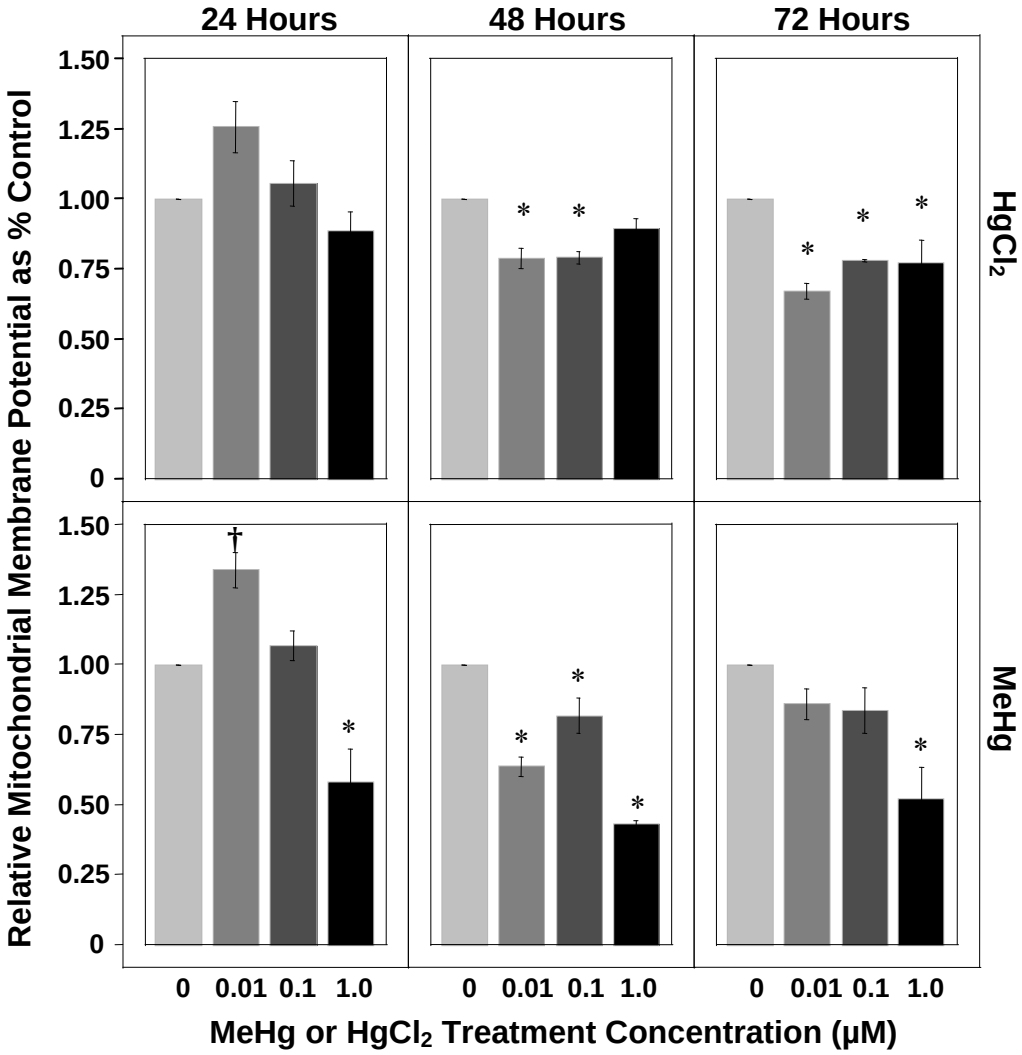

FIG. IV-5. Relative mitochondrial membrane potential (MMP) in mitochondria from SY5Y cells following exposure to 0, 0.01, 0.1, or 1.0 µM MeHg or $HgCl_2$ for 24, 48, or 72 hours. Cells were incubated with 150.0 nM TMRM for 20 min and imaged by fluorescence microscopy. Data were collected for individual mitochondria within the SY5Y cells, and then analyzed by three-way ANOVA to determine differences associated with exposure time, toxicant, and treatment concentration, followed by Tukey's HSD or Student's t post hoc analyses when appropriate. Analysis indicated a main effect for treatment, and interactions for time and treatment, and for toxicant and treatment. MMP was increased at 0.01 µM MeHg (†), but decreased at 1.0 µM MeHg compared to controls at 24 hours (*). At 48 hours, MMP was decreased in all MeHg treatments compared to controls (*). MMP was decreased in the 1.0 µM MeHg treatment compared to controls at 72 hours (*). For cells exposed to $HgCl_2$, MMP in the 0.01 and 0.1 µM $HgCl_2$ treated cells was decreased compared to controls at 48 hours. MMP in all three $HgCl_2$ treatments was decreased compared to controls at 72 hours. The indicated interactions suggested that MMP decreased with increased exposure time, and was decreased in the MeHg treatments compared to the $HgCl_2$ treatments. Data are represented as percentage of control and mean ± standard error of the mean. Three-way ANOVA main effect for treatment, F (3, 72) = 32.46, $p < 0.0001$, and interactions for time and treatment, F (3, 72) = 12.52, $p < 0.0001$, and for toxicant and treatment, F (3, 72) = 4.46, $p = 0.0062$; $\alpha = 0.05$.

Basal free intracellular Ca^{2+}

Calcium ion homeostasis was examined by measuring the relative basal intracellular calcium ion concentration ($[Ca^{2+}]_i$) in SY5Y cells exposure to 0, 0.01, 0.1 or 1.0 μM MeHg or $HgCl_2$ for 24, 48, or 72 hours. SY5Y cells were incubated with 1.0 μM Calcium Green-1 AM dye for 20 min. Relative $[Ca^{2+}]_i$ was determined by microplate reader analysis. The relative cell number was determined for each well. The $[Ca^{2+}]_i$ value from each well was normalized by the relative cell number measured for that same well. The $[Ca^{2+}]_i$ experiment was conducted three times with a sample size of eight for each experiment. Data from each experiment were independently analyzed by three-way ANOVA to determine differences and interactions associated with treatment time, toxicant, and treatment concentration. Analysis of $[Ca^{2+}]_i$ data indicated similar results for all three experiments. Data reported are representative of one of the three experiments conducted. Analysis indicated a main effect for treatment, F (3, 142) = 10.86, $p < 0.0001$, and an interaction effect between treatment and time, F (3, 142) = 6.25, $p < 0.0001$ (Fig IV-6). No differences were indicated for toxicant. Tukey's HDS post hoc analysis indicated that $[Ca^{2+}]_i$ was increased in the 1.0 μM treatment compared to controls at 24 hours, but decreased compared to controls at 48 hours. Data also indicated that $[Ca^{2+}]_i$ was decreased at 48 and 72 hours compared to 24 hours for the 1.0 μM treated cells. The indicated interaction between time and treatment suggested that $[Ca^{2+}]_i$ decreased over time with increased treatment concentration (Fig IV-6). Thapsigargin was added to control SY5Y cells as a method control to validate the measurement of changes in $[Ca^{2+}]_i$. Thapsigargin is an inhibitor of sarco-endoplasmic reticulum Ca^{2+} ATPases and raises cytosolic free Ca^{2+} by blocking the ability of the cell to pump Ca^{2+} into the endoplasmic reticulum (Treiman *et al.*, 1998). Addition of thapsigargin to control SY5Y cells (positive method control) resulted in a substantial increase in the fluorescence within the cells, indicating an increase in $[Ca^{2+}]_i$; no auto-fluorescence was observed in samples without Calcium Green-1, nor in samples without cells that contained Calcium Green-1 (negative controls), indicating minimal atmospheric and/or photo-oxidation (data not shown).

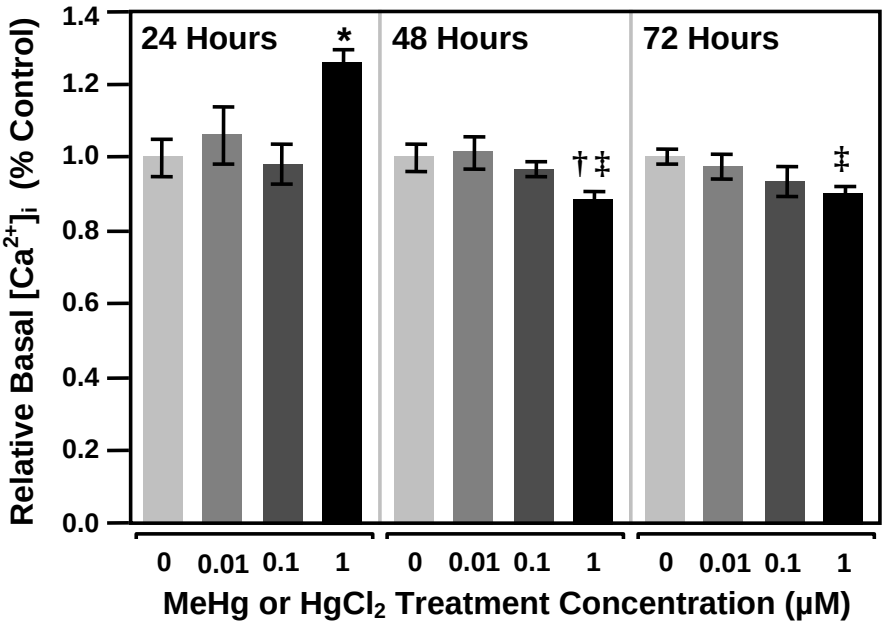

FIG. IV-6. Relative basal intracellular calcium ion concentration ($[Ca^{2+}]_i$) in SY5Y cells exposed to MeHg or $HgCl_2$ for 24, 48, or 72 hours. Cells were incubated with 1.0 µM Calcium Green-1 AM dye for 20 min and fluorescence data was collected by microplate reader analysis. Data from three experiments were analyzed independently by three-way ANOVA to determine differences associated with exposure time, toxicant, and treatment concentration. Analysis indicated similar results for all three experiments. Graphical data are representative of one of the three experiments conducted. Data were analyzed by Tukey's HSD or Student's t post hoc analyses when appropriate. Analysis indicated a main effect for treatment, and an interaction between treatment and time. No differences were indicated for toxicant. $[Ca^{2+}]_i$ was increased in the 1.0 µM treatment compared to controls at 24 hours (*), but decreased compared to controls at 48 hours (†). Data also indicated that $[Ca^{2+}]_i$ was decreased at 48 and 72 hours compared to 24 hours for the 1.0 µM treated cells (‡). The indicated interaction between time and treatment suggested that $[Ca^{2+}]_i$ decreased over time with increased treatment concentration. Data are presented as percentage of control and mean ± standard error of the mean. Three-way ANOVA main effect for treatment, F (3, 142) = 10.86, $p < 0.0001$, and interaction effect for treatment and time, F (3, 142) = 6.25, $p < 0.0001$. $\alpha = 0.05$.

Production of reactive oxygen species

The rate of generation of and the level of ROS were determined for SY5Y cells exposed to 0, 0.01, 0.1, or 1.0 µM MeHg or $HgCl_2$ for 24, 48, or 72 hours. SY5Y cells were incubated with 1.0 µM CM-H_2DCFDA dye for 5 min and then analyzed for ROS production every 2.5 min for 30 min in a plate reader. ROS data were analyzed by three-way MANOVA with repeated measures for reading time. Analysis of ROS data indicated similar results for all three experiments. Data reported are representative of one

of the three experiments conducted. Analysis indicated a between-subject difference in the rate of ROS production for exposure time, F (2, 192) = 54.46, $p < 0.0001$ (Fig IV-7). The condition of sphericity was not met; therefore, subsequent within-subject analyses were conducted using the Greenhouse-Geisser adjusted univariate analysis (Grieve, 1984). Within-subject differences for rate of ROS production were indicated for exposure time, F (4, 350) = 85.11, $p < 0.0001$, for treatment, F (6, 350) = 5.19, $p < 0.0001$, and for a toxicant and treatment interaction, F (6, 350) = 3.59, $p = 0.0016$. For both MeHg and $HgCl_2$, and for all treatment concentrations, the rate of ROS production in the 24 hour exposure time was increased compared to the rates in the 48 and 72 hour exposure times, and the rate of ROS production in the 48 hour exposure time was increased compared to the rate in the 72 hour exposure time. At 24 hours, the 0.01 μM $HgCl_2$ treated cells exhibited a decreased rate of ROS production compared to controls. The decreased rate of ROS production in the 0.01 μM $HgCl_2$ treated cells was exhibited at reading times eleven and twelve. At 24 hours, the 1.0 μM MeHg treated cells exhibited a decreased rate of ROS production compared to controls. The decreased rate of ROS production in the 1.0 μM $HgCl_2$ treated cells began at reading time two and continued to reading time twelve. At 48 hours, the 1.0 μM MeHg treated cells exhibited a decreased rate of ROS production compared to controls. The decreased rate of ROS production in the 1.0 μM MeHg treated cells began at reading time seven and continued to reading time twelve.

FIG. IV-7. Relative rate of reactive oxygen species (ROS) production in SY5Y cells exposed to 0. 0.01, 0.1, or 1.0 μM MeHg or $HgCl_2$ for 24, 48, or 72 hours. SY5Y cells were incubated with 1.0 μM CM-H_2DCFDA fluorescent dye for 5 min, and then the rate of ROS production as fluorescence was measured every 2.5 min for 30 min using a microplate reader. Data from three experiments were analyzed independently by three-way MANOVA with repeated measures for time, followed by the Greenhouse-Geisser adjusted univariate analysis to determine between- and within-subject differences and interactions associated with exposure time, toxicant, and treatment concentration over the 30 min time period. Analysis indicated similar results for all three experiments. Graphical data are representative of one of the three experiments conducted. Analysis indicated a between-subject difference in the rate of ROS production for exposure time. For both MeHg and $HgCl_2$, and for all treatment concentrations, the rate of ROS production in the 24 hour exposure time was increased compared to the rates in the 48 and 72 hour exposure times (*), and the rate of ROS production in the 48 hour exposure time was increased compared to the rate in the 72 hour exposure time (†). Within-subject differences for rate of ROS production were indicated for exposure time, for treatment, and for a toxicant and treatment interaction. At 24 hours, the 0.01 μM $HgCl_2$ treated cells exhibited a decreased rate of ROS production compared to controls at reading times eleven and twelve (0.01 < Controls), and the 1.0 μM MeHg treated cells exhibited a decreased rate of ROS production compared to controls at reading times two through twelve (1.0 < Controls). At 48 hours, the 1.0 μM MeHg treated cells exhibited decreased rate of ROS production compared to controls at reading times seven through twelve (1.0 < Controls). Three-way MANOVA between-subject difference for exposure time, F (2, 192) = 54.46, $p < 0.0001$. Within-subject differences for exposure time, F (4, 350) = 85.11, $p < 0.0001$, for treatment, F (6, 350) = 5.19, $p < 0.0001$, and for a toxicant and treatment interaction, F (6, 350) = 3.59, $p = 0.0016$; $\alpha = 0.05$.

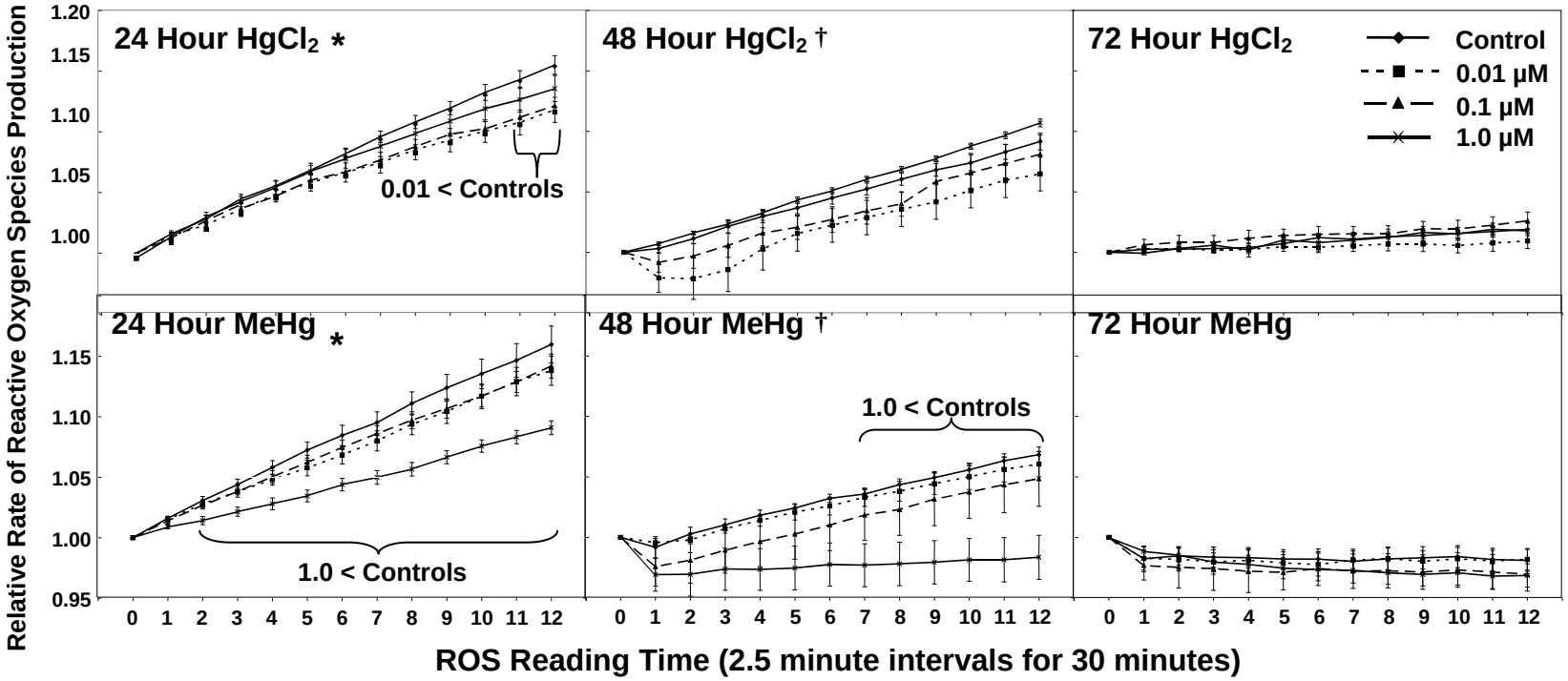
24 Hour HgCl2 *
48 Hour HgCl2 †
72 Hour HgCl2
Control
0.01 µM
0.1 µM
1.0 µM
0.01 < Controls
24 Hour MeHg *
48 Hour MeHg †
72 Hour MeHg
1.0 < Controls
1.0 < Controls
Relative Rate of Reactive Oxygen Species Production
ROS Reading Time (2.5 minute intervals for 30 minutes)

In addition to the rate of ROS production, data were analyzed by three-way MANOVA with repeated measures for reading time to determine the amount of ROS produced. No between-subject differences were indicated for the amount of ROS produced. The condition of sphericity was not met; therefore, data were subsequently analyzed using the Greenhouse-Geisser adjusted univariate analysis to determine within-subject differences and interactions (Grieve, 1984). Data indicated no within-subject differences in the level of ROS produced over the 30 minute reading time. *Tertiary* butyl hydroperoxide (*t*BHP) was added to control SY5Y cells as a method control to validate the measurement of changes in $[Ca^{2+}]_i$. *t*BHP penetrates the cell membrane and reacts with heme-proteins to produce alkoxyl radicals. Addition of *t*BHP to control SY5Y cells (positive control) resulted in a dramatic increase in the fluorescence within the cells indicating an increase in the level of ROS; no auto-fluorescence was observed in samples without CMH_2DCFDA dye, nor in samples without cells that contained CMH_2DCFDA (negative control), indicating minimal atmospheric and/or photo-oxidation (data not shown).

DISCUSSION

The accumulation of total Hg was measured in SY5Y cells exposed to 0. 0.01, 0.1, and 1.0 μM MeHg or $HgCl_2$ for 24, 48, or 72 hours. We hypothesized that the uptake of total Hg would be concentration- and time-dependent, and would be higher with MeHg treatment than with $HgCl_2$ treatment. As expected, both MeHg and $HgCl_2$ exposure resulted in a concentration-dependent accumulation of total Hg, and MeHg exposure resulted in higher levels of total Hg in the cells compared to $HgCl_2$ exposure. Meacham *et al*. (2005) showed that MeHg is taken up by PC12 cells, primary cultures of rat neocortical cells, and adult rat hippocampal slices in a concentration- and time-dependent manner. MeHg is lipophilic and can enter cells more readily than the inorganic form of Hg (Philbert *et al.*, 2000). In addition, MeHg is likely transported across the membrane bound to cysteine by the neutral amino acid transport carrier system (Aschner and Clarkson, 1989) providing multiple access points for MeHg into

the cell. Nakada and Imura (1982) showed that both MeHg and Hg^{2+} are taken up by mouse neuroblastoma cells, but that MeHg is taken up preferentially to Hg^{2+}.

In addition to preferential uptake of MeHg to Hg^{2+} observed in our study, total Hg uptake in all treated cells increased over time, as indicted by the time and treatment interaction effect. The uptake of total Hg in the lower exposure concentrations did not increase as rapidly as did higher concentrations, and the uptake of total Hg in the $HgCl_2$ exposed cells did not increase as rapidly as the MeHg exposed cells, as indicated by the time, treatment, and toxicant interaction effect. Studies of total Hg accumulation *in vivo* indicate that both MeHg and $HgCl_2$ can reach steady-state concentrations. Similar results have been shown by Berlin *et al.* (1975) in squirrel monkeys. After approximately four days following administration of MeHg, the MeHg concentrations in the blood and brain came into equilibrium in the closed system. The level of MeHg in the brain did not increase until there was additional exposure to MeHg. The model system in our study was also a closed system, where no additional MeHg or Hg^{2+} was being added following the initial exposure concentration. Similarly, MeHg in the blood of monkeys administered 50.0 μg/kg per day MeHg for eighteen months reached steady-state concentrations (1.1 μg/g of blood) after about four months, even with the continued exposure of MeHg for another fourteen months (Vahter *et al.*, 1994). MeHg concentrations in the brain reached steady-state at 12 months, not increasing with continued MeHg exposure up to thirty nine months (Lind *et al.*, 1988; Vahter *et al.*, 1994). The total Hg accumulation in SY5Y cells in the current study appeared to model the total Hg accumulation reported in scientific literature for *in vivo* MeHg exposures.

The amount of cell death with MeHg or $HgCl_2$ exposure was measured by three methods: Trypan blue exclusion, LDH activity, and the MultiTox-Fluor Multiplex Cytotoxicity assay. We hypothesized that cell death would increase in a concentration- and time-dependent manner, and that cell death would be higher with MeHg treatment than with $HgCl_2$ treatment. Based on the three cell death assays conducted in this study, the highest (1.0 μM) concentrations of MeHg and $HgCl_2$ exposure resulted in cell death, and cell death was increased with longer exposure times. In addition, cell death was

increased with 1.0 μM MeHg treatment compared to 1.0 μM $HgCl_2$ treatment. Similar results were observed by Kunimoto (1994) in cultured cerebellar granule cells. They showed that MeHg concentrations of 0.1, 0.3, and 1.0 μM resulted in cell death after 72 hours of exposure, but not after 24 hours. Also in cultured cerebellar granule cells, Vendrell *et al.* (2007) showed that 0.3 μM MeHg resulted in cell death after 96 hours of exposure. In contrast to the study by Kunimoto (1994), we did not observe cell death with 0.1 μM MeHg treatment even after 72 hours of exposure. The discrepancy in cell death at the 0.1 μM concentration is likely because of the type of cell used in the study. Although SY5Y cells are known to be sensitive to MeHg toxicity, cerebellar granule cells, as used by Kunimoto (1994), are a specific target for MeHg toxicity *in vivo* and would likely be more sensitive to MeHg treatment than SY5Y cells.

Inconsistencies in the number of dead cells estimated by Trypan blue exclusion compared to the LDH assay are evident in the 24 and 48 hour time points for $HgCl_2$ exposure. Although cell death was increased at 24 and 48 hours, the Trypan blue exclusion measures were likely underestimated due to degradation of dying cells. Degraded cells could not be measured with Trypan blue exclusion, but the lactate dehydrogenase released from the dead cells remained active and could be measured by the LDH activity assay. By 72 hours, large enough numbers of cells had died with $HgCl_2$ exposure that statistically significant numbers of them were still intact for Trypan blue exclusion to be a valid measurement. The cytotoxicity assay data substantiates the results of the Trypan blue exclusion and the LDH assays. Although the level of cell death in the 1.0 μM $HgCl_2$ at 72 hours was not significantly different from controls in the cytotoxicity assay, the trend was evident based on the time, toxicant, and treatment interaction effect measured for the cytotoxicity assay as well as the main effect for treatment concentration indicated for the Trypan blue and LDH assays.

The three cytotoxicity assays used in this study individually contain inherent potential limitations. Therefore the three assays were used in combination to obtain a more accurate assessment of viability and cell death. Trypan blue exclusion cannot label disintegrated cells, but may be able to enter a dying cell prior to the release of LDH and

other cell death associated factors. However, Trypan blue exclusion allows for individual cell data, i.e., actual cell counts of both live and dead cells. In contrast, LDH activity and the MultiTox-Fluor Multiplex Cytotoxicity assays provide population data. Furthermore, LDH degrades after 24 hours, and therefore cells dying during early time points may be underestimated unless media is collected at regular intervals. In addition, LDH activity provides no information regarding numbers of live cells. The MultiTox-Fluor Multiplex Cytotoxicity assay was designed to overcome flaws associated with the Trypan blue exclusion and LDH activity methods. When performed as designed, the live and dead cell indicator dyes are added to the wells simultaneously and are analyzed back to back at two different absorbance wavelengths that produce two discernable emission wavelengths. Problems would result when the excitation wavelengths were not set optimally resulting in significant crossover of the two emission wavelengths. Many microplate readers are fitted with general excitation/emission filter sets that function at a fixed optimal range. This was the case for the microplate reader used in our experiment. The live and dead cell emission peaks were not separated enough for the two dyes to be analyzed in the same well at the same time; therefore, we plated two sets of cells for each run and assayed the live and dead cells separately.

Mitochondrial activity in SY5Y cells was determined by fluorescence microscopy and measuring the mitochondrial membrane potential (MMP). We hypothesized that MMP would decrease in a concentration- and time-dependent manner, and that MMP would be decreases to a greater degree with MeHg treatment compared to $HgCl_2$ treatment. Both MeHg and $HgCl_2$ treatments decreased MMP in SY5Y cells. However, $HgCl_2$-induced depolarization of mitochondria did not occur until 48 hours, compared to 24 hours for MeHg. In addition, 0.01 and 0.1 μM $HgCl_2$-induced depolarization of mitochondria beginning at 48 hours continued at 72 hours, whereas only the 1.0 μM MeHg-induced depolarization of mitochondria continued at 72 hours. Our data suggest that $HgCl_2$ may enter the cell more slowly that MeHg, thus resulting in a lag-time for mitochondrial membrane depolarization. However, once inside the cell, $HgCl_2$ depolarized the mitochondrial membrane to a greater degree and for a longer

period of time than did MeHg. Similar results were shown by Hare and Atchison (1992). Their results indicated that Hg^{2+} was more effective than MeHg at depolarizing both plasma and mitochondrial membranes. They suggested that Hg^{2+} was more effective at mitochondrial depolarization because it has a higher affinity for thiol groups (-SH) than does MeHg. However, Hg^{2+} depolarized the plasma membrane at lower concentrations than were necessary to depolarize the mitochondrial membrane, whereas MeHg depolarized the plasma membrane at concentrations that also depolarized the mitochondria membrane (Hare and Atchison, 1992). Their data were consistent with other studies that showed that Hg^{2+} was less efficient at penetrating the plasma membrane than was MeHg (Nakada and Imura, 1982). Therefore, intracellular changes associated with Hg^{2+} may appear latent to those produced by MeHg exposure.

MeHg treatment was associated with an increase in MMP at 24 hours in the lowest exposure group (0.01 μM), but this increase was followed at 48 hours by a dramatic decrease in MMP, and then a return to control levels at 72 hours. These data indicate increased mitochondrial activity, followed by a sharp decrease in mitochondrial activity, and ultimately, a shift back to normal mitochondrial activity. Initial insults to cells often initiate cytoprotective processes. For example, heat shock proteins expressed in the brain are important in the maintenance of cellular homeostasis, particularly in response to stressful conditions that adversely affect normal cellular structure and function. Transcription and translation of heat shock proteins are induced by hyperthermia and viral infection, against which the proteins act as protective molecules (Buccellato *et al.*, 2007). The increased production of heat shock proteins is powered by an increase in mitochondrial activity and an increase in MMP. TNFα is another molecule that induces cytoprotection by promoting the production of free radicals from the mitochondria. The free radicals, or ROS, stimulate the action of other cytoprotective molecules (Lacerda *et al.*, 2006). In the process of ROS production, there is an initial increase in MMP necessary to produce the excess ROS (Lacerda *et al.*, 2006). These data provide an explanation for the increased MMP observed in the first 24 hours of 0.01 μM MeHg exposure. Higher levels of MeHg (1.0 μM) or lower exposures for longer

periods of times may overwhelm the ROS defense system. The increased levels of ROS, if not metabolized, can feed back on the mitochondria and cause a dissipation of the membrane potential (Brookes *et al.*, 2004). Even with a decrease in MMP, various ROS defense molecules, such as glutathione peroxidase (Kromidas *et al.*, 1990), glutathione transferase (Custodio *et al.*, 2004), catalase (Saez *et al.*, 1982), and superoxide dismutase (Fridovich, 1995b) can act to neutralize the ROS, preventing further damage to the mitochondrial membrane, allowing the MMP to return to homeostatic levels.

The concentration of intracellular Ca^{2+} was measured using a microplate reader. We hypothesized that $[Ca^{2+}]_i$ would increase in a concentration- and time-dependent manner and would be higher in cell treated with MeHg compared to those treated with $HgCl_2$. Data indicated, however, that $[Ca^{2+}]_i$ was increased at 24 hours, was decreased at 48 hours, and returned to control levels at 72 hours in the 1.0 μM treated cells. In addition, there was no difference in $[Ca^{2+}]_i$ between MeHg and $HgCl_2$. The observed changes in $[Ca^{2+}]_i$ may be correlated with the observed changes in MMP. We observed decreases MMP and increases $[Ca^{2+}]_i$ at 24 hours in the 1.0 μM treatments, a possible result of release of Ca^{2+} from the depolarized mitochondria. Mitochondria sequester Ca^{2+} when excess Ca^{2+} is present in the cytosol (Duchen, 2000). If the Ca^{2+} concentration in mitochondria become too high, or if mitochondria are damaged by another means, the sequestered Ca^{2+} is released (Duchen, 2000), thus increasing the Ca^{2+} concentration within the cytosol, as was observed in the current study. This process may also result in cell death (Duchen, 2000), which was also observed in the 1.0 μM treatments in the present study. At 48 hours, the 1.0 μM treatments exhibit cell death and decreased MMP, but also decreased $[Ca^{2+}]_i$. By 48 hours, the cells may be damaged such that the plasma membrane has become leaky allowing Ca^{2+} to move out of the dying cell and into the media, particularly due to the presence of Hg^{2+}. Upon entry into a cell, Hg^{2+} damages and depolarizes the plasma membrane (Nakada and Imura, 1982). MeHg enters the cell without disrupting the plasma membrane, whereas Hg^{2+} disrupts the plasma membrane when gaining access to the cell (Hare and Atchison, 1992). Decreased

integrity of the plasma membrane of dying cells at 48 hours may be the reason for the observed decrease in $[Ca^{2+}]_i$.

The rate at which ROS were produced was measured by microplate assay. We hypothesized that the rate of ROS production would increase in a concentration- and time-dependent manner and that the increased rate of ROS production would be greater with MeHg treatment than $HgCl_2$ treatment. Instead, we observed a decrease in the rate of ROS production over time for all treatment concentrations, and decreased rates of ROS production for the 0.01 μM $HgCl_2$ and the 1.0 μM MeHg treatments at 24 hours, and a decreased rate of ROS production for the 1.0 μM MeHg treatment at 48 hours. Although unexpected, these data indicate no increase in ROS in conjunction with the decreased MMP observed in the 1.0 μM treatments. Several possibilities exist to explain the decrease in ROS production. First, increased mitochondrial Ca^{2+} causes an increase in ROS produced from the mitochondria when the Ca^{2+} increase is accompanied by uncoupling of Complex I of the respiratory chain (Sousa *et al.*, 2003). However, when the increase in mitochondrial Ca^{2+} is accompanied by inhibition of Complex III, no increase in ROS is observed (Sousa *et al.*, 2003). MeHg is known to inhibit Complex III (Yee and Choi, 1996). In the present study, Ca^{2+} was increased, but the rate of ROS production was decreased at 24 hours in the 1.0 μM treatments. These data suggest that ROS may not have been generated by all complexes of the electron transport chain, and the amount of ROS produced was not high enough to overwhelm the antioxidant processes within the cells. In addition, any temporal increase in the production of ROS may have resulted in the upregulation and activity of antioxidant molecules, further decreasing the level of detectable ROS. Similarly, 0.01 μM $HgCl_2$ treatment resulted in a decreased rate of ROS production compared to controls at 24 hours. This decrease in ROS production did not coincide with any changed in cell death, MMP or $[Ca^{2+}]_i$. These data indicate the possible induction of cytoprotective mechanisms (Buccellato *et al.*, 2007; Lacerda *et al.*, 2006).

Although not expected, the observed pattern of MMP, $[Ca^{2+}]_i$, ROS, and cell death changes cannot easily be explained by the known process of mitochondria-related

apoptosis. In contrast to exposures to high concentrations of MeHg, the concentrations used in the present study (0.01, 0.1, and 1.0 μM) do not appear to result in mitochondrial-related and ROS-induced apoptosis. It does appear however, that an early response of neurons exposed to low levels of MeHg may be the stimulation of mechanisms of cytoprotection. The potential to induce cytoprotective genes may play a role in determining which individuals (cells and whole organisms) exhibit negative effects at low-levels of MeHg exposure and those who do not. For example, organisms inherently exhibit genetic polymorphisms that alter one's ability to detoxify various compounds and change one's susceptibility to toxicity and disease (Bellinger, 2007; Eaton, 2000; Wolff and Weston, 1997). Some individuals may be able to sustain a greater "hit" of MeHg than others, based on these genetic differences (Klautau-Guimarães *et al.*, 2005; Weghorst and Buzard, 1993).

Not only were the pattern of changes in MMP, $[Ca^{2+}]_i$, and ROS not consistent with those known to be associated with apoptotic cell death, but at the lowest MeHg and $HgCl_2$ concentrations (0.01 and 0.1 μM), no cell death occurred at all, even though MMP, $[Ca^{2+}]_i$, and ROS were altered. MMP, Ca^{2+}, and ROS have many functions in neurons other than induction of apoptosis. Neurons exhibit $[Ca^{2+}]_i$ oscillations that may be associated with synaptic strengthening among neurons in the same domain (Singer, 1993; Stryker *et al.*, 1990). In neuronal spines and dendrites, $[Ca^{2+}]_i$ changes are mediated by the NMDA receptor which is crucial for the generation of long-term potentiation (LTP) which is associated with learning and memory (Alford *et al.*, 1993; Collingridge and Bliss, 1995). $[Ca^{2+}]_i$ changes in neurons initiate signaling pathways that trigger gene transcription (Bailey *et al.*, 1996; Martin *et al.*, 1997). Mitochondria are involved in more than energy production and induction of apoptosis (Green and Reed, 1998). They function in xenobiotic metabolism and glucose sensing (Maechler, 2002), as well as steroid hormone synthesis and lipid metabolism (Brookes *et al.*, 2004). In addition, ROS are involved not only in damage of membranes by lipid peroxidation (Gardner, 1989) and the crosslinking of proteins (Davies, 2005), but are important for

cell signaling (Brookes and Darley-Usmar, 2002; Brookes *et al.*, 2002) and cell proliferation (Burdon *et al.*, 1989).

The human population is exposed to chronic low levels of MeHg, and MeHg is highly toxic to the developing fetus, infant, and young child. The incomplete blood-brain barrier allows increased access of MeHg to the developing brain. Proliferation and migration of neurons in developing young is time-dependent, and alterations in the timing or rate of these events could significantly alter normal brain development. Once neurons are placed, proper synaptic development and function are necessary for the neurons to function normally. Changes in mitochondrial activity, $[Ca^{2+}]_i$, and levels of ROS could adversely affect proliferation, migration, or synaptic plasticity, and ultimately function, of the neurons in developing brains, without causing the death of the neurons. Data from our study indicate that SY5Y cells are sensitive to low levels of both MeHg and $HgCl_2$, and respond to MeHg and $HgCl_2$ exposure in ways known to occur in the brains of humans and animals, thus making them realistic candidates for mechanistic studies that may mimic the responses of the cerebellar granule cell to MeHg exposure *in vivo*. In addition, changes in MMP, $[Ca^{2+}]_i$, and ROS were observed at MeHg and $HgCl_2$ concentrations that did not produce cell death. These changes, specifically at very low MeHg concentrations, have not been previously indicated in current scientific literature and further studies of these effects and associated mechanisms are warranted. Understanding the mechanism of low-level MeHg toxicity is necessary for the protection of the developing central nervous system.

CHAPTER V

CONCLUSIONS

SUMMARY AND CONCLUSIONS

The objective of this dissertation was to better understand the mechanism of MeHg induced neurotoxicity by comparing sub-cellular changes between mice exposed to MeHg as young adults to mouse pups exposed during gestation, and to develop an *in vitro* model to more fully investigate *in vivo* MeHg exposure.

Previously, four mechanistic processes have been considered for MeHg neurotoxicity: 1) dissipation of mitochondrial membrane potential (MMP), 2) increase in $[Ca^{2+}]_i$ to cytotoxic levels, 3) increased production of reactive oxygen species (ROS), and 4) apoptosis. In the 1950's and 1970's during the Japanese and Iraqi poisonings, the bulk of pathological data indicated large amounts of apoptosis in the brains of sick individuals. Therefore, historically, MeHg experiments have investigated apoptosis. Early *in vivo* exposure studies employed high doses of MeHg, although they were similar to or lower than those experienced in the Minamata and Iraq human poisonings. The high concentrations used in early MeHg studies are no longer relevant to the lower-level human exposures experienced today from diet and environment. MeHg is found in the daily diet of most everyone in developed countries and in developing countries with high fish-eating populations. Along with the benefits of omega-3 fatty acids and selenium in the "oh so healthful" fish we eat, comes MeHg, an insidious and quiet "predator of the CNS".

MeHg is ingested orally and distributed throughout the body via the blood stream. On average, ten percent of ingested MeHg enters the brain through the blood-brain barrier and becomes trapped within. Three sets of total Hg accumulation data were presented in this dissertation. MeHg was provided to young adult and fetal mice at or near environmentally relevant exposure levels, through oral ingestion of food. The experimental dosing designs were: 1) administration to young adult animals from

postnatal day (P) 35 to 39, with examination at P40, 2) administration to pregnant females from gestational day (G) 8 to 18, whose pups were examined at P0 and P10, and 3) exposure of SH-SY5Y human neuroblastoma cells to MeHg or $HgCl_2$ in growth media. MeHg exposure levels were selected such that the lowest levels were within range of what could be experienced by a portion of today's human population. The results of these experiments indicated that even the lowest concentrations of MeHg are taken up into the brains of mice as young adults and during gestation, and into SY5Y cells at levels that are significantly higher than control levels. Cell culture total Hg accumulation results were consistent with *in vivo* findings.

Included in the cell culture study, in addition to MeHg exposure, was the exposure of the cells to the inorganic form of Hg as $HgCl_2$. The aspect of the study involving either MeHg or $HgCl_2$ was important because when MeHg enters the brain, it is demethylated. Studies have shown that in primates and humans exposed to moderate and high levels of MeHg, 10 – 33% of the original MeHg in the brain will be converted into the inorganic form after one year; 80 – 100% of the original MeHg in the brain will be converted to the inorganic form after 20 years. Previous studies indicate that even after five days of exposure to MeHg in mice, a measurable portion of total Hg in the brain is converted to the inorganic form. Some studies have shown that the concentration of inorganic Hg in specific brain regions correlates with the degree of cellular damage in that area. However, many other studies, mainly *in vitro,* indicate MeHg to be more directly cytotoxic than inorganic Hg. SY5Y cells in the present study showed a concentration-dependent accumulation of total Hg for both MeHg and $HgCl_2$, but the concentration of total Hg in the $HgCl_2$ exposed cells was significantly less than the concentration in those exposed to MeHg.

Cell death, typically by apoptosis, is a hallmark of MeHg toxicity, at least at high concentrations. Associated with apoptosis are dissipation of the MMP, increase in $[Ca^{2+}]_i$, and increase in ROS. These events were expected upon MeHg exposure. Therefore, the presence of these events was monitored in young adult mice, pups, and SY5Y cells. Cell death was increased in SY5Y cells with MeHg and $HgCl_2$ exposure,

but only at the highest concentrations used in these experiments. In addition, with similar treatment concentrations, cell death of SY5Y cells was either increased to a lesser degree in the $HgCl_2$ treated cells compared to those treated with MeHg, or cell death was observed starting at a later time point in cells exposed to $HgCl_2$ compared to MeHg. These results are in agreement with other *in vitro* studies indicating that MeHg is more directly cytotoxic at similar concentrations of $HgCl_2$. Two techniques were used to determine cell death in mice, Fluoro-Jade B staining and activated caspase 3 immunohistochemistry. Cell death was observed in the molecular and granule cell layers of adult cerebella with 1.0 mg/kg MeHg treatment. In contrast, mouse pups at P0 showed no MeHg associated increase in cell death within the cerebellum as analyzed by Fluoro-Jade B. However, cell death was increased in the Purkinje cell layer in the cerebellum of P0 mouse pups as analyzed by activated caspase 3 immunohistochemistry. Previous studies have shown that Bergmann glia are involved in the migration of granule cells from the external germinal cell layer to the internal granule cell layer. In addition, caspase 3 is activated in Bergmann glia during development. Instead of measuring cell death in the Purkinje cell layer at P0, we may have inadvertently measured the activation of caspase 3 in Bergmann glia. However, the caspase 3 activation was MeHg exposure dependent, suggesting that MeHg may affect Bergmann glia and the migration of granule cells rather than causing cell death in early postnatally developing cerebella.

Also in contrast to the increased cell death observed in adult cerebella, the cerebella of mice at P10 exhibited MeHg associated decreases in the number of dying cells with the 0.1 mg/kg MeHg treatment in the external germinal cell layer. The external germinal cell layer of the cerebellum is an area of high cell proliferation. These newly formed cells then migrate to the internal granule cell layer. Areas of high cell proliferation will naturally have a percentage of cells that die. If, however, the cells are not proliferating as rapidly as normal, the observed number of dying cells may decrease as well. The P10 data suggest, similar to the P0 data, that cell proliferation may be altered by MeHg exposure as opposed to MeHg increasing cell death. In future work, the

TUNEL assay for apoptosis, rather than detection of activated caspase 3 might be a better choice for determining cell death in developing animals.

MMP, $[Ca^{2+}]_i$, and ROS are involved in many processes within the cell other than apoptosis. All three play roles in cell cycle progression, proliferation, migration, and differentiation. They also function in the induction of transcription and translation of genes and proteins involved in regular cell processes as well as cytoprotection. To use a term from the paper by Brookes *et al.* (2004), the three are a "love-hate triangle". There are endless numbers of permutations and combinations in which changes in MMP, $[Ca^{2+}]_i$, and ROS may interact, not only directly, but indirectly as well. In addition, the degree of increased or decreased adds multiple layers of interaction to further confound this complex interplay.

Although we know the difficulties in understanding the interaction of MMP, $[Ca^{2+}]_i$, and ROS, we investigated these processes specifically for the purpose of determining whether low-levels of MeHg would produce effects similar to those known to occur with high MeHg exposure levels. As mentioned previously, the insidious nature of low levels of MeHg may manifest as subtle alterations in learning and behavior, which have been observed in children in the Faroe Islands and in Brazil, following exposure to chronic low levels of MeHg.

MMP in adult cerebella was increased in both the 0.2 and 1.0 mg/kg MeHg treatments, and increased in female hippocampi at 1.0 mg/kg MeHg. MMP in P0 pups was decreased in cerebella at 0.1 m/kg MeHg (highest dose); but increased in cerebella and female hippocampi with 0.01 mg/kg MeHg (lowest dose). In SY5Y cells, MMP was decreased compared to controls in the highest (1.0 μM) MeHg treatment at 24, 48, and 72 hours, but only at 48 and 72 hours for 1.0 μM $HgCl_2$ treatment. However, MMP was increased at 0.01 μM MeHg (lowest dose) at 24 hours. These data indicated that MMP is affected by MeHg and $HgCl_2$ exposure. However, both increases and decreases in MMP were observed in the present study. Increased MMP is not what the previously published literature suggests for high exposure levels of MeHg. Our data indicate that MeHg at low concentrations affects MMP, but does not always result in the decreased MMP typically

associated with higher MeHg concentrations. In addition, the male hippocampus appeared particularly protected from changes in MMP associated with MeHg exposure.

Basal $[Ca^{2+}]_i$ was changed throughout the *in vivo* experiments in a manner that was age- and sex- and brain region-dependent. In adults, female hippocampi exhibited increased $[Ca^{2+}]_i$, whereas no differences in $[Ca^{2+}]_i$ were observed in male hippocampi or in male or female cerebella. For pups exposed to MeHg during gestation and analyzed at P0, no differences were observed in $[Ca^{2+}]_i$ in the hippocampus, but $[Ca^{2+}]_i$ was increased in MeHg treated cerebella. For pups analyzed at P10, female hippocampi and both male and female cerebella exhibited increased $[Ca^{2+}]_i$, with the 0.1 mg/kg MeHg treatment. In the *in vitro* experiment using SY5Y cells, increased $[Ca^{2+}]_i$ was observed in the high $HgCl_2$ exposure after 24 hours, but after 48 hours, $[Ca^{2+}]_i$ in the high exposure level had decreased and was lower than controls. No difference in $[Ca^{2+}]_i$ was indicated between treatment with MeHg and $HgCl_2$ in SY5Y cells. Overall, $[Ca^{2+}]_i$ was generally increased with MeHg treatment, particularly in cerebella and female hippocampi. Increases in $[Ca^{2+}]_i$ can be cytotoxic. However, a major function of mitochondria is to sequester Ca^{2+} to prevent Ca^{2+}-induced cytotoxicity. In our study, we observed increases in MMP, which typically indicates increased mitochondrial activity. Because we observed increases in $[Ca^{2+}]_i$, without synchronous cell death and increased MMP, our data suggested that mitochondrial may be sequestering Ca^{2+} and preventing cell death at the low-level MeHg concentrations used.

The rate at which ROS were produced over time was measured for adult and developing mice, and in SY5Y cells. Upon investigation we discovered that across the experiments the rate at which ROS were produced changed very little. We did notice, however, that the total quantity of ROS appeared different among treatments. Therefore, we investigated both the rate and level of ROS production. The rate of ROS production in adult mice was decreased at both the 0.2 and 1.0 mg/kg MeHg treatments and the decrease was greater in males than females. For P0 mouse pups, no difference was observed in the rate of ROS production, but the level of ROS production was dependent on brain region. In the cerebellum, ROS levels were decreased with MeHg treatment, but

in the hippocampus, ROS levels were increased with MeHg treatment. For P10 mouse pups, no difference was observed in the rate of ROS production, but the level of ROS production was again dependent on brain region. In the cerebellum, the 0.1 mg/kg MeHg treatment exhibited decreased ROS levels compared to controls, whereas, in the hippocampus, there was no difference in the levels of ROS produced. In SY5Y cells, the rate of ROS production was time-, toxicant-, and treatment-dependent. Over time, the rate of ROS production decreased for all treatments, including controls. Differences in the rate of ROS production was greater for MeHg treatments compared to $HgCl_2$ treatments. $HgCl_2$ 0.1 μM treatment resulted in decreased rate of ROS production at 24 hours, whereas, 1.0 μM MeHg treatment resulted in decreased ROS production at 24 and 48 hours. Overall, the rate and levels of ROS production were decreased with MeHg and $HgCl_2$ treatment, suggesting that increased generation of ROS and the induction of oxidative stress is not a major factor in low and moderate MeHg concentrations. These data are in contrast to what current literature suggests concerning ROS production and oxidative stress at higher concentrations of MeHg and $HgCl_2$.

IMPORTANCE AND FUTURE STUDIES

Our data indicate that low and moderate MeHg exposure, both *in vivo* and *in vitro* produce effects in mitochondrial function, Ca^{2+} homeostasis, and oxidative stress unlike those reported in previous literature for higher MeHg exposures. In addition, data from our study indicate that SY5Y cells are sensitive to low levels of both MeHg and $HgCl_2$, and respond to MeHg and $HgCl_2$ exposure in ways similar to those observed in the whole animal studies, thus making them realistic candidates for mechanistic studies that may mimic the responses of neurons to MeHg exposure *in vivo*.

MMP, Ca^{2+}, and ROS have many functions in neurons other than induction of apoptosis. Neurons exhibit $[Ca^{2+}]_i$ oscillations that may be associated with synaptic strengthening among neurons in the same domain. In neuronal spines and dendrites, $[Ca^{2+}]_i$ changes are mediated by NMDA receptors, which is crucial for the generation of long-term potentiation (LTP) which is associated with learning and memory. $[Ca^{2+}]_i$

changes in neurons initiate signaling pathways that trigger gene transcription. Mitochondria are involved in more than energy production and induction of apoptosis. They function in xenobiotic metabolism and glucose sensing, as well as steroid hormone synthesis and lipid metabolism. In addition, ROS are involved not only in damage of membranes by lipid peroxidation (Gardner, 1989)and the crosslinking of proteins, but are important for cell signaling and cell proliferation.

Literature suggests that neuronal dysfunction may be of particular importance in diseases such as Alzheimer's, Parkinson's, mood, and autism (Bauman and Kemper, 2005; Monnet-Tschudi *et al.*, 2006), all of which are becoming increasingly more prevalent in our aging society. In addition, the developing CNS is particularly susceptible to adverse affects of toxicants. The incomplete blood-brain barrier allows increased access of MeHg to the developing brain. Proliferation and migration of neurons in developing young is time-dependent, and alterations in the timing or rate of these events could significantly alter normal brain development. Once neurons are placed, proper synaptic development and function are necessary for the neurons to function normally. Changes in mitochondrial activity, $[Ca^{2+}]_i$, and levels of ROS could adversely affect proliferation, migration, or synaptic plasticity, and ultimately function, of the neurons in developing brains without causing the death of the neurons.

MeHg exposure in today's human population, although low, is chronic and measurable. The United States Environmental Protection Agency (U.S. E.P.A.) has set the reference dose (RfD) for MeHg at 0.1 μg/kg body weight per day. RfD is considered to be a concentration at which a chemical can be consumed on a daily basis over a lifetime without expectation of adverse effects. Whole animal adults and developmental behavioral and neuronal functional studies at chronic low levels of MeHg are limited. Also limited are low level MeHg and inorganic Hg neuronal functional studies in cultured cells. Our data indicated that low levels of MeHg may affect neuronal function, and therefore suggested that further chronic low-level MeHg studies are warranted.

Research involving very low concentrations of MeHg should be continued both *in vivo* and *in vitro*. In addition, long-term, repeated exposure studies should be

incorporated because MeHg is rarely ingested only once, but many times over many years. Advancing technology allows visualization of cytoplasmic microdomains within cells over several hours to days. Cultured neurons could be set up in a heated / humidified / CO_2 infused flow-through system and visualized by fluorescence microscopy. MeHg or $HgCl_2$ as well as various levels of extracellular Ca^{2+}, or specific mitochondrial or plasma membrane channel inhibitors or stimulators could be administered in a times sequence and the reaction of the cell, or areas within the cell could be monitored in real time.

The developing nervous system is particularly sensitive to MeHg toxicity. The brains of animals exposed to MeHg *in utero* often display altered cytoarchitecture. Daily, along the developmental time-line, neurological changes occur, both morphologically and internally within the cell. Appropriate and timely gene expression is a necessity for orderly and complete neural development. Cells from the brains of developing pups exposed to MeHg *in utero* could be harvested at various times during gestation and analyzed for changes in expression of mRNA or proteins critical for neural development at those specific time points. Proteins associated with cell proliferation and migration would be an appropriate starting point.

In the adult hippocampus, new cells are formed in the subgranular layer of the dentate gyrus. Processes such as proliferation, migration, differentiation, and synaptogenesis are vital for these new cells to become incorporated into the functioning brain. Learning and memory take place, not only during development, but during the lifetime of an individual. Synaptic plasticity, dendritic processing, and long-term potentiation are necessary for sustained learning and retention of memories. The proper function of the brain and all its neural components are of utmost importance to the human population from developing fetuses to the aged.

REFERENCES

MSNBC. (2008). Scientists study mercury in the Great Salt Lake: Source and danger of poison to birds, other wildlife remains a mystery. MSNBC.com news report on the environment. Associated Press.

Abbott, N. J., Revest, P. A. and Romero, I. A. (1992). Astrocyte-endothelial interaction: Physiology and pathology. *Neuropathol Appl Neurobiol* **18**, 424-433.

Aberg, B., Ekman, L., Falk, R., Greitz, U., Persson, G. and Snihs, J. O. (1969). Metabolism of methyl mercury (203Hg) compounds in man. *Arch Environ Health* **19**, 478-484.

Acquas, E., Carboni, E., de Ree, R. H., Da Prada, M. and Di Chiara, G. (1992). Extracellular concentrations of dopamine and metabolites in the rat caudate after oral administration of a novel catechol-O-methyltransferase inhibitor Ro 40-7592. *J Neurochem* **59**, 326-330.

Adams, J. and Lammer, E. J. (1993). Neurobehavioral teratology of isotretinoin. *Reprod Toxicol* **7**, 175-177.

Akbarian, S., Vinuela, A., Kim, J. J., Potkin, S. G., Bunney, W. E., Jr. and Jones, E. G. (1993). Distorted distribution of nicotinamide-adenine dinucleotide phosphate-diaphorase neurons in temporal lobe of schizophrenics implies anomalous cortical development. *Arch Gen Psychiatry* **50**, 178-187.

Alberdi, E., Sánchez-Gómez, M. V. and Matute, C. (2005). Calcium and glial cell death. *Cell Calcium* **38**, 417-425.

Albus, J. S. (1971). A theory of cerebellar function. *Math Biosci* **10**, 25-61.

Alford, S., Frenguelli, B. G., Schofield, J. G. and Collingridge, G. L. (1993). Characterization of calcium signals induced in hippocampal CA1 neurones by the synaptic activation of NMDA receptors. *J Physiol* **469**, 693-716.

Ali, S. F., LeBel, C. P. and Bondy, S. C. (1992). Reactive oxygen species formation as a biomarker of methylmercury and trimethyltin neurotoxicity. *Neurotoxicology* **13**, 637-648.

Allen, J. W., El-Oqayli, H., Aschner, M., Syversen, T. and Sonnewald, U. (2001). Methylmercury has a selective effect on mitochondria in cultured astrocytes in the presence of [U-13C] glutamate. *Brain Res* **908**, 149-154.

Alnaes, E. and Rahamimoff, R. (1975). On the role of mitochondria in transmitter release from motor nerve terminals. *J Physiol* **248**, 285-306.

Alonso, A. and Köhler, C. (1984). A study of the reciprocal connections between the septum and the entorhinal area using anterograde and retrograde axonal transport methods in the rat brain. *J Comp Neurol* **225**, 327-343.

Alonso, M. T., Villalobos, C., Chamero, P., Alvarez, J. and García-Sancho, J. (2006). Calcium microdomains in mitochondria and nucleus. *Cell Calcium* **40**, 513-525.

Altman, J. (1962). Are new neurons formed in the brains of adult mammals? *Science* **135**, 1127-1128, 10.1126/science.135.3509.1127.

Altman, J. (1972a). Postnatal development of the cerebellar cortex in the rat. I. The external germinal layer and the transitional molecular layer. *J Comp Neurol* **145**, 353-397.

Altman, J. (1972b). Postnatal development of the cerebellar cortex in the rat. II. Phases in the maturation of Purkinje cells and of the molecular layer. *J Comp Neurol* **145**, 399-463.

Altman, J. (1972c). Postnatal development of the cerebellar cortex in the rat. III. Maturation of the components of the granular layer. *J Comp Neurol* **145**, 465-513.

Altman, J., Anderson, W. J. and Strop, M. (1971). Retardation of cerebellar and motor development by focal X-irradiation during infancy. *Physiol Behav* **7**, 143-150.

Altman, J. and Bayer, S. A. (1990). Migration and distribution of two populations of hippocampal granule cell precursors during the perinatal and postnatal periods. *J Comp Neurol* **301**, 365-381.

Altman, J. and Bayer, S. A. (1997). Development of the Cerebellar System: In Relation to its Evolution, Structure, and Functions. CRC Press, Boca Raton.

Altman, J. and Das, G. D. (1965). Autoradiographic and histological evidence of postnatal hippocampal neurogenesis in rats. *J Comp Neurol* **124**, 319-335.

Altmann, R. (1890). Die Elementarorganismen und ihre Beziehungen zu den Zellen. Veit Co, Leipzig.

Amaral, D. G. (1978). A Golgi study of cell types in the hilar region of the hippocampus in the rat. *J Comp Neurol* **182**, 851-914.

Amaral, D. G. and Dent, J. A. (1981). Development of the mossy fibers of the dentate gyrus: I. A light and electron microscopic study of the mossy fibers and their expansions. *J Comp Neurol* **195**, 51-86.

Amin-Zaki, L., Elhassani, S., Majeed, M. A., Clarkson, T. W., Doherty, R. A., Greenwood, M. R. and Giovanoli-Jakubczak, T. (1976). Perinatal methylmercury poisoning in Iraq. *Am J Dis Child* **130**, 1070-1076.

Anderson, P., Bliss, T. V. and Skrede, K. K. (1971). Lamellar organization of hippocampal pathways. *Exp Brain Res* **13**, 222-238.

Andersen, P., Holmquist, B. and Voorhoeve, P. E. (1966). Entorhinal activation of dentate granule cells. *Acta Physiol Scand* **66**, 448-460.

Angaut, P. and Brodal, A. (1967). Etude anatomique des projections du "vestibulocervelet" sur les noyaux vestibulaires chez le chat. *J Physiol (Paris)* **59**, 327.

Angevine, J. B., Jr. (1965). Time of neuron origin in the hippocampal region. An autoradiographic study in the mouse. *Exp Neurol* **13**, 1-70.

Angevine, J. B., Mancall, E. L. and Yakovlev, P., I. (1961). The Human Cerebellum: An Atlas of Gross Topography in Serial Sections. Little Brown, Boston.

Arnold, S. E. and Trojanowski, J. Q. (1996). Human fetal hippocampal development: I. Cytoarchitecture, myeloarchitecture, and neuronal morphologic features. *J Comp Neurol* **367**, 274-292.

Aschner, M. and Clarkson, T. W. (1987). Mercury-203 distribution in pregnant and nonpregnant rats following systemic infusions with thiol-containing amino acids. *Teratology* **36**, 321-328.

Aschner, M. and Clarkson, T. W. (1989). Methyl mercury uptake across bovine brain capillary endothelial cells *in vitro*: The role of amino acids. *Pharmacol Toxicol* **64**, 293-297.

Aschner, M., Eberle, N. B. and Kimelberg, H. K. (1991). Interactions of methylmercury with rat primary astrocyte cultures: methylmercury efflux. *Brain Res* **554**, 10-14.

Atchison, W. D. (1986). Extracellular calcium-dependent and -independent effects of methylmercury on spontaneous and potassium-evoked release of acetylcholine at the neuromuscular junction. *J Pharmacol Exp Ther* **237**, 672-680.

Atchison, W. D., Joshi, U. and Thornburg, J. E. (1986). Irreversible suppression of calcium entry into nerve terminals by methylmercury. *J Pharmacol Exp Ther* **238**, 618-624.

Averdunk, R. (1970). Effect of various detachment procedures on the permeability and metabolism of permanent tissue culture cells. *Res Exp Med (Berl)* **153**, 51-58.

Bailey, C. H., Bartsch, D. and Kandel, E. R. (1996). Toward a molecular definition of long-term memory storage. *Proc Natl Acad Sci U S A* **93**, 13445-13452.

Baimbridge, K. G., Celio, M. R. and Rogers, J. H. (1992). Calcium-binding proteins in the nervous system. *Trends Neurosci* **15**, 303-308.

Bakir, F., Damluji, S. F., Amin-Zaki, L., Murtadha, M., Khalidi, A., Al-Rawi, N. Y., Tikriti, S., Dahahir, H. I., Clarkson, T. W., Smith, J. C. and Doherty, R. A. (1973). Methylmercury poisoning in Iraq. *Science* **181**, 230-241.

Bakir, F., Rustam, H., Tikriti, S., Al-Damluji, S. F. and Shihristani, H. (1980). Clinical and epidemiological aspects of methylmercury poisoning. *Postgrad Med J* **56**, 1-10.

Baldelli, S., Aquilano, K., Rotilio, G. and Ciriolo, M. R. (2008). Glutathione and copper, zinc superoxide dismutase are modulated by overexpression of neuronal nitric oxide synthase. *Int J Biochem Cell Biol* **40**, 2660-2670.

Barbara, J. G. (2002). IP3-dependent calcium-induced calcium release mediates bidirectional calcium waves in neurones: functional implications for synaptic plasticity. *Biochim Biophys Acta* **1600**, 12-18.

Barhoumi, R., Awooda, I., Mouneimne, Y., Safe, S. and Burghardt, R. C. (2006). Effects of benzo-a-pyrene on oxytocin-induced Ca^{2+} oscillations in myometrial cells. *Toxicol Lett* **165**, 133-141.

Barhoumi, R., Faske, J., Liu, X. and Tjalkens, R. B. (2004). Manganese potentiates lipopolysaccharide-induced expression of NOS2 in C6 glioma cells through

mitochondrial-dependent activation of nuclear factor kappaB. *Mol Brain Res* **122**, 167-179.

Barhwal, K., Singh, S. B., Hota, S. K., Jayalakshmi, K. and Ilavazhagan, G. (2007). Acetyl-l-Carnitine ameliorates hypobaric hypoxic impairment and spatial memory deficits in rats. *Eur J Pharmacol* **570**, 97-107.

Bauman, M. and Kemper, T. L. (1985). Histoanatomic observations of the brain in early infantile autism. *Neurology* **35**, 866-874.

Bauman, M. L. and Kemper, T. L. (2005). Neuroanatomic observations of the brain in autism: A review and future directions. *Int J Dev Neurosci* **23**, 183-187.

Bayer, S. A. (1980). Development of the hippocampal region in the rat II. Morphogenesis during embryonic and early postnatal life. *J Comp Neurol* **190**, 115-134.

Bear, M. F., Connors, B. W. and Paradiso, M. A. (2001). The action potential. In Neuroscience: Exploring the Brain (M. F. Bear, B. W. Connors and M. A. Paradiso, Eds.), pp. 74-98. Lippincott Williams & Wilkins, Baltimore.

Bégin, M. E. (1987). Effects of polyunsaturated fatty acids and of their oxidation products on cell survival. *Chem Phys Lipids* **45**, 269-313.

Behl, C., Widmann, M., Trapp, T. and Holsboer, F. (1995). 17-β εstradiol protects neurons from oxidative stress-induced cell death *in vitro*. *Biochem Biophys Res Commun* **216**, 473-482.

Bellinger, D. C. (2007). Children's cognitive health: The influence of environmental chemical exposures. *Altern Ther Health Med* **13**, S140-144.

Bellum, S., Bawa, B., Thuett, K. A., Stoica, G. and Abbott, L. C. (2007a). Changes in biochemical processes in cerebellar granule cells of mice exposed to methylmercury. *Int J Toxicol* **26**, 261-269.

Bellum, S., Thuett, K. A., Grajeda, R. and Abbott, L. C. (2007b). Coordination deficits induced in young adult mice treated with methylmercury. *Int J Toxicol* **26**, 115-121.

Bellum, S., Thuett, K. A., Taylor, R. J. and Abbott, L. C. (2007c). Assessment of mercury concentrations in mouse brain using different routes of administration and different tissue preparations. *Toxicol Mech Meth* **17**, 165-173.

Benda, C. (1989). Ueber Die Spermatogenese der Vertebraten und hoeherer Evertebraten. II. Theil. Die Histiogenese der Spermien. *Arch Anat Physiol*, 393-398.

Bergmann, E. (1857). Notiz uber einige Structureverhaltnisse des Cerebellum und Ruckenmarks. *Z Ration Med* **8**, 360-364.

Berlin, M., Carlson, J. and Norseth, T. (1975). Dose-dependence of methylmercury metabolism: A study of distribution, biotransformation, and excretion in the squirrel monkey. *Arch Environ Health* **30**, 307-313.

Bernhagen, J. (2005). Macrophage migration and function: From recruitment in vascular disease to redox regulation in the immune and neuroendocrine networks. *Antioxid Redox Signal* **7**, 1182-1188, doi:10.1089/ars.2005.7.1182.

Berridge, M. J., Lipp, P. and Bootman, M. D. (2000). The versatility and universality of calcium signalling. *Nat Rev Mol Cell Biol* **1**, 11-21.

Bertipaglia, I. and Carafoli, E. (2007). Calpains and human disease. *Subcell Biochem* **45**, 29-53.

Bezin, S., Charpentier, G., Fossier, P. and Cancela, J.-M. (2006). The Ca^{2+}-releasing messenger NAADP, a new player in the nervous system. *J Physiol* **99**, 111-118.

Biedler, J. and Spengler, B. (1976). Metaphase chromosome anomaly: Association with drug resistance and cell-specific products. *Science* **191**, 185-187, 10.1126/science.942798.

Biedler, J. L., Helson, L. and Spengler, B. A. (1973). Morphology and Growth, Tumorigenicity, and Cytogenetics of Human Neuroblastoma Cells in Continuous Culture. *Cancer Res* **33**, 2643-2652.

Blackstad, T., Brink, K., Hem, J. and June, B. (1970). Distribution of hippocampal mossy fibers in the rat. An experimental study with silver impregnation methods. *J Comp Neurol* **138**, 433-449.

Blaustein, M. P., Ratzlaff, R. W., Kendrick, N. C. and Schweitzer, E. S. (1978). Calcium buffering in presynaptic nerve terminals. I. Evidence for involvement of a nonmitochondrial ATP-dependent sequestration mechanism. *J Gen Physiol* **72**, 15-41.

Bliss, T. V. P. and Gardner-Medwin, A. R. (1973). Long-lasting potentiation of synaptic transmission in the dentate area of the unanaesthetized rabbit following stimulation of the perforant path. *J Physiol (Lond)* **232**, 357-374.

Bondy, S. C. and McKee, M. (1991). Disruption of the potential across the synaptosomal plasma membrane and mitochondria by neurotoxic agents. *Toxicol Lett* **58**, 13-21.

Borrás, C., Sastre, J., García-Sala, D., Lloret, A., Pallardó, F. V. and Viña, J. (2003). Mitochondria from females exhibit higher antioxidant gene expression and lower oxidative damage than males. *Free Rad Biol Med* **34**, 546-552.

Boss, B. D., Turlejski, K., Stanfield, B. B. and Cowan, W. M. (1987). On the numbers of neurons on fields CA1 and CA3 of the hippocampus of Sprague-Dawley and Wistar rats. *Brain Res* **406**, 280-287.

Boveris, A., Cadenas, E. and Stoppani, A. O. M. (1976). Role of ubiquinone in the mitochondrial generation of hydrogen peroxide. *Biochem J* **156**, 435-444.

Brigelius-Flohé, R. (1999). Tissue-specific functions of individual glutathione peroxidases. *Free Rad Biol Med* **27**, 951-965.

Broca, P. (1878). Anatomie comparee des circonvolutions cerebrales. Le grand lobe limbique et la scissure limbique dans la serie des mammiferes. *Rev Anthropol* **1**, 385-498.

Brookes, P. and Darley-Usmar, V. M. (2002). Hypothesis: The mitochondrial NO-signaling pathway, and the transduction of nitrosative to oxidative cell signals: An alternative function for cytochrome C oxidase. *Free Rad Biol Med* **32**, 370-374.

Brookes, P. S., Levonen, A.-L., Shiva, S., Sarti, P. and Darley-Usmar, V. M. (2002). Mitochondria: Regulators of signal transduction by reactive oxygen and nitrogen species. *Free Rad Biol Med* **33**, 755-764.

Brookes, P. S., Yoon, Y., Robotham, J. L., Anders, M. W. and Sheu, S.-S. (2004). Calcium, ATP, and ROS: A mitochondrial love-hate triangle. *Am J Physiol Cell Physiol* **287**, C817-833, 10.1152/ajpcell.00139.2004.

Brubaker, P. E., Klein, R., Herman, S. P., Lucier, G. W., Alexander, L. T. and Long, M. D. (1973). DNA, RNA, and protein synthesis in brain, liver, and kidneys of asymptomatic methylmercury treated rats. *Exp Mol Pathol* **18**, 263-280.

Brune, D., Nordberg, G. F., Vesterberg, O., Gerhardsson, L. and Wester, P. O. (1991). A review of normal concentrations of mercury in human blood. *Sci Total Environ* **100**, 235-282.

Buccellato, M. A., Carsillo, T., Traylor, Z., Oglesbee, M. and Hari Shanker, S. (2007). Heat shock protein expression in brain: A protective role spanning intrinsic thermal resistance and defense against neurotropic viruses. *Prog Brain Res* **162**, 395-415.

Buisseret-Delmas, C. and Angaut, P. (1993). The cerebellar olivo-corticonuclear connections in the rat. *Prog Neurobiol* **40**, 63-87.

Buisseret-Delmas, C., Yatim, N., Buisseret, P. and Angaut, P. (1993). The X zone and CX subzone of the cerebellum in the rat. *Neurosci Res* **16**, 195-207.

Burdon, R. H., Gill, V. and Rice-Evans, C. (1989). Cell proliferation and oxidative stress. *Free Rad Res* **7**, 149 - 159.

Burke, K., Cheng, Y., Li, B., Petrov, A., Joshi, P., Berman, R. F., Reuhl, K. R. and DiCicco-Bloom, E. (2006). Methylmercury elicits rapid inhibition of cell proliferation in the developing brain and decreases cell cycle regulator, cyclin E. *Neurotoxicology* **27**, 970-981.

Cameron, H. A., Woolley, C. S., McEwen, B. S. and Gould, E. (1993). Differentiation of newly born neurons and glia in the dentate gyrus of the adult rat. *Neuroscience* **56**, 337-344.

Campbell, N. C. and Armstrong, D. M. (1983). The olivocerebellar projection in the rat: An autoradiographic study. *Brain Res* **275**, 215-233.

Campbell, S. and Macqueen, G. (2004). The role of the hippocampus in the pathophysiology of major depression. *J Psychiatry Neurosci* **29**, 417-426.

Carafoli, E. (1974). Mitochondrial uptake of calcium ions and the regulation of cell function. *Biochem Soc Symp*, 89-109.

Carafoli, E. (2004). Calcium-mediated cellular signals: A story of failures. *Trends Biochem Sci* **29**, 371-379.

Carden, D. L. and Granger, D. N. (2000). Pathophysiology of ischaemia-reperfusion injury. *J Pathol* **190**, 255-266.

Carrillo, M.-C., Kanai, S., Sato, Y. and Kitani, K. (1992). Age-related changes in antioxidant enzyme activities are region and organ, as well as sex, selective in the rat. *Mech Ageing Dev* **65**, 187-198.

Carugo, O. and Carugo, K. D. (2005). When X-rays modify the protein structure: Radiation damage at work. *Trends Biochem Sci* **30**, 213-219.

Castoldi, A. F., Barni, S., Turin, I., Gandini, C. and Manzo, L. (2000). Early acute necrosis, delayed apoptosis and cytoskeletal breakdown in cultured cerebellar granule neurons exposed to methylmercury. *J Neurosci Res* **59**, 775-787.

Castoldi, A. F., Blandini, F., Randine, G., Samuele, A., Manzo, L. and Coccini, T. (2006). Brain monoaminergic neurotransmission parameters in weanling rats after perinatal exposure to methylmercury and 2,2',4,4',5,5'-hexachlorobiphenyl (PCB153). *Brain Res* **1112**, 91-98.

Ceccatelli, S., Tamm, C., Zhang, Q. and Chen, M. (2007). Mechanisms and modulation of neural cell damage induced by oxidative stress. *Physiol Behav* **92**, 87-92.

Cernichiari, E., Brewer, R., Myers, G. J., Marsh, D. O., Lapham, L. W., Cox, C., Shamlaye, C. F., Berlin, M., Davidson, P. W. and Clarkson, T. W. (1995a). Monitoring methylmercury during pregnancy: Maternal hair predicts fetal brain exposure. *Neurotoxicology* **16**, 705-710.

Cernichiari, E., Toribara, T. Y., Liang, L., Marsh, D. O., Berlin, M. W., Myers, G. J., Cox, C., Shamlaye, C. F., Choisy, O. and Davidson, P. (1995b). The biological monitoring of mercury in the Seychelles study. *Neurotoxicology* **16**, 613-628.

Chambers, W. W. and Sprague, J. M. (1955a). Functional localization in the cerebellum. I. Organization in longitudinal cortico-nuclear zones and their contribution to the control of posture, both extrapyramidal and pyramidal. *J Comp Neurol* **103**, 105-129.

Chambers, W. W. and Sprague, J. M. (1955b). Functional localization in the cerebellum. II. Somatotopic organization in cortex and nuclei. *AMA Arch Neurol Psychiatry* **74**, 653-680.

Chan-Palay, V., Nilaver, G., Palay, S. L., Beinfeld, M. C., Zimmerman, E. A., Wu, J. Y. and O'Donohue, T. L. (1981). Chemical heterogeneity in cerebellar Purkinje cells: Existence and coexistence of glutamic acid decarboxylase-like and motilin-like immunoreactivities. *Proc Natl Acad Sci U S A* **78**, 7787-7791.

Chance, B., Sies, H. and Boveris, A. (1979). Hydroperoxide metabolism in mammalian organs. *Physiological Reviews* **59**, 527-605.

Chang, D. T. W. and Reynolds, I. J. (2006). Mitochondrial trafficking and morphology in healthy and injured neurons. *Prog Neurobiol* **80**, 241-268.

Chang, L. W. (1977). Neurotoxic effects of mercury--A review. *Environ Res* **14**, 329-373.

Chang, L. W. and Hartmann, H. A. (1972). Blood-brain barrier dysfunction in experimental mercury intoxication. *Acta Neuropathol* **21**, 179-184.

Chang, L. W. and Verity, M. A. (1995). Mercury neurotoxicity: Effects and mechanisms. In Handbook of Neurotoxicology (L. W. Chang and R. G. Dyer, Eds.), pp. 41. Marcel Kekker, Inc., New York.

Charleston, J. S., Body, R. L., Mottet, N. K., Vahter, M. E. and Burbacher, T. M. (1995). Autometallographic determination of inorganic mercury distribution in the cortex of the calcarine sulcus of the monkey *Macaca fascicularis* following long-term subclinical exposure to methylmercury and mercuric chloride. *Toxicol Appl Pharmacol* **132**, 325-333.

Chen, G., Yuan, P.-X., Jiang, Y.-M. and Huang, L.-D. (1998). Lithium increases tyrosine hydroxylase levels both *in vivo* and *in vitro*. *J Neurochem* **70**, 1768-1771.

Chen, X., Jennings, D. B. and Medeiros, D. M. (2002). Impaired cardiac mitochondrial membrane potential and respiration in copper-deficient rats. *J Bioenerg Biomembr* **34**, 397-406.

Cheung, M. K. and Verity, M. A. (1985). Experimental methyl mercury neurotoxicity: Locus of mercurial inhibition of brain protein synthesis in vivo and in vitro. *J Neurochem* **44**, 1799-1808.

Chiriboga, C. A. (1998). Neurological correlates of fetal cocaine exposure. In Cocaine: Effects on the developing brain (J. A. Harvey and B. E. Kosofsky, Eds.), pp. 109-125. The New York Academy of Sciences, New York.

Chronister, R. B., Sikes, R. W. and White Jr, L. E. (1975). Postcommissural fornix: Origin and distribution in the rodent. *Neurosci Lett* **1**, 199-202.

Choi, B. H. and Kim, R. C. (1985). Expression of glial fibrillary acidic protein by immature oligodendroglia and its implications. *J Neuroimmunol* **8**, 215-235.

Choi, B. H. and Lapham, L. W. (1980). Evolution of Bergman glia in developing human fetal cerebellum: A Golgi, electron microscopic and immunofluorescent study. *Brain Res* **190**, 369-383.

Clapham, D. E. (2003). TRP channels as cellular sensors. *Nature* **426**, 517-524.

Clarkson, T. W. (1987). Metal toxicity in the central nervous system. *Environ Health Perspect* **75**, 59-64.

Clarkson, T. W. (2002). The three modern faces of mercury. *Environ Health Perspect* **110**, 11-23.

Clarkson, T. W., Amin-Zaki, L. and Al-Tikriti, S. K. (1976). An outbreak of methylmercury poisoning due to consumption of contaminated grain. *Fed Proc* **35**, 2395-2399.

Clarkson, T. W. and Magos, L. (2006). The toxicology of mercury and its chemical compounds. *Crit Rev Toxicol* **36**, 609 - 662.

Collingridge, G. L. and Bliss, T. V. P. (1995). Memories of NMDA receptors and LTP. *Trends Neurosci* **18**, 54-56.

Cooney, J. R., Hurlburt, J. L., Selig, D. K., Harris, K. M. and Fiala, J. C. (2002). Endosomal compartments serve multiple hippocampal dendritic spines from a widespread rather than a local store of recycling membrane. *J Neurosci* **22**, 2215-2224.

Cooper, C. E., Mason, M. G., Nicholls, P., Cooper, C. E., Mason, M. G. and Nicholls, P. (2008). A dynamic model of nitric oxide inhibition of mitochondrial cytochrome c oxidase. *Biochim Biophys Acta* **1777**, 867-876.

Corti, C., L'Hostis, E. L., Quadroni, M., Schmid, H., Durussel, I., Cox, J., Hatt, P. D., James, P. and Carafoli, E. (1999). Tyrosine phosphorylation modulates the interaction of calmodulin with its target proteins. *Eur J Biochem* **262**, 790-802.

Costa, L. G., Fattori, V., Giordano, G. and Vitalone, A. (2007). An *in vitro* approach to assess the toxicity of certain food contaminants: Methylmercury and polychlorinated biphenyls. *Toxicology* **237**, 65-76.

Counter, S. A. and Buchanan, L. H. (2004). Mercury exposure in children: A review. *Toxicol Appl Pharmacol* **198**, 209-230.

Courville, J. and Faraco-Cantin, F. (1978). On the origin of the climbing fibers of the cerebellum. An experimental study in the cat with an autoradiographic tracing method. *Neuroscience* **3**, 797-809.

Cowan, W., Fawcett, J., O'Leary, D. and Stanfield, B. (1984). Regressive events in neurogenesis. *Science* **225**, 1258-1265, 10.1126/science.6474175.

Custodio, H. M., Broberg, K., Wennberg, M., Jansson, J. H., Vessby, B., Hallmans, G., Stegmayr, B. and Skerfving, S. (2004). Polymorphisms in glutathione-related genes affect methylmercury retention. *Arch Environ Health* **59**, 588-595.

Dager, S. R., Wang, L., Friedman, S. D., Shaw, D. W., Constantino, J. N., Artru, A. A., Dawson, G. and Csernansky, J. G. (2007). Shape mapping of the hippocampus in young children with autism spectum disorder. *Am J Neuroradiol* **28**, 672-677.

Das, J. (2006). The role of mitochondrial respiration in physiological and evolutionary adaptation. *BioEssays* **28**, 890-901.

Davidson, A. M. and Halestrap, A. P. (1990). Partial inhibition by cyclosporin A of the swelling of liver mitochondria *in vivo* and *in vitro* induced by sub-micromolar [Ca^{2+}], but not by butyrate. Evidence for two distinct swelling mechanisms. *Biochem J* **268**, 147-152.

Davies, M. J. (2005). The oxidative environment and protein damage. *Biochim Biophys Acta* **1703**, 93-109.

Davis, J. M., Otto, D. A., Weil, D. E. and Grant, L. D. (1990). The comparative developmental neurotoxicity of lead in humans and animals. *Neurotoxicol Teratol* **12**, 215-229.

de Groot, H. and Littauer, A. (1989). Hypoxia, reactive oxygen, and cell injury. *Free Rad Biol Med* **6**, 541-551.

Dey, P. M., Gochfeld, M. and Reuhl, K. R. (1999). Developmental methylmercury administration alters cerebellar PSA-NCAM expression and Golgi sialyltransferase activity. *Brain Res* **845**, 139-151.

De Zeeuw, C. I., Wylie, D. R., Digiorgi, P. L. and Simpson, J. I. (1994). Projections of individual Purkinje cells of identified zones in the flocculus to the vestibular and cerebellar nuclei in the rabbit. *J Comp Neurol* **349**, 428-447.

Dhandapani, K. and Brann, D. (2002). Estrogen-astrocyte interactions: Implications for neuroprotection. *BMC Neurosci* **3**, 6.

DiMauro, S. and Schon, E. A. (2008). Mitochondrial disorders in the nervous system. *Annu Rev Neurosci* **31**, 91-123, doi:10.1146/annurev.neuro.30.051606.094302.

Diño, M. R., Schuerger, R. J., Liu, Y. B., Slater, N. T. and Mugnaini, E. (2000). Unipolar brush cell: A potential feedforward excitatory interneuron of the cerebellum. *Neuroscience* **98**, 625-636.

Domingo, J. L. (2007). Omega-3 fatty acids and the benefits of fish consumption: Is all that glitters gold? *Environ Int* **33**, 993-998.

Domoráková, I., Burda, J., Mechírová, E. and Feriková, M. (2006). Mapping of rat hippocampal neurons with NeuN after ischemia/reperfusion and ginkgo biloba extract (EGb 761) pretreatment. *Cell Mol Neurobiol* **26**, 1191-1202.

Dourdin, N., Bhatt, A. K., Dutt, P., Greer, P. A., Arthur, J. S. C., Elce, J. S. and Huttenlocher, A. (2001). Reduced cell migration and disruption of the actin cytoskeleton in calpain-deficient embryonic fibroblasts. *J Biol Chem* **276**, 48382-48388, 10.1074/jbc.M108893200.

Drahota, Z., Krivakova, P., Cervinkova, Z., Kmonickova, E., Lotkova, H., Kucera, O. and Houstek, J. (2005). Tert-butyl hydroperoxide selectively inhibits mitochondrial respiratory-chain enzymes in isolated rat hepatocytes. *Physiol Res* **54**, 67-72.

Dreiem, A. and Seegal, R. F. (2007). Methylmercury-induced changes in mitochondrial function in striatal synaptosomes are calcium-dependent and ROS-independent. *Neurotoxicology* **28**, 720-726.

Driscoll, C. D., Streissguth, A. P. and Riley, E. P. (1990). Prenatal alcohol exposure: Comparability of effects in humans and animal models. *Neurotoxicol Teratol* **12**, 231-237.

Dubin, M. and Stoppani, A. O. M. (2000). Programmed cell death and apoptosis. The role of mitochondria. *Medicina* **60**, 375-386.

Duchen, M. R. (1999). Contributions of mitochondria to animal physiology: From homeostatic sensor to calcium signalling and cell death. *J Physiol (Lond)* **516**, 1-17.

Duchen, M. R. (2000). Mitochondria and calcium: From cell signalling to cell death. *J Physiol (Lond)* **529**, 57-68.

Duchen, M. R. (2004). Mitochondria in health and disease: Perspectives on a new mitochondrial biology. *Mol Aspects Med* **25**, 365-451.

Duchen, M. R. and Biscoe, T. J. (1992). Relative mitochondrial membrane potential and $[Ca^{2+}]_i$ in type I cells isolated from the rabbit carotid body. *J Physiol (Lond)* **450**, 33-61.

Eaton, D. L. (2000). Biotransformation enzyme polymorphism and pesticide susceptibility. *Neurotoxicology* **21**, 101-111.

Eberhard, M. and Erne, P. (1991). Calcium binding to fluorescent calcium indicators: Calcium green, calcium orange and calcium crimson. *Biochem Biophys Res Commun* **180**, 209-215.

Eccles, J., Llinas, R. and Sasaki, K. (1964). Excitation of cerebellar Purkinje cells by the climbing fibres. *Nature* **203**, 245-246.

Eccles, J. C. (1967). Circuits in the cerebellar control of movement. *Proc Natl Acad Sci U S A* **58**, 336-343.

Edwards, G. N. (1865). Two cases of poisoning by mercuric methide. *St. Bartholomew's Hospital Reports* **1**, 141-150.

Ehrich, M. (1995). Using neuroblastoma cell lines to address differential specificity to organophophates. *Clin Exp Pharmacol Physiol* **22**, 291-292.

Eisler, R. (2004). Mercury hazards from gold mining to humans, plants, and animals. *Rev Environ Contam Toxicol* **181**, 139-198.

Ekerot, C. F. and Kano, M. (1985). Long-term depression of parallel fibre synapses following stimulation of climbing fibres. *Brain Res* **342**, 357-360.

Ekerot, C. F. and Oscarsson, O. (1981). Prolonged depolarization elicited in Purkinje cell dendrites by climbing fibre impulses in the cat. *J Physiol (Lond)* **318**, 207-221.

Elliott, S. J., Meszaros, J. G. and Schilling, W. P. (1992). Effect of oxidant stress in calcium signaling in vascular endothelial cells. *Free Rad Biol Med* **13**, 635-650.

Engert, F. and Bonhoeffer, T. (1999). Dendritic spine changes associated with hippocampal long-term synaptic plasticity. *Nature* **399**, 66-70.

EPA (2000). Benchmark dose technical guidance document. *EPA/630/R-00/001*, 1-87.

Eriksson, P. S., Perfilieva, E., Bjork-Eriksson, T., Alborn, A. M., Nordborg, C., Peterson, D. A. and Gage, F. H. (1998). Neurogenesis in the adult human hippocampus. *Nat Med* **4**, 1313-1317.

Eto, K. (1997). Pathology of Minamata disease. *Toxicol Pathol* **25**, 614-623.

Eto, K., Takizawa, Y., Akagi, H., Haraguchi, K., Asano, S., Takahata, N. and Tokunaga, H. (1999). Differential diagnosis between organic and inorganic mercury poisoning in human cases: The pathologic point of view. *Toxicol Pathol* **27**, 664-671.

Evans, H. L., Garman, R. H. and Weiss, B. (1977). Methylmercury: Exposure duration and regional distribution as determinants of neurotoxicity in nonhuman primates. *Toxicol Appl Pharmacol* **41**, 15-33.

Evans, H. L., Laties, V. G. and Weiss, B. (1975). Behavioral effects of mercury and methylmercury. *Fed Proc* **34**, 1858-1867.

Evans, P. H. (1993). Free radicals in brain metabolism and pathology. *Br Med Bull* **49**, 577-587.

Falconer, M. M., Vaillant, A., Reuhl, K. R., Laferriere, N. and Brown, D. L. (1994). The molecular basis of microtubule stability in neurons. *Neurotoxicology* **15**, 109-122.

Falluel-Morel, A., Sokolowski, K., Sisti, H. M., Zhou, X., Shors, T. J. and Dicicco-Bloom, E. (2007). Developmental mercury exposure elicits acute hippocampal cell death, reductions in neurogenesis, and severe learning deficits during puberty. *J Neurochem* **103**, 1968-1981.

Falluel-Morel, A., Zhou, X., Smith, E., Sisti, H., Shors, T. and DiCicco-Bloom, E. (2006). Methylmercury selectively alters neurogenesis in the neonatal rat hippocampus. *Int J Dev Neurosci* **24**, 589-589.

Farina, M., Franco, J. L., Ribas, C. M., Meotti, F. C., Missau, F. C., Pizzolatti, M. G., Dafre, A. L. and Santos, A. R. S. (2005). Protective effects of *Polygala paniculata* extract against methylmercury-induced neurotoxicity in mice. *J Pharm Pharmacol* **57**, 1503-1508.

Faro, L. R. F., Durán, R., do Nascimento, J. L. M., Alfonso, M. and Picanço-Diniz, C. W. (1997). Effects of methylmercury on the *in vivo* release of dopamine and its acidic metabolites DOPAC and HVA from striatum of rats. *Ecotoxicol Environ Saf* **38**, 95-98.

Faustman, E. M., Ponce, R. A., Ou, Y. C., Mendoza, M. A. C., Lewandowski, T. and Kavanagh, T. (2002). Investigations of methylmercury-induced alterations in neurogenesis. *Environ Health Perspect* **110**, 859-864.

Ferrer, I., Serrano, T. and Soriano, E. (1990). Naturally occurring cell death in the subicular complex and hippocampus in the rat during development. *Neurosci Res* **8**, 60-66.

Fifková, E. and Anderson, C. L. (1981). Stimulation-induced changes in dimensions of stalks of dendritic spines in the dentate molecular layer. *Exp Neurol* **74**, 621-627.

Finch, D. M. and Babb, T. L. (1981). Demonstration of caudally directed hippocampal efferents in the rat by intracellular injection of horseradish peroxidase. *Brain Res* **214**, 405-410.

Finger, S. (2004). Paul Broca (1824-1880). *J Neurol* **251**, 769-770.

Fischer, M., Kaech, S., Knutti, D. and Matus, A. (1998). Rapid actin-based plasticity in dendritic spines. *Neuron* **20**, 847-854.

Fonfria, E., Dare, E., Benelli, M., Sunol, C. and Ceccatelli, S. (2002). Translocation of apoptosis-inducing factor in cerebellar granule cells exposed to neurotoxic agents inducing oxidative stress. *Eur J Neurosci* **16**, 2013-2016.

Fonfria, E., Vilaro, M. T., Babot, Z., Rodriguez-Farre, E. and Sunol, C. (2005). Mercury compounds disrupt neuronal glutamate transport in cultured mouse cerebellar granule cells. *J Neurosci Res* **79**, 545-553.

Fonnum, F. and Lock, E. A. (2004). The contributions of excitotoxicity, glutathione depletion and DNA repair in chemically induced injury to neurones: Exemplified with toxic effects on cerebellar granule cells. *J Neurochem* **88**, 513-531.

Fox, J. H., Patel-Mandlik, K. and Cohen, M. M. (1975). Comparative effects of organic and inorganic mercury on brain slice respiration and metabolism. *J Neurochem* **24**, 757-762.

Franco, J. L., Braga, H. C., Stringari, J., Missau, F. C., Posser, T., Mendes, B. G., Leal, R. B., Santos, A. R., Dafre, A. L., Pizzolatti, M. G. and Farina, M. (2007). Mercurial-induced hydrogen peroxide generation in mouse brain mitochondria: Protective effects of quercetin. *Chem Res Toxicol* **20**, 1919-1926.

Frank, T. C., Nunley, M. C., Sons, H. D., Ramon, R. and Abbott, L. C. (2003). Fluoro-jade identification of cerebellar granule cell and purkinje cell death in the α1A calcium ion channel mutant mouse, leaner. *Neuroscience* **118**, 667-680.

Fridovich, I. (1995a). Superoxide radical and superoxide dismutases. *Annu Rev Biochem* **64**, 97.

Fridovich, I. (1995b). Superoxide radical and superoxide dismutases. *Annu Rev Biochem* **64**, 97-112, doi:10.1146/annurev.bi.64.070195.000525.

Fried, P. A., Watkinson, B. and Gray, R. (1999). Growth from birth to early adolescence in offspring prenatally exposed to cigarettes and marijuana. *Neurotoxicol Teratol* **21**, 513-525.

Friede, R. (1954). [Quantitative share of the glia in development of the cortex.]. *Acta Anat* **20**, 290-296.

Fujiyama, J., Hirayama, K. and Yasutake, A. (1994). Mechanism of methylmercury efflux from cultured astrocytes. *Biochem Pharmacol* **47**, 1525-1530.

Furukawa, Y., Torres, A. S. and O'Halloran, T. V. (2004). Oxygen-induced maturation of SOD1: A key role for disulfide formation by the copper chaperone CCS. *Eur Mol Biol Organ J* **23**, 2872-2881.

Futatsuka, M., Kitano, T., Shono, M., Fukuda, Y., Ushijima, K., Inaoka, T., Nagano, M., Wakamiya, J. and Miyamoto, K. (2000). Health surveillance in the population living in a methyl mercury-polluted area over a long period. *Environ Res* **83**, 83-92.

Gaarskjaer, F. B. (1986). The organization and development of the hippocampal mossy fiber system. *Brain Res* **396**, 335-357.

Gage, F. H., Kempermann, B. Palmer, T.D., Peterson, D.A., Ray, J. (1998). Multipotent progenitor cells in the adult dentate gyrus. *J Neurobiol* **36**, 249-266.

Gaggi, C., Zino, F., Duccini, M. and Renzoni, A. (1996). Levels of mercury in scalp hair of fishermen and their families from Camara de Lobos-Madeira (Portugal): A preliminary study. *Bull Environ Contam Toxicol* **56**, 860-865.

Ganther, H. E. (1978). Modification of methylmercury toxicity and metabolism by selenium and vitamin E: Possible mechanisms. *Environ Health Perspect* **25**, 71-76.

Ganther, H. E., Goudie, C., Sunde, M. L., Kopecky, M. J. and Wagner, P. (1972). Selenium: Relation to decreased toxicity of methylmercury added to diets containing tuna. *Science* **175**, 1122-1124.

Garcia, M. L. and Strehler, E. E. (1999). Plasma membrane calcium ATPases as critical regulators of calcium homeostasis during neuronal cell function. *Front Biosci* **4**, D869-882.

Gardner, H. W. (1989). Oxygen radical chemistry of polyunsaturated fatty acids. *Free Rad Biol Med* **7**, 65-86.

Garman, R. H., Weiss, B. and Evans, H. L. (1975). Alkyl mercurial encephalopathy in the monkey *Saimiri sciureus* and *Macaca arctoides* a histo pathologic and auto radiographic study. *Acta Neuropathol* **32**, 61-74.

Gartner, L. P. and Hiatt, J. L. (1997). Color Textbook of Histology. W.B. Saunders Company, Philadelphia.

Gasso, S., Sunol, C., Sanfeliu, C., Rodriguez-Farre, E. and Cristofol, R. M. (2000). Pharmacological characterization of the effects of methylmercury and mercuric chloride on spontaneous noradrenaline release from rat hippocampal slices. *Life Sci* **67**, 1219-1231.

Gatti, R., Belletti, S., Uggeri, J., Vettori, M. V., Mutti, A., Scandroglio, R. and Orlandini, G. (2004). Methylmercury cytotoxicity in PC12 cells is mediated by primary glutathione depletion independent of excess reactive oxygen species generation. *Toxicology* **204**, 175-185.

Gerard, M., Abitbol, M., Delezoide, A. L., Dufier, J. L., Mallet, J. and Vekemans, M. (1995). PAX-genes expression during human embryonic development, a preliminary report. *C R Acad Sci III* **318**, 57-66.

Ghez, C. and Thach, T. W. (2000). The cerebellum. In Principles of Neural Science (E. R. Kandel, J. H. Schwartz and T. M. Jessell, Eds.), 4th ed., pp. 832-852. McGraw-Hill, New York.

Gilbertson, M. W., Williston, S. K., Paulus, L. A., Lasko, N. B., Gurvits, T. V., Shenton, M. E., Pitman, R. K. and Orr, S. P. (2007). Configural cue performance in identical twins discordant for posttraumatic stress disorder: Theoretical implications for the role of hippocampal function. *Biol Psychiatry* **62**, 513-520.

Gilroy, S. and Jones, R. L. (1992). Gibberellic acid and abscisic acid coordinately regulate cytoplasmic calcium and secretory activity in barley aleurone protoplasts. *Proc Natl Acad Sci U S A* **89**, 3591-3595.

Ginsburg, J. (1971). Placental drug transfer. *Annu Rev Pharmacol* **11**, 387-408.

Gould, E., Reeves, A. J., Fallah, M., Tanapat, P., Gross, C. G. and Fuchs, E. (1999). Hippocampal neurogenesis in adult Old World primates. *Proc Natl Acad Sci U S A* **96**, 5263-5267.

Graeber, M. B., Kösel, S., Egensperger, R., Banati, R. B., Müller, U., Bise, K., Hoff, P., Möller, H. J., Fujisawa, K. and Mehraein, P. (1997). Rediscovery of the case described by Alois Alzheimer in 1911: Historical, histological and molecular genetic analysis. *Neurogenetics* **1**, 73-80.

Graff, R. D., Falconer, M. M., Brown, D. L. and Reuhl, K. R. (1997). Altered sensitivity of posttranslationally modified microtubules to methylmercury in differentiating embryonal carcinoma-derived neurons. *Toxicol Appl Pharmacol* **144**, 215-224.

Grandjean, P., Budtz-Jorgensen, E., White, R. F., Jorgensen, P. J., Weihe, P., Debes, F. and Keding, N. (1999a). Methylmercury exposure biomarkers as indicators of neurotoxicity in children aged 7 years. *Am J Epidemiol* **150**, 301-305.

Grandjean, P., Nielsen, G. D., Jorgensen, P. J. and Horder, M. (1992a). Reference intervals for trace elements in blood: Significance of risk factors. *Scand J Clin Lab Invest* **52**, 321-337.

Grandjean, P., Weihe, P., Jorgensen, P. J., Clarkson, T., Cernichiari, E. and Videro, T. (1992b). Impact of maternal seafood diet on fetal exposure to mercury, selenium, and lead. *Arch Environ Health* **47**, 185-195.

Grandjean, P., Weihe, P., White, R. F. and Debes, F. (1998). Cognitive performance of children prenatally exposed to "safe" levels of methylmercury. *Environ Res* **77**, 165-172.

Grandjean, P., Weihe, P., White, R. F., Debes, F., Araki, S., Yokoyama, K., Murata, K., Sørensen, N., Dahl, R. and Jørgensen, P. J. (1997). Cognitive deficit in 7-year-old children with prenatal exposure to methylmercury. *Neurotoxicol Teratol* **19**, 417-428.

Grandjean, P., White, R. F., Nielsen, A., Cleary, D. and de Oliveira Santos, E. C. (1999b). Methylmercury neurotoxicity in Amazonian children downstream from gold mining. *Environ Health Perspect* **107**, 587-591.

Grateron, L., Gonzalo, L. M. and Insausti, R. (1996). Postnatal development of the human entorhinal cortex. *Society for Neuroscience Abstracts* **22**, 1014.

Green, D. R. and Reed, J. C. (1998). Mitochondria and apoptosis. *Science* **281**, 1309-1312.

Greenwood, M. R., Clarkson, T. W., Doherty, R. A., Gates, A. H., Amin-Zaki, L., Elhassani, S. and Majeed, M. A. (1978). Blood clearance half-times in lactating and nonlactating members of a population exposed to methylmercury. *Environ Res* **16**, 48-54.

Grieve, A. P. (1984). Tests of sphericity of normal distributions and the analysis of repeated measures designs. *Psychometrika* **49**, 257-267.

Groenewegen, H. J., Room, P., Witter, M. P. and Lohman, A. H. M. (1982). Cortical afferents of the nucleus accumbens in the cat, studied with anterograde and retrograde transport techniques. *Neuroscience* **7**, 977-996.

Gross, C. G. (2000). Neurogenesis in the adult brain: Death of a dogma. *Nat Rev Neurosci* **1**, 67-73.

Grove, E. A. and Tole, S. (1999). Patterning events and specification signals in the developing hippocampus. *Cereb Cortex* **9**, 551-561, 10.1093/cercor/9.6.551.

Guidi, S., Ciani, E., Severi, S., Contestabile, A. and Bartesaghi, R. (2005). Postnatal neurogenesis in the dentate gyrus of the guinea pig. *Hippocampus* **15**, 285-301.

Gunter, T. E. (1998). The Ca^{2+} transport mechanisms of mitochondria and Ca^{2+} uptake from physiological-type Ca^{2+} transients. *Biochim Biophys Acta*.

Gunter, T. E., Buntinas, L., Sparagna, G., Eliseev, R. and Gunter, K. (2000). Mitochondrial calcium transport: Mechanisms and functions. *Cell Calcium* **28**, 285-296.

Gurunluoglu, R. and Gurunluoglu, A. (2008). Giulio Cesare Arantius (1530-1589): A surgeon and anatomist: His role in nasal reconstruction and influence on Gaspare Tagliacozzi. *Ann Plast Surg* **60**, 717-722.

Hall, B. D. and St. Louis, V. L. (2004). Methylmercury and total mercury in plant litter decomposing in upland forests and flooded landscapes. *Environ Sci Technol* **38**, 5010-5021, doi:10.1021/es049800q.

Halliwell, B. (2003). Oxidative stress in cell culture: An under-appreciated problem? *FEBS Lett* **540**, 3-6.

Halliwell, B. and Gutteridge, J. M. (2007). Free Radicals in Biology and Medicine. 4th ed. Oxford University Press, New York.

Hamberger, A. C., Chiang, G. H., Nylén, E. S., Scheff, S. W. and Cotman, C. W. (1979). Glutamate as a CNS transmitter. I. Evaluation of glucose and glutamine as precursors for the synthesis of preferentially released glutamate. *Brain Res* **168**, 513-530.

Han, D., Williams, E. and Cadenas, E. (2001). Mitochondrial respiratory chain-dependent generation of superoxide anion and its release into the intermembrane space. *Biochem. J.* **353**, 411-416.

Hansen, O. N., Trillingsgaard, A., Beese, I., Lyngbye, T. and Grandjean, P. (1989). A neuropsychological study of children with elevated dentine lead level: Assessment of the effect of lead in different socio-economic groups. *Neurotoxicol Teratol* **11**, 205-213.

Harada, M. (1977). Congenital Minamata disease. Intrauterine methylmercury poisoning. *Teratology* **18**, 285.

Harada, M. (1995). Minamata disease: Methylmercury poisoning in Japan caused by environmental pollution. *Crit Rev Toxicol* **25**, 1-24.

Harada, M., Fujino, T., Akagi, T. and Nishigaki, S. (1976). Epidemiological and clinical study and historical background of mercury pollution on Indian reservations in

Northwestern Ontario Canada. *Bulletin of the Institute of Constitutional Medicine Kumamoto University* **26**, 169-184.

Hare, M. F. and Atchison, W. D. (1992). Comparative action of methylmercury and divalent inorganic mercury on nerve terminal and intraterminal mitochondrial membrane potentials. *J Pharmacol Exp Ther* **261**, 166-172.

Hare, M. F., McGinnis, K. M. and Atchison, W. D. (1993). Methylmercury increases intracellular concentrations of Ca++ and heavy metals in NG108-15 cells. *J Pharmacol Exp Ther* **266**, 1626-1635.

Hasegawa, K., Omata, S. and Sugano, H. (1988). *In vivo* and *in vitro* effects of methylmercury on the activities of aminoacyl-tRNA synthetases in rat brain. *Arch Toxicol* **62**, 470-472.

Hastings, N. B. and Gould, E. (1999). Rapid extension of axons into the CA3 region by adult-generated granule cells. *J Comp Neurol* **413**, 146-154.

Hatten, M., Furie, M. and Rifkin, D. (1982). Binding of developing mouse cerebellar cells to fibronectin: A possible mechanism for the formation of the external granular layer. *J Neurosci* **2**, 1195-1206.

Hatten, M. E. (1999). Central nervous system neuronal migration. *Annu Rev Neurosci* **22**, 511-539, doi:10.1146/annurev.neuro.22.1.511.

Hawkins, A. and Olszewski, J. (1957). Glia/nerve cell index for cortex of the whale. *Science* **126**, 76-77, 10.1126/science.126.3263.76.

Hebb, D. O. (1950). Organization of behavior. *J Clin Psychol* **6**, 307.

Heiss, W. D. (1981). Cerebral blood flow: Physiology, pathophysiology and pharmacological effects. *Adv Otorhinolaryngol* **27**, 26-39.

Henderson, M. (2003). Autism is linked to mercury poisoning. Times Online: News International Group. www.timesonline.co.uk/tol/news/uk/article1099295.ece

Henze, K. and Martin, W. (2003). Evolutionary biology: Essence of mitochondria. *Nature* **426**, 127-128.

Herrup, K. and Kuemerle, B. (1997). The compartmentalization of the cerebellum. *Annu Rev Neurosci* **20**, 61-90, doi:10.1146/annurev.neuro.20.1.61.

Herrup, K. and Wilczynski, S. L. (1982). Cerebellar cell degeneration in the leaner mutant mouse. *Neuroscience* **7**, 2185-2196.

Hess, E. J. and Wilson, M. C. (1991). Tottering and leaner mutations perturb transient developmental expression of tyrosine hydroxylase in embryologically distinct Purkinje cells. *Neuron* **6**, 123-132.

Heyes, A., Mason, R. P., Kim, E.-H. and Sunderland, E. (2006). Mercury methylation in estuaries: Insights from using measuring rates using stable mercury isotopes. *Mar Chem* **102**, 134-147.

Hirose, M., Stuyvers, B., Dun, W., ter Keurs, H. and Boyden, P. A. (2008). Wide long lasting perinuclear Ca^{2+} release events generated by an interaction between ryanodine and IP3 receptors in canine Purkinje cells. *J Mol Cell Cardiol* **45**, 176-184.

Hittelman, K. J., Lindberg, O. and Cannon, B. (1969). Oxidative phosphorylation and compartmentation of fatty acid metabolism in brown fat mitochondria. *Eur J Biochem* **11**, 183-192.

Houser, C. R., Swartz, B. E., Walsh, G. O. and Delgado-Escueta, A. V. (1992). Granule cell disorganization in the dentate gyrus: Possible alterations of neuronal migration in human temporal lobe epilepsy. *Epilepsy Res Suppl* **9**, 41-49.

Huang, Z. J., Di Cristo, G. and Ango, F. (2007). Development of GABA innervation in the cerebral and cerebellar cortices. *Nat Rev Neurosci* **8**, 673-686.

Humphrey, T. (1967). The development of the human hippocampal fissure. *J Anat* **101**, 655-676.

Hunter, D., Bomford, R. R. and Dorothy Russell, S. (1940). Poisoning by methylmercury compounds. *Q J Med* **9**, 193-213.

Hunter, D. and Russell, D. S. (1954). Focal cerebellar and cerebellar atrophy in a human subject due to organic mercury compounds. *J Neurol Neurosurg Psychiatry* **17**, 235-241.

Hyman, B., Van Hoesen, G., Damasio, A. and Barnes, C. (1984). Alzheimer's disease: Cell-specific pathology isolates the hippocampal formation. *Science* **225**, 1168-1170, 10.1126/science.6474172.

Ichas, F., Jouaville, L. S., Sidash, S. S., Mazat, J.-P. and Holmuhamedov, E. L. (1994). Mitochondrial calcium spiking: A transduction mechanism based on calcium-induced permeability transition involved in cell calcium signalling. *FEBS Lett* **348**, 211-215.

Ichas, F. and Mazat, J. P. (1998). From calcium signaling to cell death: Two conformations for the mitochondrial permeability transition pore. Switching from low- to high-conductance state. *Biochim Biophys Acta* **1366**, 33-50.

Ingram, V. M., Ogren, M. P., Chatot, C. L., Gossels, J. M. and Owens, B. B. (1985). Diversity among Purkinje cells in the monkey cerebellum. *Proc Natl Acad Sci U S A* **82**, 7131-7135.

Insausti, R. and Amaral, D. G. (2004). Hippocampal formation. In The Human Nervous System (G. Paxinos and J. K. Mai, Eds.), 2 ed., pp. 871-914. Elsevier Academic Press, New York.

Insausti, R., Insausti, A. M., Sobreviela, M. T., Salinas, A. and Martínez-Peñuela, J. M. (1998). Human medial temporal lobe in aging: Anatomical basis of memory preservation. *Microsc Res Tech* **43**, 8-15.

InSug, O., Datar, S., Koch, C. J., Shapiro, I. M. and Shenker, B. J. (1997). Mercuric compounds inhibit human monocyte function by inducing apoptosis: Evidence for formation of reactive oxygen species, development of mitochondrial membrane permeability transition and loss of reductive reserve. *Toxicology* **124**, 211-224.

International Programme on Chemical Safety, I. (1990). Methylmercury. World Health Organization, Geneva.

Irukayama, K., Tsubaki, T. and Takizawa, I. (1977). History and background. In Minamata Disease: Methylmercury Poisoning in Minamata and Niigata, Japan (T. Tsubaki and K. Irukayama, Eds.), pp. 1-102. Elsevier, New York.

Ishida, Y., Ichimura, T., Sumi, H., Horigome, T. and Omata, S. (1997). Methylmercury alters the tyrosination status of tubulin in the brains of acutely intoxicated rats. *Toxicology* **122**, 171-181.

Ishizuka, N., Weber, J. and Amaral, D. G. (1990). Organization of intrahippocampal projections originating from CA3 pyramidal cells in the rat. *J Comp Neurol* **295**, 580-623.

Ito, M. (1982). Cerebellar control of the vestibulo-ocular reflex--around the flocculus hypothesis. *Annu Rev Neurosci* **5**, 275-296.

Ito, M. (1984a). The Cerebellum and Neural Control, pp. 580. Raven Press, New York.

Ito, M. (1984b). Granule cells. In The Cerebellum and Neural Control (M. Ito, Ed.), pp. 74-85. Raven Press, New York.

Ito, M. (1984c). Purkinje cells: Morphology and development. In The Cerebellum and Neural Control (M. Ito, Ed.), pp. 21-39. Raven Press, New York.

Ito, M. (1986). Long-term depression as a memory process in the cerebellum. *Neurosci Res* **3**, 531-539.

Ito, M., Sakurai, M. and Tongroach, P. (1982). Climbing fibre induced depression of both mossy fibre responsiveness and glutamate sensitivity of cerebellar Purkinje cells. *J Physiol (Lond)* **324**, 113-134.

Jakob, H. and Beckmann, H. (1986). Prenatal developmental disturbances in the limbic allocortex in schizophrenics. *J Neural Transm Gen Sect* **65**, 303-326.

Jakob, H. and Beckmann, H. (1994). Circumscribed malformation and nerve cell alterations in the entorhinal cortex of schizophrenics. Pathogenetic and clinical aspects. *J Neural Transm Gen Sect* **98**, 83-106.

Jansen, J. (1954). On the morphogenesis and the morphology of the mammalian cerebellum. In Aspects of Cerebellar Anatomy (J. Jansen and A. Brodal, Eds.), pp. 13-81. Tanum, Oslo.

Jessell, T. M. and Sanes, J. R. (2000). The induction and patterning of the nervous system. In Principles of Neural Science (E. R. Kandel, J. H. Schwartz and T. M. Jessell, Eds.), pp. 1019-1049. McGraw-Hill, New York.

Jones, K. L. (1973). Pattern of malformation in offspring of chronic alcoholic mothers. *Lancet* **1**, 1267-1271.

Jourdain, P., Fukunaga, K. and Muller, D. (2003). Calcium/calmodulin-dependent protein kinase II contributes to activity-dependent filopodia growth and spine formation. *J Neurosci* **23**, 10645-10649.

Juchau, M. R. (1972). Mechanisms of drug biotransformation reactions in the placenta. *Fed Proc* **31**, 48-51.

Julian, D., April, K. L., Patel, S., Stein, J. R. and Wohlgemuth, S. E. (2005). Mitochondrial depolarization following hydrogen sulfide exposure in erythrocytes from a sulfide-tolerant marine invertebrate. *J Exp Biol* **208**, 4109-4122, 10.1242/jeb.01867.

Kakkar, P. and Singh, B. (2007). Mitochondria: A hub of redox activities and cellular distress control. *Mol Cell Biochem* **305**, 235-253.

Kandel, E. R., Schwartz, J. H. and Jessell, T. M. (2000). Principles of Neural Science, 4th ed., pp. 1414. McGraw-Hill, New York.

Kandel, E. R. and Siegelbaum, S. A. (2000). Synaptic integration. In Principles of Neural Science (E. R. Kandel, J. H. Schwartz and T. Jessell, Eds.), pp. 207-228. McGraw-Hill, New York.

Kauppinen, R. A., Komulainen, H. and Taipale, H. (1989). Cellular mechanisms underlying the increase in cytosolic free calcium concentration induced by methylmercury in cerebrocortical synaptosomes from guinea pig. *J Pharmacol Exp Ther* **248**, 1248-1254.

Kaur, P., Schulz, K., Aschner, M. and Syversen, T. (2007). Role of docosahexaenoic acid in modulating methylmercury-induced neurotoxicity. *Toxicol Sci* **100**, 423-432.

Kerper, L. E., Ballatori, N. and Clarkson, T. W. (1992). Methylmercury transport across the blood-brain barrier by an amino acid carrier. *Am J Physiol* **262**, R761-765.

Kershaw, T. G., Clarkson, T. W. and Dhahir, P. H. (1980). The relationship between blood levels and dose of methylmercury in man. *Arch Environ Health* **35**, 28-36.

Kierszenbaum, A. L. (2002). Histology and Cell Biology: An Introduction to Pathology. Mosby, Inc., St. Louis.

Kim, Y.-J., Chai, Y.-G. and Ryu, J.-C. (2005a). Selenoprotein W as molecular target of methylmercury in human neuronal cells is down-regulated by GSH depletion. *Biochem Biophys Res Commun* **330**, 1095-1102.

Kim, Y.-J., Kim, Y.-S., Kim, M.-S. and Ryu, J.-C. (2007). The inhibitory mechanism of methylmercury on differentiation of human neuroblastoma cells. *Toxicology* **234**, 1-9.

Kim, Y.-S., Zhuang, H., Koehler, R. C. and Doré, S. (2005b). Distinct protective mechanisms of HO-1 and HO-2 against hydroperoxide-induced cytotoxicity. *Free Rad Biol Med* **38**, 85-92.

Kimbrough, R. D. (1995). Polychlorinated biphenyls (PCBs) and human health: An update. *Crit Rev Toxicol* **25**, 133-163.

Kirchhoff, S. R., Gupta, S. and Knowlton, A. A. (2002). Cytosolic heat shock protein 60, apoptosis, and myocardial Injury. *Circulation* **105**, 2899-2904, 10.1161/01.cir.0000019403.35847.23.

Kirischuk, S., Voitenko, N., Kostyuk, P. and Verkhratsky, A. (1996). Calcium signalling in granule neurones studied in cerebellar slices. *Cell Calcium* **19**, 59-71.

Klautau-Guimarães, M. d. N., DAscenção, R., Caldart, F. A., Grisolia, C. K., Souza, J. R. d., Barbosa, A. C., Cordeiro, C. M. T. and Ferrari, I. (2005). Analysis of genetic susceptibility to mercury contamination evaluated through molecular biomarkers in at-risk Amazon Amerindian populations. *Genet Mol Biol* **28**, 827-832.

Klee, C. B. and Means, A. R. (2002). Keeping up with calcium: Conference on calcium-binding proteins and calcium function in health and disease. *EMBO Rep* **3**, 823-827.

Komsta-Szumska, E., Czuba, M., Reuhl, K. R. and Miller, D. R. (1983). Demethylation and excretion of methyl mercury by the guinea pig. *Environ Res* **32**, 247-257.

Kondo, T., Takahashi, S., Sato, H., Yamada, M., Kikuchi, T. and Furuya, K. (1993). Cytotoxicity of size-density fractionated coal fly ash in rat alveolar macrophages cultured *in vitro*. *Toxicol In Vitro* **7**, 61-67.

Kostyniak, P. J. (1980). Differences in elimination rates of methylmercury between two genetic variant strains of mice. *Toxicol Lett* **6**, 405-410.

Krettek, J. E. and Price, J. L. (1977). Projections from the amygdaloid complex and adjacent olfactory structures to the entorhinal cortex and to the subiculum in the rat and cat. *J Comp Neurol* **172**, 723-752.

Kriegstein, A. R. and Noctor, S. C. (2004). Patterns of neuronal migration in the embryonic cortex. *Trends Neurosci* **27**, 392-399.

Kromidas, L., Trombetta, L. D. and Jamall, I. S. (1990). The protective effects of glutathione against methylmercury cytotoxicity. *Toxicol Lett* **51**, 67-80.

Kunimoto, M. (1994). Methylmercury induces apoptosis of rat cerebellar neurons in primary culture. *Biochem Biophys Res Commun* **204**, 310-317.

Kunimoto, M., Aoki, Y., Shibata, K. and Miura, T. (1992). Differential cytotoxic effects of methylmercury and organotin compounds on mature and immature neuronal cells and non-neuronal cells *in vitro*. *Toxicol In Vitro* **6**, 349-355.

Kunimoto, M. and Suzuki, T. (1997). Migration of granule neurons in cerebellar organotypic cultures is impaired by methylmercury. *Neurosci Lett* **226**, 183-186.

Kunimoto, M. and Suzuki, T. (1995). Selective down-regulation of 440 kDa ankyrin-B associated with neurite retraction. *Neuroreport* **6**, 2545-2548.

Kupferberg, H. J. and Way, E. L. (1963). Pharmacologic basis for the increased sensitivity of the newborn rate to morphine. *J Pharmacol Exp Ther* **141**, 105-112.

Kutala, V. K., Parinandi, N. L., Pandian, R. P. and Kuppusamy, P. (2004). Simultaneous measurement of oxygenation in intracellular and extracellular compartments of lung microvascular endothelial cells. *Antioxid Redox Signal* **6**, 597-603, doi:10.1089/152308604773934350.

Kuznetsov, D. A. and Richter, V. (1987). Modulation of messenger RNA metabolism in experimental methyl mercury neurotoxicity. *Int J Neurosci* **34**, 1-17.

Kuznetsov, D. A., Zavijalov, N. V., Govorkov, A. V. and Richter, V. (1987). Suppression of aminoacyladenylate synthesis by methyl mercury *in vitro* and *in vivo*. *Toxicol Lett* **36**, 161-165.

Lacerda, L., Smith, R. M., Opie, L. and Lecour, S. (2006). TNFα-induced cytoprotection requires the production of free radicals within mitochondria in C2C12 myotubes. *Life Sci* **79**, 2194-2201.

Langston, J. W., Forno, L. S., Rebert, C. S. and Irwin, I. (1984). Selective nigral toxicity after systemic administration of 1-methyl-4-phenyl-1,2,5,6-tetrahydropyrine (MPTP) in the squirrel monkey. *Brain Res* **292**, 390-394.

Lankas, G. R., Wise, L. D., Cartwright, M. E., Pippert, T. and Umbenhauer, D. R. (1998). Placental P-glycoprotein deficiency enhances susceptibility to chemically induced birth defects in mice. *Reprod Toxicol* **12**, 457-463.

Lau, F. C., Frank, T. C., Nahm, S. S., Stoica, G. and Abbott, L. C. (2004). Postnatal apoptosis in cerebellar granule cells of homozygous leaner (tg1a/tg1a) mice. *Neurotox Res* **6**, 267-280.

Laurberg, S. and Sørensen, K. E. (1981). Associational and commissural collaterals of neurons in the hippocampal formation (Hilus fasciae dentatae and subfield CA3). *Brain Res* **212**, 287-300.

LeBel, C. P., Ali, S. F., McKee, M. and Bondy, S. C. (1990). Organometal-induced increases in oxygen reactive species: The potential of 2',7'-dichlorofluorescin diacetate as an index of neurotoxic damage. *Toxicol Appl Pharmacol* **104**, 17-24.

LeBel, C. P., Ischiropoulos, H. and Bondy, S. C. (1992). Evaluation of the probe 2',7'-dichlorofluorescin as an indicator of reactive oxygen species formation and oxidative stress. *Chem Res Toxicol* **5**, 227-231, doi:10.1021/tx00026a012.

Leclerc, N., Schwarting, G. A., Herrup, K., Hawkes, R. and Yamamoto, M. (1992). Compartmentation in mammalian cerebellum: Zebrin II and P-path antibodies define three classes of sagittally organized bands of Purkinje cells. *Proc Natl Acad Sci U S A* **89**, 5006-5010.

Lee, S.-K., Lee, J.-Y., Lee, M.-Y., Chung, S.-M. and Chung, J.-H. (1999). Advantages of Calcium Green-1 over other fluorescent dyes in measuring cytosolic calcium in platelets. *Anal Biochem* **273**, 186-191.

Legros, H., Dingeval, M.-G., Janin, F., Costentin, J. and Bonnet, J.-J. (2004). Toxicity of a treatment associating dopamine and disulfiram for catecholaminergic neuroblastoma SH-SY5Y cells: Relationships with 3,4-dihydroxyphenylacetaldehyde formation. *Neurotoxicology* **25**, 365-375.

Lehotsky, J., Kaplan, P., Matejovicova, M., Murin, R., Racay, P. and Raeymaekers, L. (2002). Ion transport systems as targets of free radicals during ischemia reperfusion injury. *Gen Physiol Biophys* **21**, 31-37.

Lemasters, J. J., Nieminen, A. L., Qian, T., Trost, L. C., Elmore, S. P., Nishimura, Y., Crowe, R. A., E., C. W., Bradham, C. A., Brenner, D. A. and Herman, B. (1998). The mitochondrial permeability transition in cell death: A common mechanism in necrosis, apoptosis and autophagy. *Biochim Biophys Acta* **1366**, 177-196.

Levesque, P. C. and Atchison, W. D. (1987). Interactions of mitochondrial inhibitors with methylmercury on spontaneous quantal release of acetylcholine. *Toxicol Appl Pharmacol* **87**, 315-324.

Levesque, P. C. and Atchison, W. D. (1991). Disruption of brain mitochondrial calcium sequestration by methylmercury. *J Pharmacol Exp Ther* **256**, 236-242.

Li, X., Weber, L. W. D. and Rozman, K. K. (1995). Toxicokinetics of 2,3,7,8-tetrachlorodibenzo-p-dioxin in female Sprague-Dawley rats including placental and lactational transfer to fetuses and neonates. *Fundam Appl Toxicol* **27**, 70-76.

Li, Y., Pan, Y. and Zhu, H. (1998). Relation between methylmercury chloride-induced programmed cell death and the development of nervous system in rats. *Wei Sheng Yen Chiu* **27**, 241-244.

Lim, M. L. R., Minamikawa, T. and Nagley, P. (2001). The protonophore CCCP induces mitochondrial permeability transition without cytochrome c release in human osteosarcoma cells. *FEBS Lett* **503**, 69-74.

Limke, T. L. and Atchison, W. D. (2002). Acute exposure to methylmercury opens the mitochondrial permeability transition pore in rat cerebellar granule cells. *Toxicol Appl Pharmacol* **178**, 52-61.

Lind, B., Friberg, L. and Nylander, M. (1988). Preliminary studies on methylmercury biotransformation and clearance in the brain of primates II. Demethylation of mercury in brain. *J Trace Elem Exp Med* **1**, 49-56.

LoPachin, R. M. and Aschner, M. (1999). Neuronal-glial interactions as potential targets of neurotoxicant effect. In Neurotoxicology (H. A. Tilson and G. J. Harry, Eds.), 2nd ed. Taylor & Francis, Philadelphia, PA.

Lopez-Artiguez, M., Grilo, A., Martinez, D., Soria, M. L., Nunez, L., Ruano, A., Moreno, E., Garcia Fuente, F. and Repetto, M. (1994). Mercury and methylmercury in population risk groups on the Atlantic coast of southern Spain. *Arch Environ Contam Toxicol* **27**, 415-419.

Lord, C., Cook, E. H., Leventhal, B. L. and Amaral, D. G. (2000). Autism spectrum disorders. *Neuron* **28**, 355-363.

Lorente de No, R. (1933). Studies on the structure of the cerebral cortex. II. Continuation of the study of the ammonic system. *J Psychol Neurol* **46**, 113-177.

Loveland, K. A., Bachevalier, J., Pearson, D. A. and Lane, D. M. (2008). Fronto-limbic functioning in children and adolescents with and without autism. *Neuropsychologia* **46**, 49-62.

Lowndes, H. E., Philbert, M. A., Beiswanger, C. M., Kauffman, F. C. and Reuhl, K. R. (1995). Keynote introduction: Xenobiotic metabolism in the brain as mechanistic bases for neurotoxicity. In Handbook of Neurotoxicology (L. W. Chang and R. S. Dyer, Eds.), pp. 1-27. Marcel Dekker, Inc., New York.

Luft, R. (1997). Historical overview of mitochondrial diseases. In Mitochondria and Free Radicals in Neurodegenerative Diseases (M. F. Beal, N. Howell and I. Bodis-Wollner, Eds.), pp. 3-14. Wiley-Liss, Inc., New York.

Maechler, P. (2002). Mitochondria as the conductor of metabolic signals for insulin exocytosis in pancreatic ß-cells. *Cell Mol Life Sci* **59**, 1803-1818.

Magi, S., Castaldo, P., Carrieri, G., Scorziello, A., Di Renzo, G. and Amoroso, S. (2005). Involvement of Na^{+}-Ca^{2+} exchanger in intracellular Ca^{2+} increase and neuronal injury induced by polychlorinated biphenyls in human neuroblastoma SH-SY5Y cells. *J Pharmacol Exp Ther* **315**, 291-296, 10.1124/jpet.105.088948.

Magos, L., Bakir, F., Clarkson, T. W., Al-Jawad, A. M. and Al-Soffi, M. H. (1976). Tissue levels of mercury in autopsy specimens of liver and kidney. *Bull World Health Organ* **53 (suppl)**, 93-97.

Magos, L. and Butler, W. H. (1976). The kinetics of methylmercury administered repeatedly to rats. *Arch Toxicol* **35**, 25-39.

Magos, L., Peristianis, G. C., Clarkson, T. W., Brown, A., Preston, S. and Snowden, R. T. (1981). Comparative study of the sensitivity of male and female rats to methylmercury. *Arch Toxicol* **48**, 11-20.

Mahaffey, K. R. and Mergler, D. (1998). Blood levels of total and organic mercury in residents of the upper St. Lawrence River basin, Quebec: Association with age, gender, and fish consumption. *Environ Res* **77**, 104-114.

Malenka, R. C. and Bear, M. F. (2004). LTP and LTD: An embarrassment of riches. *Neuron* **44**, 5-21.

Malenka, R. C. and Nicoll, R. A. (1999). Long-term potentiation--a decade of progress? *Science* **285**, 1870-1874, 10.1126/science.285.5435.1870.

Malinow, R. (2003). AMPA receptor trafficking and long-term potentiation. *Philos Trans R Soc Lond B Biol Sci* **358**, 707-714.

Malviya, A. N. and Klein, C. (2006). Mechanism regulating nuclear calcium signaling. *Can J Physiol Pharmacol* **84**, 403-422.

Manáková, S., Puttonen, K. A., Raasmaja, A. and Männistö, P. T. (2004). The roles of dopamine transporter and Bcl-2 protein in the protection of CV1-P cells from 6-OHDA-induced toxicity. *Toxicol Lett* **154**, 117-123.

Mangina, C. A. and Sokolov, E. N. (2006). Neuronal plasticity in memory and learning abilities: Theoretical position and selective review. *Int J Psychophysiol* **60**, 203-214.

Mannella, C. A. (2006). Structure and dynamics of the mitochondrial inner membrane cristae. *Biochim Biophys Acta* **1763**, 542-548.

Marani, E. (1986). Topographic histochemistry of the cerebellum. 5'-nucleotidase, acetylcholinesterase, immunology of FAL. *Prog Histochem Cytochem* **16**, 1-169.

Marani, E. and Voogd, J. (1979). The morphology of the mouse cerebellum. *Acta Morphol Neerl Scand* **17**, 33-52.

Margulis, L. (1971). The origin of plant and animal cells. *Am Sci* **59**, 230-235.

Marr, D. (1969). A theory of cerebellar cortex. *J Physiol (Lond)* **202**, 437-470.

Marsh, D. O., Myers, G. J., Clarkson, T. W., Amin-Zaki, L. and Tikriti, S. (1977). Fetal methylmercury poisoning: New data on clinical and toxicological aspects. *Trans Am Neurol Assoc* **102**, 69-71.

Martin, C., Beshel, J. and Kay, L. M. (2007). An olfacto-hippocampal network is dynamically involved in odor-discrimination learning. *J Neurophysiol* **98**, 2196-2205, 10.1152/jn.00524.2007.

Martin, J. H. (1996). Neuroanatomy: Text and Atlas. 2nd ed. Appleton & Lange, Stamford.

Martin, K. C., Barad, M. and Kandel, E. R. (2000). Local protein synthesis and its role in synapse-specific plasticity. *Curr Opin Neurobiol* **10**, 587-592.

Martin, K. C., Michael, D., Rose, J. C., Barad, M., Casadio, A., Zhu, H. and Kandel, E. R. (1997). MAP kinase translocates into the nucleus of the presynaptic cell and is required for long-term facilitation in aplysia. *Neuron* **18**, 899-912.

Martin, T. A., Keating, J. G., Goodkin, H. P., Bastian, A. J. and Thach, W. T. (1996a). Throwing while looking through prisms: I. Focal olivocerebellar lesions impair adaptation. *Brain* **119**, 1183-1198, 10.1093/brain/119.4.1183.

Martin, T. A., Keating, J. G., Goodkin, H. P., Bastian, A. J. and Thach, W. T. (1996b). Throwing while looking through prisms: II. Specificity and storage of multiple gaze-throw calibrations. *Brain* **119**, 1199-1211, 10.1093/brain/119.4.1199.

Martindale, J. L. and Holbrook, N. J. (2002). Cellular response to oxidative stress: Signaling for suicide and survival. *J Cell Physiol* **192**, 1-15.

Marty, M. S. and Atchison, W. D. (1997). Pathways mediating Ca^{2+} entry in rat cerebellar granule cells following *in vitro* exposure to methyl mercury. *Toxicol Appl Pharmacol* **147**, 319-330.

Marty, M. S. and Atchison, W. D. (1998). Elevations of intracellular Ca^{2+} as a probable contributor to decreased viability in cerebellar granule cells following acute exposure to methylmercury. *Toxicol Appl Pharmacol* **150**, 98-105.

Massaro, E. J. (1996). The developmental cytotoxicity of mercurials: A review. In Toxicology of Metals (L. W. Chang, Ed.), pp. 1047-1082. CRC Press-Taylor & Francis Group, LLC, Boca Raton, FL.

Matsumoto, H., Koya, G. and Takeuchi, T. (1965). Fetal Minamata disease. A neuropathological study of two cases of intrauterine intoxication by a methyl mercury compound. *J Neuropathol Exp Neurol* **24**, 563-574.

Matthews, A. D. (1983). Mercury content of commercially important fish of the Seychelles, and hair mercury levels of a selected part of the population. *Environ Res* **30**, 305-312.

Mattson, M. P., Gleichmann, M. and Cheng, A. (2008). Mitochondria in neuroplasticity and neurological disorders. *Neuron* **60**, 748-766.

McBride, H. M., Neuspiel, M. and Wasiak, S. (2006). Mitochondria: More than just a powerhouse. *Curr Biol* **16**, R551-560.

McBride, W. G. (1961). Thalidomide and congenital abnormalities. *Lancet* **278**, 1358.

McCord, J. M. and Fridovich, I. (1968). The reduction of cytochrome c by milk xanthine oxidase. *J Biol Chem* **243**, 5753-5760.

McCord, J. M. and Fridovich, I. (1969). Superoxide dismutase. An enzymic function for erythrocuprein (hemocuprein). *J Biol Chem* **244**, 6049-6055.

McCormick, D. and Thompson, R. (1984). Cerebellum: Essential involvement in the classically conditioned eyelid response. *Science* **223**, 296-299, 10.1126/science.6701513.

McMahon, A. P. and Bradley, A. (1990). The Wnt-1 (int-1) proto-oncogene is required for development of a large region of the mouse brain. *Cell* **62**, 1073-1085.

Meacham, C. A., Freudenrich, T. M., Anderson, W. L., Sui, L., Lyons-Darden, T., Barone, S., Jr., Gilbert, M. E., Mundy, W. R. and Shafer, T. J. (2005). Accumulation of methylmercury or polychlorinated biphenyls in *in vitro* models of rat neuronal tissue. *Toxicol Appl Pharmacol* **205**, 177-187.

Meldolesi, J. (2001). Rapidly exchanging Ca^{2+} stores in neurons: Molecular, structural and functional properties. *Prog Neurobiol* **65**, 309-338.

Meldolesi, J. and Pozzan, T. (1998). The heterogeneity of ER Ca^{2+} stores has a key role in nonmuscle cell signaling and function. *J Cell Biol* **142**, 1395-1398, 10.1083/jcb.142.6.1395.

Meldrum, B. S. and Corsellis, J. A. N. (1984). Epilepsy. In Greenfield's Neuropathology (J. H. Adams, J. A. N. Corsellis and L. W. Duchen, Eds.), 4th ed., pp. 921-950. Wiley, New York.

Mendoza, M. A. C., Ponce, R. A., Ou, Y. C. and Faustman, E. M. (2002). p21WAF1/CIP1 inhibits cell cycle progression but not G2/M-phase transition following methylmercury exposure. *Toxicol Appl Pharmacol* **178**, 117-125.

Miale, I. L. and Sidman, R. L. (1961). An autoradiographic analysis of histogenesis in the mouse cerebellum. *Exp Neurol* **4**, 277-296.

Mielke, H. W., Powell, E., Alston, S., Manuel, J. and Gonzales, C. (2006). Environmental accumulation and synergy of multiple neurotoxicants and children's learning achievement in New Orleans, Louisiana, USA. *Neurotoxicology* **27**, 875-930.

Mikac, N., Picer, M., Stegnar, P. and Tusek-Znidaric, M. (1985). Mercury distribution in a polluted marine area, ratio of total mercury, methyl mercury and selenium in sediments, mussels and fish. *Water Res* **19**, 1387-1392.

Mikhaylova, M., Sharma, Y., Reissner, C., Nagel, F., Aravind, P., Rajini, B., Smalla, K. H., Gundelfinger, E. D., Kreutz, M. R., Mikhaylova, M., Sharma, Y., Reissner, C., Nagel, F., Aravind, P., Rajini, B., Smalla, K.-H., Gundelfinger, E. D. and Kreutz, M. R. (2006). Neuronal Ca^{2+} signaling via caldendrin and calneurons. *Biochim Biophys Acta* **1763**, 1229-1237.

Miller, C. T., Krewski, D. and Tryphonas, L. (1985). Methylmercury-induced mitochondrial DNA synthesis in neural tissue of cats. *Fundam Appl Toxicol* **5**, 251-264.

Mitchell, P. (1993). David Keilin's respiratory chain concept and its chemiosmotic consequences. In Nobel Lectures, Chemistry 1971-1980 (T. Frangsmyr and S. Forsen, Eds.), pp. 295-330. World Scientific Publishing Co., Singapore.

Miura, K. (1998). Neurotoxic mechanisms of methylmercury. *Jap J Toxicol Env Health* **44**, 393-412.

Miura, K., Suzuki, K. and Imura, N. (1978). Effects of methylmercury on mitotic mouse glioma cells. *Environ Res* **17**, 453-471.

Miura, K., Inokawa, M. and Imura, N. (1984). Effects of methylmercury and some metal ions on microtubule networks in mouse glioma cells and *in vitro* tubulin polymerization. *Toxicol Appl Pharmacol* **73**, 218-231.

Miura, K., Kobayashi, Y., Toyoda, H. and Imura, N. (1998). Methylmercury-induced microtubule depolymerization leads to inhibition of tubulin synthesis. *J Toxicol Sci* **23**, 379-388.

Miura, K., Koide, N., Himeno, S., Nakagawa, I. and Imura, N. (1999). The involvement of microtubular disruption in methylmercury-induced apoptosis in neuronal and nonneuronal cell lines. *Toxicol Appl Pharmacol* **160**, 279-288.

Moghrabi, N., Sutherland, L., Wooster, R., Povey, S., Boxer, M. and Burchell, B. (1992). Chromosomal assignment of human phenol and bilirubin UDP-glucuronosyltransferase genes (UGT1A-subfamily). *Ann Hum Genet* **56**, 81-91.

Monnet-Tschudi, F., Zurich, M. G., Boschat, C., Corbaz, A. and Honegger, P. (2006). Involvement of environmental mercury and lead in the etiology of neurodegenerative diseases. *Rev Environ Health* **21**, 105-117.

Monnet-Tschudi, F., Zurich, M. G. and Honegger, P. (1996). Comparison of the developmental effects of two mercury compounds on glial cells and neurons in aggregate cultures of rat telencephalon. *Brain Res* **741**, 52-59.

Montal, M. (1998). Mitochondria, glutamate neurotoxicity and the death cascade. *Biochim Biophys Acta* **1366**, 113-126.

Montell, C. (2005). The latest waves in calcium signaling. *Cell* **122**, 157-163.

Montgomery, K. S., Mackey, J., Thuett, K. A., Ginestra, S., Bizon, J. L. and Abbott, L. C. (2008). Chronic, low-dose prenatal exposure to methylmercury impairs motor and mnemonic function in adult C57/B6 mice. *Behav Brain Res* **191**, 55-61.

Moretto, M. B., Funchal, C., Zeni, G., Pessoa-Pureur, R. and Rocha, J. B. (2005). Selenium compounds prevent the effects of methylmercury on the *in vitro* phosphorylation of cytoskeletal proteins in cerebral cortex of young rats. *Toxicol Sci* **85**, 639-646.

Mori, N., Yasutake, A. and Hirayama, K. (2007). Comparative study of activities in reactive oxygen species production/defense system in mitochondria of rat brain and liver, and their susceptibility to methylmercury toxicity. *Arch Toxicol* **81**, 769-776.

Morris, R. G. (2003). Long-term potentiation and memory. *Philos Trans R Soc Lond* **358**, 643-647.

Moser, M. B., Trommald, M. and Andersen, P. (1994). An increase in dendritic spine density on hippocampal CA1 pyramidal cells following spatial learning in adult rats suggests the formation of new synapses. *Proc Natl Acad Sci U S A* **91**, 12673-12675.

Mukai, K., Morimoto, H., Okauchi, Y. and Nagaoka, S.-I. (1993). Kinetic study of reactions between tocopheroxyl radicals and fatty acids. *Lipids* **28**, 753-756.

Mullen, R., Buck, C. and Smith, A. (1992). NeuN, a neuronal specific nuclear protein in vertebrates. *Development* **116**, 201-211.

Muller, F. (2000). The nature and mechanism of superoxide production by the electron transport chain: Its relevance to aging. *J Amer Aging Assoc* **23**, 227-253.

Muller, F. and O'Rahilly, R. (2004). Embryonic development of the central nervous system. In The Human Nervous System (G. Paxinos and J. K. Mai, Eds.), 2nd ed., pp. 22-48. Elsevier Academic Press, San Diego.

Munday, R. (1989). Toxicity of thiols and disulphides: Involvement of free-radical species. *Free Rad Biol Med* **7**, 659-673.

Mundy, W. R. and Freudenrich, T. M. (2000). Sensitivity of immature neurons in culture to metal-induced changes in reactive oxygen species and intracellular free calcium. *Neurotoxicology* **21**, 1135-1144.

Myers, G. J. and Davidson, P. W. (1998). Prenatal methylmercury exposure and children: Neurologic, developmental, and behavioral research. *Environ Health Perspect* **106**, 841-847.

Myhrer, T. (2007). Neuronal structures involved in the induction and propagation of seizures caused by nerve agents: Implications for medical treatment. *Toxicology* **239**, 1-14.

Naganuma, A., Miura, K., Tanaka-Kagawa, T., Kitahara, J., Seko, Y., Toyoda, H. and Imura, N. (1998). Overexpression of manganese-superoxide dismutase prevents methylmercury toxicity in HeLa cells. *Life Sci* **62**, 157-161.

Nagashima, K., Fujii, Y., Tsukamoto, T., Nukuzuma, S., Satoh, M., Fujita, M., Fujioka, Y. and Akagi, H. (1996). Apoptotic process of cerebellar degeneration in experimental methylmercury intoxication of rats. *Acta Neuropathol* **91**, 72-77.

Nakada, S. and Imura, N. (1980). Stimulation of DNA synthesis and pyrimidine deoxyribonucleoside transport systems in mouse glioma and mouse neuroblastoma cells by inorganic mercury. *Toxicol Appl Pharmacol* **53**, 24-28.

Nakada, S. and Imura, N. (1982). Uptake of methyl mercury and inorganic mercury by mouse glioma and mouse neuro blastoma cells. *Neurotoxicology* **3**, 249-258.

Nakada, S., Nomoto, A. and Imura, N. (1980). Effect of methylmercury and inorganic mercury on protein synthesis in mammalian cells. *Ecotoxicol Environ Saf* **4**, 184-190.

Nakai, A., Taniuchi, Y., Asakura, H., Oya, A., Yokota, A., Koshino, T. and Araki, T. (2000). Developmental changes in mitochondrial activity and energy metabolism in fetal and neonatal rat brain. *Dev Brain Res* **121**, 67-72.

Nass, M. M. K. and Nass, S. (1963). Intramitochondrial fibers with DNA characteristics. I. Fixation and electron staining reactions. *The Journal of Cell Biology* **19**, 593-611.

Nat, R., Voiculescu, B., Stanciu, C., Vidulescu, C., Cergan, R., Badiu, C. and Popescu, L. M. (2001). Apoptosis in human embryo development: 2. Cerebellum. *J Cell Mol Med* **5**, 179-187.

Ndountse, L. T. and Chan, H. M. (2009). Role of N-methyl-D-aspartate receptors in polychlorinated biphenyl mediated neurotoxicity. *Toxicol Lett* **184**, 50-55.

Nemoto, S., Takeda, K., Yu, Z.-X., Ferrans, V. J. and Finkel, T. (2000). Role for mitochondrial oxidants as regulators of cellular metabolism. *Mol Cell Biol* **20**, 7311-7318, 10.1128/mcb.20.19.7311-7318.2000.

Nestor, P. G., Kubicki, M., Kuroki, N., Gurrera, R. J., Niznikiewicz, M., Shenton, M. E. and McCarley, R. W. (2007). Episodic memory and neuroimaging of hippocampus and fornix in chronic schizophrenia. *Psychiatry Res Neuroimaging* **155**, 21-28.

Neylan, T. C. (2000). Memory and the medial temporal lobe: Patient H. M. *J Neuropsychiatry Clin Neurosci* **12**, 103-113, 10.1176/appi.neuropsych.12.1.103.

Nichlas (1992). Mitochondrial mechanisms of neurotoxicity. *Ann N Y Acad Sci* **648**, 28-36.

Nicholls, D. G. and Ferguson, S. J. (2002). Bioenergetics 3. Academic Press, Amsterdam.

Nicholls, D. G., Johnson-Cadwell, L., Vesce, S., Jekabsons, M. and Yadava, N. (2007). Bioenergetics of mitochondria in cultured neurons and their role in glutamate excitotoxicity. *J Neurosci Res* **85**, 3206-3212.

Nicholls, D. G. and Scott, I. D. (1980a). The regulation of brain mitochondrial calcium-ion transport. The role of ATP in the discrimination between kinetic and membrane-potential-dependent calcium-ion efflux mechanisms. *Biochem J* **186**, 833-839.

Nicholls, D. G. and Scott, I. D. (1980b). The role of mitochondria in the regulation of calcium ion transport in synaptosomes. *Biochem Soc Trans* **8**, 264-266.

Nielsen, J. B. and Andersen, O. (1991). Methyl mercuric chloride toxicokinetics in mice II. Sexual differences in whole-body retention and deposition in blood hair skin muscles and fat. *Pharmacol Toxicol* **68**, 208-211.

Niles, A. L., Moravec, R. A., Scurria, M., Daily, W., Bernad, L., McNamara, B., Guthmiller, P., Rashka, K., Lange, D., Arduengo, M. and Riss, T. (2006). Monitor the ratio of live and dead cells within a population: MultiTox-Fluor Multiplex Cytotoxicity Assay. *Promega Notes* **94**.

Nolte, J. and Sundsten, J. W. (2001). The Human Brain : An Introduction to its Functional Anatomy. 5th ed. Mosby, St. Louis.

Null, D. H., Gartside, P. S. and Wei, E. (1973). Methylmercury accumulation in brains of pregnant, non-pregnant and fetal rats. *Life Sci II* **12**, 65-72.

O'Kusky, J. (1983). Methylmercury poisoning of the developing nervous system: Morphological changes in neuronal mitochondria. *Acta Neuropathol* **61**, 116-122.

Oberdoerster, J. (2001). Isolation of cerebellar granule cells from neonatal rats, Unit 12.7. In Current Protocols in Toxicology (M. D. Maines, L. G. Costa, E. Hodgson, D. J. Reed and I. G. Sipes, Eds.). John Wiley and Sons, Inc, Hoboken.

OECD. (2007). Developmental neurotoxicity study. OECD Guidelines for the Testing of Chemicals Section 4: Health Effects, pp. 1-26. Organisation for Economic Co-operation and Development, Paris, France.

Onishchenko, N., Tamm, C., Vahter, M., Hokfelt, T., Johnson, J. A., Johnson, D. A. and Ceccatelli, S. (2007). Developmental exposure to methylmercury alters learning and induces depression-like behavior in male mice. *Toxicol Sci* **97**, 428-437.

Oomman, S., Strahlendorf, H., Dertien, J. and Strahlendorf, J. (2006). Bergmann glia utilize active caspase-3 for differentiation. *Brain Res* **1078**, 19-34.

Orrenius, S., Zhivotovsky, B. and Nicotera, P. (2003). Regulation of cell death: The calcium-apoptosis link. *Nat Rev Mol Cell Biol* **4**, 552-565.

Oyama, Y., Hayashi, A., Ueha, T. and Maekawa, K. (1994). Characterization of 2',7'-dichlorofluorescin fluorescence in dissociated mammalian brain neurons: Estimation on intracellular content of hydrogen peroxide. *Brain Res* **635**, 113-117.

Padayatty, S. J., Katz, A., Wang, Y., Eck, P., Kwon, O., Lee, J.-H., Chen, S., Corpe, C., Dutta, A., Dutta, S. K. and Levine, M. (2003). Vitamin C as an antioxidant: Evaluation of its role in disease prevention. *Journal of the American College of Nutrition* **22**, 18-35.

Palade, G. E. (1952). The fine structure of mitochondria. *The Anatomical Record* **114**, 427-451.

Palkovits, M., Magyar, P. and Szentágothai, J. (1971). Quantitative histological analysis of the cerebellar cortex in the cat. III. Structural organization of the molecular layer. *Brain Res* **34**, 1-18.

Papez, J. W. (1937). A proposed mechanism of emotion. *Arch Neurol Psychiatry* **38**, 725.

Parkinson, A. (2001). Biotransformation of xenobiotics. In Casarett and Doull's Toxicology: The Basic Science of Poisons (C. D. Klaassen, Ed.), 6th ed., pp. 133-224. McGraw-Hill, New York.

Patten, B. M. and Carlson, B. M. (1974). Foundations of Embryology. McGraw-Hill, New York.

Peart, J. N. and Headrick, J. P. (2007). Adenosinergic cardioprotection: Multiple receptors, multiple pathways. *Pharmacol Therapeut* **114**, 208-221.

Pedersen, P. (1999). Mitochondrial events in the life and death of animal cells: A brief overview. *J Bioenerg Biomembr* **31**, 291-304.

Penfield, W. (1958a). Functional localization in temporal and deep sylvian areas. *Res Publ Assoc Res Nerv Ment Dis* **36**, 210-226.

Penfield, W. (1958b). Memory deficit produced by bilateral lesions in the hippocampal zone. *AMA Arch Neurol Psychiatry* **79**, 475-497.

Penfield, W. (1958c). Some mechanisms of consciousness discovered during electrical stimulation of the brain *Proc Natl Acad Sci U S A* **44**, 51-66.

Pentschew, A. and Garro, F. (1966). Lead encephalomyelopathy of the suckling rat and its implications on the porphyrinopathic nervous diseases. With special reference to the permeability disorders of the nervous system's capillaries. *Acta Neuropathol* **6**, 266-278.

Perez-Polo, J. R., Werrbach-Perez, K. and Tiffany-Castiglioni, E. (1979). A human clonal cell line model of differentiating neurons. *Dev Biol* **71**, 341-355.

Perkins, G. A., Renken, C. W., Frey, T. G. and Ellisman, M. H. (2001). Membrane architecture of mitochondria in neurons of the central nervous system. *J Neurosci Res* **66**, 857-865.

Philbert, M. A., Beiswanger, C. M., Waters, D. K., Reuhl, K. R. and Lowndes, H. E. (1991). Cellular and regional distribution of reduced glutathione in the nervous system of the rat: Histochemical localization by mercury orange and o-phthaldialdehyde-induced histofluorescence. *Toxicol Appl Pharmacol* **107**, 215-227.

Philbert, M. A., Billingsley, M. L. and Reuhl, K. R. (2000). Mechanisms of injury in the central nervous system. *Toxicol Pathol* **28**, 43-53.

Piantadosi, C. A. and Zhang, J. (1996). Mitochondrial generation of reactive oxygen species after brain ischemia in the rat. *Stroke* **27**, 327-332.

Pietrobon, D. (2002). Calcium channels and channelopathies of the central nervous system. *Molecular Neurobiology* **25**, 31-50.

Pietrobon, D. (2005). Function and dysfunction of synaptic calcium channels: Insights from mouse models. *Curr Opin Neurobiol* **15**, 257-265.

Platonow, N. (1968). Comparative effects of the chelators on the distribution of organic mercury and inorganic mercury in young pigs. *Can Vet J* **9**, 142-148.

Polla, B. S., Kantengwa, S., Francois, D., Salvioli, S., Franceschi, C., Marsac, C. and Cossarizza, A. (1996). Mitochondria are selective targets for the protective effects of heat shock against oxidative injury. *Proc Natl Acad Sci U S A* **93**, 6458-6463.

Porter, W. L. (1993). Paradoxical behavior of antioxidants in food and biological systems. *Toxicol Ind Health* **9**, 93-122.

Pramanik, R., Ishido, M. and Kunimoto, M. (2002). Methylmercury-mediated down-regulation of mtHSP70 and phospholipase A2 mRNA expression in human neuroblastoma NB-1 cells identified by cDNA macroarray analysis. *J Health Sci* **48**, 381-384.

Prasad, K. N. (1991). New opportunities with neuronal cultures to study the mechanisms of neurotoxic injuries. *Neurotoxicology* **12**, 493-503.

Price, J. L., Ko, A. I., Wade, M. J., Tsou, S. K., McKeel, D. W. and Morris, J. C. (2001). Neuron number in the entorhinal cortex and CA1 in preclinical Alzheimer disease. *Arch Neurol* **58**, 1395-1402, 10.1001/archneur.58.9.1395.

Rahola, T., Hattula, T., Korolainen, A. and Miettinen, J. K. (1973). Elimination of free and protein bound ionic mercury mercury-203 in man. *Ann Clin Res* **5**, 214-219.

Rakic, P. (1971). Neuron-glia relationship during granule cell migration in developing cerebellar cortex. A Golgi and electonmicroscopic study in *Macacus rhesus*. *J Comp Neurol* **141**, 283-312.

Rakic, P. (1972). Extrinsic cytological determinants of basket and stellate cell dendritic pattern in the cerebellar molecular layer. *J Comp Neurol* **146**, 335-354.

Rakic, P. and Sidman, R. L. (1973). Weaver mutant mouse cerebellum: Defective neuronal migration secondary to abnormality of bergmann glia. *Proc Natl Acad Sci U S A* **70**, 240-244.

Raynaud, F. and Marcilhac, A. (2006). Implication of calpain in neuronal apoptosis. *FEBS J* **273**, 3437-3443.

Reichenbach, A., Siegel, A., Rickmann, M., Wolff, J. R., Noone, D. and Robinson, S. R. (1995). Distribution of Bergmann glial somata and processes: Implications for function. *J Hirnforsch* **36**, 509-517.

Reid, T. J., Murthy, M. R., Sicignano, A., Tanaka, N., Musick, W. D. and Rossmann, M. G. (1981). Structure and heme environment of beef liver catalase at 2.5 A resolution. *Proc Natl Acad Sci U S A* **78**, 4767-4771.

Renken, C., Siragusa, G., Perkins, G., Washington, L., Nulton, J., Salamon, P. and Frey, T. G. (2002). A thermodynamic model describing the nature of the crista junction: A structural motif in the mitochondrion. *Journal of Structural Biology* **138**, 137-144.

Repetto, G., Sanz, P. and Repetto, M. (1993). *In vitro* effects of mercuric chloride and methylmercury chloride on neuroblastoma cells. *Toxicol In Vitro* **7**, 353-357.

Reuhl, K. R., Lagunowich, L. A. and Brown, D. L. (1994). Cytoskeleton and cell adhesion molecules: Critical targets of toxic agents. *Neurotoxicology* **15**, 133-145.

Reuter, H. and Porzig, H. (1995). Localization and functional significance of the Na^{+}/Ca^{2+}-exchanger in presynaptic boutons of hippocampal cells in culture. *Neuron* **15**, 1077-1084.

Reynolds, B. and Weiss, S. (1992). Generation of neurons and astrocytes from isolated cells of the adult mammalian central nervous system. *Science* **255**, 1707-1710, 10.1126/science.1553558.

Reynolds, W. A. and Pitkin, R. M. (1975). Transplacental passage of methylmercury and its uptake by primate fetal tissues (38576). *Proc Soc Exp Biol Med* **148**, 523-526.

Ribak, C. E. and Seress, L. (1983). Five types of basket cell in the hippocampal dentate gyrus: A combined Golgi and electron microscopic study. *J Neurocytol* **12**, 577-597.

Rice, D. and Barone, S., Jr. (2000). Critical periods of vulnerability for the developing nervous system: Evidence from humans and animal models. *Environ Health Perspect* **108**, 511-533.

Rieck, P., Peters, D., Hartmann, C. and Courtois, Y. (1993). A new, rapid colorimetric assay for quantitative determination of cellular proliferation, growth inhibition, and viability. *J Tissue Cult Methods* **15**, 37-41.

Robinson, K. M., Janes, M. S. and Beckman, J. S. (2008). The selective detection of mitochondrial superoxide by live cell imaging. *Nat Protoc* **3**, 941-947.

Rodier, P. M., Aschner, M. and Sager, P. R. (1984). Mitotic arrest in the developing CNS after prenatal exposure to methylmercury. *Neurobehav Toxicol Teratol* **6**, 379-385.

Rojas, D., Peterson, E., Winterrowd, E., Reite, M., Rogers, S. and Tregellas, J. (2006). Regional gray matter volumetric changes in autism associated with social and repetitive behavior symptoms. *BMC Psychiatry* **6**, 56-68.

Rowe, M. J., Bieszczad, R. R., Neymark, M. A. and Dimino, M. J. (1981). Synthesis of mitochondrial proteins after stimulation of ovarian follicles by luteinizing hormone. *Endocrinology* **108**, 127-132.

Rozenblum, G. T. and Gimona, M. (2008). Calponins: Adaptable modular regulators of the actin cytoskeleton. *Int J Biochem Cell Biol* **40**, 1990-1995.

Rozman, K. K. and Klaassen, C. D. (2001). Absorption, distribution, and excretion of toxicants. In Casarett and Doull's Toxicology: The Basic Science of Poisons (C. D. Klaassen, Ed.), 6th ed., pp. 107-132. McGraw-Hill, New York.

Sadler, T. W. (2006). Langman's Medical Embryology. 10th ed. Lippincott Williams & Wilkins, Philadelphia.

Saez, G., Thornalley, P. J., Hill, H. A., Hems, R. and Bannister, J. V. (1982). The production of free radicals during the autoxidation of cysteine and their effect on isolated rat hepatocytes. *Biochim Biophys Acta* **719**, 24-31.

Sager, P. R. (1988). Selectivity of methyl mercury effects on cytoskeleton and mitotic progression in cultured cells. *Toxicol Appl Pharmacol* **94**, 473-486.

Sager, P. R., Aschner, M. and Rodier, P. M. (1984). Persistent, differential alterations in developing cerebellar cortex of male and female mice after methylmercury exposure. *Brain Res* **314**, 1-11.

Sager, P. R., Doherty, R. A. and Olmsted, J. B. (1983). Interaction of methylmercury with microtubules in cultured cells and i*n vitro*. *Exp Cell Res* **146**, 127-137.

Sager, P. R. and Syversen, T. L. M. (1984). Differential responses to methyl mercury exposure and recovery in neuro blastoma and glioma cells and fibroblasts. *Exp Neurol* **85**, 371-382.

Saji, M. and Miura, M. (1991). Coexistence of glutamate and choline acetyltransferase in a major subpopulation of laryngeal motoneurons of the rat. *Neurosci Lett* **123**, 175-178.

Salvata, N. and Pirola, C. (1994). Analysis of mercury traces by means of solid sample atomic-absorption spectrometry. *Industrie Alimentari* **33**, 1229-1238.

Sanfeliu, C., Sebastia, J. and Kim, S. U. (2001). Methylmercury neurotoxicity in cultures of human neurons, astrocytes, neuroblastoma cells. *Neurotoxicology* **22**, 317-327.

Sano, K., Shimojo, N., Suzuki, M. and Yamaguchi, S. (1987). [Distribution of methylmercury and alteration of biogenic monoamines in various regions of the brain in methylmercury-administered rats]. *Nippon Eiseigaku Zasshi* **42**, 821-826.

Sarafian, T. and Verity, M. A. (1990). Altered patterns of protein phosphorylation and synthesis caused by methyl mercury in cerebellar granule cell culture. *J Neurochem* **55**, 922-929.

Sarafian, T. A. (1993). Methyl mercury increases intracellular Ca^{2+} and inositol phosphate levels in cultured cerebellar granule neurons. *J Neurochem* **61**, 648-657.

Sarafian, T. A., Cheung, M. K. and Verity, M. A. (1984). *In vitro* methyl mercury inhibition of protein synthesis in neonatal cerebellar perikarya. *Neuropathol Appl Neurobiol* **10**, 85-100.

Satoh, H. and Suzuki, T. (1983). Embryonic and fetal death after in utero methylmercury exposure and resultant organ mercury concentrations in mice. *Ind Health* **21**, 19-24.

Scaduto Jr, R. C. and Grotyohann, L. W. (1999). Measurement of mitochondrial membrane potential using fluorescent rhodamine derivatives. *Biophys J* **76**, 469-477.

Scarlett, J. L. and Murphy, M. P. (1997). Release of apoptogenic proteins from the mitochondrial intermembrane space during the mitochondrial permeability transition. *FEBS Lett* **418**, 282-286.

Schinkel, A. H., Smit, J. J. M., van Tellingen, O., Beijnen, J. H., Wagenaar, E., van Deemter, L., Mol, C. A. A. M., van der Valk, M. A., Robanus-Maandag, E. C., te Riele, H. P. J., Berns, A. J. M. and Borst, P. (1994). Disruption of the mouse mdr1a P-glycoprotein gene leads to a deficiency in the blood-brain barrier and to increased sensitivity to drugs. *Cell* **77**, 491-502.

Schmahmann, J. D. (1997). Rediscovery of an early concept. *Int Rev Neurobiol* **41**, 3-27.

Schmahmann, J. D. and Sherman, J. C. (1997). Cerebellar cognitive affective syndrome. *Int Rev Neurobiol* **41**, 433-440.

Schmued, L., Slikker, W. and Bowyer, J. (1997a). Demonstration and localization of *d*-fenfluramine induced neuronal degeneration in the rat: A Fluoro-Jade study. *Abstr Soc Neurosci* **23**, 275.

Schmued, L. C., Albertson, C. and Slikker, W. (1997b). Fluoro-Jade: A novel fluorochrome for the sensitive and reliable histochemical localization of neuronal degeneration. *Brain Res* **751**, 37-46.

Schmued, L. C. and Hopkins, K. J. (2000). Fluoro-Jade B: A high affinity fluorescent marker for the localization of neuronal degeneration. *Brain Res* **874**, 123-130.

NRC (2006). Guide for the care and use of laboratory animals. National Research Council. pp. 128. National Academy Press, Washington, DC.

Segal, M. and Landis, S. (1974). Afferents to the hippocampus of the rat studied with the method of retrograde transport of horseradish peroxidase. *Brain Res* **78**, 1-15.

Seidenbecher, C. I., Langnaese, K., Sanmarti-Vila, L., Boeckers, T. M., Smalla, K.-H., Sabel, B. A., Garner, C. C., Gundelfinger, E. D. and Kreutz, M. R. (1998). Caldendrin, a novel neuronal calcium-binding protein confined to the somato-dendritic compartment. *J Biol Chem* **273**, 21324-21331, 10.1074/jbc.273.33.21324.

Seress, L. (1988). Interspecies comparison of the hippocampal formation shows increased emphasis on the regio superior in the Ammon's horn of the human brain. *J Hirnforsch* **29**, 335-340.

Shafer, T. J., Contreras, M. L. and Atchison, W. D. (1990). Characterization of interactions of methylmercury with Ca^{2+} channels in synaptosomes and pheochromocytoma cells: Radiotracer flux and binding studies. *Mol Pharmacol* **38**, 102-113.

Shanker, G. and Aschner, M. (2001). Identification and characterization of uptake systems for cystine and cysteine in cultured astrocytes and neurons: Evidence for methylmercury-targeted disruption of astrocyte transport. *J Neurosci Res* **66**, 998-1002.

Shaul, U., Ben-Shachar, D., Karry, R. and Klein, E. (2003). Modulation of frequency and duration of repetitive magnetic stimulation affects catecholamine levels and tyrosine hydroxylase activity in human neuroblastoma cells: Implication for the antidepressant effect of rTMS. *Int J Neuropsychopharmacol* **6**, 233-241.

Shenker, B. J., Guo, T. L. and Shapiro, I. M. (1998). Low-level methylmercury exposure causes human T-cells to undergo apoptosis: Evidence of mitochondrial dysfunction. *Environ Res* **77**, 149-159.

Shiga, T., Ichikawa, M. and Hirata, Y. (1983). Spatial and temporal pattern of postnatal proliferation of Bergmann glial cells in rat cerebellum: An autoradiographic study. *Anat Embryol (Berl)* **167**, 203-211.

Shin, D.-M., Jeon, J.-H., Kim, C.-W., Cho, S.-Y., Lee, H.-J., Jang, G.-Y., Jeong, E. M., Lee, D.-S., Kang, J.-H., Melino, G., Park, S.-C. and Kim, I.-G. (2008). TGFβ mediates activation of transglutaminase 2 in response to oxidative stress that leads to protein aggregation. *FASEB J* **22**, 2498-2507, 10.1096/fj.07-095455.

Shoeman, D. W., Kauffman, R. E., Azarnoff, D. L. and Boulos, B. M. (1972). Placental transfer of diphenylhydantoin in the goat. *Biochem Pharmacol* **21**, 1237-1243.

Shors, T. J. (2004). Memory traces of trace memories: Neurogenesis, synaptogenesis and awareness. *Trends Neurosci* **27**, 250-256.

Sillitoe, R. V., Marzban, H., Larouche, M., Zahedi, S., Affanni, J. and Hawkes, R. (2005). Conservation of the architecture of the anterior lobe vermis of the cerebellum across mammalian species. *Prog Brain Res* **148**, 283-297.

Simic, G., Kostovic, I., Winblad, B. and Bogdanovic, N. (1997). Volume and number of neurons of the human hippocampal formation in normal aging and Alzheimer's disease. *J Comp Neurol* **379**, 482-494.

Simonyi, A., Serfozo, P., Shelat, P. B., Dopheide, M. M., Coulibaly, A. P. and Schachtman, T. R. (2007). Differential roles of hippocampal metabotropic glutamate receptors 1 and 5 in inhibitory avoidance learning. *Neurobiol Learn Mem* **88**, 305-311.

Singer, W. (1993). Neuronal representations, assemblies and temporal coherence. *Prog Brain Res* **95**, 461-474.

Sirois, J. E. and Atchison, W. D. (2000). Methylmercury affects multiple subtypes of calcium channels in rat cerebellar granule cells. *Toxicol Appl Pharmacol* **167**, 1-11.

Slivka, A., Mytilineou, C. and Cohen, G. (1987). Histochemical evaluation of glutathione in brain. *Brain Res* **409**, 275-284.

Smaili, S. S., Hsu, Y. T., Carvalho, A. C. P., Rosenstock, T. R., Sharpe, J. C. and Youle, R. J. (2003). Mitochondria, calcium and pro-apoptotic proteins as mediators in cell death signaling. *Braz J Med Biol Res* **36**, 183-190.

Smaili, S. S., Hsu, Y. T., Youle, R. J. and Russell, J. T. (2000). Mitochondria in Ca^{2+} signaling and apoptosis. *J Bioenerg Biomembr* **32**, 35-46.

Smaili, S. S. and Russell, J. T. (1999). Permeability transition pore regulates both mitochondrial membrane potential and agonist-evoked Ca^{2+} signals in oligodendrocyte progenitors. *Cell Calcium* **26**, 121-130.

Smith, J. C., Allen, P. V. and Von Burg, R. (1997). Hair methylmercury levels in U.S. women. *Arch Environ Health* **52**, 476-480.

Sobreviela, T. and Mufson, E. J. (1995). Reduced nicotinamide adenine dinucleotide phosphate-diaphorase/nitric oxide synthase profiles in the human hippocampal formation and perirhinal cortex. *J Comp Neurol* **358**, 440-464.

Soderstrom, S. and Ebendal, T. (1995). *In vitro* toxicity of methylmercury: Effects on nerve growth factor (NGF)-responsive neurons and on NGF synthesis in fibroblasts. *Toxicol Lett* **75**, 133-144.

Somjen, G. G., Herman, S. P., Klein, R., Brubaker, P. E., Briner, W. H., Goodrich, J. K., Krigman, M. R. and Haseman, J. K. (1973a). The uptake of methyl mercury mercury-203 in different tissues related to its neurotoxic effects. *J Pharmacol Exp Ther* **187**, 602-611.

Somjen, G. G., Herman, S. P., Klein, R., Brubaker, P. E., Briner, W. H., Goodrich, J. K., Krigman, M. R. and Haseman, J. K. (1973b). The uptake of methylmercury (203Hg) in different tissues related to its neurotoxic effects. *J Pharmacol Exp Ther* **187**, 602-611.

Sommer, W. (1880). Erkrankung des Ammonshorns als aetiologisches Moment der Epilepsie. *Arch Psychiatr Nervenkr* **10**, 631-675.

Sone, N., Larsstuvold, M. K. and Kagawa, Y. (1977). Effect of methyl mercury on phosphorylation, transport, and oxidation in mammalian mitochondria. *J Biochem (Tokyo)* **82**, 859-868.

Song, D., Chalepakis, G., Gruss, P. and Joyner, A. (1996). Two Pax-binding sites are required for early embryonic brain expression of an *Engrailed-2* transgene. *Development* **122**, 627-635.

Sørensen, K. E. and Shipley, M. T. (1979). Projections from the subiculum to the deep layers of the ipsilateral presubicular and entorhinal cortices in the guinea pig. *J Comp Neurol* **188**, 313-333.

Sousa, S. C., Maciel, E. N., Vercesi, A. E. and Castilho, R. F. (2003). Ca^{2+}-induced oxidative stress in brain mitochondria treated with the respiratory chain inhibitor rotenone. *FEBS Lett* **543**, 179-183.

Sparagna, G. C., Gunter, K. K., Sheu, S.-S. and Gunter, T. E. (1995). Mitochondrial calcium uptake from physiological-type pulses of calcium. *J Biol Chem* **270**, 27510-27515, 10.1074/jbc.270.46.27510.

Spurgeon, A. (2006). Prenatal methylmercury exposure and developmental outcomes: Review of the evidence and discussion of future directions. *Environ Health Perspect* **114**, 307-312.

Stagaard, J. M., Nowakowski, R. S. and Mollgard, K. (1991). Glial cell differentiation in neuron-free and neuron-rich regions. II. Early appearance of S-100 protein positive astrocytes in human fetal hippocampus. *Anat Embryol (Berl)* **184**, 559-569.

Stern, S., Cox, C., Cernichiari, E., Balys, M. and Weiss, B. (2001). Perinatal and lifetime exposure to methylmercury in the mouse: Blood and brain concentrations of mercury to 26 months of age. *Neurotoxicology* **22**, 467-477.

Steuerwald, U., Weihe, P., Jørgensen, P. J., Bjerve, K., Brock, J., Heinzow, B., Budtz-Jørgensen, E. and Grandjean, P. (2000). Maternal seafood diet, methylmercury exposure, and neonatal neurologic function. *J Pediatr* **136**, 599-605.

Stewart, P. A. and Hayakawa, K. (1994). Early ultrastructural changes in blood-brain barrier vessels of the rat embryo. *Dev Brain Res* **78**, 25-34.

Stock, D., Leslie, A. G. W. and Walker, J. E. (1999). Molecular architecture of the rotary motor in ATP synthase. *Science* **286**, 1700-1705, 10.1126/science.286.5445.1700.

St-Pierre, J., Buckingham, J. A., Roebuck, S. J. and Brand, M. D. (2002). Topology of superoxide production from different sites in the mitochondrial electron transport chain. *J Biol Chem* **277**, 44784-44790, 10.1074/jbc.M207217200.

Strauss, R. S. (1997). Effects of the intrauterine environment on childhood growth. *Br Med Bull* **53**, 81-95.

Stryker, M. P., Chapman, B., Miller, K. D. and Zahs, K. R. (1990). Experimental and theoretical studies of the organization of afferents to single orientation columns in visual cortex. *Cold Spring Harbor Symp Quant Biol: The Brain* **55**, 1082.

Sugrue, M. M. and Tatton, W. G. (2001). Mitochondrial membrane potential in aging cells. *Biol Signals Recept* **10**, 176-188.

Sunderland, E. M., Gobas, F. A. P. C., Branfireun, B. A. and Heyes, A. (2006). Environmental controls on the speciation and distribution of mercury in coastal sediments. *Mar Chem* **102**, 111-123.

Supèr, H. and Soriano, E. (1994). The organization of the embryonic and early postnatal murine hippocampus. II. Development of entorhinal, commissural, and septal connections studied with the lipophilic tracer DiI. *J Comp Neurol* **344**, 101-120.

Swanson, L. W. and Cowan, W. M. (1977). An autoradiographic study of the organization of the efferent connections of the hippocampal formation in the rat. *J Comp Neurol* **172**, 49-84.

Syversen, T. L. (1974). Biotransformation of Hg-203 labelled methyl mercuric chloride in rat brain measured by specific determination of Hg^{2+}. *Acta Pharmacol Toxicol (Copenh)* **35**, 277-283.

Syversen, T. L. M. (1982). Changes in protein and RNA synthesis in rat brain neurons after a single dose of methylmercury. *Toxicol Lett* **10**, 31-34.

Syversen, T. L. M., Totland, G. and Flood, P. R. (1981). Early morphological changes in rat cerebellum caused by a single dose of methyl mercury. *Arch Toxicol* **47**, 101-112.

Szentagothai, J. and Rajkovits, K. (1959). Uber den Ursprung der Kletterfasern des Kleinhirns. *Z Anat Entw Gesch* **121**, 131-141.

Takahashi, T., Deng, Y., Maruyama, W., Dostert, P., Kawai, M. and Naoi, M. (1994). Uptake of a neurotoxin-candidate, (R)-1,2-dimethyl-6,7-dihydroxy-1,2,3,4-tetrahydroisoquinoline into human dopaminergic neuroblastoma SH-SY5Y cells by dopamine transport system. *J Neural Transm Gen Sect* **98**, 107-118.

Takeuchi, T. (1977). Pathology and pathogenesis of Minamata disease. In Minamata Disease: Methylmercury Poisoning in Minamata and Niigata, Japan (T. Tsubaki and K. Irukayama, Eds.), pp. 103-141. Elsevier, New York.

Takeuchi, T., Eto, K. and Eto, N. (1979). Neuropathology of childhood cases of methylmercury poisoning with prolonged symptoms, with particular reference to the decortication syndrome. *Neurotoxicology* **1**, 1-20.

Takeuchi, T., Eto, K. and Tokunaga, H. (1989). Mercury level and histochemical distribution in a human brain with Minamata disease following a long-term clinical course of twenty-six years. *Neurotoxicology* **10**, 651-657.

Takeuchi, T., Morikawa, N., Matsumoto, H. and Shiraishi, Y. (1962). A pathological study of Minamata disease in Japan. *Acta Neuropathol* **2**, 40.

Taskiran, D., Kutay, F. Z., Sozmen, E. and Pogun, S. (1997). Sex differences in nitrite/nitrate levels and antioxidant defense in rat brain. *Neuroreport* **8**, 881-884.

Taupin, P. (2007). The Hippocampus: Neurotransmission and Plasticity in the Nervous System. Nova Science Publishers, New York.

Taupin, P. and Gage, F. H. (2002). Adult neurogenesis and neural stem cells of the central nervous system in mammals. *J Neurosci Res* **69**, 745-749.

Thannickal, V. J. and Fanburg, B. L. (2000). Reactive oxygen species in cell signaling. *Am J Physiol Lung Cell Mol Physiol* **279**, L1005-1028.

Thieme, R., Pai, E. F., Schirmer, R. H. and Schulz, G. E. (1981). 3-dimensional structure of glutathione reductase at 2 angstrom resolution. *J Mol Biol* **152**, 763-782.

Thomas, D. J., Fisher, H. L., Sumler, M. R., Mushak, P. and Hall, L. L. (1987). Sexual differences in the excretion of organic and inorganic mercury by methyl mercury-treated rats. *Environ Res* **43**, 203-216.

Thompson, P. M., Hayashi, K. M., de Zubicaray, G. I., Janke, A. L., Rose, S. E., Semple, J., Hong, M. S., Herman, D. H., Gravano, D., Doddrell, D. M. and Toga, A. W. (2004). Mapping hippocampal and ventricular change in Alzheimer disease. *NeuroImage* **22**, 1754-1766.

Tilson, H. A., Jacobson, J. L. and Rogan, W. J. (1990). Polychlorinated biphenyls and the developing nervous system: Cross-species comparisons. *Neurotoxicol Teratol* **12**, 239-248.

Tiruppathi, C., Minshall, R. D., Paria, B. C., Vogel, S. M. and Malik, A. B. (2002). Role of Ca^{2+} signaling in the regulation of endothelial permeability. *Vascul Pharmacol* **39**, 173-185.

Toimela, T. and Tähti, H. (2004). Mitochondrial viability and apoptosis induced by aluminum, mercuric mercury and methylmercury in cell lines of neural origin. *Arch Toxicol* **78**, 565-574.

Tokuomi, H. (1960). Clinical observation and pathologenesis of Minamata disease. *Psychiatr Neurol Jpn* **62**, 1816-1850.

Tokuomi, H., Uchino, M., Imamura, S., Yamanaga, H., Nakanishi, R. and Ideta, T. (1982). Minamata disease (organic mercury poisoning): Neuroradiologic and electrophysiologic studies. *Neurology* **32**, 1369-1375.

Treiman, M., Caspersen, C. and Christensen, S. B. (1998). A tool coming of age: Thapsigargin as an inhibitor of sarco-endoplasmic reticulum Ca^{2+}-ATPases. *Trends Pharmacol Sci* **19**, 131-135.

Tsubaki, T. and Irukayama, K. (1977). Minamata Disease: Methylmercury Poisoning in Minamata and Niigata, Japan. Elsevier, New York.

Turner, M. D., Marsh, D. O., Smith, J. C., Inglis, J. B., Clarkson, T. W., Rubio, C. E., Chiriboga, J. and Chiriboga, C. C. (1980). Methylmercury in populations eating large quantities of marine fish. *Arch Environ Health* **35**, 367-378.

Turrens, J. F. and Boveris, A. (1980). Generation of super oxide anion by the NADH dehydrogenase of bovine heart mitochondria. *Biochem J* **191**, 421-428.

Turville, S. G., Aravantinou, M., Stossel, H., Romani, N. and Robbiani, M. (2008). Resolution of de novo HIV production and trafficking in immature dendritic cells. *Nature Methods* **5**, 75-85.

Ueha-Ishibashi, T., Oyama, Y., Nakao, H., Umebayashi, C., Nishizaki, Y., Tatsuishi, T., Iwase, K., Murao, K. and Seo, H. (2004). Effect of thimerosal, a preservative in vaccines, on intracellular Ca^{2+} concentration of rat cerebellar neurons. *Toxicology* **195**, 77-84.

Uki, M. and Narahashi, T. (1996). Modulation of serotonin-induced currents by metals in mouse neuroblastoma cells. *Arch Toxicol* **70**, 652-660.

UNEP (2002). Global mercury assessment. United Nations Environment Programme Chemicals: Inter-Organization Programme for the Sound Management of Chemicals, Geneva.

Uzman, L. L. (1960). The histogenesis of the mouse cerebellum as studied by its tritiated thymidine uptake. *J Comp Neurol* **114**, 137-159.

Vahter, M., Mottet, N. K., Friberg, L., Lind, B., Shen, D. D. and Burbacher, T. (1994). Speciation of mercury in the primate blood and brain following long-term exposure to methyl mercury. *Toxicol Appl Pharmacol* **124**, 221-229.

Vahter, M. E., Mottet, N. K., Friberg, L. T., Lind, S. B., Charleston, J. S. and Burbacher, T. M. (1995). Demethylation of methyl mercury in different brain sites of *Macaca fascicularis* monkeys during long-term subclinical methyl mercury exposure. *Toxicol Appl Pharmacol* **134**, 273-284.

Vanlangenakker, N., Berghe, T. V., Krysko, D. V., Festjens, N. and Vandenabeele, P. (2008). Molecular mechanisms and pathophysiology of necrotic cell death. *Curr Mol Med* **8**, 207-220.

van Praag, H., Schinder, A. F., Christie, B. R., Toni, N., Palmer, T. D. and Gage, F. H. (2002). Functional neurogenesis in the adult hippocampus. *Nature* **415**, 1030-1034.

Vendrell, I., Carrascal, M., Vilaro, M. T., Abian, J., Rodriguez-Farre, E. and Sunol, C. (2007). Cell viability and proteomic analysis in cultured neurons exposed to methylmercury. *Hum Exp Toxicol* **26**, 263-272.

Venkatachalam, K., van Rossum, D. B., Patterson, R. L., Ma, H.-T. and Gill, D. L. (2002). The cellular and molecular basis of store-operated calcium entry. *Nat Cell Biol* **4**, E263-272.

Verity, M. A., Brown, W. J. and Cheung, M. (1975). Organic mercurial encephalopathy: *In vivo* and *in vitro* effects of methyl mercury on synaptosomal respiration. *J Neurochem* **25**, 759-766.

Verity, M. A., Brown, W. J., Cheung, M. and Czer, G. (1977). Methyl mercury inhibition of synaptosome and brain slice protein synthesis: *In vivo* and *in vitro* studies. *J Neurochem* **29**, 673-679.

Vieille-Grosjean, I., Hunt, P., Gulisano, M., Boncinelli, E. and Thorogood, P. (1997). Branchial HOX gene expression and human craniofacial development. *Dev Biol* **183**, 49-60.

Voet, D. and Voet, J. G. (2004). Biochemistry. 3rd ed. J. Wiley & Sons, Hoboken, NJ.

Volk, B., Hettmannsperger, U., Papp, T., Amelizad, Z., Oesch, F. and Knoth, R. (1991). Mapping of phenytoin-inducible cytochrome P450 immunoreactivity in the mouse central nervous system. *Neuroscience* **42**, 215-235.

Voogd, J. and Glickstein, M. (1998). The anatomy of the cerebellum. *Trends Neurosci* **21**, 370-375.

Wakabayashi, K., Kakita, A., Sakamoto, M., Su, M., Iwanaga, K. and Ikuta, F. (1995). Variability of brain lesions in rats administered methylmercury at various postnatal development phases. *Brain Res* **705**, 267-272.

Wallenstein, G. V. and Vago, D. R. (2001). Intrahippocampal scopolamine impairs both acquisition and consolidation of contextual fear conditioning. *Neurobiol Learn Mem* **75**, 245-252.

Wassef, M., Zanetta, J. P., Brehier, A. and Sotelo, C. (1985). Transient biochemical compartmentalization of Purkinje cells during early cerebellar development. *Dev Biol* **111**, 129-137.

Waterhouse, N. J. (2003). The cellular energy crisis: Mitochondria and cell death. *Med Sci Sports Exerc* **35**, 105-110.

Weghorst, C. M. and Buzard, G. S. (1993). Enhanced single-strand conformation polymorphism (SSCP) detection of point mutations utilizing methylmercury hydroxide. *Biotechniques* **15**, 396.

Weiss, B., Stern, S., Cox, C. and Balys, M. (2005). Perinatal and lifetime exposure to methylmercury in the mouse: Behavioral effects. *Neurotoxicology* **26**, 675-690.

Weiss, G. M. and Pysh, J. J. (1978). Evidence for loss of Purkinje cell dendrites during late development: A morphometric Golgi analysis in the mouse. *Brain Res* **154**, 219-230.

West, M. J. (1993). Regionally specific loss of neurons in the aging human hippocampus. *Neurobiol Aging* **14**, 287-293.

West, M. J., Coleman, P. D., Flood, D. G. and Troncoso, J. C. (1994). Differences in the pattern of hippocampal neuronal loss in normal ageing and Alzheimer's disease. *Lancet* **344**, 769-772.

Westoo, G. (1973). Methylmercury as percentage of total mercury in flesh and viscera of salmon and sea trout of various ages. *Science* **181**, 567-568, 10.1126/science.181.4099.567.

Weyer, A. and Schilling, K. (2003). Developmental and cell type-specific expression of the neuronal marker NeuN in the murine cerebellum. *J Neurosci Res* **73**, 400-409.

WGMF (1980). Working Group on Mercury in Fish & Australian Fisheries Council, Co-ordinating Committee on Metals in Fish and Fish Products. Report on Mercury in Fish and Fish Products. pp. 371. Australian Govt. Pub. Service, Canberra, Australia.

WHO (1991). Inorganic Mercury: EHC 118. World Health Organization, Geneva.

WHO. (1990). Methylmercury: EHC 101. World Health Organization, Geneva.

Wilke, R. A., Kolbert, C. P., Rahimi, R. A. and Windebank, A. J. (2003). Methylmercury induces apoptosis in cultured rat dorsal root ganglion neurons. *Neurotoxicology* **24**, 369-378.

Winneke, G., Brockhaus, A., Ewers, U., Krämer, U. and Neuf, M. (1990). Results from the European multicenter study on lead neurotoxicity in children: Implications for risk assessment. *Neurotoxicol Teratol* **12**, 553-559.

Witter, M. P. and Amaral, D. G. (1991). Entorhinal cortex of the monkey: V. Projections to the dentate gyrus, hippocampus, and subicular complex. *J Comp Neurol* **307**, 437-459.

Wojda, U., Salinska, E., Kuznicki, J., Wojda, U., Salinska, E. and Kuznicki, J. (2008). Calcium ions in neuronal degeneration. *IUBMB Life* **60**, 575-590.

Wolff, M. S. and Weston, A. (1997). Breast cancer risk and environmental exposures. *Environ Health Perspect* **105 Suppl 4**, 891-896.

Yamada, K. and Watanabe, M. (2002). Cytodifferentiation of Bergmann glia and its relationship with Purkinje cells. *Anat Sci Int* **77**, 94-108.

Yang, W. and Tiffany-Castiglioni, E. (2007). The bipyridyl herbicide paraquat induces proteasome dysfunction in human neuroblastoma SH-SY5Y cells. *J Toxicol Environ Health A* **70**, 1849-1857.

Yee, S. and Choi, B. H. (1994). Methylmercury poisoning induces oxidative stress in the mouse brain. *Exp Mol Pathol* **60**, 188-196.

Yee, S. and Choi, B. H. (1996). Oxidative stress in neurotoxic effects of methylmercury poisoning. *Neurotoxicology* **17**, 17-26.

Yeo, C. H., Hardiman, M. J. and Glickstein, M. (1984). Discrete lesions of the cerebellar cortex abolish the classically conditioned nictitating membrane response of the rabbit. *Behav Brain Res* **13**, 261-266.

Yin, Z., Jiang, H., Syversen, T., Rocha, J. B. T., Farina, M. and Aschner, M. (2008). The methylmercury-l-cysteine conjugate is a substrate for the L-type large neutral amino acid transporter. *J Neurochem* **107**, 1083-1090.

Yin, Z., Milatovic, D., Aschner, J. L., Syversen, T., Rocha, J. B., Souza, D. O., Sidoryk, M., Albrecht, J. and Aschner, M. (2007). Methylmercury induces oxidative injury, alterations in permeability and glutamine transport in cultured astrocytes. *Brain Res* **1131**, 1-10.

Yokoo, E., Valente, J., Grattan, L., Schmidt, S., Platt, I. and Silbergeld, E. (2003). Low level methylmercury exposure affects neuropsychological function in adults. *Environ Health* **2**, 8.

Yoshida, Y., Niki, E. and Noguchi, N. (2003). Comparative study on the action of tocopherols and tocotrienols as antioxidant: Chemical and physical effects. *Chem Phys Lipids* **123**, 63-75.

Yoshino, Y., Mozai, T. and Nakao, K. (1966). Biochemical changes in the brain in rats poisoned with an alkylmercury compound, with special reference to the inhibition of protein synthesis in brain cortex slices. *J Neurochem* **13**, 1223-1230.

Yuasa, S. (1996). Bergmann glial development in the mouse cerebellum as revealed by tenascin expression. *Anat Embryol (Berl)* **194**, 223-234.

Zhang, L., Yu, L. and Yu, C.-A. (1998). Generation of superoxide anion by succinate-cytochrome c reductase from bovine heart mitochondria. *J Biol Chem* **273**, 33972-33976, 10.1074/jbc.273.51.33972.

Ziehen, T. (1934). Centralnervensystem. In Handbuch der Anatomie des Menschen (v. Bardeleben and Eggeling, Eds.), pp. 863-1546. G. Fischer, Jena, Germany.

Zimmer, J. (1978). Development of the hippocampus and fascia dentata: Morphological and histochemical aspects. *Prog Brain Res* **48**, 171-190.

Zola-Morgan, S., Squire, L. and Amaral, D. (1986). Human amnesia and the medial temporal region: Enduring memory impairment following a bilateral lesion limited to field CA1 of the hippocampus. *J Neurosci* **6**, 2950-2967.

Zou, J. Y., Petney, R. and Roth, J. A. (1990). Immunohistochemical detection of phenol sulfotransferase-containing neurons in human brain. *J Neurochem* **55**, 1154-1158.

VITA

Name: Kerry Almeda Thuett

Address: 1610 County Road 125, Post, TX 79356

Email Address: kthuett@gmail.com

Education: B.S., Biology / Mathematics, Texas Tech University, 1993
M.S., Environmental Toxicology, Texas Tech University, 2001
Ph.D., Toxicology, Texas A&M University, 2009

Publications:

1. Montgomery, K. S., Mackey, J., **Thuett, K. A.,** Ginestra, S., Bizon, J. L. and Abbott, L. C. (2008). Chronic, low-dose prenatal exposure to methylmercury impairs motor and mnemonic function in adult C57/B6 mice. *Behav Brain Res* **191**, 55-61.
2. Bellum, S., **Thuett, K. A.,** Grajeda, R. and Abbott, L. C. (2007). Coordination deficits induced in young adult mice treated with methylmercury. *Int J Toxicol* **26**, 115-121.
3. Bellum, S., **Thuett, K. A.,** Taylor, R. J. and Abbott, L. C. (2007). Assessment of mercury concentrations in mouse brain using different routes of administration and different tissue preparations. *Toxicol Mech Meth* **17**, 165-173.
4. Bellum, S., Bawa, B., **Thuett, K. A.,** Stoica, G. and Abbott, L. C. (2007). Changes in biochemical processes in cerebellar granule cells of mice exposed to methylmercury. *Int J Toxicol* **26**, 261-269.
5. Carr, J. A., Gentles, A., Smith, E. E., Goleman, W. L., Urquidi, L. J., **Thuett, K.,** Kendall, R. J., Giesy, J. P., Gross, T. S., Solomon, K. R. and Van Der Kraak, G. (2003). Response of larval *Xenopus Laevis* to atrazine: Assessment of growth, metamorphosis, and gonadal and laryngeal morphology. *Env Toxicol Chem* **22**, 396-405.
6. **Thuett, K. A.,** Roots, E. H., Mitchell, L. P., Gentles, B. A., Anderson, T., Kendall, R. J. and Smith, E. E. (2002). Effects of in utero and lactational ammonium perchlorate exposure on thyroid gland histology and thyroid and sex hormones in developing deer mice (*Peromyscus maniculatus*) through postnatal day 21. *J Toxicol Env Health A* **65**, 2119-2130.
7. **Thuett, K. A.,** Roots, E. H., Mitchell, L. P., Gentles, B. A., Anderson, T. A. and Smith, E. E. (2002). *In utero* and lactational exposure to ammonium perchlorate in drinking water: Effects on developing deer mice at postnatal day 21. *J Toxicol Env Health A* **65**, 1061-1076.